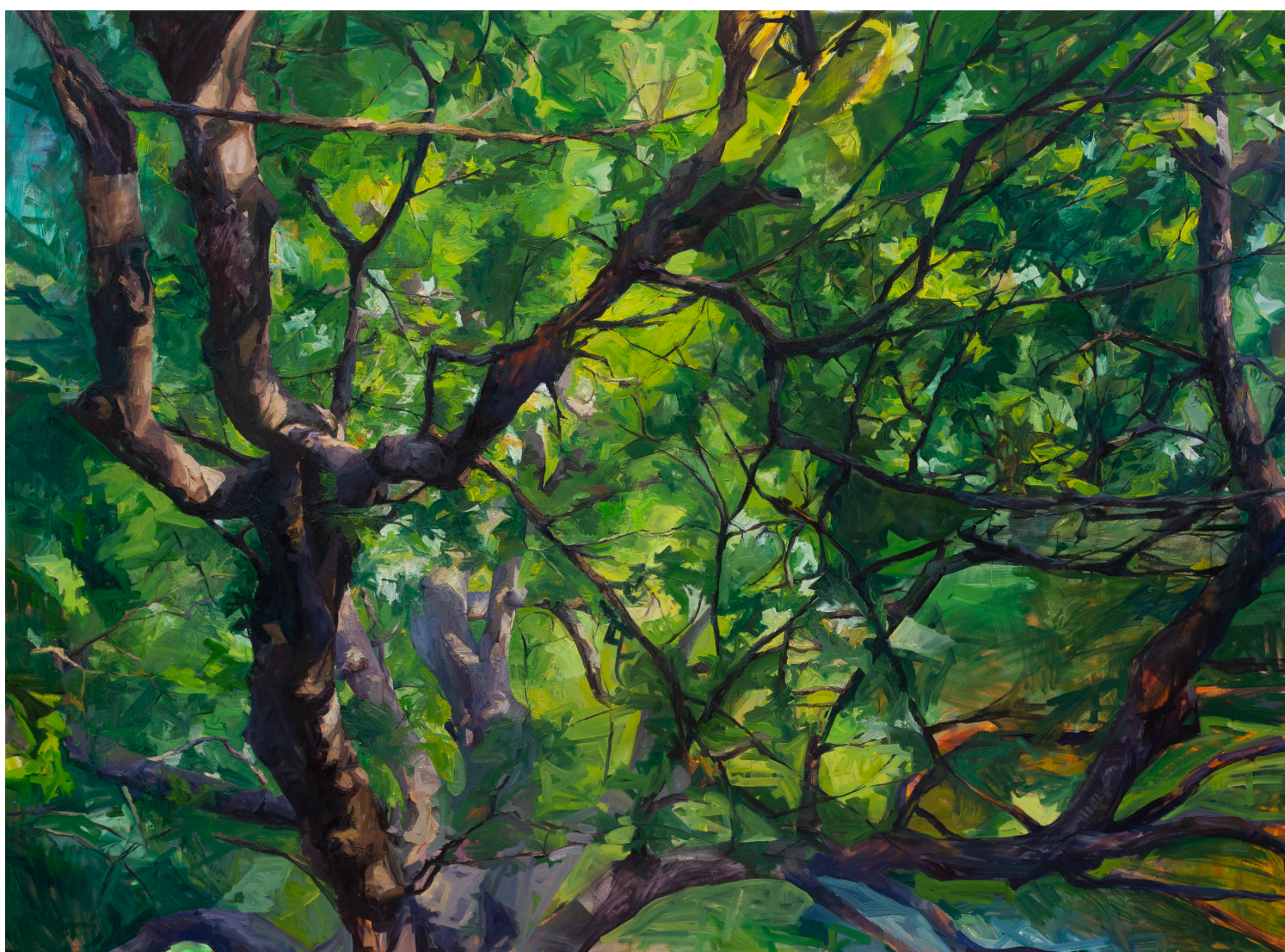UNIVERSITY OF COPENHAGEN
NIELS BOHR INSTITUTE

Quantum: Illuminated

Theory of light-matter interaction for quantum enhanced technologies

Oliver August Dall'Alba Sandberg

Supervisor:

Anders Søndberg Sørensen

Abstract

The study of the interaction between light and matter has revolutionised our under-standing of the modern world, with applications as far-reaching as the development of semiconductors to quantum technology for communication and cryptography. In this thesis, we theoretically analyse light-matter interaction using quantum emitter systems that span a range of scales, from individual quantum dots to ensembles of millions of atoms. By combining our theoretical modelling with experimental exper-tise at the Niels Bohr Institute, we further deepen our understanding of the effects of experimental losses in these diverse light-matter systems.

At an emitter number $N = 1$, we study the nonlinear scattering of individual photons off a quantum dot embedded in a photonic crystal waveguide. We use this single-photon nonlinearity to generate time-energy entanglement, which is of practi-cal importance in opening opportunities for quantum computing and cryptography, as well as quantum optical information processing, communication and measurement protocols.

We add another quantum dot to reach $N = 2$, investigating the entirely new physics arising from the ability to absorb, re-emit and then re-absorb the re-emitted light field. We show how super- and subradiance arises from this coupled system and find our theoretical model can describe the first experimental demonstration of emitter-emitter coupling in waveguide coupled quantum dots.

We then study $N = 10 - 100$ quantum emitters, arranged periodically in an atomic lattice. We propose a novel quantum sensing protocol that exploits the coop-erative enhancement arising from the coherent interaction of the lattice atoms with impurities embedded at some lattice sites. Our protocol is several orders of magni-tude more sensitive in the lattice than in free space and is robust to noise introduced by lattice disorder.

Finally, we use an atomic ensemble with $N \sim 1$ million to investigate the pro-duction of frequency dependent squeezing. This is of interest for gravitational wave interferometers, as it can improve sensitivity beyond the so-called standard quantum limit. By exploiting electromagnetically induced transparency (EIT) and motional averaging, we can produce a broadband suppression of the quantum noise in a grav-itational wave interferometer, even when accounting for experimental losses. Lower noise opens the door to more sensitive gravitational wave astronomy, allowing us to see further than ever before.

Resumé

Undersøgelserne af interaktionen mellem stof og lys har revolutioneret forståelsen af den moderne verden med vidtgående applikationer som udviklingen af halvledere to kvanteteknologier for kommunikation og kryptografi. I denne afhandling, analyserer vi interaktionen mellem stof og lys teoretisk, ved hjælp af kvanteudsendere, som dækker over en lang række forskellige størrelser, fra individuelle kvanteprikker til ensembler af millioner af atomer. Ved at kombinere vores teoretiske modellering med eksperimentel ekspertise ved Niels Bohr Instituttet, forøger vi yderligere vores forståelse af effekterne ved eksperimentelle tab i disse forskelligartede systemer.

Ved udsendertallet $N = 1$, undersøger vi den ikkelineære spredning af enkelte fotoner fra en kvanteprik indlejret i en fotonisk krystal bølgeleder. Vi bruger denne enkelt fotons ikke-linearitet til at generere tid-energi forvikling, hvilket er af praktisk betydning, da det åbner muligheder for kvantekomputering, kryptografi og kvanteoptisk informationsbehandling, kommunikation af måleprotokoller.

Vi tilføjer yderligere en kvanteprik, for at opnå $N = 2$, og undersøger den komplet nye fysik, som opstår fra muligheden for absorption, genudsendelse og så genabsorption af det genudsendte lys. Vi viser hvordan super- og subradiant opstår fra det koblede system og vi finder at vores teoretiske model passer godt på den første eksperimentelle demonstration af udsender-udsender kobling i bølgeledere koblet til kvanteprikker.

Vi undersøger så $N = 10 - 100$ kvanteudsendere, ordnet periodisk i et atomart gitter. Vi forslår en hidtil ukendt kvanteregistreringsprotokol, som udnytter forstærkningen, der kommer fra den kohærente interaktion mellem atomerne i gitteret og urenhederne ved nogle af gitterpladserne. Vi finder ud af, at vores protokol er flere størrelsesordner mere følsom i gitteret end i vakuum og er robust imod støj fra uorden i gitteret.

Endelig, undersøger vi atomiske ensembler med $N \sim 1$ million til at undersøge produktionen af frekvensafhængigt sammentrykning. Dette er interessant for tyngdebølgeinterferometre, da det kan øge følsomhed udover den såkaldt normale kvantegrænse. Ved at udnytte elektromagnetisk induceret transparens (EIT) og bevægelsesgennemsnit finder vi, at vi kan fremstille en bredbåndet undertrykkelse af kvantestøjen i et tyngdebølgeinterferometer, selv hvis vi tager hensyn til eksperimentelle tab.

Acknowledgements

Although my name sits on the front cover as the author, a work of this magnitude is only possible with the help of a whole village of others.

Firstly, and most significantly, is the contribution made by my supervisor Anders Sørensen. Anders, it has been an honour and a privilege to sit in your office and feel stupid each week. I have learned so much through the process – I didn't come here because I thought it would be easy, but despite the challenge, I did manage to have quite a lot of fun. It cannot be overstated how much you have contributed to my development as a physicist, and I am immensely grateful for the opportunity to work with you and glad that I decided to come to Copenhagen.

It is hard for me to imagine a more welcoming environment than the Niels Bohr Institute. From my near-hospitalisation during my initial interview all the way until the submission of this thesis, I have been made to feel at home here. There are simply too many people to name them all here, but a few merit a special mention. (I write the above sentence so as not to forget somebody's name, but I will inevitably forget someone important here. To whomever this ends up being, I'm sorry – my brain currently resembles a half-cooked omelette).

Björn Schrinski taught me how to work my way around master equations, Liouvillians and the quantum regression theorem. My work would be immeasurably worse without you: you saved my PhD. Vasso, regardless of what you think, you are an excellent physicist and an even better person. It has been a blast working with you, and I am grateful to call you my friend. Do not forget your Greek soul. Shikai, it has been a privilege to work alongside you. Your hard work and passion for physics inspires me. Evi, thank you for sharing your music with me. It has opened doors that I never thought possible. αύτος ο κόσμος δε θ᾽ αλλαξει ποτέ. Patrik, thank you for the discussions that always went on some strange tangent, they have enriched my time in Copenhagen. Felix, thank you for your energy, laughter and the spontaneous Copenhagen adventures. Love, thanks for the Swedish-speaking lunches when surrounded by all the Danes, it helped me to feel less outnumbered. To Emil Hellebek, thank you for helping me translate my abstract into Danish and for our entertaining discussions about your peculiar country. To Emil Zeuthen, thank you for trying to teach me Danish during our chats in the office. I think I understand less than when I started, but it was a lot of fun anyway.

I am grateful to Susanne Yelin for the opportunity to work in her group at Harvard University. The time I spent in Cambridge was some of the most rewarding parts of my PhD, and I am looking forward to coming back in the future. I am indebted also to Stefan Ostermann, with whom I worked on the cooperative sensing project.

Thank you for believing in my ideas, and I am glad I could do the same for you.

To the ever-effervescent Hannah, thank you for allowing me to use my favourite painting on the cover[1] of this thesis. Every time I look at it, I smile. I hope my work will do justice to yours.

To Ellie, thanks for taking care of me during the final, intensive weeks of writing, when eating seemed an inconvenience and an afterthought. Maybe it was a small gesture for you, but your food meant so much to me. Thanks for listening to my rants about physics, and for helping me with my figures.

To Eliot, my dear brother, thank you for always being there when I needed to talk, for your Python expertise (although, now ChatGPT is getting pretty good at teaching me) and for always being enthusiastic when I shared some small win with you.

Lastly, to my parents, your belief in me has never been in doubt. Thank you for giving me the gift of curiosity, it has given me so much. To my father, thank you for always wanting me to push myself and reach my potential, you have made me reach higher than I thought possible. To my mother, thank you for reinforcing that critical inquiry is valuable, a gift that allows me to remain joyful whenever I am lost or confused. I love you both dearly.

<div align="right">

Oliver August Dall'Alba Sandberg,
Niels Bohr Institute, September 2023.

</div>

---

[1]Cover art: original painting (*European Beech Tree*, Oil on canvas, 84x62in., 2022), Hannah Steele

List of Publications

The work presented in this thesis has lead to the following publications and manuscripts.

1. A. Tiranov, V. Angelopoulou, C. J. van Diepen, B. Schrinski, **O. A. D. Sandberg**, Y. Wang, L. Midolo, S. Scholz, A. D. Wieck, A. Ludwig, A. S. Sørensen, and P. Lodahl, Collective super- and subradiant dynamics between distant optical quantum emitters, *Science*, vol. 379, no. 6630, pp. 389393, Jan. 2023

2. S. Liu, **O. A. D. Sandberg**, M. L. Chan, B. Schrinski, Y. Anyfantaki, R. B. Nielsen, R. G. Larsen, A. Skalkin, Y. Wang, L. Midolo, S. Scholz, A. D. Wieck, A. Ludwig, A. S. Sørensen, A. Tiranov, and P. Lodahl, Violation of Bell inequality by photon scattering on a two-level emitter, *Submitted to Nature Physics.*

3. **O. A. D. Sandberg**, and A. S. Sørensen, Generation of frequency dependent squeezing via motionally-averaged electromagnetically induced transparency in a room temperature atomic ensemble, *In preparation.*

4. **O. A. D. Sandberg**, S. Ostermann, and S. F. Yelin, Cooperative Sensing with Impurities in a Two-Dimensional Subwavelength Array, *In preparation.*

5. **O. A. D. Sandberg**, B. Schrinski, A. Tiranov, V. Angelopoulou, C. J. van Diepen, P. Lodahl, and A. S. Sørensen, Master equation description of collective super- and subradiance from coupled quantum dots, *In preparation*

6. **O. A. D. Sandberg**, B. Schrinski, S. Liu, A. Tiranov, P. Lodahl, and A. S. Sørensen, Nonlinear photon scattering off a quantum dot in a photonic crystal waveguide, *In preparation.*

7. A. Tiranov, V. Angelopoulou, C. J. van Diepen, A. Ahmad, **O. A. D. Sandberg**, B. Schrinski, Y. Wang, L. Midolo, S. Scholz, A. D. Wieck, A. Ludwig, A. S. Sørensen, and P. Lodahl, Anti-dip in photon coincidences from coupled quantum dots," *In preparation.*

Table of Contents

List of Figures

Chapter 1

On matters of light

1.1 Quantum light, quantum matter: pioneers to present

The study of light-matter interaction in quantum mechanics has been one of the most transformative areas of research in modern science. It has revolutionized our understanding of the microscopic world and has had significant applications in technology, from enabling the development of semiconductors to propelling the rise of quantum technology for communication and cryptography.

At the turn of the 20th century, the classical understanding of physics was challenged by the revelations of quantum mechanics. Early pioneers like Max Planck, Niels Bohr and Albert Einstein made groundbreaking discoveries that marked the dawn of a new era in physics.

Max Planck's investigation of black-body radiation led to the formulation of quantum theory, introducing the concept of quantization of energy. This development laid the foundation for wave-particle duality, suggesting light can exhibit both wave-like and particle-like behaviour. Niels Bohr gave the electron a wave-like nature, producing a model of the atom that did not collapse by radiating energy, as predicted by classical physics. His model additionally provided a microscopic understanding for the empirical Rydberg formula for the spectral emission lines of hydrogen. Albert Einstein's work on the photoelectric effect further supported the idea of a wave-particle duality by demonstrating light could behave as discrete packets of energy, later called photons.

The concept of wave-particle duality not only helped to reconcile classical physics with quantum phenomena but also played a crucial role in various scientific advancements. For instance, understanding the dual nature of light and matter has been pivotal in comprehending semiconductor physics, leading to the development of electronic devices that power our modern technology.

In contemporary research, a shift is taking place, with a focus on harnessing quantum mechanics to create advanced technologies. Instead of being passive observers simply understanding the quantum world, we are now working to produce and manipulate quantum states to our own ends. In other words, we are making the transition to engineering. As Dowling and Milburn put it, "we are currently in the midst of a second quantum revolution. The first quantum revolution gave us new rules that govern physical reality. The second quantum revolution will take these rules and use them to develop new technologies" [6].

Quantum computers, quantum communication, quantum cryptography, quantum sensing and metrology, quantum simulation and quantum networking are all

examples of advancements that we hope will arise out of this revolution. These technologies will harness both light and matter in various capacities, building on the strengths of each.

Light is ideal for information transport, due to its high propagation speed, low loss and dispersion, minimal interference, and ease of detection. Exploiting these advantages, light in linear media has become the foundation for various communication systems, including fiber-optic communication, laser-based communication and free-space communication. While linear light is excellent for efficient information transport, the processing of information requires nonlinear media [7]. Nonlinear media refers to materials or systems in which the output response is not directly proportional to the input signal. Classically, it is only high intensity light beams that can produce such a power-dependent response. This is why early experimental realisations of nonlinear optical phenomena were only possible with the development of powerful lasers [8]. However, there have been both theoretical [9, 10, 11] and experimental [12, 13] advances in nonlinear optics in the quantum regime, where nonlinearities are present at the level of only a few photons. Such nonlinearities have the potential to unlock photonic information processing and storage at the quantum level.

On the other hand, matter-based quantum systems, such as trapped ions [14, 15, 16], superconducting qubits [17, 18, 19] and quantum dots [20, 21], provide excellent platforms for encoding and processing quantum information. These systems can represent quantum bits (qubits) and perform quantum operations with high fidelity, forming the foundation for quantum computing and quantum information processing.

In order to achieve the ambitious goals of quantum technology, scientists are working to interface light with individual quantum systems, enabling operations such as photonic gates and Bell state analysis. Such capabilities would pave the way for secure communication and quantum computing. Consequently, research in the field of light-matter interaction is experiencing a resurgence.

Researchers are now pushing the boundaries of nonlinear optics into the quantum regime. Nonlinear interactions at the level of a single photon have demonstrated several advantages. For instance, they can be employed for ultra-sensitive measurements, quantum state engineering and quantum simulation. Incorporating nonlinear optics into quantum systems necessitates a toolbox of highly controllable light-matter systems, where light and matter are strongly correlated. Novel phenomena like super-radiance and subradiance, as well as entanglement, come into play in these systems. Moreover, advances in quantum technologies have shifted entanglement generation from individual atoms to solid-state devices, offering scalability and better control, such as in superconducting qubits and quantum dots.

In recent years, the exploration of quantum systems has opened new frontiers in the field of quantum information processing and quantum sensing. The ability to manipulate and control individual quantum emitters has led to groundbreaking discoveries in various quantum phenomena. Building on these discoveries, this thesis aims to investigate the behaviour and applications of quantum emitters in systems across various scales, from individual quantum dots to ensembles of millions of atoms. Through collaboration with experimentalists in conjunction with our theoretical modelling, we study the properties and potential applications of quantum emitters in diverse contexts. In this research, we have positioned ourselves to take advantage of new technological capabilities in modern experiments. We exploit the newfound ability to couple quantum dots in photonic crystal waveguides [22], control atoms to produce arrays [23] and interface light with atomic ensembles [24]. The research presented herein not only contributes to our fundamental understanding of quantum phenomena, but also opens up exciting possibilities for practical quantum technologies and precision sensing applications.

1.2   The structure of this thesis

This thesis is organised as a collection of manuscripts, with an introductory chapter giving theoretical background where needed to understand the content in the coming chapter.

In Chapter 2, we develop the necessary theoretical background for the proceeding two chapters investigating quantum dots in photonic crystal waveguides. We derive the Hamiltonian and equations of motion for relevant operators in this system, and write down a useful effective operator formalism. We additionally describe the quantum regression theorem, which is extensively used to compute two-time correlation functions, most notably the second order correlation function $g^{(2)}(\tau)$.

In Chapter 3, we theoretically investigate the generation of time-energy entanglement via the scattering off a single quantum dot embedded in a photonic crystal waveguide. The entanglement that is produced is evidence of a single-photon nonlinearity induced by the scattering. This type of optical response, occurring at the level of a single quantum of light, opens the door to improved classical nonlinear optics, as well as quantum information processing and communication.

We then shift our focus to a system with $N = 2$ quantum emitters in Chapter 4. We introduce a second quantum dot into the system and show we can generate coupling between the emitters. We explore the phenomena of super- and subradiance arising from this coupled quantum dot system. A theoretical model is presented

to describe the behaviour of the two interacting emitters, generating insights into quantum coherence and correlated emission.

Next, in Chapter 5 we investigate a setting where $N \sim 10 - 100$ – arrays of periodically spaced atoms in a so-called atomic lattice. In this context, a novel quantum sensing protocol is proposed, involving the embedding of two impurity atoms in a sub-wavelength atomic array. Through dipole-dipole coupling with the array, the emitters exhibit long-range collective coupling, leading to heightened sensitivity to detuning, suggesting potential applications for sensing electric and magnetic fields. We show that this model is not only several orders of magnitude more sensitive than coupled emitters in free space, but is also robust to the noise introduced by lattice disorder. The protocol's generality suggests potential applications in diverse quantum systems, including the previously discussed coupled quantum dot system.

Finally, in Chapters 6 and 7 we investigate an atomic ensemble where $N \sim 1$ million quantum emitters are considered. Here, we explore the utilization of electromagnetically induced transparency (EIT) in an atomic ensemble to produce frequency-dependent squeezing. In Chapter 6, we show how this phenomenon can significantly enhance the sensitivity of gravitational wave detectors, such as the Laser Interferometer Gravitational-Wave Observatory (LIGO). In Chapter 7, we demonstrate how motional averaging inside the cell containing the ensemble atoms facilitates the desired squeezing rotation. This leads to a broadband suppression of noise in a way that can be integrated into LIGOs existing infrastructure without major redesigns.

Chapter 2

Quantum dots in photonic crystal waveguides
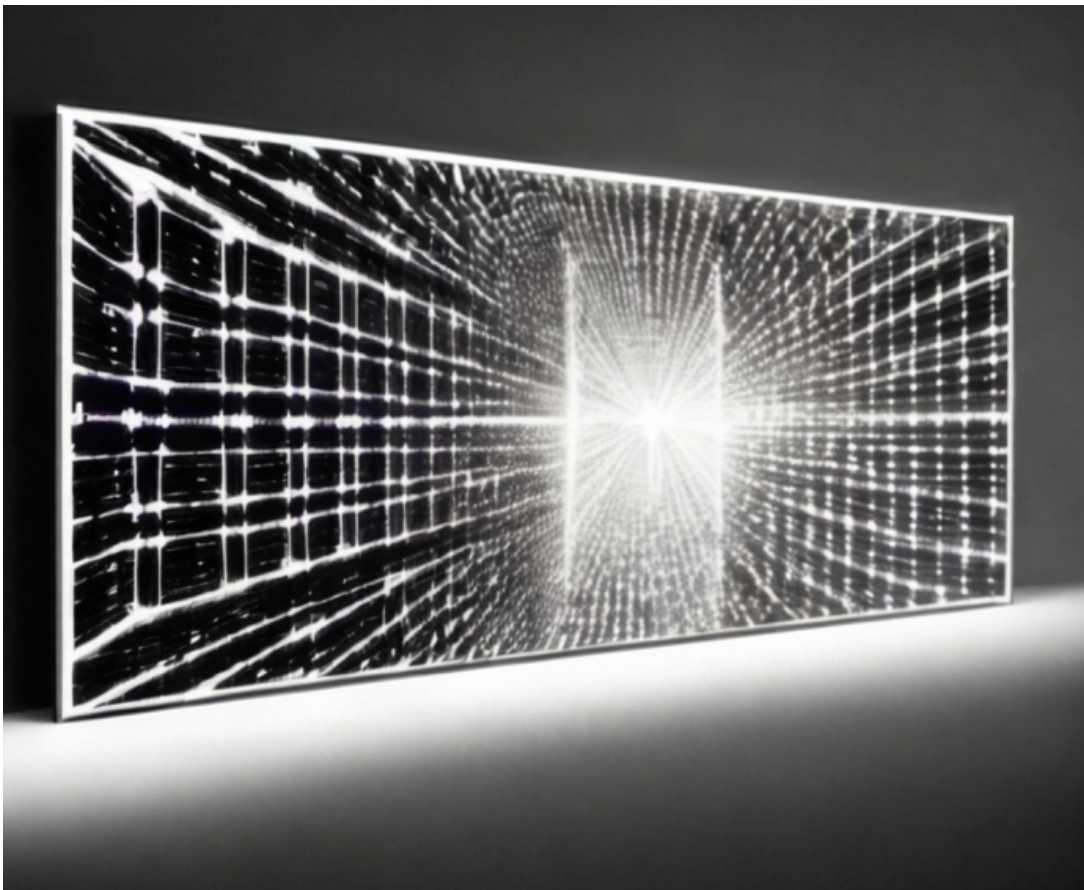
Despite many decades of study [25, 26] and a plethora of applications [27], the interaction between light and N quantum emitters is still producing novel and surprising results. One of the most well-known of these phenomena is Dicke superradiance [28] which has been extensively studied [29] since Dicke's seminal 1954 paper. Recent developments [24, 7] have led to the development of waveguides (see Fig. 2.1), platforms that allow for the ordered arrangement of quantum emitters, which allows the underlying collective effects to be seen more clearly. The confine-
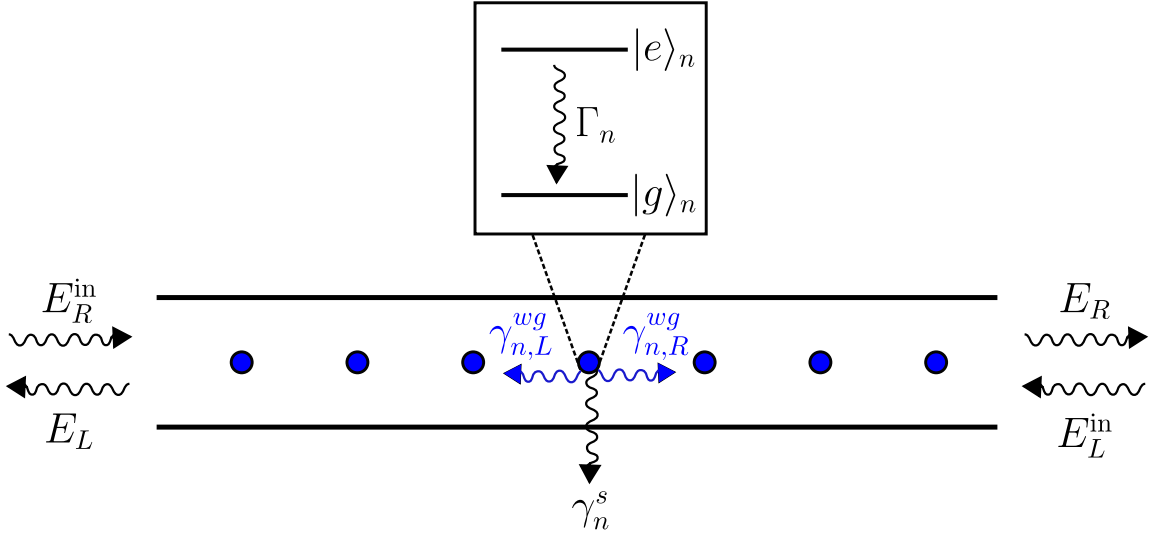
Figure 2.1: **Quantum emitters embedded in a photonic crystal waveguide**. We write a description for N quantum emitters with label n inside a waveguide. Each emitter is a two level system with excited state $|e\rangle_n$ and ground state $|g\rangle_n$. The decay rate from excited to ground is Γ_n, which is then emitted into the waveguide, to the left with rate $\gamma^{wg}_{n,L}$, to the right with rate $\gamma^{wg}_{n,R}$ or to the side (as a loss) with rate γ^s_n. The dots are driven with the input fields $E^{\text{in}}_{L/R}$, which are shown here going through the waveguide. In principle, driving through the top is also possible, such that the detected fields E_L and E_R do not contain a contribution from the input light.

ment of the emitters inside the waveguide also drastically increases the coupling between emitter and photon to levels much higher than in free space, similar to the coupling enhancement found in cavity QED [30]. The following two chapters will investigate systems of quantum dots embedded in a photonic crystal waveguide. We begin with the case $N = 1$, where we exploit the single-photon nonlinearity produced

by photonic scattering off a single quantum dot to produce quantum states entangled in time and energy. We then analyse the case $N = 2$, where we couple two dots and demonstrate super- and sub-radiance arises from the system.

In this chapter, we will outline the theoretical background for these two proceeding chapters. First, by modelling the dipole-dipole interaction between the light fields and quantum emitters, we write down an effective Hamiltonian description of the dynamics of waveguide quantum dots, within the master equation framework. We then outline the Quantum Regression Theorem, which will be used to evaluate expectation values in the developed framework. This primarily allows us to compute correlation functions, particularly the second order correlation function $g^{(2)}(\tau)$.

2.1 Dipole-dipole coupling between light fields and quantum dots

We describe a system of N emitters inside a waveguide, as shown in Fig. 2.1. The Hamiltonian describing the dipole-dipole interaction between a quantised electromagnetic field and matter is

$$H = H_{\text{F}} + H_{\text{QD}} + H_{\text{I}}, \tag{2.1}$$

where the Hamiltonian describing the electromagnetic field is

$$H_{\text{F}} = \int dk \hbar \omega_k a_k^\dagger a_k \tag{2.2}$$

for bosonic creation and annihilation operators $a_k^\dagger$ and a_k with wavenumbers k and corresponding frequencies ω_k. Each quantum dot is described as a two-level system where

$$H_{\text{QD}} = \sum_j \hbar \omega_{eg} \sigma_{ee}^{(j)}, \tag{2.3}$$

where $\sigma_{ee} = |e\rangle \langle e|$ and $\omega_{eg} = \omega_e - \omega_g$, the frequency difference between the ground and excited state of the dipole transition $|g\rangle \leftrightarrow |e\rangle$. The interaction between the light fields and quantum dots is given by

$$H_{\text{I}}^{(j)} = -\hbar \sum_m \int dk \mathcal{G}_{m,k}^{(j)} \sigma_{eg}^{(j)} a_m e^{ikz_j(-1)^m} + \text{H.c.} \tag{2.4}$$

where $m = 0$ corresponds to the right-going field to the right and $m = 1$ corresponds to the left-going field. The coupling constant $\mathcal{G}_{m,k}^{(j)}$ describes the directional coupling to the jth dot. We assume the frequency components of the field addressing the dots are centred on a narrow frequency interval about ω_0, with corresponding wavenumber k_0. We can expand the frequencies as $\omega_k \approx \omega_0 + v_g(k - k_0)$ where $v_g = \partial\omega/\partial k$ is the group velocity. We approximate the coupling constant independent of frequency on this frequency range, i.e., $\mathcal{G}_{m,k}^{(j)} \approx \mathcal{G}_m^{(j)}$. We now transform into a rotating frame with respect to the drive frequency ω_0, obtaining the interaction picture Hamiltonian

$$\tilde{H}^{(j)} = \hbar\Delta\sigma_{ee}^{(j)} + \hbar \int dk(\omega_k - \omega_0)a_k^\dagger a_k$$
$$- \hbar\sum_m \mathcal{G}_m^{(j)} \int dk \left(\sigma_{eg}^{(j)}a_k e^{ikz_j(-1)^m} + \text{H.c.}\right) \tag{2.5}$$

where the detuning $\Delta = \omega_{eg} - \omega_0$ is now defined with respect to the drive. We can then use the slowly-varying field operator to describe the light-matter interaction

$$E_m(z) = \frac{\sqrt{v_g}}{\sqrt{2\pi}} \int_0^\infty dk a_k e^{i(k-k_0)z(-1)^m}, \tag{2.6}$$

which obeys the bosonic commutation relation $\left[E(z), E^\dagger(z')\right] = v_g\delta(z - z')$. We can therefore write the total Hamiltonian as

$$\tilde{H} = \sum_j \hbar\Delta\sigma_{ee}^{(j)} - i\hbar\sum_m \int dz(-1)^m E_m^\dagger(z)\frac{\partial E_m(z)}{z}$$
$$- \hbar\sum_j \sum_m \sqrt{2\pi/v_g}\mathcal{G}_m^{(j)} \left(\sigma_{eg}^{(j)}E_m(z_j)e^{ik_0z_j} + \text{H.c.}\right) \tag{2.7}$$

We assume a symmetric dispersion relation such that $|v_g^L| = |v_g^R| = v_g$, i.e., the left and right-going group velocities have the same magnitude. The integral over k is thus split into a left and right block, centred about $\pm k_0$, i.e.,

$$\int dk \, \omega(k)a_k^\dagger a_k \approx \underbrace{\int_{-k_0-\Delta k}^{-k_0+\Delta k} dk \, \omega(k)a_{k,L}^\dagger a_{k,L}}_{\text{Left-going}} + \underbrace{\int_{k_0-\Delta k}^{k_0+\Delta k} dk \, \omega(k)a_{k,R}^\dagger a_{k,R}}_{\text{Right-going}}. \tag{2.8}$$

We are interested in driving the emitters with coherent light, with a field we will call $\mathcal{E}(t)$. This driving can be achieved either through the waveguide, in which case the coherent field will be included as an input to the detected field, or from above, such

that we only need to treat the effect of the field on the atomic operators. We take the initial state of the system to be a tensor product of this coherent state with the emitters all in their respective ground states [31]

$$|\psi_0\rangle = \hat{D}(\alpha_k)|\emptyset\rangle \otimes \prod_j \left(|g\rangle_j\right), \tag{2.9}$$

where $D(\alpha_k)$ is the displacement operator acting on the photonic vacuum state $|\emptyset\rangle$. We are interested in coherent light as an input and thus wish to apply a displacement to the interaction Hamiltonian with the operator $\hat{D}(\alpha_k) = \exp\left[\int dk(\hat{a}_k^\dagger \alpha_k - \hat{a}_k \alpha_k^*)\right]$ so that

$$\tilde{H}' = D^\dagger(\tilde{\alpha}_k)\tilde{H}D(\tilde{\alpha}_k) - i\hbar D^\dagger(\tilde{\alpha}_k)\frac{dD(\tilde{\alpha}_k)}{dt}, \tag{2.10}$$

where $\tilde{a}_k = \alpha_k e^{-i(\omega_k-\omega_0)t}$, such that the displaced state $|\psi'(t)\rangle = D^\dagger(\tilde{\alpha})|\psi(t)\rangle$ obeys the interaction picture Schrödinger equation

$$i\hbar\partial_t|\psi'(t)\rangle = \tilde{H}'|\psi'(t)\rangle. \tag{2.11}$$

The quantum dot H_{QD} and field H_F Hamiltonians are invariant under this displacement, but the interaction Hamiltonian in the rotating frame changes to

$$H_I' = -\hbar\sum_j \sqrt{2\pi/v_g}\sum_m g_m^{(j)}\left[\sigma_{eg}^{(j)}E_m(z_j)e^{ik_0z_j(-1)^m} + \sigma_{ge}^{(j)}E_m^\dagger(z_j)e^{-ik_0z_j(-1)^m}\right]$$
$$+ \frac{\Omega_j}{2}\left(\sigma_{eg}^{(j)}e^{ik_0z_j} - \hbar\sigma_{ge}^{(j)}e^{-ik_0z_j}\right), \tag{2.12}$$

where $\Omega_j = 2\sqrt{2\pi}\mathcal{E}^{(j)}\mathcal{G}$ and

$$\mathcal{E}^{(j)}(t) = \frac{1}{\sqrt{2\pi}}\int dk\alpha_k e^{i[(k-k_0)z_j-(\omega_k-\omega_0)t]}, \tag{2.13}$$

is the coherent input field. We can obtain equations of motion using $\dot{A} = -\frac{i}{\hbar}[A, H]$. For the jth quantum dot de-excitation operator σ_{ge}, we have

$$\dot{\sigma}_{ge}^{(j)} = \sqrt{2\pi/v_g}i\sum_m g_m^{(j)}\sigma_z^{(j)}E_m(z_j)e^{ik_0z_j(-1)^m} + i\frac{\Omega_j}{2}\sigma_z^{(j)}e^{ik_0z_j} \tag{2.14}$$

$$= \sqrt{2\pi/v_g}i\left[g_L^{(j)}\sigma_z^{(j)}E_L(z_j)e^{-ik_0z_j} + g_R^{(j)}\sigma_z^{(j)}E_R(z_j)e^{ik_0z_j}\right] + i\frac{\Omega_j}{2}\sigma_z^{(j)}e^{ik_0z_j} \tag{2.15}$$

The equations of motion for the field operators E_L and E_R are

$$\dot{E}_m(z_j) = -v_g(-1)^m \frac{\partial E_m(z)}{\partial z} - i\sqrt{2\pi v_g} \sum_j \delta(z - z_j) e^{ik_0 z_j (-1)^m} g_m^{(j)} \sigma_{ge}^{(j)}(t) \qquad (2.16)$$

$$\Rightarrow \underbrace{\left(\frac{\partial}{\partial z} + \frac{(-1)^m}{v_g} \frac{\partial}{\partial t} \right)}_{\text{Directional derivative}} E_m(z,t) = -i\sqrt{2\pi} \sum_j \delta((z - z_j)(-1)^m) e^{ik_0 z_j (-1)^m} \frac{g_m^{(j)}}{\sqrt{v_g}} \sigma_{ge}^{(j)}(t)$$

$$(2.17)$$

The left hand side is a directional derivative and produces time-retarded solutions of the form $E_m(z,t) = f(t \pm z/v_g)$, corresponding to left- and right-going waves, respectively. This time-retardation can be neglected, i.e., $t \pm z/v_g \approx t$, since the system size $L_{\text{sys}} \ll v_g/\Gamma$. This results in a Markov approximation [32]. By making this approximation we are making the claim that the propagation speed of light in the waveguide is effectively instant compared to the decay timescales Γ that are present in the system, i.e., the interesting dynamics occur on a timescale much slower than the speed of light, and thus its propagation can be neglected. We can then formally integrate our equations and obtain

$$E_L = -\sqrt{2\pi} i \sum_j \frac{g_L^{(j)}}{\sqrt{v_g}} \sigma_{ge}^{(j)} \theta(z_j - z) e^{ik_0 z_j} + E_L^{\text{in}} \qquad (2.18)$$

$$E_R = -\sqrt{2\pi} i \sum_j \frac{g_R^{(j)}}{\sqrt{v_g}} \sigma_{ge}^{(j)} \theta(z - z_j) e^{-ik_0 z_j} + E_R^{\text{in}}, \qquad (2.19)$$

where $\theta(z)$ is the Heaviside step function, which ensures the correct coupling only to the left (right). Inserting these into the equation of motion for σ_{ge} we obtain

$$\dot{\sigma}_{ge}^{(j)} = 2\pi i \sum_\ell \left[g_L^{(j)} \sigma_z^{(j)} \sigma_{ge}^{(\ell)} \frac{g_L^{(\ell)}}{v_g} \theta(z_\ell - z_j) e^{ik_0(z_\ell - z_j)} + g_R^{(j)} \sigma_z^{(j)} \sigma_{ge}^{(\ell)} \frac{g_R^{(\ell)}}{v_g} \theta(z_j - z_\ell) e^{-ik_0(z_\ell - z_j)} \right]$$

$$+ i \left(E_L^{in} \frac{g_L^{(j)}\sqrt{2\pi}}{\sqrt{v_g}} e^{-ik_0 z_j} + E_R^{in} \frac{g_R^{(j)}\sqrt{2\pi}}{\sqrt{v_g}} e^{ik_0 z_j} + \frac{\Omega_j}{2} e^{ik_0 z_j} \right) \sigma_z^{(j)}, \qquad (2.20)$$

where when evaluating the sum, we use $\theta(0) = 1/2 + i\delta\omega$. The imaginary term $i\delta\omega$ is the Lamb shift that we neglect since we can include it directly in the reference frequency ω_0 which can be measured experimentally.

The above is a rather general treatment that includes the possibility of a chiral waveguide [33]. We will henceforth treat the non-chiral case, where the coupling to

the left and the right is equal, i.e., $g_L^{(j)} = g_R^{(j)} = g^{(j)}$. We can thus write

$$\dot{\sigma}_{ge}^{(j)} = \frac{i}{2}\Gamma_j\beta_j\sigma_z^{(j)}\sigma_{ge}^{(j)} + i\sum_{\ell \neq j}\sqrt{\beta_j\beta_\ell\Gamma_j\Gamma_\ell}e^{ik_0|z_\ell - z_j|}\sigma_z^{(j)}\sigma_{ge}^{(j)}$$

$$+ i\left[\sqrt{\frac{\beta_j\Gamma_j}{2}}\left(E_L^{in}e^{-ik_0z_j} + E_R^{in}e^{ik_0z_j}\right) + \frac{\Omega_j}{2}e^{ik_0z_j}\right]\sigma_z^{(j)}, \qquad (2.21)$$

where we have written $\Gamma_j\beta_j = 4\pi(g^{(j)})^2/v_g$. To account for dephasing γ_d and decay to the side γ_s, we write our equations of motion in a master equation ($\hbar = 1$)

$$\dot{\rho} = \mathcal{L}_{\text{tot}}[\rho] = -i\,[H,\rho] + \mathcal{L}_{\text{coup}}[\rho] + \mathcal{L}_{\text{decay}}[\rho] + \mathcal{L}_{\text{deph}}[\rho]. \qquad (2.22)$$

Here the Hamiltonian $H = \sum_m \Delta_m\sigma_m^z/2 + \Omega_m(e^{i\theta_m}\sigma_m^+ + e^{-i\theta_m}\sigma_m^-)/2$ accounts for the detuning and potential driving of the involved emitters with relative phases $\theta_m - \theta_n$. We have written three different Liouvillians: a Liouvillian corresponding to decay of the emitters to modes other than the waveguide (side modes)

$$\mathcal{L}_{\text{decay}}[\rho] = \sum_m \gamma_m^s\sigma_m^-\rho\sigma_m^+ \qquad (2.23)$$

with a decay rate γ_m^s for the mth emitter. We also include dephasing described by

$$\mathcal{L}_{\text{deph}}[\rho] = \frac{\gamma_d}{2}\sum_m\left[\sigma_m^z\rho\sigma_m^z - \rho\right], \qquad (2.24)$$

where the dephasing rate γ_d is assumed similar for all emitters for simplicity. This is the standard description of pure dephasing acting individually on each emitter.

Finally, we include a term $\mathcal{L}_{\text{coup}}[\rho]$ which describes the waveguide mediated coupling [34, 35, 36]

$$\mathcal{L}_{\text{coup}}[\rho] = i\sum_{mn}J_{mn}[\sigma_n^+\sigma_m^-,\rho] - \sum_{mn}\Gamma_{mn}\left[\sigma_m^-\rho\sigma_n^+ - \frac{1}{2}\{\sigma_n^+\sigma_m^-,\rho\}\right] \qquad (2.25)$$

with the couplings

$$\Gamma_{mn} = \frac{4\pi g^{(m)}g^{(n)}}{v_g}\text{Re}\{e^{i\phi_{mn}}\} \quad \text{and} \quad J_{mn} = \frac{2\pi g^{(m)}g^{(n)}}{v_g}\text{Im}\{e^{i\phi_{mn}}\}, \qquad (2.26)$$

which, by writing $\Gamma_m\beta_m = 4\pi(g^{(m)})^2/v_g$, corresponds to $J_{mn} = \frac{1}{2}\sqrt{\beta_m\beta_n\Gamma_m\Gamma_n}\sin\phi_{mn}$ and $\Gamma_{mn} = \sqrt{\beta_m\beta_n\Gamma_m\Gamma_n}\cos\phi_{mn}$, which can now be identified as the dispersive and

dissipative coupling rates connecting QD_m with QD_n. With these identifications, we can write the fields as

$$E_L = E_R^{\text{in}} + \sum_n -i\sqrt{\beta_n \Gamma_n/2}\,\sigma_n^- e^{i\phi_n} \tag{2.27}$$

$$E_R = E_R^{\text{in}} + \sum_n -i\sqrt{\beta_n \Gamma_n/2}\,\sigma_n^- e^{-i\phi_n} \tag{2.28}$$

where $\phi_n = k_0 z_n$ is the accumulated, relative phase to the left (right) of the field emitted at position z. In order to analytically understand the basic physics, we can neglect dephasing and work in the single-emitter subspace, where the dynamics reduce to

$$\dot{\rho} = -i\left[\mathcal{H}_{\text{eff}}\rho - \rho\mathcal{H}_{\text{eff}}^\dagger\right] \tag{2.29}$$

with an effective Hamiltonian $\mathcal{H}_{\text{eff}}$ (frame rotating at the excitation field frequency and $\hbar = 1$) [35, 36]

$$\mathcal{H}_{\text{eff}} = \sum_{m,n=1}^N \left(J_{mn} - i\frac{\Gamma_{mn}}{2}\right)\sigma_n^+\sigma_m^- + \sum_{n=1}^N \left(\Delta_n - i\frac{\gamma_n^s}{2}\right)\sigma_n^+\sigma_n^-. \tag{2.30}$$

The evolution with the effective Hamiltonian corresponds to the so-called no jump quantum Monte-Carlo wavefunction approach. The omitted jump terms, representing the state after a decay, prepare the system in the non-radiative joint ground state of the system. Since this state is non-radiative, the full system dynamics of the emitted light can be understood within this no-jump framework. However, once the system undergoes dephasing, re-excitation or is excited beyond the single-excitation subspace, these jump terms are important, and we revert to the full master equation (2.22) to solve the system dynamics. The decay rate $\Gamma_m = \gamma_m^{wg} + \gamma_m^s$ contains the decay rate into (out of) the waveguide γ_m^{wg} (γ_m^s), corresponding to β-factors $\beta_m = \gamma_m^{wg}/\Gamma_m$. Δ_m is the detuning of QD_m with respect to the excitation field frequency, such that $\Delta_{mn} = \Delta_m - \Delta_n$ is the detuning between the two QDs, $\phi_{mn} = k_0|z_{mn}|$ is the phase lag due to the emitter separation $z_{mn} = z_m - z_n$ with k_0 being the resonant wavenumber of the waveguide mode. ϕ_{mn} determines the character of the coupling between dispersive ($\Gamma_{mn} = 0$), which modifies the energy levels, to dissipative ($J_{mn} = 0$), which affects the decay dynamics.

2.2   The Quantum Regression Theorem

Given two operators acting at times t_1 and t_2, we want to compute two time correlation functions of the form [37, 38, 39]

$$\langle O_2(t_2)O_1(t_1)\rangle = \text{Tr}_{SE}\left(O_2 U(t_2,t_1)O_1 U(t_1,t_0)\rho_{SE}U^\dagger(t_1,t_0)U^\dagger(t_2,t_1)\right) \qquad (2.31)$$

where ρ_{SE} is the system + environment density matrix, and $U(t_b,t_a)$ is the time evolution operator from $t_a \rightarrow t_b$.

2.2.1   Applying the Markov approximation

The environment can be split into two parts, E_1 from $t_0 \rightarrow t_1$ and E_2 from $t_1 \rightarrow t_2$. In the Markov approximation, the trace over the environment E_1 affects the time evolution only from $t_0 \rightarrow t_1$, and is also invariant with respect to the operators $O_{1,2}$, since they are system operators. Thus, we can compute the trace over E_1 as

$$\langle O_2 O_1\rangle = \text{Tr}_S \text{Tr}_{E_2}\left(O_2 U(t_2,t_1)O_1\rho_s(t_1)U^\dagger(t_2,t_1)\right) \qquad (2.32)$$

$$= \text{Tr}_S\left(O_2\underbrace{\mathcal{D}(t_2,t_1)[O_1\rho_s(t_1)]}_{\rho_{UN}(t_2)}\right) \qquad (2.33)$$

$$= \text{Tr}_S\left(O_2\rho_{UN}(t_2)\right) \qquad (2.34)$$

here $\mathcal{D}(t_2,t_1) = \mathcal{T}\exp\left(\int_{t_1}^{t_2}\mathcal{L}(t)[\rho]dt\right)$ is the superoperator that evolves from time $t_1 \rightarrow t_2$ and the Liouvillian $\mathcal{L}(t)[\rho]$ defines the evolution of the density matrix via $\dot{\rho} = \mathcal{L}[\rho]$. The operator $\rho_{UN}(t_2)$ is not a true density operator, since it is in general unnormalised due to the action of the operator O_1. In the case that the Liouvillian is time independent, the time evolution superoperator is written as

$$\mathcal{D}(t_2,t_1) = e^{\mathcal{L}[\rho](t_2-t_1)} \qquad (2.35)$$

The resulting equation has reduced Eq. 2.31, which includes both system and environment, to the form in Eq. 2.34 which involves only the system's density matrix and operators.

2.2.2   Practical recipe

In practice, it is unnecessary to construct time evolution operators, etc formally. Below, I will describe the practical recipe (see Fig. 2.2.2 for a diagrammatic repre-

sentation of the recipe) that is actually used to compute second order correlation functions of the form

$$G^{(2)}(\tau) = \text{Tr}\left(\hat{a}(t+\tau)\hat{a}(t)\hat{\rho}\hat{a}^\dagger(t)\hat{a}^\dagger(t+\tau)\right) \tag{2.36}$$

0. Solve the equation of motion for ρ.

1. Compute a time evolution from the initial time $\rho(t_0) \to \rho(t)$. Often this step is trivial as either $t_0 = t$ or the density matrix is initially in the steady state and has a trivial time evolution.

2. Act with the operators at t, obtaining a new density matrix $\rho_1(t)$

3. $\rho_1(t)$ is then evolved to the time $t + \tau$.

4. Finally, act with the operators at time $t_2 = t + \tau$

$$G^{(2)}(\tau) = \text{Tr}\left(\hat{a}(t+\tau)\rho_1(t+\tau)\hat{a}^\dagger(t+\tau)\right) \tag{2.37}$$

which is simply matrix multiplication and the computation of the trace.

This recipe (and indeed the quantum regression theorem in general) can be physically thought of as acting with operators at the given times after evolution with the density matrix.

2.2.2.1 Factoring of traces at long times

Suppose we want to compute the trace $\text{Tr}\left(a(t)a(t')\rho_{ss}\right)$, where $\dot{\rho} = \mathcal{L}[\rho]$, which has a steady state solution ρ_{ss}. When t and t' are sufficiently separated that the system has had time to relax back into the steady state, the trace factors since

$$\text{Tr}\left(a(t)\underbrace{a(t')\rho_{ss}}_{=\rho_{\text{UN}}}\right) = \text{Tr}\left(a(t)\rho_{\text{UN}}\right) \tag{2.38}$$

$$= \text{Tr}\left(a(t)A\rho_{ss}\right) \tag{2.39}$$
$$= \text{Tr}\left(a(t)\rho_{ss}\right)A \tag{2.40}$$
$$= \text{Tr}\left(a(t)\rho_{ss}\right)\text{Tr}\left(a(t')\rho_{ss}\right) \tag{2.41}$$

i.e., the product $\rho_{\text{UN}} = a(t')\rho_{ss}$ can be thought of as a new, in general unnormalised, density matrix that will eventually evolve back to $A\rho_{ss}$, where A is the normalisation factor.
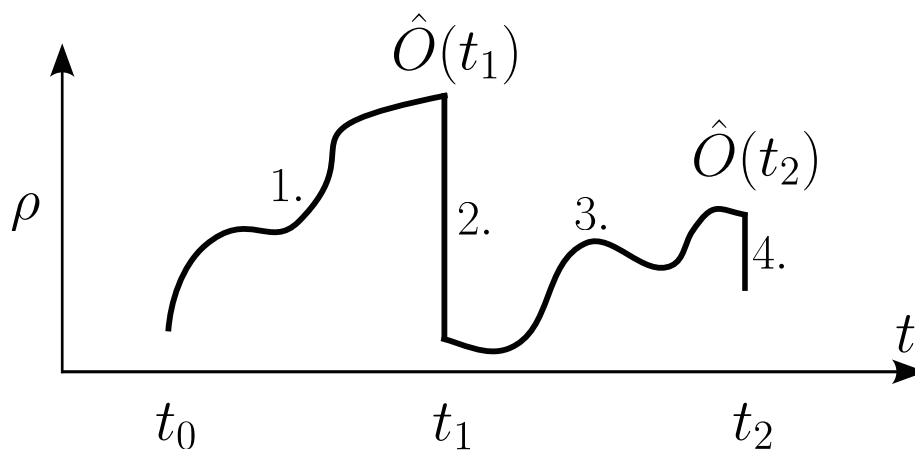
Figure 2.2: **The action of the quantum regression theorem** in each step of the recipe. Here, $t_1 = t$, and $t_2 = t + \tau$. The squiggly lines represent time evolution of the density matrix, whereas the vertical lines represent the discrete change to the quantum state upon the application of the operator $\hat{O}(t)$ at time t. The process of applying the operators can be thought of as a measurement process that extracts information from the state and changes it through measurement back-action.

Chapter 3

Generation of time-energy entanglement via scattering off a quantum dot

This chapter will form the basis of a theory paper accompanying our recent experimental work [1]. I was responsible for developing the theory, with input from Björn Schrinski and Anders Søndberg Sørensen. Shikai Liu, Alexey Tiranov, myself and Peter Lodahl wrote the manuscript with input from the other authors. The operator transformations, quantum dot dynamics, spectral diffusion + time jitter and spectral filtering sections of the appendix that I was responsible for have been reproduced in this thesis with minimal changes. The figure Fig. 3.9 is a modification of several figures that appear in the work [1], originally produced by S.L., with input from myself, A.S.S and P.L.

3.1 Introduction

Quantum entanglement, or the non-local correlations between the states of two or more particles, is a fundamental and counterintuitive phenomenon of quantum mechanics that has far-reaching implications for our understanding of fundamental physics and the development of next-generation technologies. Its importance in quantum computing [40], quantum cryptography [41, 42], and quantum teleportation [43] make it a key focus of ongoing research [44, 45]. The entanglement of light can be achieved by interaction with matter, although the required nonlinearity is typically weak. At low optical power, most materials are in the linear optical regime, exhibiting e.g., reflection and absorption, which can be described by a complex refractive index [7]. With a sufficiently high optical power some materials experience a modification of the index of refraction [8], such that the response to the light becomes power-dependent, i.e., we have a nonlinear response to the number of photons. Implementing nonlinear effects at progressively lower optical power has been the focus of a research effort in optical science for some decades. Devices that display nonlinear interactions at the level of a single photon could improve the performance of classical nonlinear devices [46], enable quantum optical information processing and communication [47] and enable quantum measurement protocols making use of non-classical light fields [48, 49].

In a recent experimental work, [1], we measured time-energy entanglement generated via scattering off a quantum dot embedded in a photonic crystal waveguide. The waveguide works to enhance the radiative coupling of the quantum dot, which is typically otherwise weak, such that it dominates the decoherence processes. The basic mechanism works as follows: low power continuous wave (CW) laser light is shone onto the quantum dot. The coherent interference between the dot field and the waveguide field results in reflection of single photons, but allows two photon states to pass through (see Fig. 3.1). In the ideal case, all two photon states are produced via a single photon exciting the dot, and then a subsequent photon passing through the dot and stimulating the emission of the dot excitation. This produces a pair of entangled photons which then travels through a Franson interferometer [8] that acts as a measurement device quantifying the amount of entanglement. In contrast to a Hong-Ou-Mandel measurement [50], which is local since it requires both photons to be present at the same location in spacetime, Franson measurements can be performed when the two photons are space-like separated [51].

Below, we show in more detail the model used to theoretically describe this experiment and show some surprising physics that can occur when we deviate from the specific parameters needed to fit the model to the experiment.

Photon scattering process
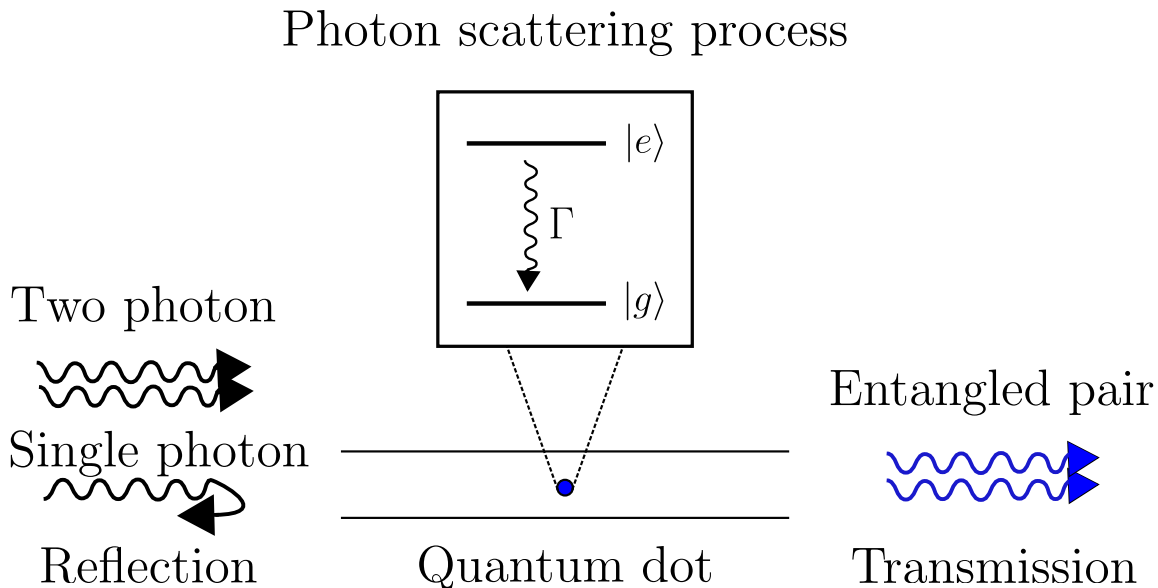
Figure 3.1: **Schematic of the photon scattering process producing a single-photon nonlinearity.** When single photons are incident on the quantum dot in the waveguide, the destructive interference between the incident and transmitted field cause perfect reflection. However, when two photons are incident, the dot saturates, and the second photon causes stimulated emission of the first, resulting in an entangled pair.

3.2 Model – early early, late late

We describe the system with a density matrix, where we keep the regions corresponding to two detector clicks and trace out the remaining regions (see Fig. 3.2), giving a representation in terms of early and late photons. The density matrix in terms of photon numbers is given by (for low power, and thus low photon number) to second order

$$\rho = \rho_0 + \rho_1 + \rho_2, \tag{3.1}$$

where ρ_n is the density matrix corresponding to n photons. We post select on only the two photon density matrix $\rho_2 \approx |\psi\rangle \langle\psi|$ which has two component parts, described below.

19

Figure 3.2: Our density matrix is constructed by tracing out the gray sections, giving a representation in terms of early and late photons $|e\rangle$ and $|\ell\rangle$.

3.2.1 General state

The general state that comes out from the scattering off the dot is

$$|\psi\rangle = g(\beta)(|e\rangle + |\ell\rangle)^2 - f(\beta)(|ee\rangle + |\ell\ell\rangle) \tag{3.2}$$

for some functions g and f that describe how much light is transmitted vs scattered by the dot. $g(\beta)$ is the laser (elastic scattering) component, which should decrease as a function β as less light leaks into the waveguide. $f(\beta)$ is the inelastic scattering function that gives the probability of correlated two photon pairs. Perfect single photon reflection is only achieved if $\beta = \frac{\Gamma}{\gamma_s + \Gamma} = 1$, i.e., if all the light from the dot is emitted into the waveguide. The presence of some γ_s (decay into non-waveguide 'side' modes) allows single photons to leak past the quantum dot, described by the function $g(\beta)$. Hence, for $\beta = 1$, we expect $g(\beta) = 0$. Since scattering off the dot gives a phase of π, and the $|ee\rangle$ and $|\ell\ell\rangle$ photons scatter only **once** vs twice for the $|e\ell\rangle$ or $|\ell e\rangle$ photons, there is a relative phase of π between the two, and thus the minus sign on $f(\beta)$.

When $g(\beta) = 0$ we get the entangled state $|ee\rangle + |\ell\ell\rangle$ and and when $f(\beta) = 0$, we get the separable state $(|e\rangle + |\ell\rangle)^2$. The functions g and f are unknown *a priori*. At some value of β, $g(\beta)$ will have decayed enough for them to cross $f(\beta) = g(\beta)$ and we will obtain the maximally entangled state

$$(|e\rangle + |\ell\rangle)^2 - (|ee\rangle + |\ell\ell\rangle) = |e\ell\rangle + |\ell e\rangle. \tag{3.3}$$

This state picture allows us to treat much of the experimental apparatus (e.g., the interferometers, detectors, etc) as a measurement device, allowing us to treat the dot

20

as the important physical system that prepares the state of interest. Thus, we can (and do) focus on the interaction of the dot and the incident light to theoretically analyse the system. An experimentally inclined reader is encouraged to consult [1] for a more comprehensive description of the experiment itself.

3.2.2 Computation of $g(\beta)$ and $f(\beta)$

First, we will expand the wavefunction (3.2) into one and two photon components.

$$|\psi\rangle = g(\beta)\left(|e\ell\rangle + |\ell e\rangle\right) + \left(g(\beta) - f(\beta)\right)\left(|ee\rangle + |\ell\ell\rangle\right) \tag{3.4}$$

The (unnormalised) transmission coefficient for the scattering can be computed (in the low power limit) with

$$\left[\lim_{n\to 0}\frac{\langle a\rangle}{\sqrt{n}}\right]^2 = \tilde{g} \tag{3.5}$$

where the tilde reflects the fact that the coefficient is as yet unnormalised. We similarly have the coefficient of the two photon component

$$\left[\lim_{n\to 0}\frac{\langle a^2\rangle}{n}\right]^2 = \tilde{g} - \tilde{f} \tag{3.6}$$

To evaluate these expectation values, we solve the dynamics in a density matrix formalism, using the master equation

$$\dot{\rho} = -i\left[H, \rho\right] + \mathcal{L}_{\text{decay}}[\rho] + \mathcal{L}_{\text{deph}}[\rho], \tag{3.7}$$

with Hamiltonian

$$H = \frac{\Omega}{2}\sigma_x + \Delta\sigma_{ee}, \tag{3.8}$$

corresponding to driving of the quantum dot with Rabi frequency Ω and detuning Δ. σ_x is the usual Pauli matrix, and $\sigma_{ij} = |i\rangle\langle j|$. The waveguide field is given by $a = \sqrt{n\Gamma}\mathbb{1} - i\sqrt{\beta\Gamma/2}\sigma_-$, where Γ is the decay rate of the quantum dot, n is the photon number per quantum dot lifetime and $\mathbb{1}$ is the identity matrix. The standard decay and dephasing Liouvillians have been given in general in the previous chapter (2.22) and are discussed in more detail for this specific system in Appendix 3.8.1. Since the

21

state picture breaks down with the presence of dephasing, we ignore its effects here. We obtain

$$\tilde{g}(\beta) = \frac{\Gamma(-\beta\Gamma + \Gamma + 2i\Delta)^2}{(\Gamma + 2i\Delta)^2} \tag{3.9}$$

$$\tilde{f}(\beta) - \tilde{g}(\beta) = -\frac{\Gamma^2(-2\beta\Gamma + \Gamma + 2i\Delta)^2}{(\Gamma + 2i\Delta)^2}, \tag{3.10}$$

where expectation values have been evaluated with respect to the steady state solution to Eq. (3.7). When on resonance, the coefficients are both real, and we obtain the expressions

$$\tilde{g}(\beta) = (\beta - 1)^2\Gamma \tag{3.11}$$

$$\tilde{f}(\beta) - \tilde{g}(\beta) = -(1 - 2\beta)^2\Gamma^2 \tag{3.12}$$

By ensuring that the state (3.2) is properly normalised, i.e., by dividing by $\mathcal{N} = 2\tilde{g}^2 + 2(\tilde{g} - \tilde{f})^2$, we can also compute the normalised coefficients $f(\beta)$ and $g(\beta)$. We have plotted these coefficients in Fig. 3.3b). As we predicted with our heuristic arguments, the function $\tilde{g}$ crosses $\tilde{f}$. As it happens, the value at the crossing is exactly $\beta = \frac{1}{2}$. That is, the point at which we expect to obtain the entangled state $|e\ell\rangle + |\ell e\rangle$ is at $\beta = 1/2$.

In Fig. 3.4, we additionally plot the normalisation constant, which is proportional to the success rate $\mathcal{N}(\beta)$. Interestingly, $\mathcal{N}$ does not have an extremal value at $\beta = 1/2$, and the rate is higher for $\beta = 1$.
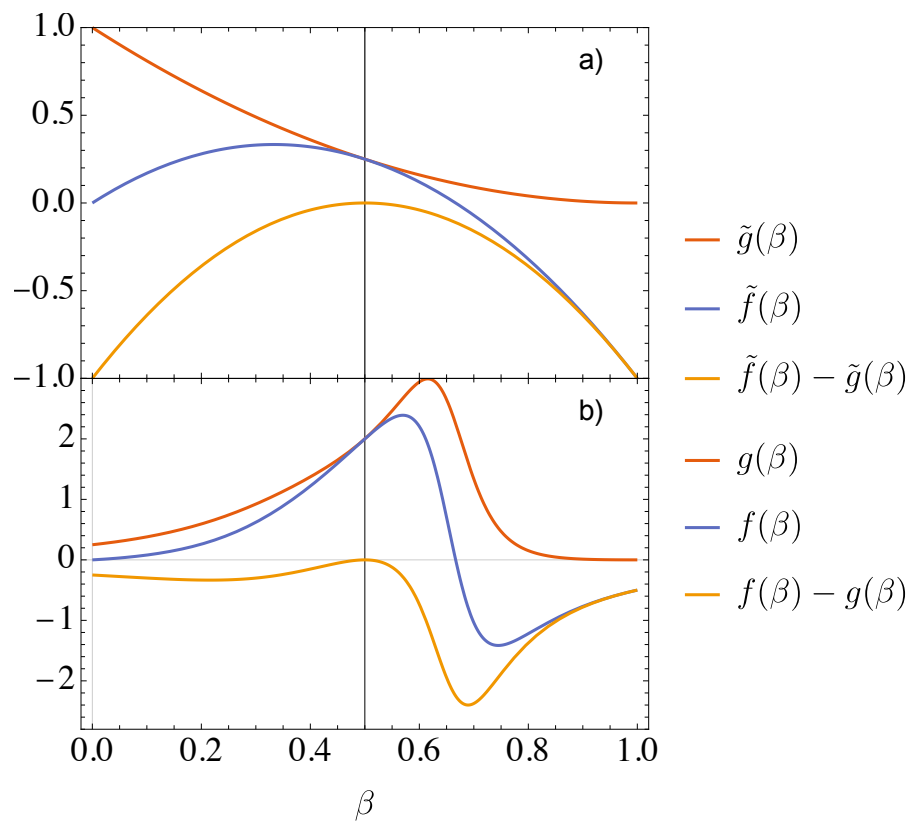
Figure 3.3: **The coefficients of the general scattering wavefunction** $|\psi\rangle$ given by Eq. (3.2). In panel **a)** we show the unnormalised coefficients, and in **b)** we show the normalised ones. As predicted by our heuristic arguments, the curves $f(\beta)$ and $g(\beta)$ cross. The vertical black line is placed to show this crossing point.

23
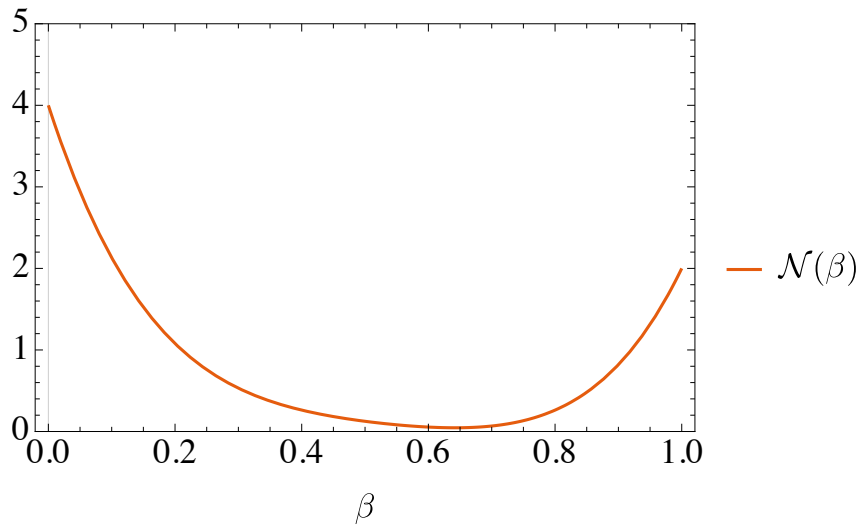
Figure 3.4: **The normalisation constant $\mathcal{N}(\beta)$.**

3.3 Computation of second order correlation function (transmission in pairs)

As mentioned earlier, the basic mechanism of action for our protocol is the reflection of single photons and the transmission of photon pairs. This mechanism can be measured quantitatively using the second order correlation function $g^{(2)}(\tau)$, where we expect a bunching[1] effect at $\tau = 0$ due to the enhanced probability of detecting photon pairs produced at the same time. Note that in principle the photon scattering can produce entanglement in frequency due to energy exchange between photon pairs, however since our detection window is very narrow, this entanglement is erased. Here we consider imperfections such as laser leaking into the waveguide (corresponding to non-unity β), as well as dephasing, which destroys the coherence between the dot field and waveguide field. Both of these effects will reduce the relative probability that the two collected photons are produced by the desired excitation and spontaneous emission process, thus suppressing the height of the $g^{(2)}(0)$ peak.

3.3.1 Second order correlation function before the interferometer

Since we interpret the interferometer as functioning as a measurement device, it is of interest to understand the second order correlation function before it passes through the interferometer. We would like to know $g^{(2)}(0)$, as a function of the imperfections γ_d and β. This calculation is relatively straightforward (see Appendix 3.8.1) using quantum regression theorem, as we only need to calculate the steady state density matrix, which can be done analytically. Since we are interested in the correlation at zero time delay (i.e., $\tau = 0$), no time evolution step is necessary.

Because we are interested in the photon nonlinearity produced by the scattering off the quantum dot, we compute the height of the $g^{(2)}(0)$ peak using the Quantum Regression Theorem (see 2.2). A large anti-bunching peak is a signature of the entangled state $|ee\rangle + |\ell\ell\rangle$ which will produce a strong violation of the Clauser-Horne-Shimony-Holt (CHSH) inequality.

$$g^{(2)}(0) = \frac{(\Gamma + 4\beta\Gamma n + \gamma_d)(\Gamma + 4\beta\Gamma(\beta + n - 1) + \gamma_d)}{(\Gamma + \beta\Gamma(\beta + 4n - 2) + \gamma_d)^2} \tag{3.13}$$

---

[1]By bunching, we refer to a second order correlation function $g^{(2)} > 1$, which characterises two photon detection events that have occurred at a higher rate than expected compared with uncorrelated light.

which, in the limit of low power is

$$g^{(2)}(0) = \frac{(\Gamma + \gamma_d)(4(\beta - 1)\beta\Gamma + \Gamma + \gamma_d)}{((\beta - 1)^2\Gamma + \gamma_d)^2}$$

(3.14)

Expanding around $\gamma_d = 0$ we have

$$g^{(2)}(0) = \frac{(1 - 2\beta)^2}{(\beta - 1)^4} + \frac{2\beta^2(2(\beta - 3)\beta + 3)\gamma_d}{(\beta - 1)^6\Gamma} + O\left(\gamma_d^2\right),$$

(3.15)

and in the limit of perfect coupling, we have

$$g^{(2)}(0) = \frac{(\Gamma + \gamma_d)^2}{\gamma_d^2} + \frac{4(\beta - 1)\Gamma(\Gamma + \gamma_d)}{\gamma_d^2} + O\left((\beta - 1)^2\right)$$

(3.16)

Eq. (3.15) clarifies the plot shown in Fig. 3.5. At $\gamma_d = 0$, we have a $g^{(2)}(0)$ that diverges at $\beta = 1$, representing the bunching of the $|ee\rangle + |\ell\ell\rangle$ state. At $\beta = 1/2$, $g^{(2)}(0) = 0$, and corresponds to the antibunching $|e\ell\rangle + |\ell e\rangle$ state which is composed of single photons.
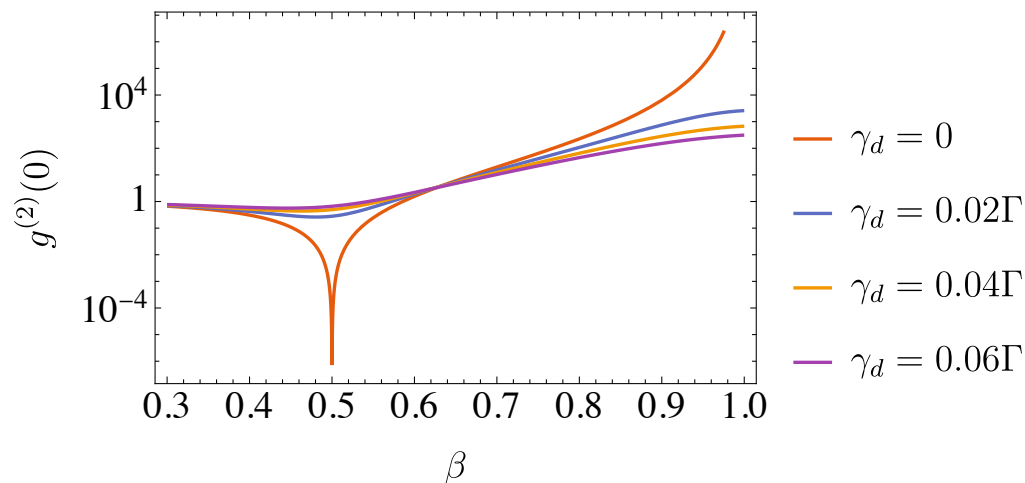
Figure 3.5: $g^{(2)}$ **peak as a function of β for various values of γ_d.** At $\gamma_d = 0$, we are able to use the wavefunction picture described by (3.2). Here we find that at $\beta = 1/2$, when we have only single photon states $|e\ell\rangle + |\ell e\rangle$, we see anti-bunching, as expected. At $\beta = 1$, we see strong bunching, since we expect to recover the two photon entangled state $|ee\rangle + |\ell\ell\rangle$. The introduction of dephasing produces a reduction in the size of both the bunching peak and anti-bunching dip due to the loss of coherence between the waveguide and scattering modes.
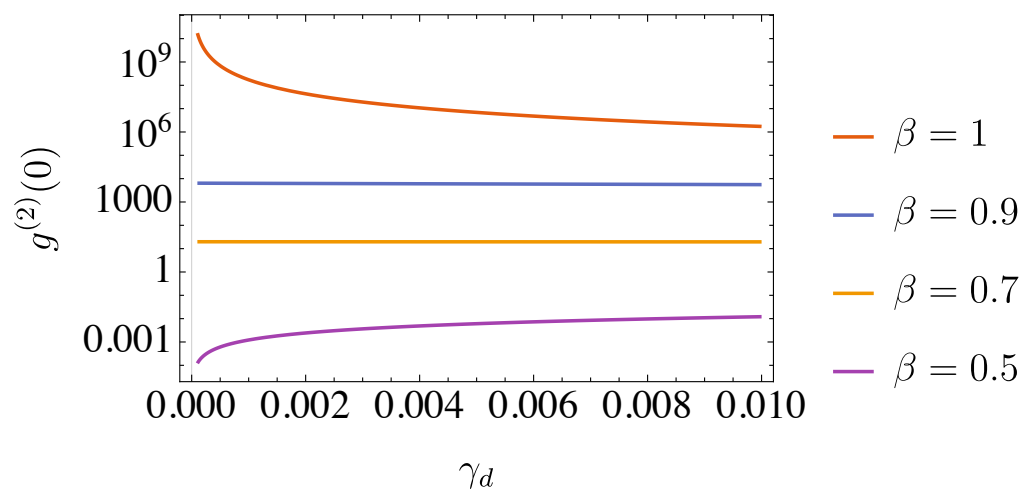
Figure 3.6: $g^{(2)}(0)$ **as a function of** γ_d **for various values of** β. In the limit of vanishing dephasing $\gamma_d = 0$, we return to our expected strong bunching at $\beta = 1$ and antibunching at $\beta = 1/2$. As dephasing is increased, we have more leakage into the waveguide, and a corresponding loss of coherence, reducing the bunching (anti-bunching).

3.4 Bell (standard basis and optimised basis)

To quantify the amount of entanglement, we compute quantum correlations

$$E(\phi_a, \phi_b) = \frac{G^{(2)}(\phi_a, \phi_b) + G^{(2)}(\phi_{a\perp}, \phi_{b\perp}) - G^{(2)}(\phi_a, \phi_{b\perp}) - G^{(2)}(\phi_{a\perp}, \phi_b)}{G^{(2)}(\phi_a, \phi_b) + G^{(2)}(\phi_{a\perp}, \phi_{b\perp}) + G^{(2)}(\phi_a, \phi_{b\perp}) + G^{(2)}(\phi_{a\perp}, \phi_b)} \quad (3.17)$$

after the interferometer, using the central Franson interference peak (see Appendix 3.8.2 for details), such that we can compute the CHSH parameter

$$S = |E(\phi_a, \phi_b) + E(\phi_a, \phi_{b'}) - E(\phi_{a'}, \phi_b) + E(\phi_{a'}, \phi_{b'})| \quad (3.18)$$

where $\phi_{a\perp}$ and $\phi_{a'}$ represent the orthogonal (differing by π) and diagonal phase (differing by $\pi/2$) basis relative to ϕ_a. This is the standard basis for the CHSH inequality. However, in performing this measurement, we have the freedom to alter our basis, and in particular to optimise it to produce the maximum violation. Below, we will show that for $\beta \sim 1$, the standard basis is optimal, but for other values of β, this is not the case. We will further show that we can saturate (or violate) S for any value of β, and indeed violate it for almost all values of β.

We can compute an expression for the low power limit with β being the only imperfection. In this case, we have

$$\lim_{n \to 0} \frac{G^{(2)}(\phi_1, \phi_2, \beta)}{\Omega^4} = \frac{\left(\beta^2 \sin\left(\frac{\phi_1}{2}\right) \sin\left(\frac{\phi_2}{2}\right) + ((\beta - 4)\beta + 2) \cos\left(\frac{\phi_1}{2}\right) \cos\left(\frac{\phi_2}{2}\right)\right)^2}{\beta^2 \Gamma^2}$$

$$(3.19)$$

where we recall that $\Omega^2 = 2\beta\Gamma^2 n$, and n is the photon number per lifetime. Using this $G^{(2)}$ (and noting that the factor $\beta^2\Gamma^2$ is divided out) we compute an expression for S as a function of general phase angles $\phi_a, \phi'_a, \phi_b, \phi'_b$

$$S = \frac{((\beta - 4)\beta + 2)\beta^2 \left(\sin(\phi_b)(\sin(\phi'_a) + \sin(\phi_a)) + (\sin(\phi_a) - \sin(\phi'_a))\sin(\phi'_b)\right)}{\beta(\beta((\beta - 4)\beta + 10) - 8) + 2}$$

$$(3.20)$$

$$+ \cos(\phi'_a)(\cos(\phi_b) - \cos(\phi'_b)) + \cos(\phi_a)(\cos(\phi'_b) + \cos(\phi_b)).$$

If $\phi'_a = \phi_a + \pi/2$ and $\phi'_b = -\phi_b$, this expression reduces to

$$S = 2\cos(\phi_a)\left(\frac{((\beta - 4)\beta + 2)\beta^2 \sin(\phi_b)}{\beta(\beta((\beta - 4)\beta + 10) - 8) + 2} + \cos(\phi_b)\right) \quad (3.21)$$

We can fix $\phi_a = 0$ without loss of generality and find the optimal S by setting

$$\phi_b = \tan^{-1}\left(\frac{\beta^2\left(\beta^2 - 4\beta + 2\right)}{\beta^4 - 4\beta^3 + 10\beta^2 - 8\beta + 2}\right), \tag{3.22}$$

giving an expression for the optimal S in terms of β

$$S_{\text{opt}} = \frac{2\sqrt{2}\sqrt{\beta^8 - 8\beta^7 + 28\beta^6 - 56\beta^5 + 86\beta^4 - 88\beta^3 + 52\beta^2 - 16\beta + 2}}{\beta^4 - 4\beta^3 + 10\beta^2 - 8\beta + 2} \tag{3.23}$$

Using the standard basis $\phi_a = 0, \phi_a' = \pi/2, \phi_b = -\pi/4, \phi_{b'} = \pi/4$ we obtain the expression

$$S = \frac{2\sqrt{2}(1 - 2\beta)^2}{\beta(\beta((\beta - 4)\beta + 10) - 8) + 2} \tag{3.24}$$

Expanding about $\beta = 1$, we see

$$S_{\text{opt}} \approx 2\sqrt{2}\left(1 - (\beta - 1)^4\right) + \mathcal{O}\left((\beta - 1)^5\right) \tag{3.25}$$

and similarly, expanding about $\beta = 1/2$, we see

$$S_{\text{opt}} \approx 2\sqrt{2} - 128\sqrt{2}\left(\beta - \frac{1}{2}\right)^2 + \mathcal{O}\left(\left(\beta - \frac{1}{2}\right)^3\right) \tag{3.26}$$

The optimal S is obtained both at $\beta = 1$ and $\beta = 1/2$, however, the series expansions about $\beta = 1$ has a leading order term at 4th order, whereas the expansion at $\beta = 1/2$ has a second order term. A similar pattern is observed if we expand the optimal phase angle ϕ_b

$$\phi_b \approx -\frac{\pi}{4} + (\beta - 1)^4 + \mathcal{O}\left((\beta - 1)^5\right) \tag{3.27}$$

$$\phi_b \approx \frac{\pi}{4} - 64\left(\beta - \frac{1}{2}\right)^2 + \mathcal{O}\left(\left(\beta - \frac{1}{2}\right)^3\right) \tag{3.28}$$

Thus, although in principle an optimal violation can occur at both these values, $\beta = 1$ is significantly more robust to variations in β. In terms of the coefficients of (3.2), computed above, the maximum violations correspond to $g(1) = 0, f(1) = 1$, where the resulting pure state is $|\psi\rangle = |ee\rangle + |\ell\ell\rangle$ and $g(1/2) = f(1/2)$, where the pure state is $|e\ell\rangle + |\ell e\rangle$. Note that $\beta = 1/2$ and $\beta = 1$ are universally the points at which we can reach maximum S, i.e., this is still true if we have complex scattering coefficients due to some detuning Δ. In Fig. 3.8, we show the optimal S depends on Δ and β.
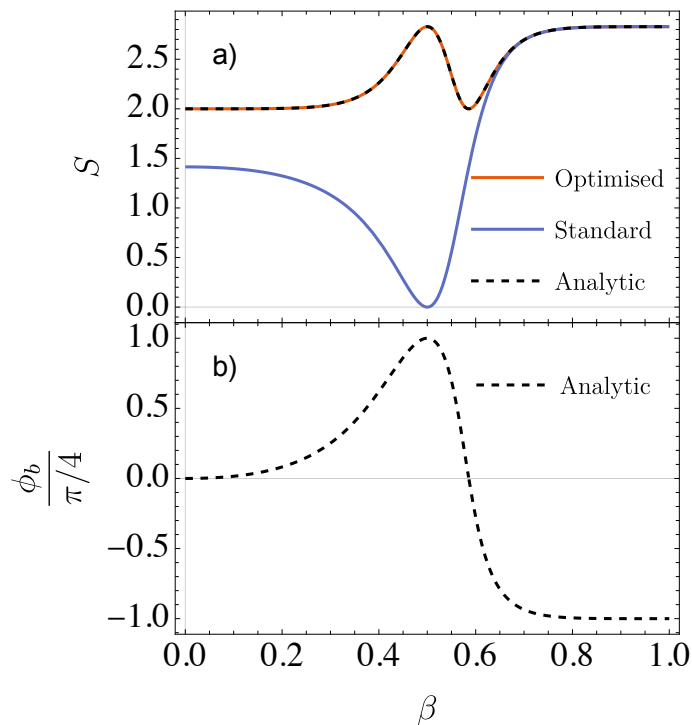
Figure 3.7: **CHSH parameter S as a function of β.** In panel **a)**, we plot the numerically optimised (orange, solid) as well as the analytic expression (3.22) (black, dashed). We also plot S with the standard basis (blue, solid). The standard basis is optimal for large values of β, but is poor for small values. The optimal basis has $S \geq 2$ for all β. In particular at $\beta = 1/2$, we can see the signature of the maximally entangled state $|e\ell\rangle + |\ell e\rangle$. **b)** The optimal phase angle ϕ_b (3.22) as a function of β. The analytic phase agrees exactly with the one found with numerical optimisation.
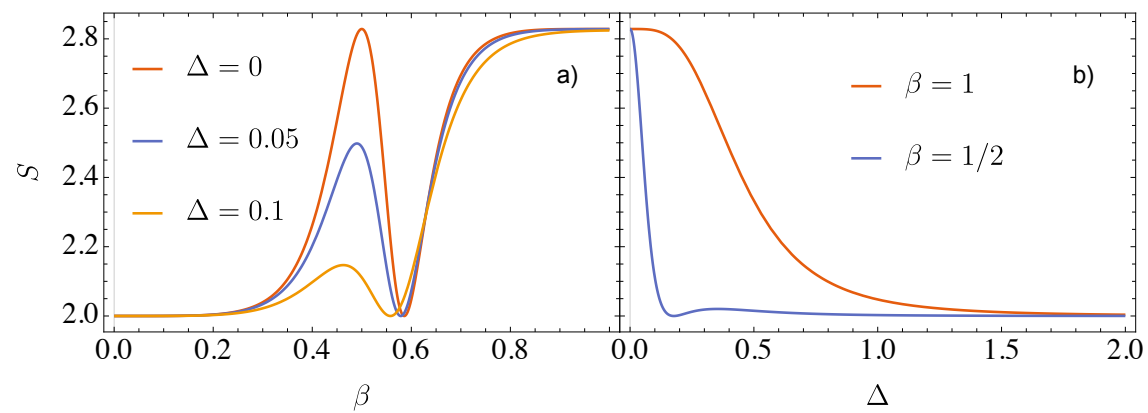
Figure 3.8: **Optimised CHSH parameter S as a function of Δ and β. a)** CHSH parameter as a function of β for selected values of the detuning Δ. We can see that the location of the maxima remain the same, regardless of the value of Δ. **b)** S as a function of Δ for the peak values $\beta = 1$ and $\beta = 1/2$. The peak at $\beta = 1$ remains high for a much larger range of detunings than the peak at $\beta = 1/2$, reflecting again the robustness to variations of the $\beta = 1$ peak in comparison to the $\beta = 1/2$ peak.
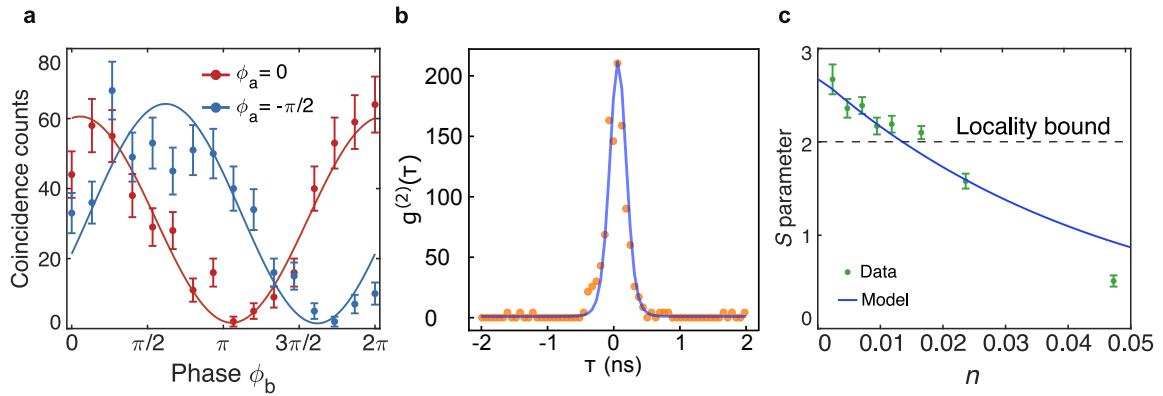
Figure 3.9: **Comparison between experimental data [1] and theory. a.** The coincidence counts as the phase ϕ_b is swept, for $\phi_a = 0$ (red) and $\phi_a = -\pi/2$ (blue). The points are the data from the experiment [1], and the solid lines are the theoretical model given by Eq. (3.19). **b.** The second order correlation function $g^{(2)}(\tau)$ for the filtered data (orange points) along with the theory (blue line). We obtain a bunching peak with a height > 200, showing strong evidence of a single-photon linearity. **c.** The CHSH parameter as a function of photon number per wavelength n. In the low power limit, we observe a pronounced violation of the CHSH Bell inequality $S = 2.67(16) > 2$ by more than four standard deviations. In **b** and **c**, we use the full model with spectral diffusion and time jitter included.

3.5 Filtering and experimental imperfections

3.5.1 Spectral diffusion and detector time jitter

Below, we consider two important effects relevant to modelling experimental imperfections of QD spectral diffusion and time jitter of the single-photon detector. Spectral diffusion corresponds to a slow (compared to the QD lifetime) frequency drift of the QD that can be modelled as a normal distribution of QD detunings:

$$P_{\mathrm{SD}}(\Delta, \sigma_{\mathrm{SD}}) = \frac{1}{\sqrt{2\pi\sigma_{\mathrm{SD}}^2}} \exp\left(-\frac{\Delta^2}{2\sigma_{\mathrm{SD}}^2}\right), \qquad (3.29)$$

where σ_{SD} is the standard deviation of the spectral diffusion. We compute the effect of spectral diffusion on $G^{(2)}$ by taking the integral over all possible detunings

$$G^{(2)}(\sigma_{\mathrm{SD}}, t, \Gamma, n, \beta, \gamma_d) = \int P_{\mathrm{SD}}(\Delta, \sigma_{\mathrm{SD}}) G^{(2)}(\Delta, t, \Gamma, n, \beta, \gamma_d) d\Delta. \qquad (3.30)$$

Similarly, we consider the instrument response function (IRF) due to the time jitter of the single-photon detector, which is modelled as a Gaussian distribution:

$$P_{\mathrm{IRF}}(t, \sigma_{\mathrm{IRF}}) = \frac{1}{\sqrt{2\pi\sigma_{\mathrm{IRF}}^2}} \exp\left(-\frac{t^2}{2\sigma_{\mathrm{IRF}}^2}\right), \qquad (3.31)$$

that influences the correlation function $G^{(2)}$ according to

$$G^{(2)}(\sigma_{\mathrm{SD}}, \tau, \sigma_{\mathrm{IRF}}, \Gamma, n, \beta, \gamma_d) = \int P_{\mathrm{IRF}}(t - \tau, \sigma_{\mathrm{IRF}}) G^{(2)}(\sigma_{\mathrm{SD}}, t, \Gamma, n, \beta, \gamma_d) dt \qquad (3.32)$$
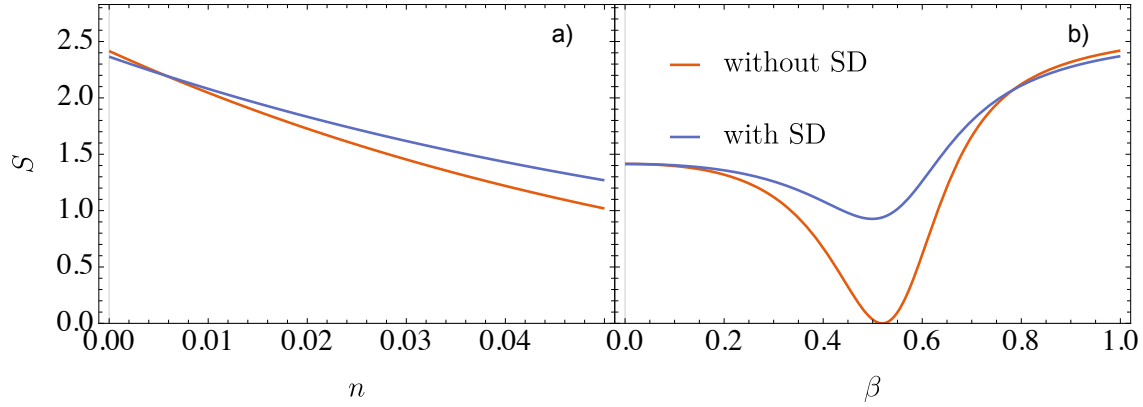
Figure 3.10: **The effect of spectral diffusion on the CHSH parameter** S
All plots use the standard basis. **a)** S as a function of the photon number per
lifetime n. We set an experimentally realistic $\beta = 0.92$. At very low n the spectral
diffusion degrades the entanglement quality, whilst at higher n it is actually slightly
improved. **b)** S as a function of β. We set $n = 0.0001$ and find that again in this low
power limit, the spectral diffusion degrades the entanglement. Since we are using
the standard basis here, S increases at $\beta = 1/2$. Using an optimised basis, we would
see a suppression of S at $\beta = 1/2$, similar to what we observed in Fig. 3.8.

3.6 Filtering and the effects of dephasing

Due to imperfections not present in the perfect world of theoretical physics, it was
necessary to introduce a spectral filter in the experiment. In the experiment, we have
some laser leakage into the waveguide, coming from a combination of non-unity β,
spectral diffusion (discussed below), and dephasing. In [1], we argue that the effect
of the filter can be effectively captured by re-fitting the spectral diffusion and the
coupling rate β, whilst keeping the dephasing rate γ_d fixed.

This can be justified by considering the illustrative spectra of the outgoing light
presented in Fig. 3.11. As seen in the figure, the outgoing spectrum consists of a
narrow elastic peak and a broad inelastic emission. The narrow peak (see Eq. (3.38))
comes from laser leakage and vanishes in the ideal limit of vanishing imperfections
($\beta = 1$, $\gamma_d = \sigma_{\text{SD}} = 0$ and $n \to 0$). Under non-perfect conditions, the central narrow
peak appears to quadratic order in the imperfection parameters ($1 - \beta$, $\sigma_{\text{SD}}/\Gamma$, n and
γ_d/Γ) or through products of them. Since for typical parameters, n and γ_d/Γ (~ 0.01)
are much smaller than $1 - \beta$ and $\sigma_{\text{SD}}/\Gamma$ (~ 0.1), the latter have a much stronger

35

influence on the coherent peak. In contrast to the narrow peak, the pure dephasing induces (via the quantum jump operator $c = \sqrt{\gamma_d/2}\sigma_z$) a spectrally broad inelastic emission linear in γ_d/Γ (with width $\sim \Gamma + \gamma_d$) from the QD's excited state [52, 53] and so does inelastic multi-photon scattering controlled by n. Upon application of the spectral filter, the narrow peak from the laser light is strongly affected, but the broad peak produced by pure dephasing and multi-photon scattering is largely unchanged.

The decoherence caused by dephasing can be thought of in two ways. Firstly, as a measurement by a photon (a mechanical excitation of the waveguide) that prepares the system in the excited state. The loss of coherence is due to the phase information being carried away by the phonon, which is not captured in our model. We can alternatively think of dephasing as an uncorrelated (white) noise process that shakes the energy levels of the emitter rapidly in time. This destroys phase coherence by producing a rapidly oscillating, random phase. The average of this process produces an exponential decay in the off diagonal elements of the density matrix. Spectral diffusion similarly produces decoherence by oscillations of the energy levels, but this noise is correlated and occurs at much slower time-scales, so its effects appear primarily in the spectrum at small frequencies around $\omega = 0$. The influence of the filter can thus be effectively captured by adjusting β and the spectral diffusion σ_{SD} (see Fig. 3.11).

Below, we show how to compute the spectrum used to justify this conclusion and discuss the justification with the help of our analytics.

3.6.1 Computation of spectrum

The goal is to find an expression for $\langle a^\dagger(\omega')a(\omega)\rangle /n$, the emission spectrum for the system normalised by the photon number per lifetime n. This is the Fourier transform of $\langle a^\dagger(t+\tau)a(t)\rangle /n$. Since we compute the time dynamics (i.e., we propagate $a\rho$ from $t \to t+\tau$) with a matrix exponential $e^{\mathbf{M}|t|}$ via Eq. (3.49), we can compute the Fourier transform at this step. We write

$$\frac{1}{\sqrt{2\pi}} \int_{-\infty}^{\infty} e^{\boldsymbol{M}|t|}e^{i\omega t}dt = \frac{1}{\sqrt{2\pi}} \int_{0}^{\infty} e^{\mathbf{M}t+i\omega t}dt + \frac{1}{\sqrt{2\pi}} \int_{-\infty}^{0} e^{\mathbf{M}t+i\omega t}dt \qquad (3.33)$$

$$= \frac{1}{\sqrt{2\pi}} \left[(-\mathbf{M} + i\omega)^{-1} - (\mathbf{M} + i\omega)^{-1}\right] \qquad (3.34)$$

where $(\cdot)^{-1}$ is the matrix inverse and $i\omega$ is understood to be multiplied by the identity matrix with the same dimension as $\mathbf{M}$. We can now compute

$$\mathbf{a}\boldsymbol{\rho}(\omega) = \frac{1}{\sqrt{2\pi}} \left[(-\mathbf{M} + i\omega)^{-1} - (\mathbf{M} + i\omega)^{-1}\right] \mathbf{a}\boldsymbol{\rho_{ss}} \qquad (3.35)$$
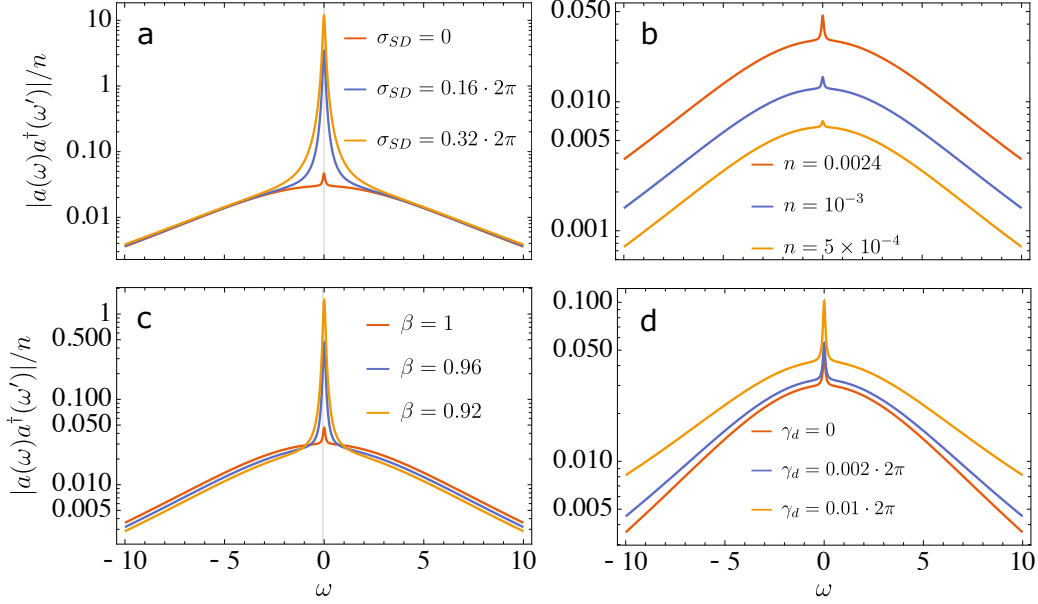
Figure 3.11: **Illustrative spectra $\langle a(\omega)a^\dagger(\omega')\rangle$ with various imperfections.** Except when otherwise stated, we use the values $n = 0.0024$, $\beta = 1$, $\sigma_{SD} = 0$ and $\gamma_d = 0$. **(a)** Spectra where the spectral diffusion σ_{SD} is gradually increased. The narrow peak at $\omega = 0$ is strongly affected, whilst the broad peak remains unchanged. **(b)** Spectra for various values of n. Both the central narrow peak and the broader peak are scaled up with increasing n. **(c)** Spectra with decreasing β. As with spectral diffusion, the dominant contribution is to increase the height of the central narrow peak, whilst the broader peak is relatively unchanged. **(d)** Spectra with gradually increasing dephasing rate γ_d. The dominant effect is to increase and broaden the wide peak. The central narrow peak remains relatively unaffected. Note that in all plots, the width of the central peak has been scaled by a factor of 100 whilst conserving the total area so that the effect can be seen more clearly.

where the boldface characters, e.g., $\boldsymbol{\rho}$ should be understood as the vectorised version of the same operator ρ. In this case, ρ is a 2×2 density matrix, but $\boldsymbol{\rho}$ is a vector with length 4. We obtain, in the low power limit,

$$\lim_{n \to 0} \frac{\mathrm{Tr}(a\rho(\omega)a^\dagger)}{n} = \frac{4\sqrt{\frac{2}{\pi}}\beta^2\Gamma^2\gamma_d}{(\Gamma + 2i\Delta + 2\gamma_d)(4\omega^2 + (\Gamma - 2i\Delta + 2\gamma_d)^2)}, \tag{3.36}$$

where now the unbolded operator $a\rho(\omega)$ represents the reshaping of the vector $\boldsymbol{a}\boldsymbol{\rho}(\omega)$ back into density matrix form. This method computes the broad part of the spectrum

37

dominated by dephasing but misses the constant term at $\omega = 0$ that produces a narrow peak with the width of the laser light.

This constant value is the value $\langle a^\dagger a \rangle$ at $t \to \infty$. Such expectation values factor at long times (see 2.2.2.1), so we may compute

$$\lim_{t \to \infty} \frac{\text{Tr}(a\rho(t)a^\dagger)}{n} = \frac{1}{n} \langle a \rangle \langle a^\dagger \rangle \tag{3.37}$$

$$= \frac{\Gamma\left(16\Delta^4 + 4\Delta^2\left(\Gamma^2(\beta(\beta+8n-2)+2)+4\Gamma\gamma_d(\beta(4n-1)+2)+8\gamma_d^2\right)+(\Gamma+2\gamma_d)^2(\Gamma+\beta\Gamma(4n-1)+2\gamma_d)^2\right)}{\left(4\Delta^2+(\Gamma+2\gamma_d)(\Gamma+4\beta\Gamma n+2\gamma_d)\right)^2} \tag{3.38}$$

To incorporate this narrow peak into the spectrum, we multiply by a Lorentzian with area 1 and with $\gamma = \Gamma_{laser}$, i.e., the full spectrum is given by

$$\frac{\langle a^\dagger(\omega)a(\omega)\rangle}{n} = \frac{\text{Tr}(a\rho(\omega)a^\dagger)}{n} + \frac{1}{n} \langle a \rangle \langle a^\dagger \rangle \underbrace{\frac{1}{\pi}\left(\frac{\Gamma_{laser}}{\omega^2 + \Gamma_{laser}^2}\right)}_{\text{normalised Lorenzian}} \tag{3.39}$$

Taking the limit of the narrow peak $n \to 0$, we obtain

$$\lim_{n \to 0} \frac{1}{n} \langle a \rangle \langle a^\dagger \rangle = \frac{\Gamma\left(4\Delta^2 + ((\beta-1)\Gamma - 2\gamma_d)^2\right)}{4\Delta^2 + (\Gamma + 2\gamma_d)^2} \tag{3.40}$$

Since $\gamma_d/\Gamma \ll 1$, we can see that the term $(\beta-1)\Gamma - 2\gamma_d = \Gamma\left(\beta - 1 - \frac{2\gamma_d}{\Gamma}\right) \approx (\beta-1)\Gamma$, i.e., the dephasing plays a minimal role in the narrow peak and will not be strongly influenced by the spectral filtering.

3.7 Conclusions and outlook

We have analysed the scattering off a quantum dot in order to investigate the single-photon nonlinearity present in this system. We made use of this nonlinearity to experimentally generate time-energy entanglement, and measured this entanglement by violating a CHSH inequality. We theoretically investigated the underlying physics with a simplified model in the state picture, where we were able to compute the one- and two-photon scattering components explicitly using the full solution to the system's master equation. We showed that *reducing* the coupling to the waveguide may enhance the measured CHSH violation, since there is another perfectly entangled state that appears when $\beta = 1/2$, alongside the state that appears at $\beta = 1$. We validated these findings by using the full model to compute the CHSH S parameter, and found that the standard basis only produces a violation for $\beta = 1$. We found

an analytic formula for the optimal basis, and showed that it agrees with numerical optimisation for all values of β. We thus found that the CHSH inequality can be at least saturated for all values of β, and is violated for almost all values. We further explored the origin of this violation by computing the second order correlation function $g^{(2)}(0)$. When dephasing is zero, we can see strong signatures of anti-bunching (when $\beta = 1/2$ and we have the single photon entangled state) and bunching (when $\beta = 1$ and we have the two-photon entangled state). We investigated the effects of spectral diffusion and detector time jitter, as these are two imperfections that are of crucial importance to modelling the experiment. By computing the emission spectrum $\langle a^\dagger(\omega')a(\omega)\rangle$, we were able to reason that the spectral filter used in the experiment would affect the effective spectral diffusion and coupling rate β, whilst keeping the dephasing rate fixed. We do not produce a full model of the filter, only try to reproduce the effects in our fitting. A possible theoretical step that would give some interesting insights is to filter the spectrum 'by hand' through adding some transformation $T(\omega)$ that would simulate the filter by suppressing the central peak. It would then in principle be possible to fit a new β analytically.

3.8   Appendix

3.8.1   Quantum dot dynamics

The QD is described by the Lindblad master equation for the system which reads $(\hbar = 1)$

$$\dot{\rho} = -i\left[H, \rho\right] + \mathcal{L}_{\text{decay}}[\rho] + \mathcal{L}_{\text{deph}}[\rho]. \tag{3.41}$$

Here, the unitary part of the time evolution is given by the Hamiltonian

$$H = \frac{\Omega}{2}\sigma_x + \Delta\sigma_{ee}, \tag{3.42}$$

which accounts for the driving of the QD with Rabi frequency Ω and detuning Δ. The Rabi frequency $\Omega = \Omega(t)$ may in general be time-dependent, σ_x is the usual Pauli matrix and $\sigma_{ij} = |i\rangle\langle j|$. The decay Liouvillian

$$\mathcal{L}_{\text{decay}}[\rho] = \Gamma\left[\sigma_-\rho\sigma_+ - \frac{1}{2}\left\{\sigma_+\sigma_-, \rho\right\}\right] \tag{3.43}$$

models the total decay of the emitter $\Gamma = \gamma + \gamma_s$ into both the waveguide mode γ and other modes γ_s (referred to as side modes). We additionally include a Liouvillian modelling dephasing

$$\mathcal{L}_{\text{deph}}[\rho] = \frac{\gamma_d}{2} \left[\sigma_z \rho \sigma_z - \rho \right], \tag{3.44}$$

where γ_d is the dephasing rate and σ_z, σ_+ and σ_- are the Pauli operators. The ratio of the waveguide decay to the total decay defines the β-factor $\beta = \frac{\gamma}{\Gamma} = \frac{\gamma}{\gamma + \gamma_s}$. The transmitted field operator entering the $G^{(2)}$ calculations is $a = a_{in}\mathrm{I} - \sqrt{\beta\Gamma/2}\sigma_{ge}$, where the input field a_{in} is a coherent state of amplitude $\alpha(t)$, and mean photon flux $|\alpha(t)|^2$. The coherent field is related to the Rabi frequency by $\Omega/2 = \sqrt{\beta\Gamma/2}\alpha(t)$ and thus the mean photon number per lifetime is $n = \frac{|\alpha|^2}{\Gamma} = \frac{\Omega^2}{2\beta\Gamma^2}$. In matrix form, the master equation reads

$$\dot{\rho} = \begin{pmatrix} -\Gamma\rho_{\text{ee}} + \frac{1}{2}i\Omega(\rho_{\text{eg}} - \rho_{\text{ge}}) & \frac{1}{2}i\Omega(\rho_{\text{ee}} - \rho_{\text{gg}}) - \frac{1}{2}\rho_{\text{eg}}(\Gamma + 2i\Delta + 2\gamma_d) \\ -\frac{1}{2}\rho_{\text{ge}}(\Gamma - 2i\Delta + 2\gamma_d) - \frac{1}{2}i\Omega(\rho_{\text{ee}} - \rho_{\text{gg}}) & \Gamma\rho_{\text{ee}} - \frac{1}{2}i\Omega(\rho_{\text{eg}} - \rho_{\text{ge}}) \end{pmatrix} \tag{3.45}$$

The QD is continuously driven by a laser field, eventually reaching an equilibrium state described by the steady state density matrix ρ_{ss}. To find ρ_{ss}, we write the master equation in the form

$$\dot{\boldsymbol{\rho}} = \mathbf{M}\boldsymbol{\rho}, \tag{3.46}$$

where

$$\mathbf{M} = \begin{pmatrix} -\Gamma & \frac{i\Omega}{2} & -\frac{i\Omega}{2} & 0 \\ \frac{i\Omega}{2} & -\frac{\Gamma}{2} - i\Delta - \gamma_d & 0 & -\frac{i\Omega}{2} \\ -\frac{i\Omega}{2} & 0 & -\frac{\Gamma}{2} + i\Delta - \gamma_d & \frac{i\Omega}{2} \\ \Gamma & -\frac{i\Omega}{2} & \frac{i\Omega}{2} & 0 \end{pmatrix} \tag{3.47}$$

is the coefficient matrix and

$$\boldsymbol{\rho} = \left(\rho_{\text{ee}}, \rho_{\text{eg}}, \rho_{\text{ge}}, \rho_{\text{gg}} \right)^T. \tag{3.48}$$

The master equation has a general time-dependent solution in terms of the matrix exponential

$$\boldsymbol{\rho}(t) = \exp\left(\mathbf{M}t\right)\boldsymbol{\rho}(0). \tag{3.49}$$

Taking $t \to \infty$ leads to an expression for ρ_{ss}. Alternatively, we can find the steady state (obtained when $\dot{\boldsymbol{\rho}} = 0$) by taking the null space of $\mathbf{M}$ and normalizing it so that it has unit trace, which gives

$$\rho_{ss} = \begin{pmatrix} \frac{\Omega^2(\Gamma+2\gamma_d)}{\Gamma(4\Delta^2+(\Gamma+2\gamma_d)^2)+2\Omega^2(\Gamma+2\gamma_d)} & -\frac{i\Gamma\Omega(\Gamma-2i\Delta+2\gamma_d)}{\Gamma(4\Delta^2+(\Gamma+2\gamma_d)^2)+2\Omega^2(\Gamma+2\gamma_d)} \\ \frac{i\Gamma\Omega(\Gamma+2i\Delta+2\gamma_d)}{\Gamma(4\Delta^2+(\Gamma+2\gamma_d)^2)+2\Omega^2(\Gamma+2\gamma_d)} & \frac{1}{\frac{\Omega^2(\Gamma+2\gamma_d)}{\Gamma\left(4\Delta^2+(\Gamma+2\gamma_d)^2\right)+\Omega^2(\Gamma+2\gamma_d)}+1} \end{pmatrix}. \tag{3.50}$$

3.8.2 Interferometer transformation

Using an input-output formalism, we find the field that comes out of the interferometers a and b to be

$$\hat{a}_{out}^{(a)} = \frac{1}{\sqrt{2}}\left(a_{in}(t) + a_{in}(t - L/c)e^{-i\phi_a}\right), \tag{3.51}$$

$$\hat{a}_{out}^{(b)} = \frac{1}{\sqrt{2}}\left(a_{in}(t) + a_{in}(t - L/c)e^{-i\phi_b}\right), \tag{3.52}$$

where a phase $\phi_{a,b}$ and a time delay L/c is picked up when travelling through the long arm of the interferometer with length difference L and speed of light c. Here a_{in} is the state that enters the interferometer, i.e., the field from the QD. The (unnormalised) second-order correlation function after the interferometer

$$G^{(2)}(\tau) = \text{Tr}\left(\hat{a}^{(a)}(t+\tau)\hat{a}^{(b)}(t)\hat{\rho}\hat{a}^{(b)}(t)^\dagger\hat{a}^{(a)}(t+\tau)^\dagger\right), \tag{3.53}$$

can be calculated using the quantum regression theorem, so that $G^{(2)}(\tau)$ inherits its functional dependence on Δ, Γ, etc from the density matrix, ρ. We assume that $t, \tau, \frac{1}{\Gamma} \ll L/c$, so that correlations between time bins vanish, implying that $G^{(2)}$ can be factored into traces containing each separate time bin. There are peaks that appear experimentally when performing this measurement, corresponding to the different possible arrival times of the photons on the detectors. For the centre peak (where $t' = t + \tau$), the factored $G^{(2)}$ is

$$G^{(2)}(\tau) = 2\text{Tr}\left(a\left(t'\right)a(t)\rho a(t)^{\dagger}a\left(t'\right)^{\dagger}\right) + 2\text{Tr}\left(a\rho_{ss}a^{\dagger}\right)^{2}$$
$$+ e^{-i(\phi_a+\phi_b)}\text{Tr}\left(a\left(t'\right)a(t)\rho\right)\text{Tr}\left(\rho a(t)^{\dagger}a\left(t'\right)^{\dagger}\right)$$
$$+ e^{-i(\phi_a-\phi_b)}\text{Tr}\left(a\left(t'\right)\rho a(t)^{\dagger}\right)\text{Tr}\left(a(t)\rho a\left(t'\right)^{\dagger}\right)$$
$$+ e^{-i\phi_a}\left[\text{Tr}\left(a\rho_{ss}\right)\text{Tr}\left(a(t)\rho a(t)^{\dagger}a\left(t'\right)^{\dagger}\right) + \text{Tr}\left(a\left(t'\right)a(t)\rho a(t)^{\dagger}\right)\text{Tr}\left(\rho_{ss}a^{\dagger}\right)\right]$$
$$+ e^{i(\phi_a-\phi_b)}\text{Tr}\left(a(t')\rho a(t)^{\dagger}\right)\text{Tr}\left(a(t)\rho a(t')^{\dagger}\right)$$
$$+ e^{-i\phi_b}\left[\text{Tr}\left(a(t')\rho a(t)^{\dagger}a(t')^{\dagger}\right)\text{Tr}\left(a\rho_{ss}\right) + \text{Tr}\left(a(t')a(t)\rho a(t)^{\dagger}\right)\text{Tr}\left(\rho_{ss}a^{\dagger}\right)\right]$$
$$+ e^{i(\phi_1+\phi_b)}\text{Tr}\left(a(t')a(t)\rho\right)\text{Tr}\left(\rho a(t)^{\dagger}a(t')^{\dagger}\right)$$
$$+ e^{i\phi_b}\left[\text{Tr}\left(a(t')a(t)\rho a(t')^{\dagger}\right)\text{Tr}\left(\rho_{ss}a^{\dagger}\right) + \text{Tr}\left(a(t')\rho a(t)^{\dagger}a(t')^{\dagger}\right)\text{Tr}\left(a\rho_{ss}\right)\right]$$
$$+ e^{i\phi_a}\left[\text{Tr}\left(a(t')a(t)\rho a(t)^{\dagger}\right)\text{Tr}\left(\rho_{ss}a^{\dagger}\right) + \text{Tr}\left(a(t)\rho a(t)^{\dagger}a(t')^{\dagger}\right)\text{Tr}\left(a\rho_{ss}\right)\right].$$

$$(3.54)$$

When $\tau = \pm L/c + \epsilon$ we obtain non-central peaks. We define $t' = t + \epsilon$. The factored $G^{(2)}(\tau)$ for the non-central peaks is then

$$G^{(2)}(\tau) = \text{Tr}\left(a\left(t'\right)a(t)\rho a(t)^{\dagger}a\left(t'\right)^{\dagger}\right) + 3\text{Tr}\left(a\rho_{ss}a^{\dagger}\right)^{2}$$
$$+ e^{i(\phi_a-\phi_b)}\text{Tr}\left(a\rho_{ss}\right)^{2}\text{Tr}\left(\rho a(t)^{\dagger}a(t')^{\dagger}\right)$$
$$+ e^{i(\phi_a+\phi_b)}\text{Tr}\left(a\rho_{ss}\right)\text{Tr}\left(a(t)\rho a(t')^{\dagger}\right)\text{Tr}\left(\rho_{ss}a^{\dagger}\right)$$
$$+ e^{i\phi_a}\left[\text{Tr}\left(a(t')\rho\right)\text{Tr}\left(a(t)\rho a(t)^{\dagger}a(t')^{\dagger}\right) + \text{Tr}\left(a\rho_{ss}\right)\text{Tr}\left(\rho_{ss}a\right)\text{Tr}\left(a(t)\rho a(t)^{\dagger}\right)\right]$$
$$+ e^{-i(\phi_a+\phi_b)}\text{Tr}\left(a(t')\rho a(t)^{\dagger}\right)\text{Tr}\left(a(t)\rho_{ss}\right)\text{Tr}\left(\rho_{ss}a^{\dagger}\right)$$
$$+ e^{-i\phi_b}\left[\text{Tr}\left(a(t')\rho a(t)^{\dagger}a(t')^{\dagger}\right)\text{Tr}\left(a(t)\rho\right) + \text{Tr}\left(a(t')\rho a(t')\right)\text{Tr}\left(a\rho_{ss}\right)\text{Tr}\left(\rho_{ss}a^{\dagger}\right)\right]$$
$$+ e^{-i(\phi_a-\phi_b)}\text{Tr}\left(a(t')a(t)\rho\right)\text{Tr}\left(\rho_{ss}a^{\dagger}\right)^{2}$$
$$+ e^{i\phi_b}\left[\text{Tr}\left(a(t')a(t)\rho a(t')^{\dagger}\right)\text{Tr}\left(\rho_{ss}a^{\dagger}\right) + \text{Tr}\left(a(t')\rho a(t')^{\dagger}\right)\text{Tr}\left(a\rho_{ss}\right)\text{Tr}\left(\rho_{ss}a^{\dagger}\right)\right]$$
$$+ e^{-i\phi_a}\left[\text{Tr}\left(a(t')a(t)\rho a(t)^{\dagger}\right)\text{Tr}\left(\rho_{ss}a^{\dagger}\right) + \text{Tr}\left(a\rho_{ss}\right)\text{Tr}\left(a(t)\rho a(t)^{\dagger}\right)\text{Tr}\left(\rho_{ss}a^{\dagger}\right)\right].$$

$$(3.55)$$

Chapter 4

Collective super- and subradiance from coupled quantum dots

This chapter will form the basis of a theory paper accompanying our recent experimental work [2]. The experimental work was primarily carried out by Alexey Tiranov, Vasiliki Angelopoulou and Cornelis Jacobus van Diepen. I developed the theory, along with Björn Schrinski and Anders Søndberg Sørensen. The figures Fig. 4.5, Fig. 4.6 and Fig. 4.12 are modifications of ones produced for the work [2], originally produced by A.T, V.A and C.J.vD using their experimental data and code containing the theory simulation that I provided.

In the previous chapter, we looked at producing a nonlinearity at the level of single photons. We were able to show theoretically that a quantum dot embedded in a photonic crystal waveguide would reflect single photons and allow two photon states to pass through. This is an important step to realising a building block that could be used for photonic information processing, e.g., a single photon gate.

Now, we add an emitter, such that $N = 2$. Going from $N = 1$ to $N > 1$ represents a drastic change in the available physics: with more than one emitter, an input field can be absorbed by one emitter, re-excited and then absorbed by another emitter, leading to the formation of collective emitter states. Due to the coherence between these emitted fields, various collective modes can result, including superradiant (symmetric) and subradiant (antisymmetric) modes [54, 55]. The nonlinearity present at $N = 1$ in principle allows for quantum information processing. It is then of interest to couple two quantum emitters to allow for the engineering of, e.g., multi-photon gates between emitters. In principle, dipole-dipole interactions between emitters would produce the appropriate coupling, but a major challenge is that these interactions decay strongly with distance [56], meaning that engineering using dipole-dipole interactions is challenging in real experiments that have imperfections. By using a waveguide, the dipole-dipole interactions between quantum dots can be enhanced by collective effects, meaning that in principle it is possible to couple emitters more distant than the typical sub-wavelength scales required for dipole-dipole interactions. The first natural question is how one can tell if there is coupling between two emitters.

For this, we look to the diagram in Fig 4.1. We see in panel a) the two emitters in their uncoupled basis, and in panel b) in the coupled basis. A signature feature of the coupled basis is super- and subradiant emission, where coherent cancellation of the decay from $|ee\rangle \rightarrow |-\rangle$ produces a so-called superradiant decay to the state $|+\rangle$ at an enhanced decay rate Γ_+. As we will show using an effective Hamiltonian approach, without imperfections, this superradiant decay rate is 2Γ (where Γ is the ordinary decay rate of the QD), whereas the subradiant state $|-\rangle = |eg\rangle - |ge\rangle$ is completely dark, as the decay rate from this state is $\Gamma_- = 0$.

We will now show how to obtain the super- and subradiant decay rates, and how these rates would be visible in an experiment. We use the master equation formalism detailed in the introduction chapter, taking the effective Hamiltonian with $N = 2$

$$\mathcal{H}_{\text{eff}} = \sum_{i,j=1}^{2} \left(J_{ij} - i\frac{\Gamma_{ij}}{2} \right) \sigma_j^+ \sigma_i^- - \sum_j^{2} \left(i\frac{\gamma_j^s}{2} + \Delta_j \right) \sigma_j^+ \sigma_j^-. \tag{4.1}$$

We will first consider the case where we have only one excitation in the system, and
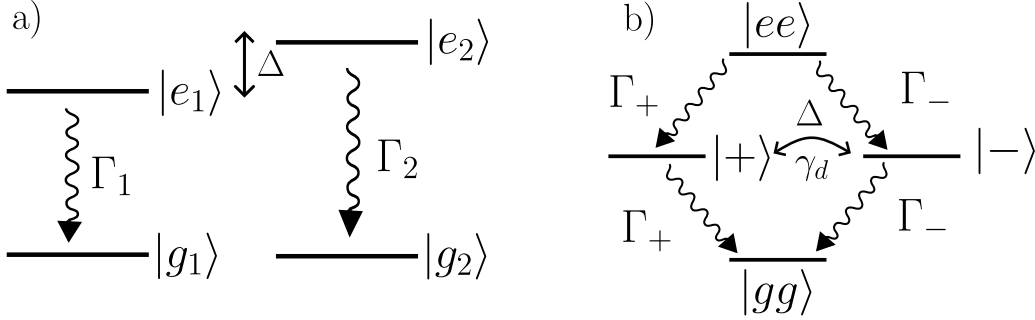
Figure 4.1: **Super- and subradiance produced by emitter-emitter coupling.**
a) Each of the quantum dots j is modelled as a two level emitter with ground state
$|g_j\rangle$ and excited state $|e_j\rangle$ with decay raters Γ_j. The two levels are separated in energy
by a detuning Δ. b) In the coupled basis, the superradiant state $|+\rangle = |eg\rangle + |ge\rangle$
radiates with higher rate Γ_+ compared with the single emitter decay rates due to
coherent cancellation of the decay to the state $|-\rangle = |eg\rangle - |ge\rangle$ which occurs with
a rate $\Gamma_- < \Gamma_j$.

work in the single excitation subspace with

$$\mathcal{H}_{\text{eff}} = \begin{pmatrix} \Delta_1 - i\frac{\Gamma_1}{2} & -\frac{1}{2}ie^{i\phi}\sqrt{\beta_1\beta_2\Gamma_1\Gamma_2} \\ -\frac{1}{2}ie^{i\phi}\sqrt{\beta_1\beta_2\Gamma_1\Gamma_2} & \Delta_2 - \frac{i\Gamma_2}{2} \end{pmatrix} \tag{4.2}$$

Since we are interested in the decay rates of the two emitters, we are interested
in the eigenvalues, which are, assuming the two emitters have the same decay rate
$\Gamma_1 = \Gamma_2 = \Gamma$ and coupling $\beta_1 = \beta_2 = \beta$

$$E_\pm = \frac{1}{2}\left(-i\Gamma + \Delta_1 + \Delta_2 \pm i\sqrt{\beta^2\Gamma^2 e^{2i\phi} - \Delta^2}\right), \tag{4.3}$$

where $\Delta = \Delta_2 - \Delta_1$. The emitter decay rate is given by $\Gamma_\pm = -2\text{Im}(E_\pm)$, so we
have the super and subradiant rates as

$$\Gamma_\pm = \Gamma \pm \text{Re}\left(\sqrt{\beta^2\Gamma^2 e^{2i\phi} - \Delta^2}\right) \tag{4.4}$$

When we have purely dissipative coupling, $\phi = N\pi$, unity β and are on resonance
$\Delta = 0$, we obtain the result $\Gamma_+ = 2\Gamma$ and $\Gamma_- = 0$, i.e., the superradiant decay occurs
at twice the rate compared to the single emitter decay rate Γ and the subradiant
state has an infinite lifetime since its decay rate is zero. The structure of these decay
rates allows us to understand much of what is occurring dynamically in the system,
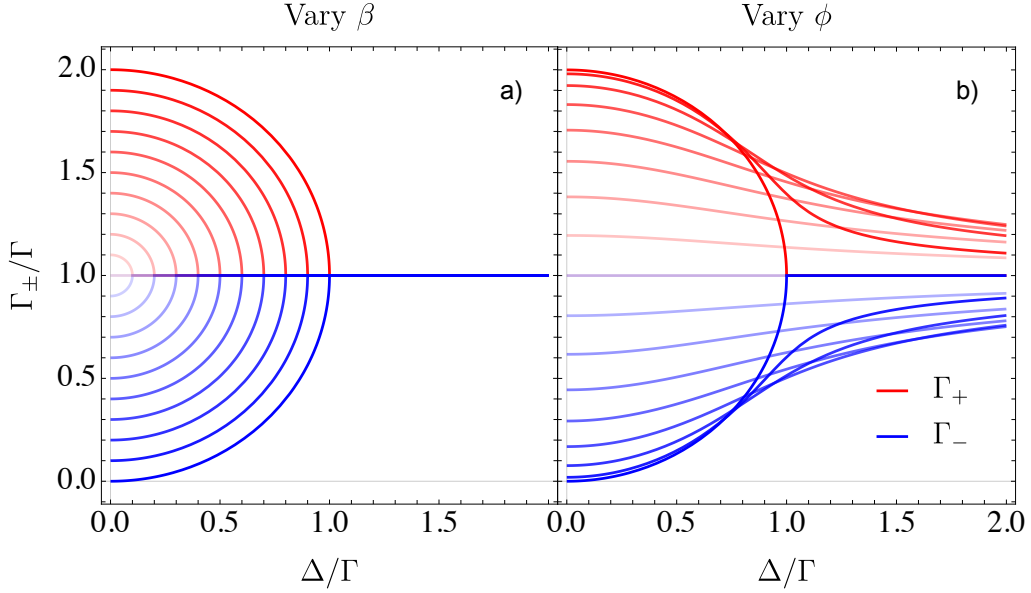
Figure 4.2: **Super- and subradiant decay rates $\Gamma_\pm$ as a function Δ/Γ.** We take $\phi = 0$ and $\beta = 1$ as a starting point for each plot, and the colour gradients show variations in **a)** β from 1 (solid lines) to 0 (faint lines) and **b)**, ϕ from 0 (solid lines) to $\pi/2$, (faint lines).

and how changes to the system parameters will affect the system behaviour. As can be seen in Fig 4.2, these rates form circles in the plane $\Gamma_\pm, \Delta$. As β decreases from 1, the radius of this circle shrinks, until $\Gamma_+ = \Gamma_- = \Gamma$ and the effects of super- and subradiance is gone. Similarly, as we sweep the phase ϕ from 0 to $\pi/2$, the circles deform and elongate, eventually reaching the same $\Gamma_\pm = 1$ state with no super- or subradiance. In the case of dissipative coupling, we also lose the distinction between super- and subradiant decays as soon as we are in the overdamped region $\Delta > \Gamma$, where $\Gamma_+ = \Gamma_- = \Gamma$. Even in an ostensibly simple system, the coupling phase ϕ and detuning Δ both introduce rich physics which merits exploration. However, in a realistic system, we expect imperfections, so a natural question is exactly how much these imperfections affect the decay dynamics.

We will attempt to answer this question by investigating both the population of each state, as well as the intensity caused by the decays that might be measured in a realistic experiment. Assuming that the initial population is $|\psi_0\rangle = (0, 1)^T$, i.e., the second dot is initially excited, the population density can be computed with

$$|\psi\rangle = \exp\left(-iH_{\text{eff}}t\right)|\psi_0\rangle \tag{4.5}$$
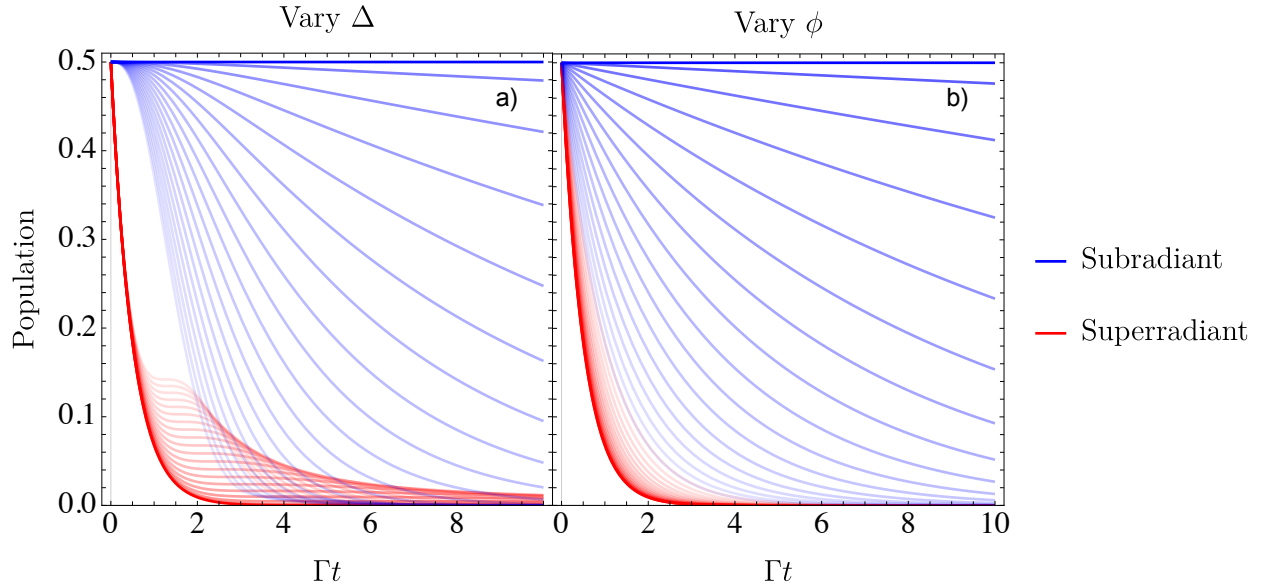
Figure 4.3: **Population of the super- and subradiant state $|+\rangle$ and $|-\rangle$ as a function of time**. The gradients show variations in *a)* Δ from 0 (solid lines) to $2/\Gamma$ (faint lines) and *b)*, ϕ from 0 (solid lines) to $\pi/2$, (faint lines).

and the left- and right-going fields incident on the detectors have the expressions

$$E_L = -i\frac{\sqrt{\beta_1\Gamma_1}\sigma_1^-}{\sqrt{2}} - i\frac{e^{i\phi}\sqrt{\beta_2\Gamma_2}\sigma_2^-}{\sqrt{2}} \tag{4.6}$$

$$E_R = -i\frac{e^{i\phi}\sqrt{\beta_1\Gamma_1}\sigma_1^-}{\sqrt{2}} - i\frac{\sqrt{\beta_2\Gamma_2}\sigma_2^-}{\sqrt{2}}, \tag{4.7}$$

with the phase $\phi = k_0 d$ and where d is the distance between the emitters. The intensity at the left/right ports can thus be computed with

$$I_{L/R} = \langle E_{L/R}^\dagger E_{L/R}\rangle \tag{4.8}$$

By computing the initial intensity $I_L(t=0) = I_R(t=0) = \frac{\beta_2\Gamma_2}{2}$ which represents half the decay from the excited dot going to each detector, we can see that the waveguide in our model is non-chiral, i.e., it does not have a preferred propagation direction.

In Fig. 4.3 we can see the effects of the structures in Fig. 4.2 on the populations of the super- and subradiant states. For $\Delta/\Gamma = 0$ (opaque line), we have a subradiant

47
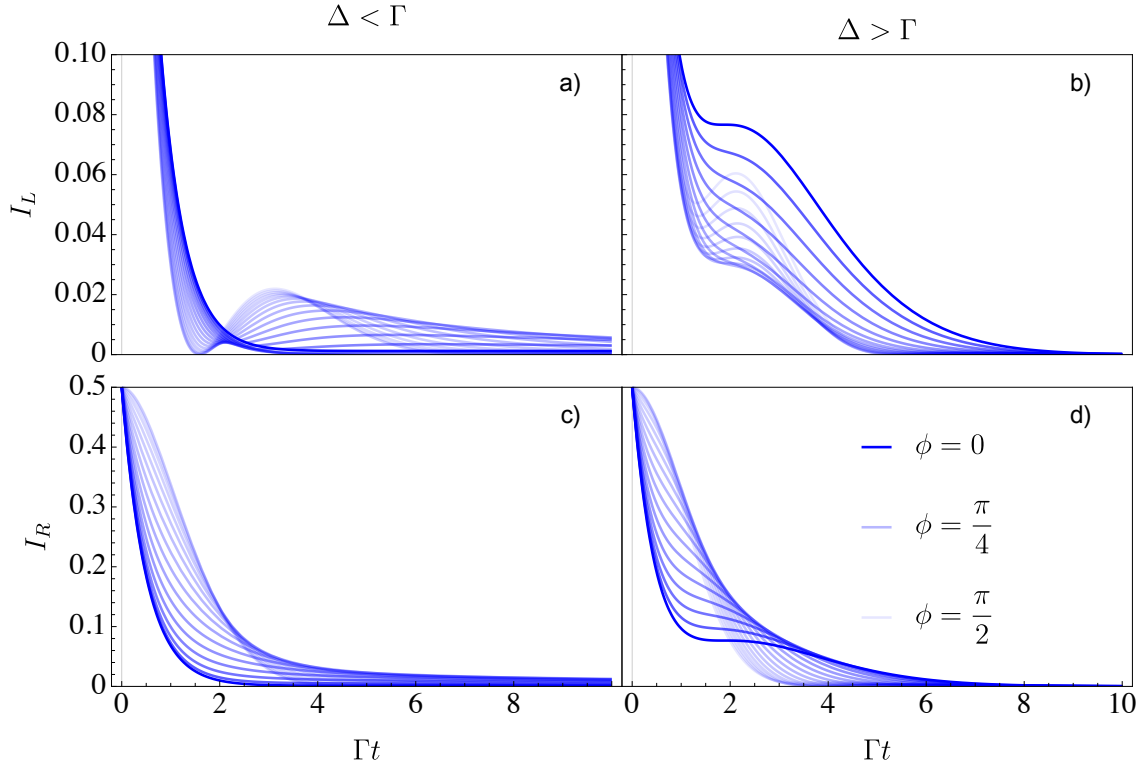
Figure 4.4: **Intensities at the left and right detectors $I_{L/R}$ for the initial state**
$|eg\rangle$. We show two different regimes, $\Delta < \Gamma$, the underdamped regime where the
decay is dominant over the population transfer due to the detuning. Here we have the
strongest signatures of super- and subradiance. We also show the overdamped regime
$\Delta > \Gamma$, where now the dominant rate is the cycling from $|eg\rangle \leftrightarrow |ge\rangle$. By altering
the opacity of the lines from $\phi = 0$ (opaque line) to $\phi = \pi/2$ (transparent line), we
can see how changing the phase between the dots alters the observed dynamics.

population remaining at 0.5 without decay, whilst the superradiant decay causes the
population to rapidly decrease to zero. As Δ is increased from resonance, we see the
resulting oscillations between the super- and subradiant states, and the population
oscillates between the two decay rates Γ_+ and Γ_-. As the phase ϕ is varied from
0 (opaque lines) we can see the result of the circle gradually broadening out, with
the two decay rates becoming equal, the populations simply decay at the same rate,
mimicking the uncoupled system.

In Fig. 4.4 we show the effects of these changing populations on the intensity. In

the underdamped regime $\Delta < \Gamma$, the decay dynamics are dominant over the coherent population transfer due to the detuning. When the coupling phase $\phi = N\pi$ the measured value at each detector is identical, due to the symmetry in the fields E_L and E_R. This symmetry was present in the experimental data shown in Fig. 4.6, where the left and right ports showed symmetric intensities, consistent with dissipative coupling $\phi = N\pi$. The data are well described by the theoretical model, shown in panel c).
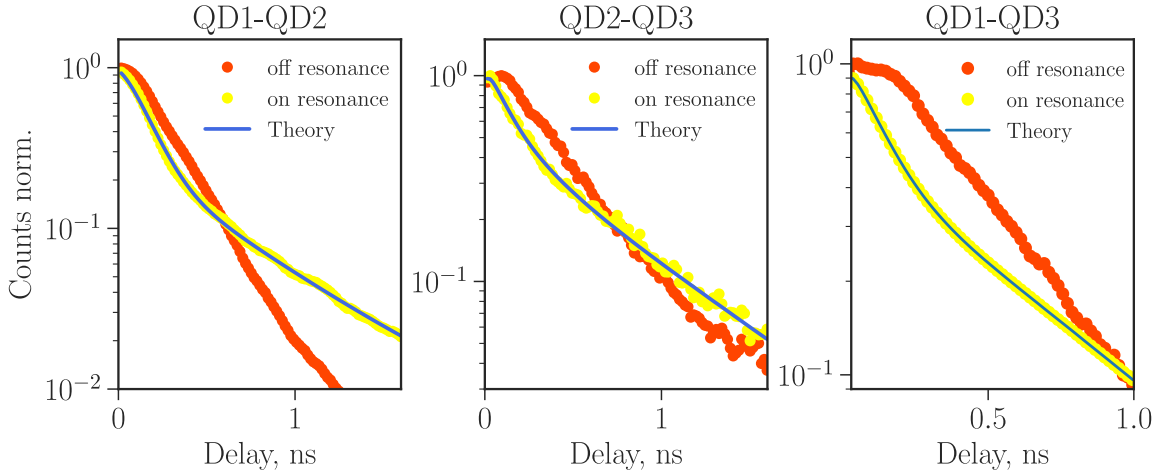
Figure 4.5: **Experimental intensity measurements of pairs of quantum dots in a photonic crystal waveguide**, fitted with the theory described above. The resonant case, shown in yellow, shows the signature of super- and subradiance, with an early superradiant decay occurring at a rate faster than the off resonant decay rate, followed by a slower subradiant decay. Experimentally, a short π pulse is used to excite one of the dots, and this pulse is also modelled in the theory. Data has been reproduced from our recent experimental work [2]

Eq. (4.4) and Fig. 4.2 imply that we will see the strongest signatures of super- and subradiance when the coupling phase $\phi = 0$ and when we are on resonance $\Delta = 0$. In Fig. 4.5, we show experimental data from the work [2], fitted with the full theory including dephasing and spectral diffusion. On resonance, we see a clear subradiant and superradiant decay which is well described by the theory.
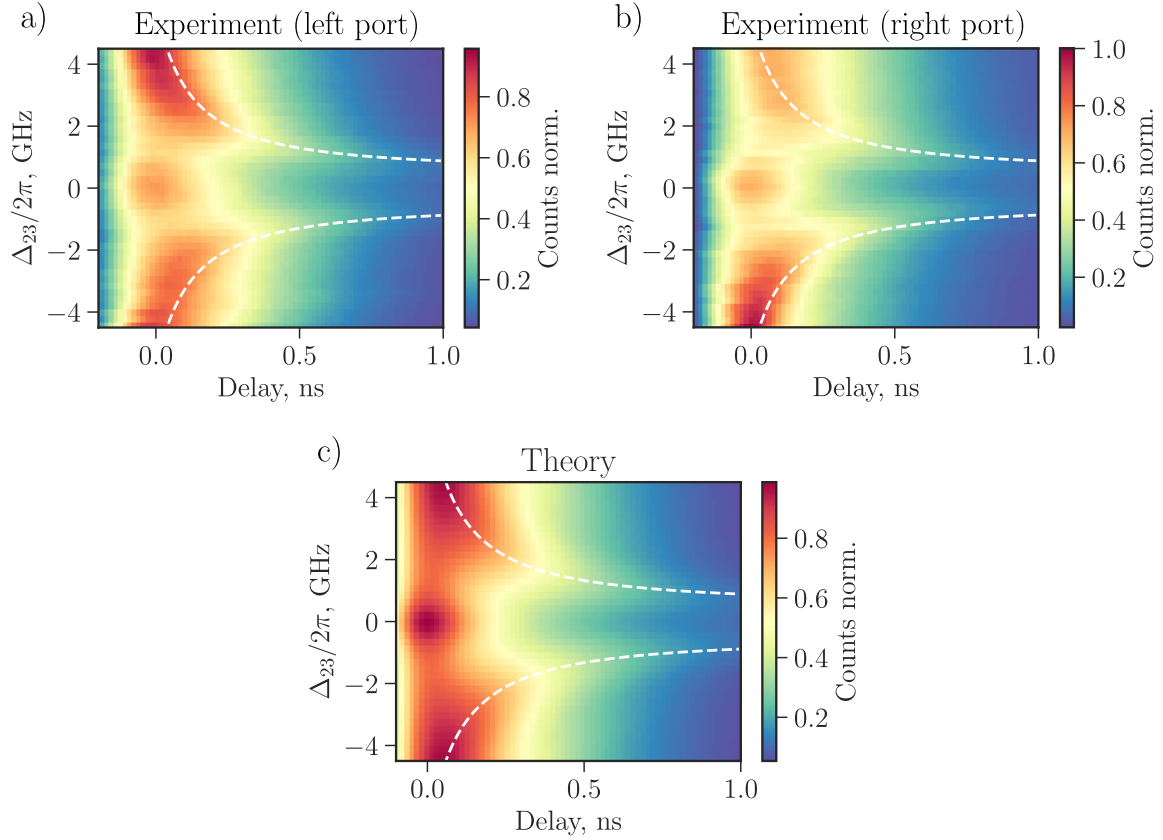
Figure 4.6: **Experimental intensity measurements of a pair of coupled quantum dots as a function of time and detuning**. Experimental data from the left port is shown in panel a), whilst data from the right port is shown in panel b). The corresponding curve predicted by the theory is shown below in panel c). The symmetric readouts from left and right ports is consistent with a coupling phase $\phi = N\pi$, i.e., we have dissipative coupling.

4.1 Driving and multiple excitations

We have until this point considered a situation where we, as theorists are often wont to do, simply assume that we can perform magic tricks with a reckless disregard to the significantly more complicated reality of actual experiments. Here, we will investigate the more realistic scenario where our dots must be excited by driving them with laser light. Indeed, this is the entire point of the coherent field Eq. (2.13)

introduced in Chapter 2. One of the important features in [2] was the ability to drive, from the top (i.e., not through the waveguide) a single dot at a time. Let us now see what is possible with this fine degree of control over our system. Firstly, it should be noted that it is no longer sufficient to work in the single-excitation sub-space for a full description of our system. Especially when we have long pulses or continuously shine light on our dots, there is a high probability of multiple excitation. In this case, we must solve the full density matrix using the master equation that we can recall from Chapter 2

$$\dot{\rho} = \mathcal{L}_{\text{tot}}[\rho] = -i\,[H, \rho] + \mathcal{L}_{\text{coup}}[\rho] + \mathcal{L}_{\text{decay}}[\rho] + \mathcal{L}_{\text{deph}}[\rho]. \tag{4.9}$$

Since we now have multiple excitations, we will also use the second order correlation function $g^{(2)}(\tau)$ to quantify our dynamics.

When we drive a single dot, we populate both the $|+\rangle$ and $|-\rangle$ states and can in principle drive from either of them to the state $|ee\rangle$. However, since the superradiant state decays with rate $\Gamma_+ > \Gamma_-$, the coupling to $|+\rangle$ is effectively suppressed. Thus the dominant pathway is circular (see Fig. 4.7) $|gg\rangle \to |-\rangle \to |ee\rangle \to |+\rangle \to |gg\rangle$. This decay pathway produces bunching since once the photon decays from $|ee\rangle$, the
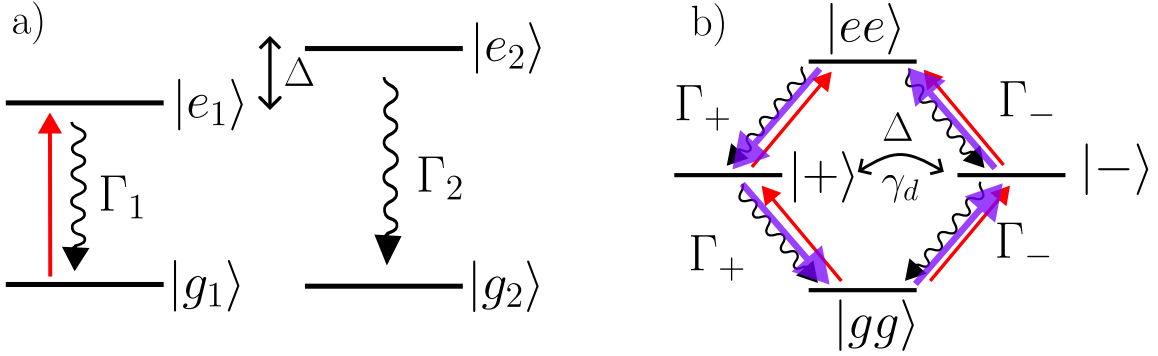
Figure 4.7: **Resonant driving of a single quantum dot. a)** One of the dots is resonantly driven with Rabi frequency Ω_1. **b)** The effective drive (purple, thick arrows) follows a circular path in the coupled basis due to the difference in decay rate $\Gamma_+ > \Gamma_-$. If $\Omega_1 \gg \Gamma_+$, then the $|ee\rangle$ state will become saturated, leading to a more pronounced bunching peak.

subradiant state decays with probability $P(t) = e^{-\Gamma_+ t}$, which is strongly peaked at $t = 0$. Thus, we expect that $g^{(2)}(\tau)$ has a contribution that has a bunching with a characteristic timescale that goes as the inverse of the superradiant decay rate $t_{\text{super}} \sim 1/\Gamma_+$.

However, there is another, broader feature that can appear in $g^{(2)}(\tau)$ stemming from imperfections in the subradiant state. This state can decay with a decay time that goes as $\Gamma_{\text{sub}} \sim 1/\Gamma_-$ which is longer than the timescale of the superradiant decay. Since there is always exactly one photon in this process, it will be antibunched. Thus, there are two features that can be detected in $g^{(2)}(\tau)$: one narrow bunching peak and a broader antibunching dip that correspond to the super- and subradiant states, respectively. These features can be seen in Fig. 4.8, where in panel a), we can see both the narrow bunching peak, and the broader anti-bunching dip. In panel b) we can see how the phase ϕ affects whether we have bunching or anti-bunching for our coincidences.
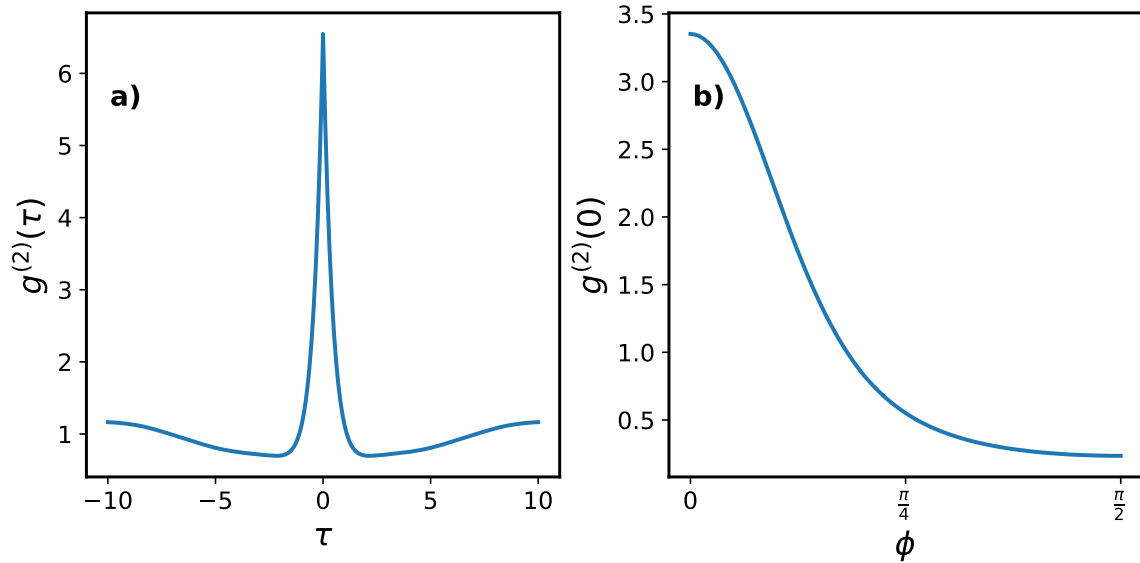
Figure 4.8: **Second order correlation function for a continuously driven single dot**. In a) we show $g^{(2)}(\tau)$ and in b) we show how the bunching peak $g^{(2)}(0)$ decays as ϕ is swept between 0 and $\pi/2$.

4.1.1 The importance of coherence

If we perform the same experiment where we off resonantly drive one dot whilst sweeping the detuning, we find something rather striking: $g^{(2)}(0)$ actually increases. We can understand this by considering the populations in perturbation theory
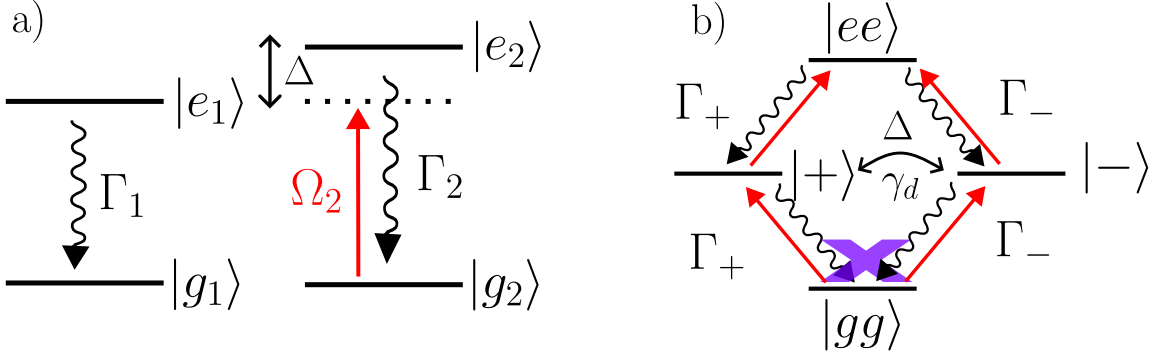
Figure 4.9: **Off resonant driving of a single quantum dot a)** Our drive is off resonance (detuning Δ) with the target dot whilst on resonance with the other. **b)** Due to coherent cancellation of the single-photon decays, the bunching of this state increases with when the detuning Δ is increased (see Fig. 4.10).

(to first order in Ω)

$$\begin{pmatrix} \dot{c}_1 \\ c_2 \end{pmatrix} = \mathcal{H}_{\text{eff}} \begin{pmatrix} c_1 \\ c_2 \end{pmatrix} - \frac{i}{2} \begin{pmatrix} \Omega_1 \\ \Omega_2 \end{pmatrix} \tag{4.10}$$

In steady state, we have the solutions

$$\begin{pmatrix} c_1 \\ c_2 \end{pmatrix} = \frac{i}{2} \mathcal{H}_{\text{eff}}^{-1} \begin{pmatrix} \Omega_1 \\ \Omega_2 \end{pmatrix} \tag{4.11}$$

When we drive only the detuned dot, i.e., $\Omega_1 = 0$, we have the amplitudes

$$\begin{pmatrix} c_1 \\ c_2 \end{pmatrix} = \begin{pmatrix} \frac{i\Gamma_2\Omega_2}{2\sqrt{\Gamma_1\Gamma_2}\Delta} \\ -\frac{i\Omega_2}{2\Delta} \end{pmatrix} \tag{4.12}$$

and when $\Gamma_1 = \Gamma_2 = \Gamma$, the amplitudes have the same magnitude but opposite sign,

$$\begin{pmatrix} c_1 \\ c_2 \end{pmatrix} = \begin{pmatrix} \frac{i\Omega_2}{2\Delta} \\ -\frac{i\Omega_2}{2\Delta} \end{pmatrix} \tag{4.13}$$

Because of this relative phase, the amplitude of the one photon decay processes cancel destructively, leaving only two-photon decay, which produces a large bunching effect. This effect can happen only when the excitation exchange happens coherently, and as such we expect it not to happen for e.g., dephasing, which produces an incoherent evolution between super- and subradiant states. Indeed, in Fig. 4.10b), we see the decay of the bunching peak $g^{(2)}(0)$ as a function of γ_d.
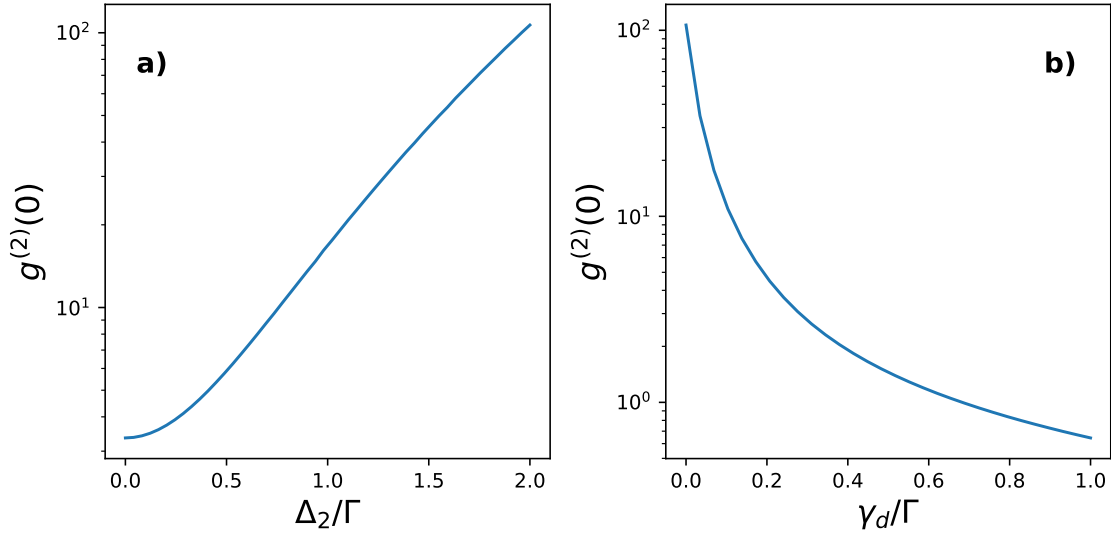
Figure 4.10: **Bunching peak $g^{(2)}(0)$ as a function of detuning and dephasing.** a) Due to coherent cancellation, the bunching peak increases as Δ_2 is swept. b) Since dephasing is incoherent, no such cancellation occurs, and the single-photon decays begin to dominate, causing anti-bunching.

4.1.2 Multiple driving

We now allow for the driving of both the dots simultaneously. The introduction of two drives introduces the possibility for new physics: a relative phase between the drives. By choosing the phase of the drive, we can deterministically populate either the super- or subradiant states. In Fig. 4.11, we see the effect of sweeping the driving phase between $\theta = 0$ and $\theta = \pi$. When the population is in the subradiant state, the decay rate is low, and so the probability for multiple excitation to the $|ee\rangle$ state is high. This means that at $\theta = \pi$, we see bunching. The superradiant state, on the other hand, decays quickly, and the probability for multiple excitation is low. Instead, the single-excitation state decays, displaying the anti-bunching effect that we see in Fig. 4.11b). We can use the same perturbation theory as in (4.10), with a driving phase $e^{i\theta}$ on one of the dots, to calculate the approximate amplitudes of the
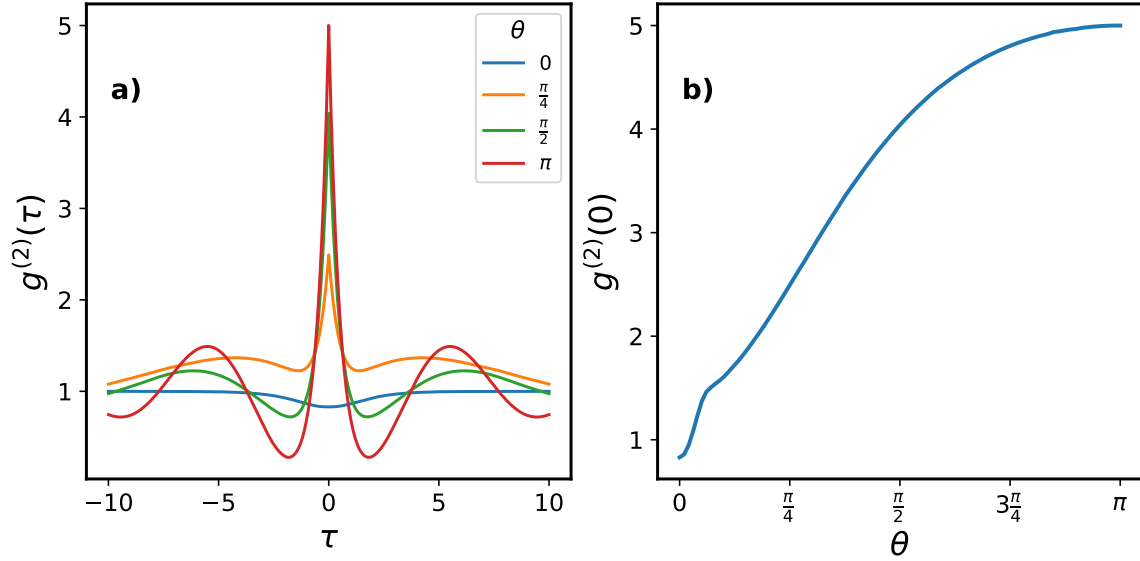
Figure 4.11: **Sweeping the driving phase for multiple driving.** Resonant driving of both dots with $\Omega_1 = \Omega_2 = \Gamma/2$, whilst sweeping the driving phase θ. **a)** The driving phase allows us to excite either the super- ($\theta = 0$) or subradiant ($\theta = \pi$) states, causing a corresponding anti-bunching or bunching. **b)** $g^{(2)}(0)$ for $\theta \in [0, \pi]$. Since the superradiant state decays quickly, the dots do not have the chance to reach the $|ee\rangle$ state, so at $\theta = 0$, we see anti-bunching. The subradiant state, on the other hand, decays slowly, allowing for multiple excitation to the $|ee\rangle$ state which decays with bunching.

super- and subradiant states, obtaining the expressions

$$c_{\text{super}} = \frac{\left(1 + e^{i\theta}\right)\Omega}{2\sqrt{2}(\Gamma + i\Delta)} \tag{4.14}$$

$$c_{\text{sub}} = \frac{i\left(-1 + e^{i\theta}\right)\Omega}{2\sqrt{2}\Delta} \tag{4.15}$$

where here we have set $\Omega_1 = \Omega_2 = \Omega$, and $\Gamma_1 = \Gamma_2 = \Gamma$. Here we can see that at $\theta = 0$, the coefficient of the subradiant state $c_{\text{sub}} \propto 1 - e^{i\theta} = 0$. Similarly, at $\theta = \pi$, the coefficient of the superradiant state $c_{\text{super}} \propto 1 + e^{i\theta} = 0$.
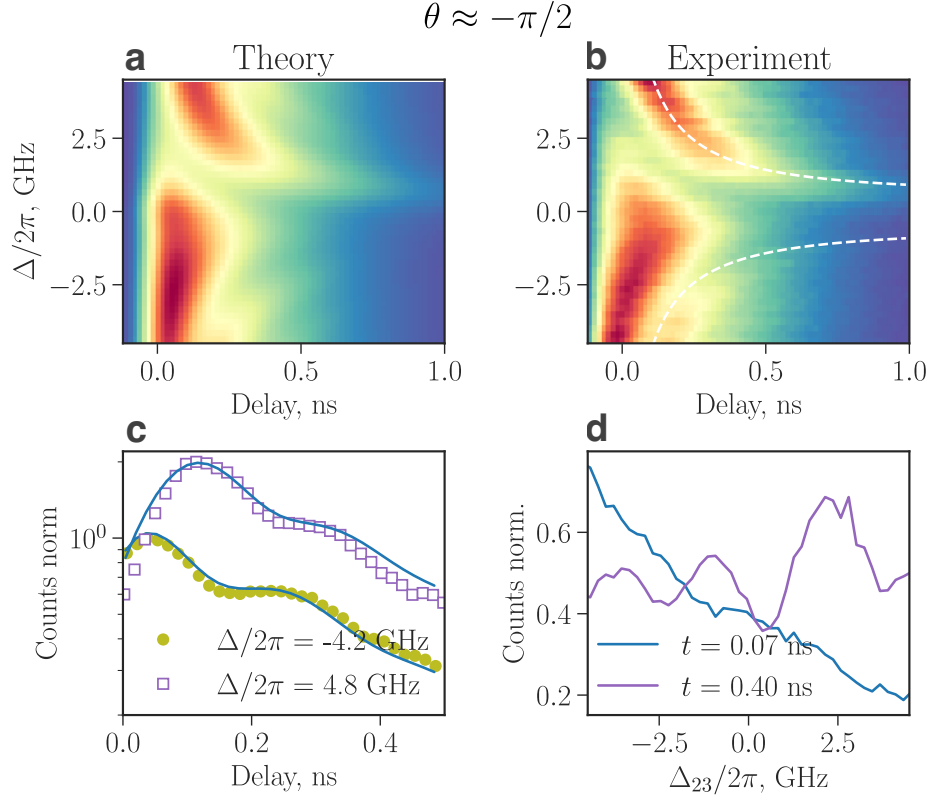
Figure 4.12: **2D lifetime measurements sweeping** θ. **a.** The theory and corresponding experimental data **b.**. The dots are simultaneously excited with a phase $\theta = -\pi/2$ determined from the theoretical fit. **c.** Trace of the normalised intensity with different detunings. With a positive detuning $\Delta > 0$, we excite into the superradiant state, as can be seen by the initial large counts, followed by a coherent oscillation to the subradiant state, characterised by a lowering of the count rate. The two detuned states oscillate out of phase with each other, as with a negative detuning $\Delta < 0$, we excite into the subradiant state. The data are well explained by the theory (solid lines). **d.** Trace along the detuning axis, taken at an early (0.07ns) and later (0.4ns) time. For $t = 0.07$ns, we see the initial excitation into either superradiant ($\Delta < 0$) or subradiant ($\Delta > 0$) states. At the later time $t = 0.4ns$, we can see the effect of the coherent oscillations between the super- and subradiant states.
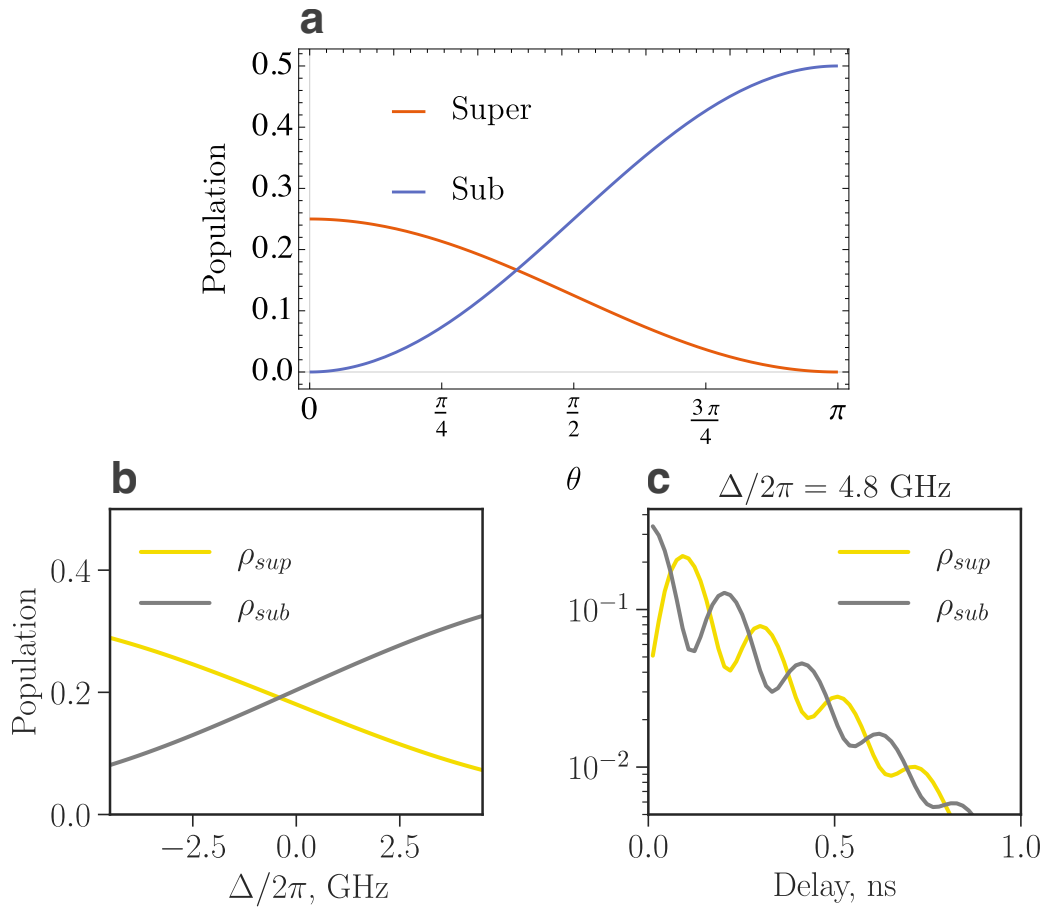
Figure 4.13: **Populations of multiple driving. a.** The steady state populations of the super- and subradiant states as a function of the driving phase θ, calculated using the perturbation theory (4.10). **b.** The populations using the full pulsed theory for the experimental run shown in Fig. 4.12 as a function of detuning Δ and **c.** time.

4.2 Conclusions and outlook

The coupling of emitters has been a long-standing goal that will open the door to many opportunities, including the generation of cluster states, photon-photon gates and the exploration of non-equilibrium many-body physics. In this chapter, we examined in more detail the theory that accompanied our recent experimental work that realised this milestone [2]. We began by examining the heart of the theoretical analysis, the effective Hamiltonian, from which many insights could be gained. Firstly, we solved the dynamics in the single-excitation subspace, finding expressions for the super- and subradiant decay rates. We showed how these decay rates affected the decay dynamics, in both population, and at the detectors. We investigated the effects of the introduction of detuning Δ finite coupling to the waveguide β and the phase between the quantum dots ϕ, and detailed two important regimes for the dynamics, the underdamped $\Delta < \Gamma$ and the overdamped $\Delta > \Gamma$. We found that the experiment, which uses pulses for excitation, is well-described by this simple model, which agreed also with the full model that included the excitation pulse. By introducing driving of a single dot, we introduced new physics: the ability to have multiple excitations in the system at once. Here, we looked at the correlation function $g^{(2)}(\tau)$ to quantify the effects of the coupling when both emitters were excited. We also investigated multiple driving, finding that by altering the driving phase, it is possible to excite into either the super- or subradiant states. Along with our effective Hamiltonian description giving analytic insights into the behaviour of the rich physics in this system, our full model, including driving pulses, was a good fit to the experimental data. In principle, the introduction of driving pulses adds another degree of freedom that is experimentally and theoretically interesting, particularly in the region between the short pulse and long pulse (continuous wave) limits. Our model and accompanying code also allows for the inclusion of driving through the waveguide, where the detector field is modified to include the driving coherent light field. Again, there are in principle some interesting effects to be explored here, including a strong asymmetry between left and right detector intensities due to the presence of the input light field. The investigation of these effects is beyond the scope of this work, but an interested reader is welcome to explore for themselves with the accompanying code.

Chapter 5

Cooperative sensing with impurities in a two-dimensional subwavelength array

The following is an unpublished manuscript composed of work that was primarily carried out during my external stay at Harvard University, in the group of Susanne F. Yelin. This work was carried out in collaboration with Stefan Ostermann, who produced the Figure 5.4, the appendix section 5.6, and additionally contributed to proofreading and editing of the manuscript, along with Prof. Yelin.

Abstract

Quantum sensing plays a vital role in future technologies. Here, we propose a versatile protocol based on two dissipatively coupled quantum emitters for highly sensitive sensing applications. Our approach, compatible with existing platforms, leverages the strong frequency dependence of efficient population transfer between distant emitters and local readout. This allows the detection of minute relative frequency shifts in the emitters' resonance frequencies. We analytically estimate achievable sensitivities as well as the dependence on various system parameters. The proposed protocol is robust against various environmental factors and perturbations, which enhances its applicability in real-world scenarios.

5.1 Introduction

Efficient light-matter interfaces are a core constituent of future quantum technologies [57]. However, establishing strong coupling between light and matter is challenging due to the small interaction cross-section between matter and single photons, which is in general proportional to the photon's wavelength squared [56]. To overcome this challenge, various platforms which alter the radiative environment by introducing dielectric media near quantum emitters have been developed over the past decade. Besides enhancing the coupling between light and matter on the single photon level, these setups also enable long-range couplings between distant emitters and modified emitter decay rates.

Prominent examples of such platforms are quantum emitters, such as quantum dots [22], nano-particles [58, 59], or atoms coupled to cavities, nano-photonic waveguides [60], photonic band-gap materials [61], or other dielectric structures, like atomic lattices with subwavelength spacing [62, 63, 64]. All these platforms offer a wide range of applications, including the generation of super- and subradiant states [65, 66, 2], as well as the generation of non-classical states of light, quantum simulation, quantum information processing, and sensing.

In this Letter we propose a versatile protocol to exploit two dissipatively coupled quantum emitters for sensing applications. The utilization of quantum platforms for quantum sensing capitalizes on a crucial feature of quantum systems: their susceptibility to external disturbances. While these effects are detrimental to quantum cryptography and quantum computing, they present an opportunity for highly sensitive measurements of electric and magnetic fields [67], time and frequency [68], rotations [69], temperature, and pressure [70, 71]. In sensors based on large dense

ensembles of emitters, cooperative effects result in systematic errors of atom based sensing protocols due to induced shifts, dephasing, and decays [72, 73, 74].

Our approach leverages the strong frequency dependence of the population transfer between distant quantum emitters and local population readout, enabling the measurement of minute frequency shifts. While the scheme is compatible with a variety of state-of-the-art platforms that allow coherent dissipative coupling of emitters, the discussion below is based on a particular setup of impurities embedded in a two-dimensional subwavelength atom array [75]. We show that the presented approach is highly sensitive while remaining robust to noise.

Model.—Pairs of cooperatively coupled quantum emitters (labelled s and q as in Fig. 5.1a) with resonance frequencies $\omega_{s,q} = 2\pi c/\lambda_0^{s,q}$ ($\lambda_0^{s,q}$ denotes the transition wavelength of emitters s and q) and decay rates $\gamma_{s,q}$ can in general be described by the effective non-Hermitian Hamiltonian

$$\mathcal{H}_{\text{eff}} = \begin{pmatrix} \Omega_s - i\Gamma_s/2 & \sqrt{\gamma_s\gamma_q}\kappa \\ \sqrt{\gamma_s\gamma_q}\kappa & \Omega_q - i\Gamma_q/2 \end{pmatrix}, \tag{5.1}$$

where the effective frequencies $\Omega_{s,q}$, effective decay rates $\Gamma_{s,q}$, and coupling strength κ are determined by the specific system used to realize the Hamiltonian.

For the remainder of this work we focus on a particular configuration where the Hamiltonian (5.1) is realised by coupling two impurities to a large two-dimensional atomic array with sub-wavelength lattice spacing, i.e., , $a < \lambda_0^{s,q}$. The atoms interact via light induced dipole-dipole interactions. The coherent and dissipative interaction strengths between the atoms are determined via the real- and imaginary-part of the Green's tensor for a point dipole in free space (see Supplementary Information 5.2). In general, the system dynamics of such a dissipative quantum system has to be modelled in the master equation formalism. In the single-excitation subspace, and without external driving, the quantum jump terms in the master equation can be neglected [76] and the system dynamics are fully described by the effective Hamiltonian (5.1). After adiabatically eliminating the lattice (see SM 5.2), the dynamics of the two coupled impurities is governed by the effective frequencies

$$\Omega_s \equiv \gamma_s \text{Re}\{\Sigma\} \tag{5.2}$$
$$\Omega_q \equiv \Delta + \gamma_q \text{Re}\{\Sigma\} \tag{5.3}$$

and effective decay rates

$$\Gamma_s \equiv \gamma_s \left(1 - 2\text{Im}\{\Sigma\}\right) = \gamma_s\Gamma_{\text{coop}} \tag{5.4}$$
$$\Gamma_q \equiv \gamma_q \left(1 - 2\text{Im}\{\Sigma\}\right) = \gamma_q\Gamma_{\text{coop}}, \tag{5.5}$$

61
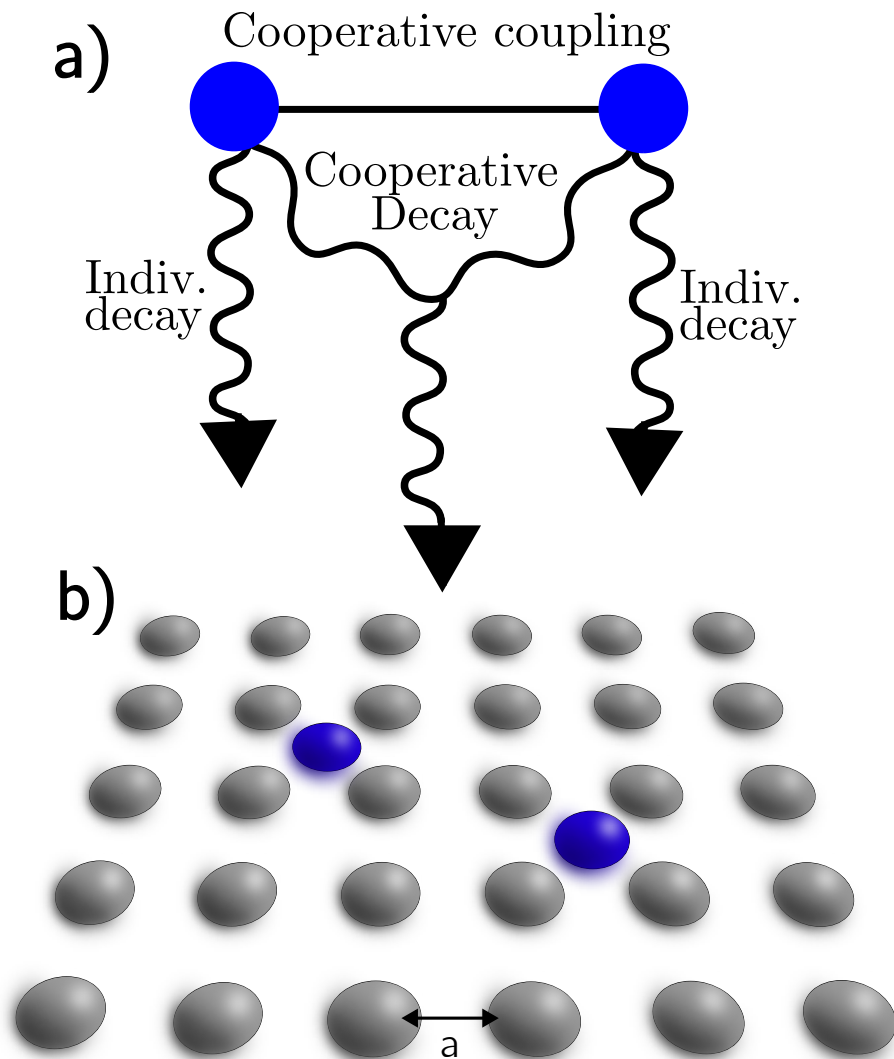
Figure 5.1: **Schematics** a) The effective dynamics of the cooperatively enhanced impurity-impurity system. In this work, this effective system is obtained via adiabatic elimination of a 2D sub-wavelength atomic lattice, giving two parameters: a self-energy Σ and effective coupling strength κ, that characterise the cooperative effects of the lattice. b) A pair of impurities (blue) placed in an sub-wavelength atomic lattice with spacing $a \lesssim \lambda$. The lattice atoms couple via optical dipole-dipole interactions and serves as a Markovian bath mediating the interactions and modifying the bare decay rates. We note that we do not invoke the assumption of independent atomic emission, instead the emitted fields of the lattice atoms interfere with each other, giving rise to a coherent collective enhancement to the coupling of the impurities.

where $0 < \Gamma_{\text{coop}} = 1 - 2\text{Im}(\Sigma) < 1$ is the cooperativity factor that describes the lengthening of the decay times and $\Delta = \omega_s - \omega_q$ is the detuning between the two impurities.

The effective frequencies and decay rates are modified by the self-energy Σ and the effective coupling strength κ which both depend on the particular lattice parameters. We define the resonant detuning Δ_0 when $\Omega_s = \Omega_q$.

$$\Delta_0 = \text{Re}(\Sigma)\,(\gamma_s - \gamma_q). \tag{5.6}$$

The parameter Δ_0 plays an important role as it incorporates the fundamental signatures of the underlying lattice structure. For example, in the inset of Figure 5.2b, we can see that the resonance peaks shift as the ratio $R = \gamma_s/\gamma_q$ is changed. The location of the maximum of these peaks is given precisely by Δ_0. The fact that Δ_0 strongly depends on the properties of the lattice, implies that external noise like position or frequency disorder for the lattice atoms will also result shifts of the resonance frequencies. Choosing the operating point of the sensing protocol (outlined below) with respect to this modified resonance point will allow operation above the noise floor of the chosen implementation.

The dynamics of the system are governed by the differential equations $(\dot{s}, \dot{q})^T = \mathcal{H}_{\text{eff}} \cdot (s, q)^T$. The solutions are therefore superpositions of exponentials of the eigenvalues of H_{eff}, which are $\omega_{\pm} = \bar{\Omega} - i\frac{\bar{\gamma}\Gamma_{\text{coop}}}{2} \pm S$ with the quasi-Rabi frequency

$$S(\Delta) = \sqrt{\frac{1}{4}\left(\Delta_0 - \Delta - i\frac{\Gamma_{\text{coop}}}{2}(\gamma_s - \gamma_q)\right)^2 + \gamma_s\gamma_q\kappa^2}, \tag{5.7}$$

the mean frequency $\bar{\Omega} = (\Omega_s + \Omega_q)/2$ and the mean decay rate $\bar{\gamma} = (\gamma_s + \gamma_q)/2$. Assuming the impurity q is initially excited, we can find an analytic expression for the dynamics of impurity s. The population of impurity s at time t is given as

$$|s(t)|^2 = -\frac{\gamma_s\gamma_q|\kappa|^2}{4|S|^2}e^{-t\bar{\gamma}\Gamma_{\text{coop}}}$$
$$\times \left[e^{-2t\text{Im}(S)} + e^{2t\text{Im}(S)} - e^{-2it\text{Re}(S)} - e^{2it\text{Re}(S)}\right], \tag{5.8}$$

where $S = S(\Delta)$. As illustrated in Fig. 5.2a, the population $|s(t)|^2$ is strongly affected by changes in the detuning, Δ, between the two impurities. This feature is at the core of our proposed sensing protocol, since it allows the measurement of minute frequency shifts via population measurements in impurity s. Such shifts can for example be imposed via Zeeman shifts induced by external magnetic or electric fields at the location of impurity q.

63

The dynamics of $s(t)$ resemble the well known behaviour of laser driven atoms performing Rabi oscillations. In our system, $S(\Delta)$ takes on the analogous role of the Rabi frequency, with the key difference being that both the quasi-detuning $\Delta_{\text{quasi}} = \Delta - \Delta_0 - i\frac{\Gamma_{\text{coop}}}{2}(\gamma_q - \gamma_s)$ given by the difference between the diagonal elements of $\mathcal{H}_{\text{eff}}$ and consequently the quasi- Rabi frequency $S(\Delta)$ have imaginary components. These imaginary components come as a consequence of the decay channels available due to the cooperative effects induced via the surrounding lattice atoms. Note that as a consequence of the non-Hermitian effective Hamiltonian (5.1) the eigenvalue spectrum of H admits exceptional points [77], which have been previously investigated as candidates for quantum sensing protocols. For the protocol presented below, the exceptional points are not optimal points for sensing, so we do not focus on them in this work (see 5.3 for more details).

Sensing protocol.—The key concept of the proposed protocol is illustrated in Fig. 5.2a. After an initial excitation of impurity q, the population in impurity s is detected after some time t_0. Note that while this time can in general be selected arbitrarily, there are specific values that maximize the protocol's sensitivity. Thus, t_0 is a degree of freedom that can be optimized. The large amplitude change in the population dynamics of impurity s exhibits the high sensitivity to small changes in the relative resonance frequencies between the quantum emitters, described by the detuning $\tilde{\Delta} = \Delta/\sqrt{\gamma_s\gamma_q}$. Therefore, an external disturbance to impurity q, e.g., a magnetic field, can be detected in the dynamics of impurity s. The long-range coupling of the two emitters allows efficient local readout. The sensitivity of this protocol can be quantified by computing the standard deviation of the change to the population in response to some signal Δ_{signal} (see Figure 5.2b)

Since the protocol requires the detection of single photons, each measurement of the population in impurity s is a Bernoulli trial (the detector clicks or it doesn't) where the probability of success is binomially distributed with probability $p = |s(t_0)|^2$, i.e., we take samples from the response curve in Figure 5.2b. From these measurements, one can estimate the quantity s_{signal}, which is the change in the population due to some additional detuning Δ_{signal}. Since the population changes with Δ_{signal}, by measuring s, we can obtain an estimate of Δ_{signal} from $|s_{\text{signal}}|^2$ as follows:

We have $|s(t_0)|^2 = f(\Delta)$. Assume we initially detune to a certain value $\Delta = \Delta_0 + \Delta_{\text{add}}$. The added detuning Δ_{add} gives an extra degree of freedom that allows us to further optimise the system to be sensitive to changes in $|s(t_0)|^2$ created by some signal detuning Δ_{signal}. We have

$$f(\Delta_{\text{add}} + \Delta_{\text{signal}}) = s + s_{\text{signal}} \tag{5.9}$$

$$\Rightarrow \Delta_{\text{signal}} = f^{-1}(s + s_{\text{signal}}) - \Delta_{\text{add}} \tag{5.10}$$

Expanding linearly around s, we obtain

$$\Delta_{\text{signal}} = \frac{s_{\text{signal}}}{\frac{\partial s}{\partial \Delta}} - \Delta_{\text{add}} \tag{5.11}$$

The standard deviation of Δ_{signal} is thus

$$\sigma_{\Delta_{\text{signal}}} = \left. \frac{\sigma_{s_{\text{signal}}}}{\frac{\partial s}{\partial \Delta}} \right|_{\Delta = \Delta_{\text{add}}}, \tag{5.12}$$

where the measurements of s_{signal} are distributed binomially, and so has the well-known (single-shot) variance $\sigma^2 = p(1-p)$ and Δ_{signal} inherits the same distribution via its dependence on $|s(t_0)|^2$. The observable of interest is the signal detuning Δ_{signal}. For a certain frequency shift, which is generated via an external *local* perturbation (e.g., a magnetic field at the location of impurity q), it can be obtained by measuring the maximum population of s. Since the system is highly sensitive to changes in Δ, the protocol is able to detect small external disturbances. We quantify this sensitivity by computing the uncertainty on the measurement of Δ via the standard deviation [see 5.2b and (5.12)].

An analytic approximation to the envelope function of $|s(t_0, \Delta)|^2$ can be found by taking t_0 equal to the time of maximum population transfer. Since it does not take into account sensitivity improvements due to the phase of the response curve for different detunings, this envelope function gives an upper bound on the sensitivity.

$$|s_{\text{max}}|^2 \approx \gamma_s \gamma_q \left| \frac{\kappa}{S} \right|^2 e^{-\frac{\pi \bar{\gamma} \Gamma_{\text{coop}}}{2 \text{Re}(S)}} \tag{5.13}$$

This equation is displayed in Figure. 5.2b as a black dashed line. The decay term containing Γ_{coop} would be absent from systems undergoing standard Rabi oscillations.

Recall the sensitivity of the sensing protocol is quantified by σ, the standard deviation of a measurement of Δ_{signal}. The lattice spacing a, the added detuning Δ_{add} and the measurement time t_0 all affect this measurement sensitivity. In Figure 5.3, σ is plotted as a function of these parameters. The broad resonances in these plots stem from the population hitting a maximum, the derivative hitting zero and subsequently causing a divergence in σ. The narrower resonances correspond to the population itself reaching zero for a given parameter set. These occur over a smaller range of parameters, hence the narrower profile. In panel a), σ is plotted as a function of the added detuning $\tilde{\Delta}_{\text{add}}$ and the measurement time t_0.
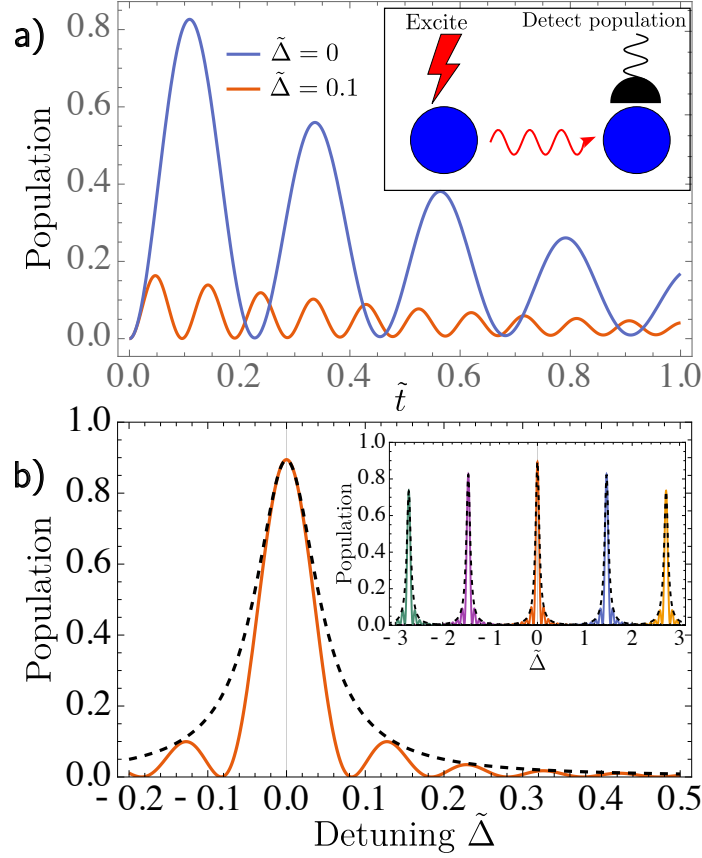
Figure 5.2: **Impurity dynamics**. a) The population of the initially unexcited impurity s as a function of the time $\tilde{t} = \sqrt{\gamma_s \gamma_q} t$ [see Eq. (5.8)] for a 10×10 lattice, with lattice spacing $a = 0.3\lambda_0^s$ and impurity distance $d = 2a$. The blue curve corresponds to maximal population transfer at $\tilde{\Delta} = 0$. A small change in detuning ($\tilde{\Delta} = 0.1$) diminishes the achievable population transfer (red curve). b) The maximum population as a function of detuning for the same parameters as a) above. In the inset, the population is shown for values of $R = \gamma_s/\gamma_q$ from left to right $R = (1/30, 1/10, 1, 10, 30)$. The height and width of the quasi-Lorenzian $|s_{\max}|^2(\Delta)$ [see (5.13)] lowers and widens as we move away from the ratio $R = \gamma_s/\gamma_q = 1$. Note that R and R^{-1} have the same shape, just shifted such that the resonance occurs at Δ_0 (5.6).

For a given t_0, $\tilde{\Delta}_{\mathrm{add}}$ has the effect of moving the resonance point. At very small values of t_0, the population is very small, little information can be extracted from the system and hence σ is very large.

In panel b), σ is plotted as a function of measurement time, t_0 and the lattice spacing a

The lattice spacing changes the timescale of the dynamics, where a smaller lattice spacing means faster exchange. This makes physical sense: the smaller the lattice spacing, the smaller the physical distance the excitation needs to traverse, and assuming equal decay rates and propagation velocity, the effective timescale is decreased.

For $a \sim 0.13$, there is a dark band where in principle the optimal σ lies. However, in the neighbourhood of this region there are a number of isolated resonances that would be very difficult to avoid in practice.

In general, small, but non-zero values of $\tilde{\Delta}_{\mathrm{add}}$ are optimal, and at the optimal detunings, avoiding resonances, a lattice spacing of $a \sim 0.2$ is optimal.

Conclusions and Outlook.—We introduced a quantum sensor which is based on the coherent photon exchange between distant quantum emitters and local population readout. We showed that these local population measurements can be used to detect minute frequency shifts at the location of one emitter. This is due to the strong sensitivity of the photon transfer efficiency on the relative detuning between the emitters. The population transfer is strongly enhanced by the collective effects present in the system. This is in contrast to other lattice based metrology applications which are in general harmed by such effects via dephasing and cooperative shifts. While the discussion in this Letter was based on a particular implementation with impurities embedded in a cooperative array, the protocol is generalizable to related platforms (quantum dots coupled to waveguides or photonic bandgap materials, solid state based implementations, NV centres etc).

The introduced approach opens up exciting avenues for cooperatively enhance quantum sensing. The proposed protocol is expected to be implementable in state-of-the-art platforms. The major challenge to overcome is local single photon readout, which however is for example becoming feasible in modern tweezer-based setups.

For the particular configuration studied here, where the sensor relies on the cooperative coupling of the lattice atoms to the impurities, the population dynamics of the two impurities can also be used to monitor the lattice dynamics. This could form the basis for a new tool for device characterisation. Another exciting future direction motivated by the findings in this work is to extend the study to systems beyond the single excitation regime, where strong photon non-linearities will occur. These could potentially improve the sensitivity.
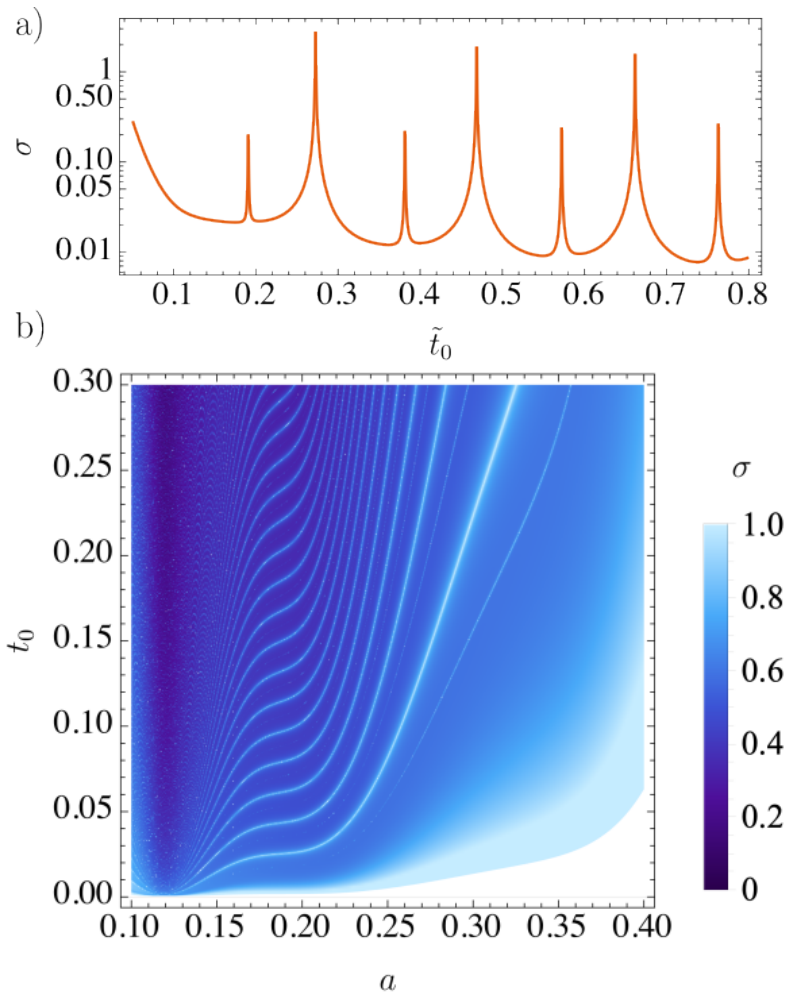
Figure 5.3: **Measurement standard deviation** (a) Standard deviation of measurements of Δ_{sig} as a function of the measurement time $\tilde{t}_0$. We set $\gamma_s = \gamma_q$ for this plot as it represents the universally optimal value for this protocol (see 5.5 for details). (b) σ as a function of the measurement time $\tilde{t}_0$ and the lattice spacing a. Again, the resonances are a result of divergences when the derivative hits an inflection point. The resonances are a result of the derivative reaching an inflection point, leading to a divergence in (5.12). σ as a function of the lattice spacing, a.

5.2 Appendix: Realisation of effective Hamiltonian

Below, we show how the effective Hamiltonian (5.1) can be obtained via adiabatic elimination of the lattice Hamiltonian in the appropriate rotating wave approximation. We model an array of ℓ atoms arranged in a lattice, as well as two impurities with annihilation operators q, s. We have a space of size N, where the first ℓ entries correspond to the lattice atoms, and the next two entries correspond to the impurities, i.e., $\ell = N - 2$.

In real space, the Hamiltonian is split into

$$H_{latt} = \sum_m^\ell \left(\omega_L - i \frac{\gamma_L}{2} \right) \sigma_m^\dagger \sigma_m + \gamma_L \sum_{m \neq n}^\ell \left(J_{mn} - i \frac{\Gamma_{mn}}{2} \right) \sigma_m^\dagger \sigma_n \qquad (5.14)$$

We have also the interaction between the lattice and the impurities (or defect)

$$H_{latt,d} = \sqrt{\gamma_L \gamma_d} \sum_m^\ell \left[\left(J_{dm} - i \frac{\Gamma_{dm}}{2} \right) d^\dagger \sigma_m + \left(J_{md} - i \frac{\Gamma_{md}}{2} \right) \sigma_m^\dagger d \right] \qquad (5.15)$$

where $d = q, s$ indicate the impurity atoms and $\sigma_z^{(d)}$ indicates a σ_z matrix acting on site d. We have also the impurity interaction that has the same form as the lattice atoms

$$H_{qs} = \sqrt{\gamma_q \gamma_s} \left[\left(J_{qs} - i \frac{\Gamma_{qs}}{2} \right) q^\dagger s + \left(J_{sq} - i \frac{\Gamma_{sq}}{2} \right) s^\dagger q \right] \qquad (5.16)$$

The bare impurity dynamics is governed by

$$H_{dd} = \sum_d \left(\omega_d - i \frac{\gamma_d}{2} \right) d^\dagger d \qquad (5.17)$$

Due to resonant dipole-dipole interactions, we obtain collective coupling J_{ij} and decay Γ_{ij} rates that are defined as

$$\sqrt{\gamma_i \gamma_j} J_{ij}(\mathbf{r}_i, \mathbf{r}_j) = -\frac{3\pi \sqrt{\gamma_i \gamma_j}}{\omega} \mathbf{d}_i^\dagger \cdot \mathrm{Re} \left[\mathbf{G}(\mathbf{r}_{ij}, \omega) \right] \cdot \mathbf{d}_j \qquad (5.18)$$

$$\sqrt{\gamma_i \gamma_j} \Gamma_{ij}(\mathbf{r}_i, \mathbf{r}_j) = -\frac{6\pi \sqrt{\gamma_i \gamma_j}}{\omega} \mathbf{d}_i^\dagger \cdot \mathrm{Im} \left[\mathbf{G}(\mathbf{r}_{ij}, \omega) \right] \cdot \mathbf{d}_j \qquad (5.19)$$

for the free space Green's tensor $\mathbf{G}(\mathbf{r}_{ij}, \omega)$ with components

$$G_{\alpha\beta}(\mathbf{r}_{ij}, \omega) = \frac{e^{i\omega r}}{4\pi r}\left[\left(1 + \frac{i}{\omega r} - \frac{1}{\omega^2 r^2}\right)\delta_{\alpha\beta} - \left(1 + \frac{3i}{\omega r} - \frac{3}{\omega^2 r^2}\right)\frac{r_{ij,\alpha}r_{ij,\beta}}{r^2}\right] - \frac{\delta(\mathbf{r}_{ij})}{3\omega^2}\delta_{\alpha\beta},$$
(5.20)

an atomic separation $\mathbf{r}_{ij} = \mathbf{r}_i - \mathbf{r}_j$, $r \equiv |\mathbf{r}_{ij}|$, individual atomic decay rates γ_i, γ_j and atomic dipole moments $\mathbf{d}_{i,j}$.

5.2.1 Momentum space representation

Writing $\sigma_m = \frac{1}{\sqrt{\ell}}\sum_{\mathbf{k}=1}^{\ell} e^{\frac{2\pi}{\ell}i\mathbf{k}\cdot\mathbf{r}_m}$, moving to the rotating frame with frequency ω_s and requiring that we are in the single-excitation subspace, we get that

$$H_{latt} = \gamma_L \sum_{\mathbf{k}}\left[\frac{\delta_{sL}}{\gamma_L} - \frac{i}{2} + J_L(\mathbf{k}) - \frac{i}{2}\Gamma_L(\mathbf{k})\right]\sigma_{\mathbf{k}}^{\dagger}\sigma_{\mathbf{k}} \tag{5.21}$$

$$H_{latt,d} = \sqrt{\gamma_L\gamma_d}\sum_{\mathbf{k}}\left[\left(J_d(\mathbf{k}) - \frac{i}{2}\Gamma_d(\mathbf{k})\right)d^{\dagger}\sigma_{\mathbf{k}} + \left(J_d^*(\mathbf{k}) - \frac{i}{2}\Gamma_d^*(\mathbf{k})\right)\sigma_{\mathbf{k}}^{\dagger}d\right] \tag{5.22}$$

$$H_{qs} = \sqrt{\gamma_s\gamma_q}\left(J_{qs} - i\frac{\Gamma_{qs}}{2}\right)q^{\dagger}s + \left(J_{sq} - i\frac{\Gamma_{sq}}{2}\right)s^{\dagger}q \tag{5.23}$$

$$H_{ss} = -i\frac{\gamma_s}{2}s^{\dagger}s \tag{5.24}$$

$$H_{qq} = \left(\Delta - i\frac{\gamma_q}{2}\right)q^{\dagger}q \tag{5.25}$$

Where $\Delta = \omega_q - \omega_s$, $\delta = \omega_L - \omega_s$ and where $\sigma_{\mathbf{k}} \to e^{-i\omega_s t}\sigma_{\mathbf{k}}$, $s \to e^{-i\omega_s t}s$ and $q \to e^{-i\omega_s t}q$.

After adiabatic elimination of the lattice, we obtain

$$\dot{s} = -i\left(\gamma_s\Sigma_s - i\frac{\gamma_s}{2}\right)s - i\sqrt{\gamma_s\gamma_q}\kappa_s q \tag{5.26}$$

$$\dot{q} = -i\left(\Delta + \gamma_q\Sigma_q - i\frac{\gamma_q}{2}\right)q - i\sqrt{\gamma_s\gamma_q}\kappa_q s \tag{5.27}$$

Where we define the self-energies

$$\Sigma_s \equiv \sum_{\mathbf{k}} \frac{(J_s(\mathbf{k}) - \frac{i}{2}\Gamma_s(\mathbf{k}))(J_s^*(\mathbf{k}) - \frac{i}{2}\Gamma_s^*(\mathbf{k}))}{\delta/\gamma_L + J_L(\mathbf{k}) - \frac{i}{2}\Gamma_L(\mathbf{k}) - i/2} \tag{5.28}$$

$$\Sigma_q \equiv \sum_{\mathbf{k}} \frac{(J_q(\mathbf{k}) - \frac{i}{2}\Gamma_q(\mathbf{k}))(J_q^*(\mathbf{k}) - \frac{i}{2}\Gamma_q^*(\mathbf{k}))}{\delta/\gamma_L + J_L(\mathbf{k}) - \frac{i}{2}\Gamma_L(\mathbf{k}) - i/2} \tag{5.29}$$

and the effective coupling strengths

$$\kappa_s \equiv \left(J_{sq} - i\frac{\Gamma_{sq}}{2} + \sum_{\mathbf{k}} \frac{(J_s(\mathbf{k}) - \frac{i}{2}\Gamma_s(\mathbf{k}))(J_q^*(\mathbf{k}) - \frac{i}{2}\Gamma_q^*(\mathbf{k}))}{\delta/\gamma_L + J_L(\mathbf{k}) - \frac{i}{2}\Gamma_L(\mathbf{k}) - i/2} \right) \tag{5.30}$$

$$\kappa_q \equiv \left(J_{qs} - i\frac{\Gamma_{qs}}{2} + \sum_{\mathbf{k}} \frac{(J_q(\mathbf{k}) - \frac{i}{2}\Gamma_q(\mathbf{k}))(J_s^*(\mathbf{k}) - \frac{i}{2}\Gamma_s^*(\mathbf{k}))}{\delta/\gamma_L + J_L(\mathbf{k}) - \frac{i}{2}\Gamma_L(\mathbf{k}) - i/2} \right) \tag{5.31}$$

Now calling $|\psi\rangle = \begin{pmatrix} s \\ q \end{pmatrix}$ and noting that $\kappa_s = \kappa_q \equiv \kappa$ and $\Sigma_s = \Sigma_q \equiv \Sigma$, these equations can be written in terms of an effective (non-Hermitian) Hamiltonian

$$\mathcal{H}_{\text{eff}} = \begin{pmatrix} -\frac{i\gamma_s}{2} + \gamma_s\Sigma & \sqrt{\gamma_s\gamma_q}\kappa \\ \sqrt{\gamma_s\gamma_q}\kappa & -\frac{i\gamma_q}{2} + \Delta + \gamma_q\Sigma \end{pmatrix} \equiv \begin{pmatrix} \Omega_s - i\Gamma_s/2 & \sqrt{\gamma_s\gamma_q}\kappa \\ \sqrt{\gamma_s\gamma_q}\kappa & \Omega_q - i\Gamma_q/2 \end{pmatrix}, \tag{5.32}$$

which is (5.1) in the main text.

5.2.2 Constraints on Σ and κ

The above derivation requires the computation of the self-energy Σ and the coupling rate κ if the dynamics of the effective Hamiltonian (5.1) are to be realised. Below, we discuss the constraints and physical meaning of these parameters.

The real part of Σ is responsible for setting an energy scale, and so does nothing whatsoever to the overall dynamics, as the only relevant quantity affecting dynamics is the energy difference. To achieve the longest lifetime, the requirement is $\text{Im}\{\Sigma\} = 1/2$, such that the decay terms Γ_s and Γ_q are zero and thus the decay time diverges. However, at $\text{Im}\{\Sigma\} = 1/2$, then $\lim_{t\to\infty} |s(t)|^2 \to \infty$, i.e., the population diverges too and is thus unphysical in this model. In general, for us to have physical parameters, we need to satisfy

$$\text{Im}\{\Sigma\} < \frac{1}{2} \quad \text{and} \quad \bar{\gamma}\Gamma_{\text{coop}} > 2\text{Im}\{S\}, \tag{5.33}$$

where the second inequality comes from ensuring that $\lim_{t\to\infty}|s(t)|^2 < \infty$. Satisfying the second inequality puts restrictions on κ. Assuming $\gamma_s = \gamma_q \equiv \gamma$, and $\Delta = 0$ we have $S = \sqrt{\gamma^2\kappa^2}$, and

$$\mathrm{Im}(S) = \frac{\gamma\,\mathrm{Im}(\kappa)\mathrm{Re}(\kappa)}{|\mathrm{Re}(\kappa)|}. \tag{5.34}$$

Thus, the general condition under our assumptions is

$$\frac{\gamma\,\mathrm{Im}(\kappa)\mathrm{Re}(\kappa)}{|\mathrm{Re}(\kappa)|} < \gamma\left(\frac{1}{2} - \mathrm{Im}(\Sigma)\right) \tag{5.35}$$

Assuming $\mathrm{Re}(\kappa) < 0$ and $\mathrm{Im}(\kappa) < 0$, we can further simplify this to the condition

$$\mathrm{Im}(\kappa) > \mathrm{Im}(\Sigma) - \frac{1}{2}. \tag{5.36}$$

5.3 Appendix: Exceptional points

In this section, we compute the exceptional points of the system and find that they lie far away from the optimal point for sensing in the presented protocol. The eigenvectors of the effective Hamiltonian (5.1) are

$$e_{\pm} = \begin{pmatrix} \frac{1}{\tilde{\kappa}}\left(\Omega_{sq} - i\frac{\Gamma_{sq}}{2} \pm S\right) \\ 1, \end{pmatrix} \tag{5.37}$$

with the eigenvalues given in the main text. The energies are degenerate when the square root term $S = \sqrt{-\left(i\Omega_{sq} + \frac{\Gamma_{sq}}{2}\right)^2 + \tilde{\kappa}^2} = 0$. Equating real and imaginary parts, we obtain

$$\gamma_{sq}\Gamma_{\mathrm{coop}} = \mathrm{Re}\{\tilde{\kappa}\} \tag{5.38}$$

$$\frac{1}{2}\left(\Delta_0 - \Delta\right) = \mathrm{Im}\{\tilde{\kappa}\} \tag{5.39}$$

and this is the same point at which the eigenvalues also coalesce, i.e., it is the exceptional point for the system. For any $\gamma_s \neq \gamma_q$, any degeneracy in the eigenvalue spectrum is an exceptional point. However, $\gamma_s = \gamma_q$ is the optimal point for the presented sensing protocol, and the exceptional points lie far away (several orders of magnitude) from this optimum. Therefore, we do not focus on the exceptional points in this work.

5.4 Fisher information

The Fisher information for a binomially distributed quantity is given by $\mathcal{I}(s) = \frac{n}{p(1-p)}$. The variance of a Bernoulli distribution with n trials is $np(1-p)$, and saturates the Cramér-Rao bound for a single shot

$$\sigma^2_{s_{\text{signal}}} \geq \frac{1}{\mathcal{I}(s)} \tag{5.40}$$

$$np(1-p) \geq \frac{p(1-p)}{n}. \tag{5.41}$$

5.5 Appendix: Optimal value of emitter decay rates

The optimal value of the gamma ratio is always $R = \gamma_s/\gamma_q = 1$, i.e., that the two impurities have the same decay rate, regardless of the value of a, and additionally any value $R = r$ gives the same value of σ as its reciprocal $R = 1/r$, mirroring the symmetry in Figure 5.2b.

5.6 Appendix: Calculating the self-energies and effective coupling strengths for non-periodic arrays

Bloch's theorem can be applied for periodic lattices to obtain the lattice dispersion used to determine the self-energies and coupling rates defined in Eqs. (5.29) and (5.31). For impurities embedded in a non-periodic lattices, the self-energy and coupling rates can be determined via an alternative method based on the real space Hamiltonian.

In the single excitation manifold the system dynamics are governed by the Schrödinger equation $i\partial_t |\psi(t)\rangle = H |\psi(t)\rangle$ with the non-Hermitian Hamiltonian $H = H_{latt} + H_{latt,d} + H_{qs} + H_{dd}$, with the individual Hamiltonians defined in Eqs. (5.14)–(5.17). The atomic wave function can be written as $|\psi(t)\rangle = a(t) |G, g_s, g_q\rangle + \sum_{m=1}^{l} b_m(t) e^{i\omega_I t} |e_i, g_s, g_q\rangle + s(t) e^{i\omega_I t} |G, e_s, g_q\rangle + q(t) e^{i\omega_I t} |G, g_s, e_q\rangle$, where $|G, g_s, g_q\rangle$ denotes the state with all atoms in the ground state, $|e_i, g_s, g_q\rangle$ the state where only the ith lattice atom is excited and $|G, e_s, g_q\rangle$ $(|G, g_s, e_q\rangle)$ is the state where only the impurity s (q) is excited.

In the frame rotating at the impurity resonance frequency ω_I, this results in a set of coupled equations for the amplitudes $b_m(t)$, $s(t)$ and $q(t)$,

$$\partial_t b_m(t) = i\left(\delta_{LI} + \frac{i}{2}\gamma_L\right)b_m(t) - i\gamma_L \sum_{n\neq m}^{l}\left(J_{mn} - \frac{i}{2}\Gamma_{mn}\right)b_n(t)$$

$$- i\sqrt{\gamma_L\gamma_s}\left(J_{ms} - \frac{i}{2}\Gamma_{ms}\right)s(t) - i\sqrt{\gamma_L\gamma_q}\left(J_{mq} - \frac{i}{2}\Gamma_{mq}\right)q(t), \qquad (5.42a)$$

$$\partial_t s(t) = -\frac{\gamma_s}{2}s(t) - i\sqrt{\gamma_L\gamma_s}\sum_{m=1}^{l}\left(J_{ms} - \frac{i}{2}\Gamma_{ms}\right)b_i(t) - i\sqrt{\gamma_s\gamma_q}\left(J_{sq} - i\frac{\Gamma_{sq}}{2}\right)q(t)$$

$$(5.42b)$$

$$\partial_t q(t) = -\frac{\gamma_q}{2}q(t) - i\sqrt{\gamma_L\gamma_s}\sum_{m=1}^{l}\left(J_{mq} - \frac{i}{2}\Gamma_{mq}\right)b_i(t) - i\sqrt{\gamma_s\gamma_q}\left(J_{qs} - i\frac{\Gamma_{qs}}{2}\right)s(t).$$

$$(5.42c)$$

We introduced the detuning $\delta_{LI} := \omega_I - \omega_L$ between the lattice and impurity atom transition frequencies. Note that the model does not contain any classical driving terms, so the derivatives of the excited state populations don't depend on the ground state population $a(t)$. This set of equations can be written in matrix form

$$i\begin{pmatrix} \dot{b}_1(t) \\ \vdots \\ \dot{b}_l(t) \\ \dot{s}(t) \\ \dot{q}(t) \end{pmatrix} = \begin{pmatrix} & & & c_{1s} & c_{1q} \\ & \mathbf{H}_L & & \vdots & \vdots \\ & & & c_{ls} & c_{lq} \\ c_{s1} & \cdots & c_{sl} & i\gamma_s/2 & c_{sq} \\ c_{q1} & \cdots & c_{ql} & c_{qs} & i\gamma_q/2 \end{pmatrix} \cdot \begin{pmatrix} b_1(t) \\ \vdots \\ b_l(t) \\ s(t) \\ q(t) \end{pmatrix} \qquad (5.43)$$

where the $l \times l$ matrix $\mathbf{H}_L$ represents the bare lattice Hamiltonian matrix containing the terms $\propto (\delta_{LI} - i\gamma_L/2)$ in the diagonal and the coupling terms $\propto (J_{mn} - i\Gamma_{mn}/2)$ in the off-diagonals [see first line in Eq. (5.42a)]. The complex numbers $c_{is,q} = c_{s,qi}$ with $i \in [1, l]$ denote the coupling terms between the lattice atoms and the impurity $\propto J_{ms} - i\Gamma_{ms}/2$, and $c_{sq} = c_{qs}$ denotes the free space coupling of the two impurities s and q.

If $\gamma_{s,q} \ll \gamma_L$, the lattice dynamics can be adiabatically eliminated. Defining the quantities $\mathbf{b}(t) := (b_1(t)\ldots b_l(t))^T$ and the lattice-impurity coupling vectors $\mathbf{C}_{Ls} := (c_{1s}\ldots c_{ls})^T$, $\mathbf{C}_{Lq} := (c_{1q}\ldots c_{lq})^T$ and setting $\dot{b}_i(t) = 0$ results in the steady state for the lattice atoms,

$$\mathbf{b}_{ss}(t) = -\mathbf{H}_L^{-1} \cdot (\mathbf{C}_{Ls}s(t) + \mathbf{C}_{Lq}q(t)). \qquad (5.44)$$

Plugging this back into Eq. (5.43), we obtain the coupled set of equation governing the impurities' dynamics

$$\dot{s}(t) = -i \left[\frac{i}{2} \gamma_s - \mathbf{C}_{sL}^T \cdot \mathbf{H}_L^{-1} \cdot \mathbf{C}_{Ls} \right] s(t) - i \left[c_{sq} - \mathbf{C}_{sL}^T \cdot \mathbf{H}^{-1} \mathbf{C}_{Lq} \right] q(t), \qquad (5.45)$$

$$\dot{q}(t) = -i \left[\frac{i}{2} \gamma_q - \mathbf{C}_{qL}^T \cdot \mathbf{H}_L^{-1} \cdot \mathbf{C}_{Lq} \right] q(t) - i \left[c_{qs} - \mathbf{C}_{qL}^T \cdot \mathbf{H}^{-1} \mathbf{C}_{Ls} \right] s(t), \qquad (5.46)$$

with $\mathbf{C}_{s,qL}^T := (c_{s,q1}, \ldots, c_{s,ql})$. To obtain the effective Hamiltonian given in Eq. (5.32) we have to bring these equations into the form

$$\dot{s}(t) = -i \left[\gamma_s \Sigma_s - i \frac{\gamma_s}{2} \right] s(t) - i \sqrt{\gamma_s \gamma_q} \kappa_s q(t), \qquad (5.47)$$

$$\dot{q}(t) = -i \left[\gamma_q \Sigma_q - i \frac{\gamma_q}{2} \right] q(t) - i \sqrt{\gamma_s \gamma_q} \kappa_q s(t). \qquad (5.48)$$

This results in the following expressions for the self energies and coupling strengths

$$\Sigma_s := -\mathbf{C}_{sL}^T \cdot \mathbf{H}_L^{-1} \cdot \mathbf{C}_{Ls}/\gamma_s, \qquad (5.49)$$

$$\Sigma_q := -\mathbf{C}_{qL}^T \cdot \mathbf{H}_L^{-1} \cdot \mathbf{C}_{Lq}/\gamma_q, \qquad (5.50)$$

$$\kappa_s := \left(c_{sq} - \mathbf{C}_{qL}^T \cdot \mathbf{H}_L^{-1} \cdot \mathbf{C}_{Ls} \right)/\sqrt{\gamma_s \gamma_q}, \qquad (5.51)$$

$$\kappa_q := \left(c_{qs} - \mathbf{C}_{sL}^T \cdot \mathbf{H}_L^{-1} \cdot \mathbf{C}_{Lq} \right)/\sqrt{\gamma_s \gamma_q}. \qquad (5.52)$$

5.7   Appendix: Robustness to noise

To illustrate the robustness of the introduced sensing protocol to external noise, we analyse the role of positional disorder of the array atoms onto the self-energy and coupling strength. Therefore, we randomly sample the lattice positions for each emitter from a Gaussian distribution with a certain width σ centred around the unperturbed lattice points. We determine Σ and κ for 100 lattice realizations (for $R = \gamma_s/\gamma_q = 1$) and plot its mean value together with the standard deviation in Fig. 5.4. Note that positional disorder breaks the lattice symmetry and Bloch's theorem, which was employed in the momentum space representation described above, is no longer valid. Therefore, we perform the adiabatic elimination in real space as outlined above.

The self-energy and the coupling strength are the two quantities at the core of the introduced protocol. The real part of the coupling constant κ changes the timescale of the dynamics, i.e., it has a similar effect as changing the lattice spacing a. As such, in Fig. 5.5a), we see a similar response to $\mathrm{Re}(\kappa_{\mathrm{dis}})$ as changing a, including crossing over resonance points. The imaginary part of κ affects the decay lifetime similarly

75
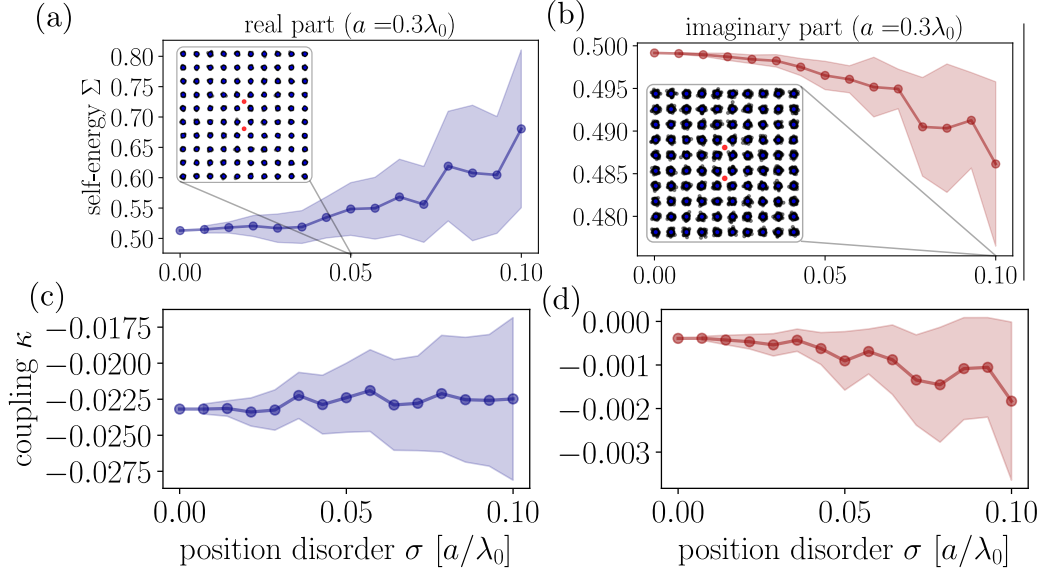
Figure 5.4: **Mean-value and standard deviation** (indicated by blue and red shaded regions) of the real- and imaginary-part of the self-energy Σ (a)-(b) and the coupling strength κ (c)-(d) as a function of position disorder. The insets show the lattice positions realized for a certain position disorder.

to Γ_{coop}. Increasing this parameter can actually *improve* the sensitivity, as seen in Fig. 5.5b). As discussed in SM 5.2.2, the real part of the self-energy Σ simply sets an absolute energy scale and does not affect the dynamics. As such, we do not see any change to σ in panel c) of Fig. 5.5. Finally, altering $\text{Im}(\Sigma)$ directly affects Γ_{coop} and thus can dramatically affect the sensitivity of the protocol. In Fig. 5.4b), we see that a relatively large amount of lattice disorder is required before a significant change in $\text{Re}(\Sigma)$ is observed. In panel d) of Fig. 5.5, we see that the sensitivity remains relatively low for small changes to Σ_{dis}. However, directly changing the imaginary part of Σ is equivalent to changing the cooperative enhancement factor Γ_{coop} directly. Since improvements to this factor exponentially improve the sensitivity, disorder that destroys this enhancement will similarly see a loss of this exponential improvement. Hence, we can see it is important that there is not too much disorder that produces a large change in $\text{Im}(\Sigma)$.
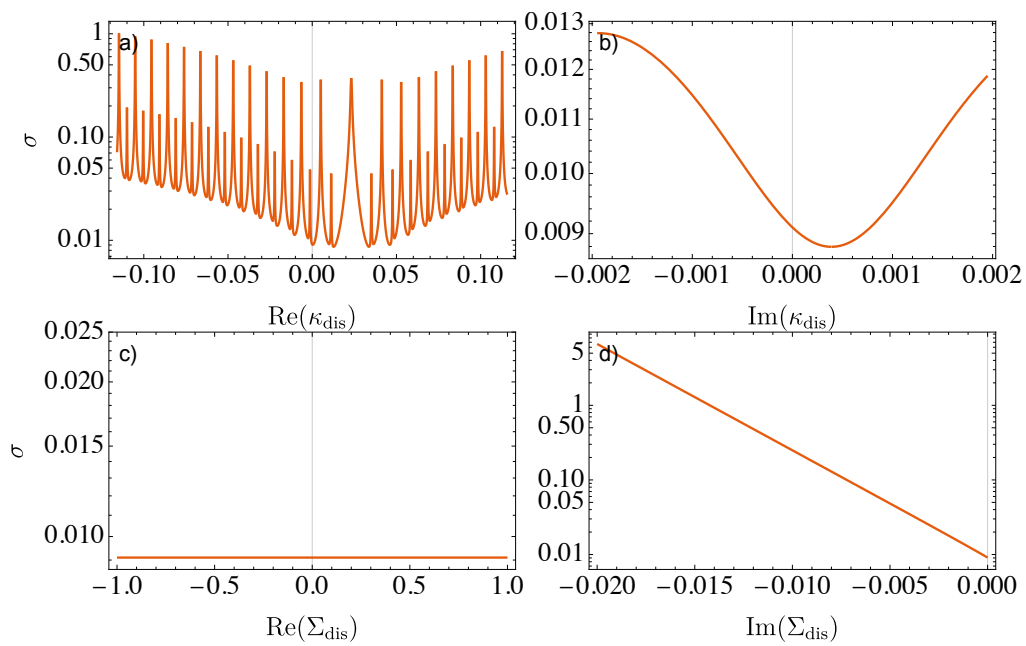
Figure 5.5: **The protocol sensitivity σ with the inclusion of lattice disorder.** a) σ with added real part of the coupling constant κ_{dis}. b) Adding an imaginary κ_{dis}. c) Adding a real part Σ_{dis} to the self-energy Σ. c) Adding an imaginary part Σ_{dis} to the self-energy Σ.

Chapter 6

Frequency dependent squeezing in gravitational wave detectors

The 2015 detection of gravitational waves by the LIGO collaboration [78] ushered in a new era in astronomy. Since then, subsequent measurements [79, 80] has cemented the place of this new era, and subsequent detectors, including LIGO and VIRGO, have made several changes to improve the sensitivity [81, 82]. It has been known since the early '80s [83, 84] that squeezed light can improve the sensitivity of gravitational wave detectors, due to the suppression of quantum noise, and we are now reaching the point where the engineering effort to remove the classical noise has been so successful that quantum noise is now dominant.

A gravitational wave interferometer uses laser light to monitor the position of suspended mirrors which act as test masses. The light produces two types of quantum noise: shot noise, which arises from the random fluctuations of photon arrival time at the photodetectors and radiation pressure noise, which arises from the fluctuations in the laser power, causing movement in the mirror that masks the motion due to the gravitational wave amplitude h.

Shot noise becomes dominant at frequencies in the tens of hertz and has Poissonian statistics, meaning it has a signal-to-noise ratio (SNR) $SNR \sim \frac{N}{\sqrt{N}} = \sqrt{N}$. i.e., the signal grows linearly with photon number, but the corresponding noise introduced only grows as the square root. Thus, shot noise can be counteracted by increasing the laser power, so that the total number of photons reaching the detector is increased.

Radiation pressure noise, on the other hand, dominates at frequencies around 1Hz, corresponding to the resonant frequency of the mirror's harmonic motion. Radiation pressure noise is worsened by increased laser power: as the total power increases, so too do the fluctuations. As expected from the quantum uncertainty principle, we can never get something for free. The tradeoff between these two noise sources has been extensively studied [85] by the quantum measurement community. For a measurement of length τ, quantum mechanics places a limit on the accuracy of a measurement of the position z of a mass, called the "standard quantum limit" [83]

$$(\Delta z)_{\text{SQL}} = \left(\frac{2\pi\tau}{m} \right)^{1/2} \tag{6.1}$$

This correspondingly limits the gravitational wave amplitude h that it is possible to detect with an interferometer

$$h_{\text{SQL}} \sim (\Delta z)_{\text{SQL}}/l \tag{6.2}$$

where l is the interferometer arm length. This scaling with the inverse of length is the reason that ground-based interferometers such as LIGO try to make the arm length as large as possible (4km, in the case of LIGO).

In this chapter, we will analyse a simple theoretical model of an interferometer, and show that by using frequency dependent squeezing, it is possible to suppress the quantum noise across the entire spectral range. In the chapter following, we will detail a scheme for producing frequency dependent squeezing for the purpose of enhancing gravitational wave detection. The figure of merit for this detection is the noise spectral density, i.e., the power spectral density of each noise component (see Fig. 6.1).
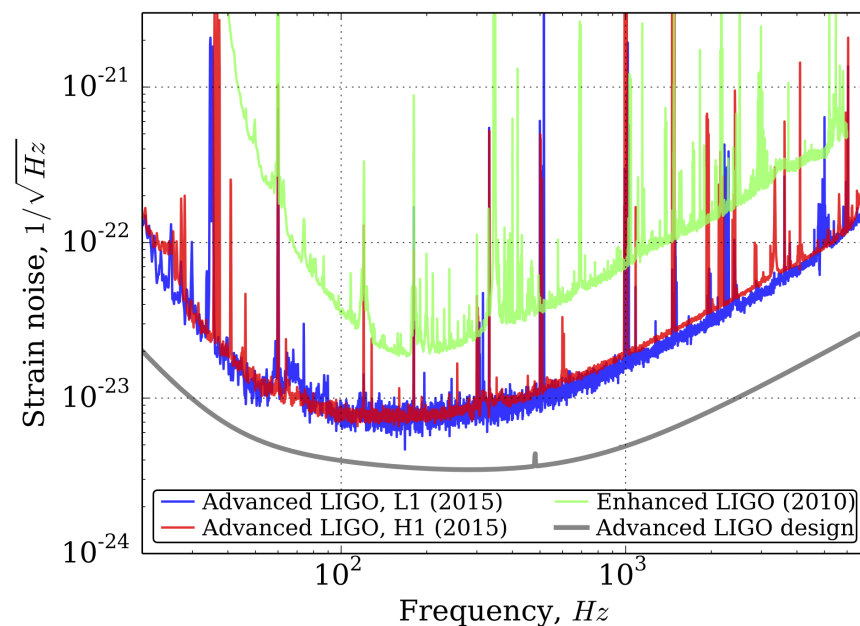
Figure 6.1: **The noise spectral density of different generations of LIGO detectors**. Reproduced from the arXiv version of [3] under the LIGO image use policy [4].

6.1   Squeezing in a toy model of LIGO

We first imagine LIGO as a Mach-Zehnder interferometer interfaced with a cavity with movable mirror on one arm. We include a frequency dependent phase shifter $\varphi(\omega)$ injecting light into the input port. For now, we are simply interested in whether such a phase element can produce any improvement to the sensitivity of LIGO in

principle, and will not pay attention to how one might produce such a phase element. We will first write down the Hamiltonian for the movable cavity mirror, and then write the equation of motion for light in the cavity. We then write down the input-output relation for the cavity and calculate the quadrature modes that will be used to calculate the noise spectral density.
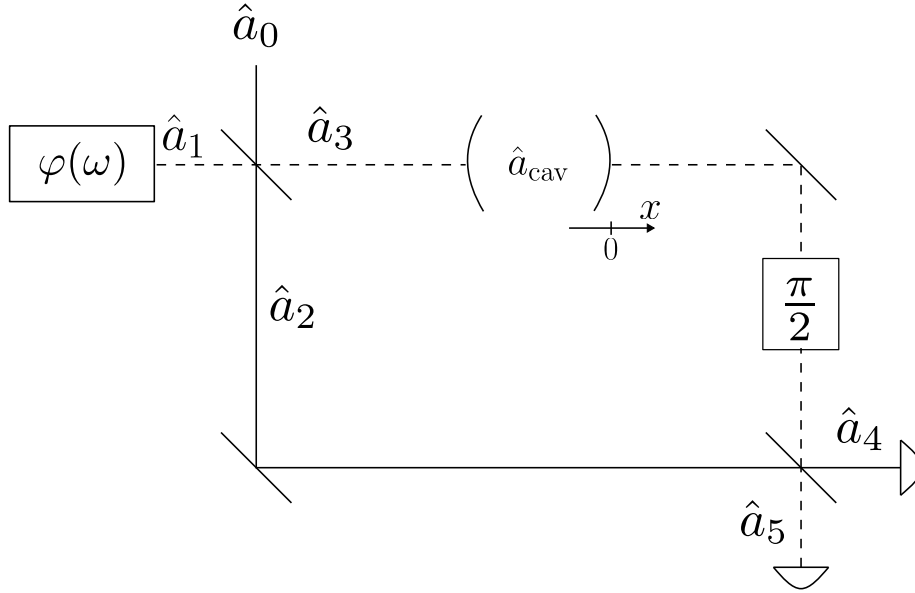
Figure 6.2: **A toy model of LIGO** where the phase difference between arms is produced by a cavity of length L with movable mirror with position coordinate x. We inject light with frequency dependent squeezing angle $\varphi(\omega)$ into the vacuum port of the interferometer. The mode $\hat{a}_0$ is used as the interferometer laser mode, i.e., it is a coherent state.

6.1.1 Hamiltonian for cavity mirror

The cavity in the top arm of Fig. 6.2 is described by a the harmonic oscillator Hamiltonian

$$H_{cav} = \hbar\omega_{cav}\hat{a}^\dagger_{cav}\hat{a}_{cav}, \tag{6.3}$$

where we have dropped the ground state energy $\frac{\hbar\omega_{cav}}{2}$ as it is simply a constant offset.

6.1.1.1 Light resonance condition for a cavity

For light to be resonant within a cavity of length L, the round trip distance $(2L)$ must be equal to an integer multiple of the wavelength, λ. This is so the light constructively interferes, forming a standing wave pattern. $2L = N\lambda$, for $N \in \mathbb{N}$.

The angular frequency of light ω is related to the ordinary frequency f by $\omega = 2\pi f$. Further $f = \frac{v}{\lambda}$, where v is the velocity of the wave. For the case of light, $v = c$. We thus have, for the cavity of length L,

$$\omega_0 = 2\pi \frac{v}{\lambda} = \frac{2\pi c}{2L} = \frac{\pi c}{L} \tag{6.4}$$

Now supposing the cavity mirror is moved some distance $\hat{x}$ from its initial length L, we have

$$\omega_{\text{cav}} = \frac{\pi c}{L + \hat{x}} \tag{6.5}$$

Since we are trying to detect minute displacements from gravitational waves we know that $\hat{x} \ll L$, so we can perform a series expansion to first order in $\hat{x}$, giving

$$\omega_{\text{cav}} \approx \omega_0 \left(1 - \frac{\hat{x}}{L} \right)$$

thus, the Hamiltonian is given by

$$\hat{H}_{\text{cav}} \approx \hbar\omega_0 \left(1 - \frac{\hat{x}}{L} \right) \hat{a}_{\text{cav}}^\dagger \hat{a}_{\text{cav}} \tag{6.6}$$

6.1.2 Mirror equation of motion

We have the equations of motion

$$\dot{\hat{x}}(t) = \frac{1}{m}\hat{p}(t) \tag{6.7}$$

$$\dot{\hat{p}}(t) = -m\omega_m^2 \hat{x}(t) - \gamma p(t) + F_{\text{ba}}(t) + F_{\text{s}}(t) + F_{\text{d}}(t) \tag{6.8}$$

Where F_{ba} is the back action, F_d is a classical diffusive force and F_s is the force due to the gravitational wave signal.

The back action can be written

$$F_{ba} = \dot{p}_{cav} = \frac{\partial H_{cav}}{\partial x} = \frac{\hbar\omega_0}{L}\hat{a}^\dagger_{cav}\hat{a}_{cav} \tag{6.9}$$

Expanding $\hat{a}_{cav} = \delta\hat{a}_{cav} + \alpha_{cav}$, we find

$$\hat{F}_{ba} = \frac{\hbar\omega_0}{L}\left(\delta\hat{a}^\dagger_{cav} + \alpha^*_{cav}\right)\left(\delta\hat{a}_{cav} + \alpha_{cav}\right) \tag{6.10}$$

$$= \frac{\hbar\omega_0}{L}\left[\cancel{\delta\hat{a}^\dagger_{cav}\delta\hat{a}_{cav}} + \delta\hat{a}^\dagger_{cav} + \alpha^*_{cav}\delta\hat{a}_{cav} + |\alpha_{cav}|^2\right] \tag{6.11}$$

We similarly expand $\hat{x} = \delta\hat{x} + \langle x\rangle$ and collect only the time dependent terms in (6.8) (neither $\langle x\rangle$ nor $|\alpha|^2$ carry time-dependence.)

$$\dot{\hat{p}}(t) = -m\omega_m^2\delta\hat{x}(t) - \gamma\hat{p}(t) + \frac{\hbar\omega_0}{L}\left(\alpha^*_{cav}\delta\hat{a}_{cav} + \alpha_{cav}\delta\hat{a}^\dagger_{cav}\right) + \hat{F}_d + \hat{F}_s \tag{6.12}$$

Taking the Fourier transform, we arrive at

$$-i\omega\hat{p}(\omega) = -m\omega_m^2\delta\hat{x}(\omega) - \gamma\hat{p}(\omega) + \frac{\hbar\omega_0}{L}\left[\alpha^*_{cav}\delta\hat{a}_{cav}(\omega) + \alpha_{cav}\delta\hat{a}^\dagger_{cav}(-\omega)\right]$$
$$+ \hat{F}_d(\omega) + \hat{F}_s(\omega) \tag{6.13}$$

Fourier transforming (6.7) gives

$$-i\omega\delta\hat{(}\omega) = \frac{\hat{p}(\omega)}{m} \tag{6.14}$$

$$\Rightarrow \hat{p}(\omega) = -i\omega m\delta\hat{x}(\omega) \tag{6.15}$$

Substituting into (6.13), we obtain

$$\delta\hat{x}(\omega)\left[m\omega_m^2 - m\omega^2 - i\gamma m\omega\right] = \frac{\hbar\omega_0}{L}\left[\alpha^*_{cav}\delta\hat{a}_{cav}(\omega) + \alpha_{cav}\delta\hat{a}^\dagger_{cav}(-\omega)\right] + \hat{F}_d(\omega) + \hat{F}_s(\omega) \tag{6.16}$$

Let $\chi_m^{-1} = m(\omega_m^2 - \omega^2 - i\gamma\omega)$ and write

$$\delta\hat{x}(\omega) = \chi_m\left[\frac{\hbar\omega_0}{L}\left(\alpha^*_{cav}\delta\hat{a}_{cav}(\omega) + \alpha_{cav}\delta\hat{a}^\dagger_{cav}(-\omega)\right) + \hat{F}_d(\omega) + \hat{F}_s(\omega)\right] \tag{6.17}$$

Writing $\delta\hat{a}^\dagger(-\omega) = \delta\hat{X}(\omega) + i\delta\hat{P}(\omega)$ and $\delta\hat{a}(\omega) = \delta\hat{X}(\omega) - \delta\hat{P}(\omega)$, we have

$$\delta\hat{x}(\omega) = \chi_m\left[\frac{\hbar\omega_0}{L}\left(i\delta\hat{P}(\omega)(\alpha_{cav} - \alpha^*_{cav}) + \delta\hat{X}(\omega)(\alpha_{cav} + \alpha^*_{cav})\right) + \hat{F}_d(\omega) + \hat{F}_s(\omega)\right] \tag{6.18}$$

6.1.3 Light equation of motion

The equation of motion for light in the cavity is

$$\dot{\hat{a}}_{cav} = -\kappa\hat{a}_{cav} + \sqrt{2\kappa}\hat{a}_{in} + \frac{i}{\hbar}[\hat{H},\hat{a}_{cav}] \tag{6.19}$$

$$\hat{a}_{out} = \hat{a}_{in} - \sqrt{2\kappa}\hat{a}_{cav} \tag{6.20}$$

Recalling that the cavity Hamiltonian (6.6) and computing the commutator $[\hat{H},\hat{a}_{cav}] = \hbar\omega_0\hat{a}_{cav}\left(\frac{\hat{x}}{L} - 1\right)$, we can write

$$\dot{\hat{a}}_{cav} = -\kappa\hat{a}_{cav} + \sqrt{2\kappa}\hat{a}_{in} + i\omega_0\hat{a}_{cav}\left(\frac{\hat{x}}{L} - 1\right) \tag{6.21}$$

We will write the operators in the laser frame with the transformation $\hat{a} \rightarrow \hat{a}e^{-i\omega_L t}$. This affects the time derivative on the left hand side but leaves the remaining terms unchanged (after multiplying through by $e^{i\omega_L t}$)

$$\dot{\hat{a}}_{cav} - i\omega_L\hat{a}_{cav} = -\kappa\hat{a}_{cav} + \sqrt{2\kappa}\hat{a}_{in} + i\omega_0\hat{a}_{cav}\left(\frac{\hat{x}}{L} - 1\right) \tag{6.22}$$

Writing our operators as a mean value + fluctuation, we can make the transformation $\hat{a} = \delta\hat{a} + \underbrace{\langle a \rangle}_{=\alpha}$ and $\hat{x} = \delta x + \langle x \rangle$ and write

$$\delta\dot{\hat{a}}_{cav} + \dot{\alpha}_{cav} + \kappa(\delta\hat{a}_{cav} + \alpha_{cav}) =$$

$$\sqrt{2\kappa}\left(\delta\hat{a}_{in} + \alpha_{in}\right) + i\left[\underbrace{\omega_0\left(\frac{\langle x \rangle}{L} - 1\right) + \omega_L}_{\Delta=\omega_L-\omega_0'=0} + \frac{\omega_0\delta\hat{x}}{L}\right](\delta_{cav} + \alpha_{cav}), \tag{6.23}$$

and linearise our equations, i.e., taking terms to first order in the fluctuations only

$$\delta\dot{\hat{a}}_{cav} + \kappa\delta\hat{a}_{cav} = \sqrt{2\kappa}\delta\hat{a}_{in} + i\frac{\omega_0\delta\hat{x}}{L}\alpha_{cav} \tag{6.24}$$

Fourier transforming, we obtain

$$(\kappa - i\omega)\delta\hat{a}_{cav}(\omega) = \sqrt{2\kappa}\delta\hat{a}_{in}(\omega) + i\frac{\omega_0\delta\hat{x}(\omega)}{L}\alpha_{cav} \tag{6.25}$$

We would like to re-write in terms of the quadrature operators $\delta\hat{X}(\omega) = \frac{1}{2}\left(\delta\hat{a}^\dagger(-\omega) + \delta\hat{a}(\omega)\right)$ and $\delta\hat{P}(\omega) = \frac{1}{2i}\left(\delta\hat{a}^\dagger(-\omega) - \delta\hat{a}(\omega)\right)$. Taking the complex conjugate and performing $\omega \to -\omega$, we obtain

$$(\kappa - i\omega)\delta\hat{a}^\dagger_{cav}(-\omega) = \sqrt{2\kappa}\delta\hat{a}^\dagger_{in}(-\omega) - i\frac{\omega_0 \delta\hat{x}(\omega)}{L}\alpha_{cav} \tag{6.26}$$

where $(\delta x(-\omega))^\dagger = \delta x(\omega)$ by the definition of the Fourier transform (see Appendix 6.5), recalling that $\delta\hat{x}^\dagger(t) = \delta\hat{x}(t)$ because $\hat{x}$ is an observable and therefore Hermitian. Performing $\frac{1}{2}((6.25) + (6.26))$ and $\frac{1}{2i}((6.25) - (6.26))$

$$(\kappa - i\omega)\,\delta\hat{X}_{cav}(\omega) + \frac{i\omega_0\delta\hat{x}(\omega)}{2L}(\alpha^*_{cav} - \alpha_{cav}) = \sqrt{2\kappa}\delta\hat{X}_{in}(\omega) \tag{6.27}$$

$$(\kappa - i\omega)\,\delta\hat{P}_{cav}(\omega) + \frac{\omega_0\delta\hat{x}(\omega)}{2L}(\alpha_{cav} + \alpha^*_{cav}) = \sqrt{2\kappa}\delta\hat{P}_{in}(\omega) \tag{6.28}$$

Combining these two equations with (6.18), we obtain the matrix equations

$$\begin{pmatrix} \kappa - i\omega & 0 & \frac{i\omega_0}{2L}\left(\alpha_{\text{cav}}{}^* - \alpha_{\text{cav}}\right) \\ 0 & \kappa - i\omega & \frac{\omega_0}{2L}\left(\alpha_{\text{cav}}{}^* + \alpha_{\text{cav}}\right) \\ \frac{\hbar\omega_0}{L}\left(\alpha_{\text{cav}}{}^* + \alpha_{\text{cav}}\right) & \frac{i\hbar\omega_0}{L}\left(\alpha_{\text{cav}} - \alpha_{\text{cav}}{}^*\right) & \frac{1}{\chi_m(\omega)} \end{pmatrix} \begin{pmatrix} \delta\hat{X}_{cav}(\omega) \\ \delta\hat{P}_{cav}(\omega) \\ \delta\hat{x} \end{pmatrix} = \begin{pmatrix} \sqrt{2\kappa}\delta\hat{X}_{in} \\ \sqrt{2\kappa}\delta\hat{P}_{in} \\ \hat{F}_s + \hat{F}_d \end{pmatrix} \tag{6.29}$$

We can invert this equation to obtain

$$\begin{pmatrix} \delta\hat{X}_{cav}(\omega) \\ \delta\hat{P}_{cav}(\omega) \\ \delta\hat{x} \end{pmatrix} = \begin{pmatrix} \frac{1}{\kappa - i\omega} & 0 & 0 \\ \frac{2\hbar|\alpha_{\text{cav}}|^2\omega_0^2\chi_m(\omega)}{L^2(\kappa - i\omega)^2} & \frac{1}{\kappa - i\omega} & -\frac{|\alpha_{\text{cav}}|\omega_0\chi_m(\omega)}{L(\kappa - i\omega)} \\ -\frac{2\hbar|\alpha_{\text{cav}}|\omega_0\chi_m(\omega)}{L(\kappa - i\omega)} & 0 & \chi_m(\omega) \end{pmatrix} \begin{pmatrix} \sqrt{2\kappa}\delta\hat{X}_{in} \\ \sqrt{2\kappa}\delta\hat{P}_{in} \\ \hat{F}_s + \hat{F}_d \end{pmatrix} \tag{6.30}$$

This equation describes the response of the system inside the cavity, but we want to additionally include the rest of the interferometer, which will input and output light.

6.1.4 Cavity input output relation and quadrature modes

As such, we begin by writing the input-output relation for the cavity mode $\hat{a}_{\text{cav}}$ and write the fluctuations about this cavity mode $\delta\hat{a}_{\text{cav}}$.

$$\hat{a}_{out} = \hat{a}_{in} - \sqrt{2\kappa}\hat{a}_{cav} \tag{6.31}$$

$$\Rightarrow \delta\hat{a}_{out} = \delta\hat{a}_{in} - \sqrt{2\kappa}\delta\hat{a}_{cav} \tag{6.32}$$

Since $\delta\hat{X}$ and $\delta\hat{P}$ are linear in $\delta\hat{a}$, we can simply write

$$\delta\hat{Y}_{out} = \delta\hat{Y}_{in} - \sqrt{2\kappa}\delta Y_{cav} \tag{6.33}$$

Where Y is a generalized quadrature operator that can be any linear combination of $\delta\hat{a}$. Combining with (6.30), we find that

$$\delta\hat{X}_{out} = -\frac{\delta\hat{X}_{in}(\kappa + i\omega)}{\kappa - i\omega} \tag{6.34}$$

$$\delta\hat{P}_{out} = \frac{\sqrt{2}\alpha\sqrt{\kappa}\chi\omega 0\left(\hat{F}_d + \hat{F}_s\right)}{L(\kappa - i\omega)} - \frac{\delta\hat{P}_{in}(\kappa^2 + \omega^2)}{(\kappa - i\omega)^2} - \frac{4\alpha^2\kappa\chi\omega 0^2\hbar\delta\hat{X}_{in}}{L^2(\kappa - i\omega)^2} \tag{6.35}$$

Now we define $g = \frac{2\alpha\omega_0\sqrt{\hbar}}{L\sqrt{\kappa m}}$ and $F_s = \delta x_s/\chi$

$$\delta\hat{P}_{out} = \frac{g\kappa\sqrt{m}\left(\chi F_d + \delta x_s\right)}{\sqrt{2}\sqrt{\hbar}(\kappa - i\omega)} - \frac{g^2\kappa^2 m\chi\delta\hat{X}_{in}}{(\kappa - i\omega)^2} - \frac{\delta\hat{P}_{in}(\kappa^2 + \omega^2)}{(\kappa - i\omega)^2} \tag{6.36}$$

$$
\begin{aligned}
P_{out} = &-P_{in}e^{2i\theta} - X_{in}\frac{g^2|\mathcal{L}(\omega)|^2}{i\gamma + \omega^2 - \omega_m^2}e^{2i\theta} \\
&+ \frac{e^{i\theta}g|\mathcal{L}(\omega)}{\sqrt{2\hbar m}(i\gamma\omega + \omega^2 - \omega_m^2)}F_d + \frac{e^{i\theta}g|\mathcal{L}(\omega)\sqrt{m}}{\sqrt{2\hbar}}\delta x_s
\end{aligned} \tag{6.37}
$$

where $\mathcal{L}(\omega) = \frac{\kappa}{\kappa + i\omega} = \frac{\kappa}{\sqrt{\kappa^2 + \omega^2}}e^{i\theta}$ i.e.,

$$|\mathcal{L}(\omega)| = \frac{\kappa}{\sqrt{\kappa^2 + \omega^2}} \tag{6.38}$$

$$\Rightarrow |\mathcal{L}(\omega)|^2 = \frac{\kappa^2}{\kappa^2 + \omega^2} \tag{6.39}$$

These output modes can be used to calculate the output intensity of the interferometer, which we can use to calculate the noise spectral density.

6.2 Noise spectral density

Analysing the interferometer modes (see appendix 6.6) allows us to express the homodyne photocurrent in terms of the P quadrature

$$I = 2i\alpha_2 P_{out} \tag{6.40}$$

Inserting P_{out} from above and normalising by dividing by the signal term (the coefficient of δx_s), we have the normalised photocurrent

$$
\begin{aligned}
I_{norm} = \Big(& (\sin(\varphi)X - \cos(\varphi)P)\, e^{i\theta} \frac{\sqrt{2\hbar}}{\sqrt{m}g|\mathcal{L}(\omega)|} - (\cos(\varphi)X + \sin(\varphi)P)\frac{g|\mathcal{L}(\omega)e^{i\theta}\sqrt{2\hbar}}{\sqrt{m}(i\gamma\omega + \omega^2 - \omega_m^2)} \\
& + \delta x_s + \frac{F_d}{m(i\gamma\omega + \omega^2 - \omega_m^2)} \Big)
\end{aligned}
\tag{6.41}
$$

We can write $I_{norm} = \delta x_s + \delta I$, i.e., split into signal and noise components. Let $\chi^{-1} = (\omega_m^2 - \omega^2 - i\gamma\omega)$ and define $\mathcal{A} = \frac{\sqrt{2\hbar}}{g\sqrt{m}|\mathcal{L}(\omega)|}$ and $\mathcal{B} = \frac{g\sqrt{2\hbar}|\mathcal{L}(\omega)|}{\sqrt{m}\chi^{-1}}$. We now write

$$
\delta I = \mathcal{A}e^{i\theta}(X\sin(\varphi) - P\cos(\varphi)) - \mathcal{B}e^{i\theta}(P\sin(\varphi) + X\cos(\varphi)) + \frac{F_d}{m\chi^{-1}}
\tag{6.42}
$$

We can then find the noise spectral density $\mathcal{S}_{\delta I}$, where we inject squeezed light into the vacuum port with squeezing parameter S. We obtain

$$
\mathcal{S}_{\delta I}\delta(\omega - \omega') = \frac{1}{2}\langle \delta I^\dagger \delta I + \delta I \delta I^\dagger \rangle
\tag{6.43}
$$

$$
\begin{aligned}
= \frac{1}{2}\Bigg(& \frac{1}{2}|\mathcal{A}|^2\left(S^{-1}\sin^2(\varphi) + S\cos^2(\varphi)\right) + |\mathcal{AB}|\left(S - S^{-1}\right)\sin(\varphi)\cos(\varphi) \\
& + \frac{1}{2}|\mathcal{B}|^2\left(S\sin^2(\varphi) + S^{-1}\cos^2(\varphi)\right) + \frac{\langle F_d^\dagger \cdot F_d\rangle}{m^2|\chi|^{-2}} + \frac{\langle F_d \cdot F_d^\dagger\rangle}{m^2|\chi|^{-2}} \Bigg)
\end{aligned}
\tag{6.44}
$$

where the cross terms cancel, and we have made use of $\langle X^\dagger X\rangle = \langle XX^\dagger\rangle = \frac{1}{4}S^{-1}$ and $\langle P^\dagger P\rangle = \langle PP^\dagger\rangle = \frac{1}{4}S$

Throwing away the classical terms given by F_d, and inserting the definitions of $\mathcal{A}, \mathcal{B}$ we have

$$
\begin{aligned}
\mathcal{S}_{\delta I}\delta(\omega - \omega') = \frac{1}{2}\Bigg(& \frac{\hbar}{g^2 m\,|\mathcal{L}(\omega)|^2}\left(S^{-1}\sin^2(\varphi) + S\cos^2(\varphi)\right) + \frac{2\hbar}{m|\chi^{-1}|}\left(S - S^{-1}\right)\sin(\varphi)\cos(\varphi) \\
& + \frac{g^2\hbar\,|\mathcal{L}(\omega)|^2}{m\,|\chi^{-1}|^2}\left(S\sin^2(\varphi) + S^{-1}\cos^2(\varphi)\right) \Bigg)
\end{aligned}
\tag{6.45}
$$

Letting $i\gamma\omega \ll \omega^2 - \omega_m^2$ and recalling that $\chi^{-1} = (\omega_m^2 - \omega^2 - i\gamma\omega)$, we can write

$$\mathcal{S}_{\delta I}\delta(\omega - \omega') = \frac{1}{2}\left(\frac{\hbar}{g^2 m\,|\mathcal{L}(\omega)|^2}\left(S^{-1}\sin^2(\varphi) + S\cos^2(\varphi)\right) + \frac{2\hbar}{m|\omega^2 - \omega_m^2|}\left(S - S^{-1}\right)\sin(\varphi)\cos(\varphi)\right.$$

$$\left. + \frac{g^2\hbar\,|\mathcal{L}(\omega)|^2}{m\,|\omega^2 - \omega_m^2|^2}\left(S\sin^2(\varphi) + S^{-1}\cos^2(\varphi)\right)\right) \tag{6.46}$$

Now we can identify a characteristic noise spectral density $\mathcal{S}_c = \frac{\hbar}{mg_{LIGO}^2}$. We can then obtain the quantity $\Sigma = \frac{\mathcal{S}_{\delta I}}{\mathcal{S}_c}$ We obtain

$$\Sigma = \frac{g_{LIGO}^2}{2g^2|\mathcal{L}(\omega)|^2}(S^{-1}\sin^2(\varphi) + S\cos^2(\varphi)) + \frac{g^2 g_{LIGO}^2|\mathcal{L}(\omega)|^2}{2|\omega^2 - \omega_m^2|^2}\left(S\sin^2(\varphi) + S^{-1}\cos^2(\varphi)\right)$$

$$+ (S - S^{-1})\sin(\varphi)\cos(\varphi)\frac{g_{LIGO}^2}{\omega^2 - \omega_m^2} \tag{6.47}$$

6.2.1 Optimal phase angle

To find the optimal phase angle, Σ is differentiated with respect to the phase angle. The extrema are given by $\frac{d\Sigma}{d\varphi} = 0$.

$$0 = \frac{d}{d\varphi}\Sigma = \left(S - S^{-1}\right)\left(\frac{g_{LIGO}^2}{\omega^2 - \omega_m^2}\cos(2\varphi) + \frac{g_{LIGO}^2\left(g^4\,|\mathcal{L}(\omega)|^4 - |\omega^2 - \omega_m^2|^2\right)}{2g^2\,|\mathcal{L}(\omega)|^2\,|\omega^2 - \omega_m^2|^2}\sin(2\varphi)\right) \tag{6.48}$$

$$\Rightarrow \tan(2\varphi) = \frac{2g^2\,|\mathcal{L}(\omega)|^2\,|\omega^2 - \omega_m^2|^2}{(\omega^2 - \omega_m^2)\left(g^4\,|\mathcal{L}(\omega)|^4 - |\omega^2 - \omega_m^2|^2\right)} \tag{6.49}$$

Assuming that $\omega_m < \omega$, we can write $|\omega^2 - \omega_m^2| = \omega^2 - \omega_m^2$ This gives

$$\tan(2\varphi) = \frac{2g^2\left(\omega^2 - \omega_m^2\right)|\mathcal{L}(\omega)|^2}{g^4\,|\mathcal{L}(\omega)|^4 - (\omega^2 - \omega_m^2)^2} \tag{6.50}$$

Now we use the identity $\tan(2\theta) = \frac{2\tan(\theta)}{1-\tan^2(\theta)}$. We have an equation in $x = \tan(\varphi)$

$$\frac{2x}{1 - x^2} = \frac{2g^2\left(\omega^2 - \omega_m^2\right)|\mathcal{L}(\omega)|^2}{g^4\,|\mathcal{L}(\omega)|^4 - (\omega^2 - \omega_m^2)^2} \tag{6.51}$$

which has solutions

$$x_{\min} = \frac{\omega^2 - \omega_m^2}{g^2\,|L(\omega)|^2}, \qquad\qquad x_{\max} = -\frac{g^2\,|L(\omega)|^2}{\omega^2 - \omega_m^2} \qquad (6.52)$$

$$\Rightarrow \varphi_{\min} = \arctan\left(\frac{\omega^2 - \omega_m^2}{g^2\,|L(\omega)|^2}\right), \qquad \varphi_{\max} = \arctan\left(-\frac{g^2\,|L(\omega)|^2}{\omega^2 - \omega_m^2}\right) \qquad (6.53)$$

6.2.2 Comparison with unsqueezed state

We then insert these extremal angles into Eq.(6.47) to give an optimal noise spectral density. Using $x\cos(\arctan(x)) = \sin(\arctan(x)) = \frac{x}{\sqrt{x^2+1}}$, we compute Σ for $\varphi_{\min}$ and $\varphi_{\max}$, respectively. We obtain

$$\Sigma_{\min} = \frac{1}{S}\left(\frac{g_{LIGO}^2}{2}\left(\frac{1}{g^2|\mathcal{L}(\omega)|^2} + \frac{g^2|\mathcal{L}(\omega)|^2}{|\omega^2 - \omega_m^2|^2}\right)\right) = \frac{\Sigma_{\text{un-squeezed}}}{S} \qquad (6.54)$$

$$\Sigma_{\max} = S\Sigma_{\text{un-squeezed}} \qquad (6.55)$$

i.e., we obtain perfect broadband squeezing across the entire spectral range. This noise spectral density is plotted in Fig. 6.3. When we throw away the classical terms $\hat{F}_d$, we have made Σ into close to a perfect square, bar the sine and cosine contributions, which are equal when $S = 1$ (i.e., when we do not have squeezing). This broadband suppression of noise has been known at least since the analysis of Kimble et al. [86].
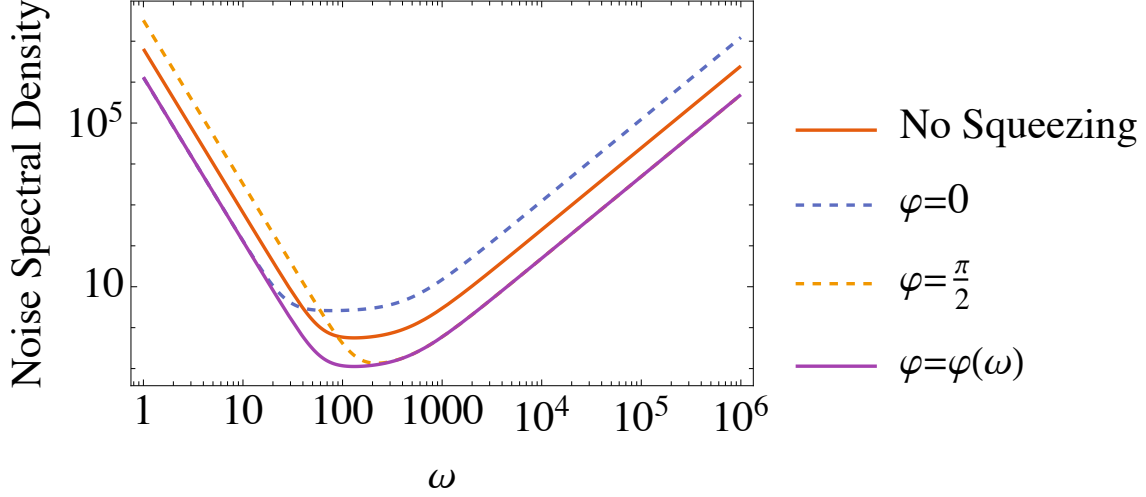
Figure 6.3: **The noise spectral density of the interferometer at different squeezing settings**. A squeezing angle of $\phi = 0$ corresponds to back action suppression at low frequencies, whilst a squeezing angle of $\varphi = \pi/2$ corresponds to shot noise suppression, which dominates at high frequencies. We also show the noise spectral density with the calculated optimal phase angle $\varphi = \varphi_{\min}(\omega)$ which shows a fixed broadband suppression across the entire spectral range.

6.3 Frequency dependent squeezing via a filter cavity

We have, as yet, not considered how one might produce the frequency dependent squeezing $\varphi(\omega)$ that we need. Below, we will consider the case of a filter cavity with cavity mode $\hat{a}$ with equation of motion in Fourier space given by

$$-i\hat{a}\omega = \hat{a}_{\rm in}\sqrt{\kappa_{\rm out}} - \frac{\hat{a}\kappa}{2} + \hat{a}_{\rm loss}\sqrt{\kappa_{\rm loss}} \tag{6.56}$$

We have here used the conventions compatible with the Langevin equations for a 3-level atom in a Lambda configuration, that will later be used for an EIT analysis. The above equation can be obtained by setting the atom-light coupling g to zero, such that the equations correspond to an empty cavity.

Solving along with the input-output relation $\hat{a} = \frac{\hat{a}_{\rm in}+\hat{a}_{\rm out}}{\sqrt{\kappa_{\rm out}}}$, we obtain a reflection coefficient
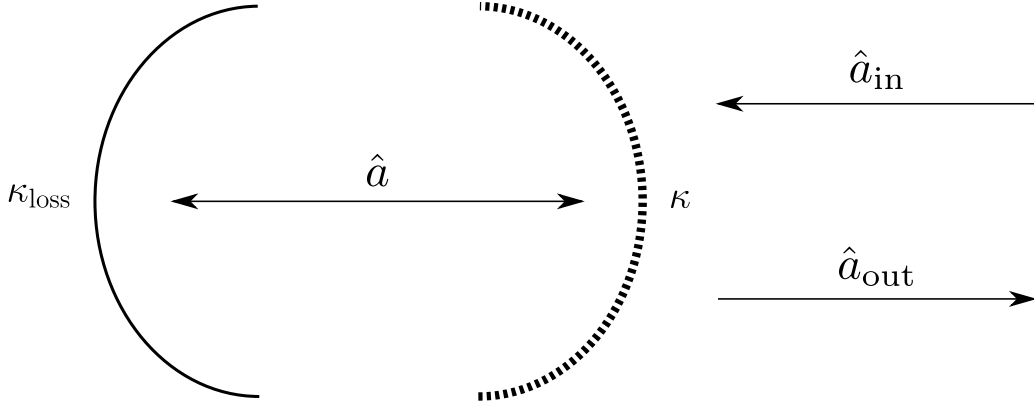
Figure 6.4: Schematic of one-sided cavity with cavity mode $\hat{a}$, along with input mode $\hat{a}_{\text{in}}$ and output mode $\hat{a}_{\text{out}}$. We consider possible losses from the 'wrong' side of the cavity κ_s, but express in terms of the cavity κ as $\kappa_{\text{loss}} = \kappa_s/\kappa$.

$$r = \frac{a_{\text{out}}}{a_{\text{in}}} = \frac{-\kappa + 2\kappa\left(1 - \kappa_{\text{loss}}\right) + 2i\omega}{\kappa - 2i\omega} \tag{6.57}$$

where we have written the cavity out-coupling in terms of the cavity coupling κ with a loss term κ_{loss}, i.e., $\kappa_{\text{out}} = \kappa\left(1 - \kappa_{\text{loss}}\right)$. The scattering angle θ in the lossy case is

$$\theta = -2\tan^{-1}\left(\frac{4\kappa\omega\left(\kappa_{\text{loss}} - 1\right)}{\kappa^2\left(\sqrt{\frac{\kappa^2(1-2\kappa_{\text{loss}})^2+4\omega^2}{\kappa^2+4\omega^2}} - 2\kappa_{\text{loss}} + 1\right) + 4\omega^2\left(\sqrt{\frac{\kappa^2(1-2\kappa_{\text{loss}})^2+4\omega^2}{\kappa^2+4\omega^2}} - 1\right)}\right) \tag{6.58}$$

In the lossless case, we have simply

$$r = \frac{\kappa + 2i\omega}{\kappa - 2i\omega} \tag{6.59}$$

and a scattering angle

$$\theta = 2\tan^{-1}\left(\frac{2\omega}{\kappa}\right) \tag{6.60}$$

Now we can define our squeezing rotation angle

$$\varphi = \frac{\theta(\omega + \omega_i) + \theta(-\omega + \omega_i)}{2} \tag{6.61}$$

$$= \tan^{-1}\left(\frac{2\left(\omega_i - \omega\right)}{\kappa}\right) + \tan^{-1}\left(\frac{2\left(\omega_i + \omega\right)}{\kappa}\right) \tag{6.62}$$

$$= \tan^{-1}\left(\frac{4\kappa\omega_i}{-4\omega_i^2 + \kappa^2 + 4\omega^2}\right) \tag{6.63}$$

where ω_i is the frequency of the interferometer laser and where we have used the identity $\tan^{-1}(u) \pm \tan^{-1}(v) = \tan^{-1}\left(\frac{u \pm v}{1 \mp uv}\right)$, and where ω_i is the frequency of the interferometer light.

Physically, we can shift our ϕ by introducing a fixed phase delay. Mathematically, a $\pi/2$ constant shift is obtained by taking the limit of the above identity as $v \to \infty$. This yields $\tan^{-1}(u) + \frac{\pi}{2} = -\tan^{-1}\left(\frac{1}{u}\right)$ We will hence work with the function

$$\phi = \tan^{-1}\left(-\frac{-4\omega_i^2 + \kappa^2 + 4\omega^2}{4\kappa\omega_i}\right) \tag{6.64}$$

We can compare this to the optimal phase for LIGO

$$\phi_{\text{LIGO}} = \tan^{-1}\left(\frac{\omega^2\left(\kappa_{\text{LIGO}}^2 + \omega^2\right)}{g_{\text{LIGO}}^2\kappa_{\text{LIGO}}^2}\right) \tag{6.65}$$

Comparing the arguments of the arctan functions, we find that

$$\frac{\omega^4}{g_{\text{LIGO}}^2\kappa_{\text{LIGO}}^2} + \frac{\omega^2}{g_{\text{LIGO}}^2} = -\frac{\omega^2}{\kappa\omega_i} + \frac{\omega_i}{\kappa} - \frac{\kappa}{4\omega_i} \tag{6.66}$$

and matching coefficients, we find that

$$\omega_i = -\frac{1}{\sqrt{2}}g_{\text{LIGO}} \tag{6.67}$$

$$\kappa = \sqrt{2}g_{\text{LIGO}} \tag{6.68}$$

where we have taken the solution with $\kappa \in \mathbb{R}_{>0}$. We note also that this matching becomes exact as $\kappa_{\text{LIGO}} \to \infty$.

6.4 Summary and conclusion

In this chapter, we have analysed a toy model of the LIGO interferometer and found that we can produce a suppression of the noise across the entire spectral range. The concept requires the production of frequency-dependent squeezing, which we showed can be produced by a filter cavity. Despite the considerable experimental difficulties, proof of principle experiments for these filter cavities have already been conducted [87, 88]. In the next chapter, we model a system that can potentially mimic the effects of the filter cavity, whilst circumventing some of the associated experimental difficulties.

6.5 Appendix: Fourier transform convention

In this appendix, we detail the Fourier transform convention used throughout the gravitational wave chapters. We have continuous operators with the following commutation rules

$$[\hat{a}(t), \hat{a}^\dagger(t')] = \delta(t - t') \tag{6.69}$$

and

$$[\hat{a}(t), \hat{a}(t')] = [\hat{a}^\dagger(t), \hat{a}^\dagger(t')] = 0. \tag{6.70}$$

In the time domain $\hat{X}(t) = \frac{1}{2}(\hat{a}^\dagger(t) + \hat{a}(t))$, we can see that $\hat{X}^\dagger(t) = \hat{X}(t)$. However, to take the Fourier transform, we need to make some choice for what to do with the transform of $\hat{a}^\dagger$

$$\hat{a}(\omega) = \frac{1}{\sqrt{2\pi}} \int_{-\infty}^{\infty} a(t)e^{i\omega t}dt \tag{6.71}$$

Since the Fourier transform takes us out of the reals, the resulting operators do not have the same properties under conjugation. In particular, if we make the following choice (taking the hermitian conjugate of the entire Fourier transform above)

$$\hat{a}^\dagger(\omega) = \frac{1}{\sqrt{2\pi}} \int_{-\infty}^{\infty} a^\dagger(t)e^{-i\omega t}dt \tag{6.72}$$

Then we will have

$$\Rightarrow \hat{a}^\dagger(-\omega) = \frac{1}{\sqrt{2\pi}} \int_{-\infty}^{\infty} \hat{a}^\dagger(t)e^{i\omega t}dt \tag{6.73}$$

This choice of convention implies that

$$(\hat{a}(\omega))^\dagger = \hat{a}^\dagger(\omega) \tag{6.74}$$

$$\Rightarrow (\hat{a}(-\omega))^\dagger = \hat{a}^\dagger(-\omega), \tag{6.75}$$

i.e., there is no ambiguity in the notation. However, it also implies that the Fourier transform of $\hat{a}^\dagger(t) \xrightarrow{F.T} \hat{a}^\dagger(-\omega)$. Since we will frequently need to manipulate our operators in either the time domain or the Fourier domain, this is a helpful choice of definition, since we only have to be careful when actually making our Fourier transforms. Everything else just works as expected.

This choice affects the commutation relation $[a(\omega), a^\dagger(\omega')]$. For our choice, we have

$$[\hat{a}(\omega), \hat{a}^\dagger(\omega')] = \frac{1}{2\pi} \int \hat{a}(t)e^{i\omega t} dt \int \hat{a}^\dagger(t')e^{-i\omega' t'} dt' - \frac{1}{2\pi} \int \hat{a}^\dagger(t')e^{-i\omega' t'} dt' \int \hat{a}(t)e^{i\omega t} dt \tag{6.76}$$

$$= \frac{1}{2\pi} \int \left(\hat{a}(t)\hat{a}^\dagger(t') - \hat{a}^\dagger(t')\hat{a}(t)\right) e^{i\omega t} e^{-i\omega' t'} dt dt' \tag{6.77}$$

$$= \frac{1}{2\pi} \int_{-\infty}^{\infty} [\hat{a}(t), \hat{a}^\dagger(t')] e^{it\omega} e^{-it'\omega'} dt dt' \tag{6.78}$$

$$= \frac{1}{2\pi} \int_{-\infty}^{\infty} \delta(t - t') e^{it\omega} e^{-it'\omega'} dt dt' \tag{6.79}$$

$$= \frac{1}{2\pi} \int_{-\infty}^{\infty} e^{it(\omega - \omega')} dt \tag{6.80}$$

$$= \delta(\omega - \omega'), \tag{6.81}$$

which is analogous to the non-Fourier relations. Choosing instead the convention

$$\hat{a}^\dagger(\omega) = \frac{1}{\sqrt{2\pi}} \int_{-\infty}^{\infty} \hat{a}^\dagger(t)e^{i\omega t} dt \tag{6.82}$$

leads to the commutation rule $[\hat{a}(\omega), \hat{a}^\dagger(\omega')] = \delta(\omega + \omega')$, since there will be the term $e^{i\omega t} e^{i\omega' t'}$ which will lead to an integral over $e^{it(\omega + \omega')}$. we also have

$$[\hat{a}(\omega), \hat{a}(\omega')] = \frac{1}{2\pi} \int_{-\infty}^{\infty} [\hat{a}(t), \hat{a}(t')] e^{it\omega} e^{it'\omega'} dt df' \tag{6.83}$$

$$= 0 \tag{6.84}$$

$$= [\hat{a}^\dagger(\omega), \hat{a}^\dagger(\omega')], \tag{6.85}$$

which is independent of our convention choice.

Below, we will compute the Fourier transforms of some useful operators using this convention.

6.5.0.1 Fourier transform of $\delta\hat{a}$.

For the operator $\delta\hat{a}(t) \equiv \hat{a}(t) - \alpha(t)$ (for a coherent state), we have the Fourier transform convention

$$\delta\hat{a}(\omega) = \frac{1}{\sqrt{2\pi}} \int_{-\infty}^{\infty} a(t)e^{i\omega t}dt - \frac{1}{\sqrt{2\pi}} \int_{-\infty}^{\infty} \alpha(t)e^{i\omega t}dt \tag{6.86}$$

$$= \hat{a}(\omega) - \alpha(\omega) \tag{6.87}$$

and

$$\delta\hat{a}^{\dagger}(\omega) = \frac{1}{\sqrt{2\pi}} \int_{-\infty}^{\infty} a^{\dagger}(t)e^{-i\omega t}dt - \frac{1}{\sqrt{2\pi}} \int_{-\infty}^{\infty} \alpha^{*}(t)e^{-i\omega t}dt \tag{6.88}$$

$$= \hat{a}^{\dagger}(\omega) - \alpha^{*}(\omega) \tag{6.89}$$

6.5.0.2 Fourier transform convention for $\delta\hat{X}$

For the operator $\delta\hat{X} = \frac{1}{2}\left(\delta\hat{a} + \delta\hat{a}^{\dagger}\right)$, we have the Fourier transform

$$\delta\hat{X}(\omega) = \frac{1}{\sqrt{2\pi}} \int_{-\infty}^{\infty} \frac{1}{2} \left(\delta\hat{a}(t) + \delta\hat{a}^{\dagger}(t)\right) e^{i\omega t}dt \tag{6.90}$$

$$= \frac{1}{2} \left(\delta\hat{a}(\omega) + \delta\hat{a}^{\dagger}(-\omega)\right) \tag{6.91}$$

6.6 Appendix: Analysis of interferometer

In this appendix, we analyse the modes of the interferometer shown in Fig. 6.5. We want to find the relationship between the input operators $\hat{a}_0, \hat{a}_1$ and the output operators $\hat{a}_4, \hat{a}_5$. We first perform an analysis without assuming the input modes $\hat{a}_0$ and $\hat{a}_1$, but later we assume squeezed vacuum and coherent light are injected into these ports, respectively. Light entering the ports $(\hat{a}_0, \hat{a}_1)$ will be split by the beamsplitter according to

$$\begin{pmatrix} a_2 \\ a_3 \end{pmatrix} = B \begin{pmatrix} a_0 \\ a_1 \end{pmatrix} \tag{6.92}$$

$$= \frac{1}{\sqrt{2}} \begin{pmatrix} a_0 + ia_1 \\ a_1 + ia_0 \end{pmatrix} \tag{6.93}$$

where
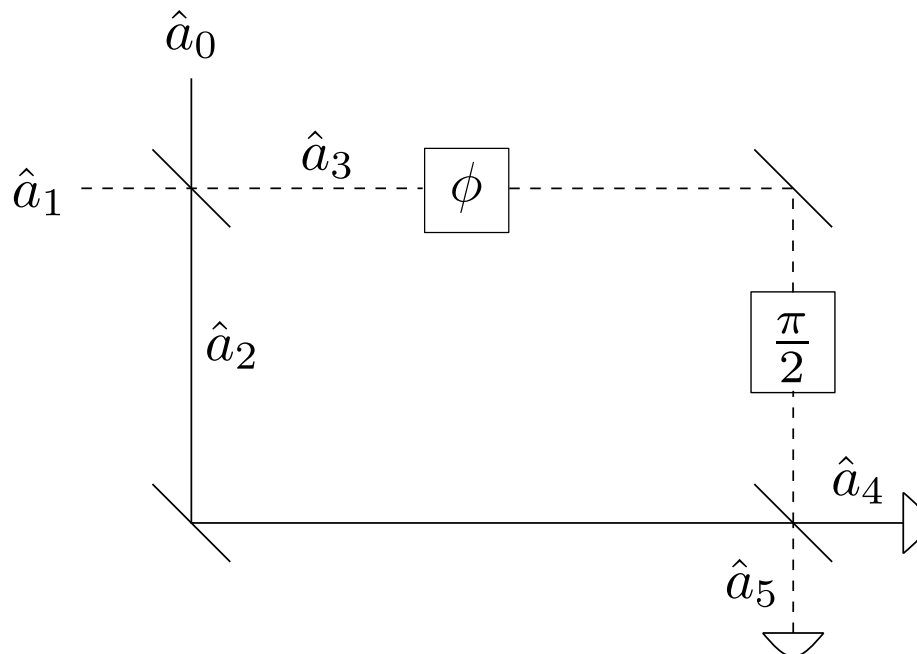
Figure 6.5: **A standard Mach-Zehnder interferometer with phase difference** ϕ **between the two arms**. The extra phase shift $\pi/2$ is included so that we operate in 'dark mode' i.e., we have no photocurrent when the phase difference is zero.

$$B = \frac{1}{\sqrt{2}} \begin{pmatrix} 1 & i \\ i & 1 \end{pmatrix} \tag{6.94}$$

is the matrix for the 50/50 beamsplitter.

The light $\hat{a}_0$ transmits to the arm denoted by $\hat{a}_2$ and the light $\hat{a}_1$ reflects (and thus picks up a $\pi/2$ phase shift) in arm two. For arm three, the transmission and reflection are reversed.

The phase shifter ϕ directly introduces a relative phase shift between the arms, and we additionally shift the relative phase by $\pi/2$ so the detection is in 'dark' mode, i.e., that there is no output signal when the lengths of the interferometer arms are the same.

After the phase shifting, the light in arm 3 changes, and we have

$$\begin{pmatrix} a_2 \\ a_3 \end{pmatrix} = \Phi\left(\phi + \frac{\pi}{2}\right) B \begin{pmatrix} a_0 \\ a_1 \end{pmatrix} \tag{6.95}$$

$$= \frac{1}{\sqrt{2}} \begin{pmatrix} a_0 + ia_1 \\ -e^{i\phi}(a_0 - ia_1) \end{pmatrix} \tag{6.96}$$

where

$$\Phi(\theta) = \begin{pmatrix} 1 & 0 \\ 0 & e^{i\theta} \end{pmatrix} \tag{6.97}$$

performs a phase shift θ on the lower arm (here arm 3). The light then enters the second beam splitter and is transformed according to the matrix B again, and we find the final output modes

$$\begin{pmatrix} a_4 \\ a_5 \end{pmatrix} = B\Phi\left(\phi + \frac{\pi}{2}\right) B \begin{pmatrix} a_0 \\ a_1 \end{pmatrix} \tag{6.98}$$

$$= \frac{1}{2} \begin{pmatrix} \left(1 - ie^{i\phi}\right) a_0 - \left(-i + e^{i\phi}\right) a_1 \\ i\left(i + e^{i\phi}\right) a_1 - \left(-i + e^{i\phi}\right) a_0 \end{pmatrix} \tag{6.99}$$

The detectors measure the photocurrent $N = a^\dagger a$. In our configuration, we will perform a homodyne measurement, i.e., we subtract the current at arm 4 from the one at arm 5 to obtain

$$\hat{I} = \hat{a}_5^\dagger \hat{a}_5 - \hat{a}_4^\dagger \hat{a}_4 \tag{6.100}$$

$$\hat{I} = \sin(\phi)\left(a_1{}^\dagger a_1 - a_0{}^\dagger a_0\right) + \cos(\phi)\left(a_0{}^\dagger a_1 + a_1{}^\dagger a_0\right) \tag{6.101}$$

6.6.1 Injection of coherent light into one port

Using a coherent state input $\beta = |\beta|e^{i\theta}$ combined with some light of interest $|\Psi\rangle$, we can obtain

$$\langle\beta, \Psi|\hat{I}|\Psi, \beta\rangle = \langle\beta, \Psi|\sin(\phi)\left(a_1{}^\dagger a_1 - a_0{}^\dagger a_0\right) + \cos(\phi)\left(a_0{}^\dagger a_1 + a_1{}^\dagger a_0\right)|\Psi, \beta\rangle \tag{6.102}$$

$$= \sin(\phi)\left(|\beta|^2 - \langle\Psi|\hat{n}_0|\Psi\rangle\right) + |\beta|\cos(\phi)\langle\Psi|\hat{a}_0^\dagger e^{i\theta} + \hat{a}_0 e^{-i\theta}|\Psi\rangle \tag{6.103}$$

$$= \sin(\phi)\left(|\beta|^2 - \langle\Psi|\hat{n}_0|\Psi\rangle\right) + 2|\beta|\cos(\phi)\langle\Psi|\hat{Y}(\theta)|\Psi\rangle \tag{6.104}$$

Where $\hat{Y}(\theta) = \frac{1}{2}\left(\hat{a}_0^\dagger e^{i\theta} + \hat{a}_0 e^{-i\theta}\right)$ and θ is the angle of the coherent state input (that will function as the local oscillator angle for homodyne detection). Note that $\hat{Y}(\theta = 0) = \hat{X}_0$ and $\hat{Y}(\theta = \pi/2) = \hat{P}_0$, so we have access to both quadrature components with this method.

We can also compute the variance

$$(\Delta I)^2 = |\beta|\sin(\phi)\cos(\phi)\left\langle\Psi|e^{i\theta}a_0{}^\dagger + a_0 e^{-i\theta}|\Psi\right\rangle + \cos^2(\phi)\left\langle\Psi|a_0{}^\dagger \cdot a_0|\Psi\right\rangle + |\beta|^2\sin^2(\phi) \tag{6.105}$$

$$= |\beta|\sin(\phi)\cos(\phi)\left\langle\Psi|Y(\theta)|\Psi\right\rangle + \cos^2(\phi)\left\langle\Psi|n_0|\Psi\right\rangle + |\beta|^2\sin^2(\phi) \tag{6.106}$$

6.6.1.1 Vacuum state in other port

If we now use $|0\rangle$ in the other port, we have

$$\langle\beta, 0|\hat{I}|0, \beta\rangle = |\beta|^2\sin(\phi) \tag{6.107}$$

We can also compute the variance of this signal

$$\Delta I^2 = |\beta|^2 \,, \tag{6.108}$$

yielding a signal-to-noise ratio

$$\text{SNR} = \frac{\langle I\rangle}{\Delta I} = \frac{|\beta|^2\sin(\phi)}{|\beta|} \tag{6.109}$$

6.6.1.2 Squeezed vacuum in second port

We now consider the case where we inject *squeezed* vacuum into the second port. We will make use of the squeeze operator relations

$$\hat{S}^\dagger(z)\hat{a}\hat{S}(z) = \hat{a}\cosh r - e^{i\theta_{sq}}\hat{a}^\dagger\sinh \tag{6.110}$$

$$\hat{S}^\dagger(z)\hat{a}^\dagger\hat{S}(z) = \hat{a}^\dagger\cosh r - e^{-i\theta_{sq}}\hat{a}\sinh r \tag{6.111}$$

where θ_{sq} is the squeezing angle and r is the squeezing parameter.

$$n_0 = a_0^\dagger a_0$$
$$\Rightarrow n_{sq} = \cosh(r)\left(a_0{}^\dagger\cosh(r) - a_0 e^{-i\theta}\sinh(r)\right)\cdot a_0$$
$$+ \sinh(r)\left(a_0\sinh(r) - e^{i\theta}a_0{}^\dagger\cosh(r)\right)\cdot a_0{}^\dagger \tag{6.112}$$

which has expectation value

$$\langle 0|n_{sq}|0\rangle = \sinh^2(r) \tag{6.113}$$

Since the expectation value of the generalized quadrature operator $Y(\theta)$ is linear in the operators $\hat{a}_0$ and $\hat{a}_0^\dagger$, it has expectation value zero, so the signal is

$$\langle I \rangle = \sin(\phi)\left(|\beta|^2 - \sinh^2(r)\right) \tag{6.114}$$

with variance

$$(\Delta I)^2 = |\beta|^2 \sin^2(\phi) + \sinh^2(r)\cos^2(\phi), \tag{6.115}$$

giving a signal-to-noise ratio

$$\mathrm{SNR} = \frac{\left||\beta|^2 \sin(\phi) - \sinh^2(r)\sin(\phi)\right|}{\sqrt{|\beta|^2 \sin^2(\phi) + \sinh^2(r)\cos^2(\phi)}} \tag{6.116}$$

$$\approx \frac{\left|\phi\left(|\beta|^2 - \sinh^2(r)\right)\right|}{|\sinh^2(r)|} + \mathcal{O}\left(\phi^2\right), \tag{6.117}$$

where in the second line we have expanded in ϕ to first order, since we expect the signal to be small. The signal-to-noise ratio grows as the squeezing parameter r is increased.

Chapter 7

Frequency dependent squeezing via electromagnetically induced transparency in a motionally-averaged room temperature atomic ensemble

7.1 Introduction

We have seen in the previous chapter that the optimal frequency dependent squeezing can be produced by a filter cavity. In order to produce this squeezing rotation, the light needs to be inside the cavity on the order of milliseconds ($g_{\text{LIGO}} = 2\pi \cdot 60$ Hz corresponds to ~ 2.5ms). Given the high propagation speed of light, this corresponds to roughly 1000km of distance travelled. Assuming a round trip loss of 0.01%, we require a cavity length of 1km to reach $> 90\%$ total loss. To alleviate some of the engineering problems associated with producing such a large cavity, we propose an alternative scheme to increase the light storage time: photon storage via electromagnetically induced transparency.

Works analysing the storage potential of EIT are relatively numerous [89, 90, 91] and the idea to apply EIT to gravitational wave detection has already been proposed [92]. However, the analysis [92] does not include the averaging effect of atoms travelling in and out of the cavity beam, nor does it rigorously treat all the noise sources. We endeavour to build on this work and do both. We will begin with a treatment of the noise that includes additional losses from the cavity and effects due to finite cooperativity and then move on to a full treatment of the dynamics of atoms moving in and out of the cavity field in the section on motional averaging.

Other recent work [93] has theoretically and experimentally analysed an optical parametric oscillator away from resonance, and found that up to a 39° rotation is possible, with a corresponding noise reduction of 5.5 dB.

7.2 Frequency dependent squeezing with EIT

We consider the 3-level system shown in Fig. 7.1. We begin with the rotating frame atomic Hamiltonian (7.172) in the rotating wave approximation derived in Appendix 7.10 of this chapter.

$$\hat{H}^{(j)} = \hbar\Delta\hat{\sigma}_{33}^{(j)} + \hbar\delta\hat{\sigma}_{22}^{(j)} - \hbar\left(\Omega_j\hat{\sigma}_{32}^{(j)} + \Omega_j^*\hat{\sigma}_{23}^{(j)} + g_j\hat{\sigma}_{31}^{(j)}\hat{a} + g_j^*\hat{\sigma}_{13}^{(j)}\hat{a}^\dagger\right) \qquad (7.1)$$

From here, we can obtain Langevin equations of motion via

$$\frac{d\hat{O}}{dt} = -\frac{i}{\hbar}\left[\hat{O}, \hat{H}\right] - \frac{\gamma_{\hat{O}}}{2}\hat{O} + \hat{\Gamma}_{\hat{O}}, \qquad (7.2)$$

where we have introduced a decay $\gamma_{\hat{O}}$ corresponding to each operator and a Langevin noise operator $\Gamma_{\hat{O}}$ such that the fluctuation dissipation theorem is satisfied (this noise
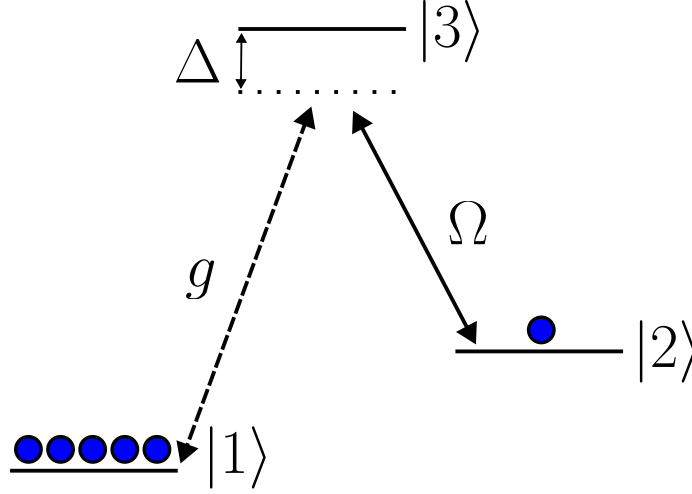
Figure 7.1: **A Λ-type 3-level atom** coupled to a classical field (solid), with Rabi frequency Ω and a quantum cavity field (dashed) with coupling strength g. Assuming each of the N atoms in the medium couples equally to the field, the quantum field couples to spin-wave excitations with an effective coupling constant $g\sqrt{N}$ due to collective enhancement [5]. The fields are detuned from the excited state $|3\rangle$ by some amount Δ to reduce the effects of Doppler broadening and absorption.

operator has the effect of ensuring that the commutation relations for the operators are conserved by the time-evolution).

$$\dot{\hat{a}} = i \sum_{j=0}^{N-1} \left(g^{(j)} \right)^* \sigma_{1,3}^{(j)} + \hat{a_{\text{in}}}\sqrt{\kappa_{\text{out}}} - \frac{\hat{a}\kappa}{2} + \hat{a_{\text{loss}}}\sqrt{\kappa_{\text{loss}}} \tag{7.3}$$

$$\dot{\hat{\sigma}}_{12}^{(j)} = i\frac{\Omega^*}{2}\hat{\sigma}_{13}^{(j)} - \left(\frac{\gamma_s}{2} + i\delta \right)\hat{\sigma}_{12}^{(j)} + \hat{\Gamma}_{\sigma_{12}} \tag{7.4}$$

$$\dot{\hat{\sigma}}_{13}^{(j)} = ig^{(j)}\hat{a} - \left(\frac{\gamma}{2} + i\Delta \right)\hat{\sigma}_{13}^{(j)} + i\frac{\Omega}{2}\hat{\sigma}_{12} + \hat{\Gamma}_{\sigma_{13}}, \tag{7.5}$$

where we have assumed the population of the state $|1\rangle$ remains high, i.e., $\sigma_{11} \approx 1$ and $\sigma_{22} \approx \sigma_{33} \approx 0$. We have set $\gamma_{\hat{a}} \to \kappa = \kappa_{\text{out}} + \kappa_{\text{loss}}$ and $\Gamma_{\hat{a}} \to \hat{a_{\text{in}}}\sqrt{\kappa_{\text{out}}} + \hat{a_{\text{loss}}}\sqrt{\kappa_{\text{loss}}}$, i.e., the decay $\hat{\Gamma}_{\hat{a}}$ is composed of the normal input-output relation for a cavity, plus an additional loss term $\hat{a}_{\text{loss}}\sqrt{\kappa_{\text{loss}}}$ that takes into account cavity losses that do not come through the in/out port. This represents a small departure from the usual (time-reversal symmetric) representation and corresponds to extra cavity loss κ_s from the other side of the cavity. We have additionally defined $\gamma_{\sigma_{12}} = \gamma_s$ and $\gamma_{\sigma_{13}} = \gamma$

7.3 Constant coupling EIT

To obtain the standard EIT equations, we will assume that each of our N atoms couples equally to the cavity field $\hat{a}$, i.e., $g_j = g$ and to the classical field such that $\Omega_j = \Omega$. This assumption is not realistic for atoms moving in and out of the laser beam, and will be treated more rigorously in the following section on motional averaging. We define two collective operators

$$\hat{P} = \frac{1}{\sqrt{N}} \sum_{j=0}^{N-1} \hat{\sigma}_{23}^{(j)} \tag{7.6}$$

$$\hat{S} = \frac{1}{\sqrt{N}} \sum_{j=0}^{N-1} \hat{\sigma}_{21}^{(j)} \tag{7.7}$$

$\hat{S}$ is the annihilation operator for the so-called 'spin wave', that a quantum memory is trying to create (i.e., mapping a pulse of light from the state $|2\rangle$ to the long-lived state $|1\rangle$ via the excited state $|3\rangle$) $\hat{P}$ is the annihilation operator for the polarisation. Setting $\delta = 0$, we obtain the equations of motion

$$\dot{\hat{a}} = \hat{a}_{\text{in}}\sqrt{\kappa_{\text{out}}} - \frac{\hat{a}\kappa}{2} + \hat{a_{\text{loss}}}\sqrt{\kappa_{\text{loss}}} + ig\sqrt{N}\hat{P} \tag{7.8}$$

$$\dot{\hat{P}} = i\hat{a}g\sqrt{N} + \sqrt{\gamma}\hat{F}_p + \hat{P}\left(-\frac{\gamma}{2} - i\Delta\right) + \frac{1}{2}i\hat{S}\Omega \tag{7.9}$$

$$\dot{\hat{S}} = \hat{F}_s\sqrt{\gamma_s} + \frac{1}{2}i\hat{P}\Omega^* - \frac{\hat{S}\gamma_s}{2} - i\delta\hat{S} \tag{7.10}$$

Where we have replaced the Langevin noise operators with force terms $\gamma_{\hat{O}}\hat{F}_{\hat{O}}$. These noise operators, along with $\hat{a}_{\text{loss}}$ have zero expectation value when expressed in terms of normal-ordered products and will thus be neglected in the following.

7.3.1 Adiabatic elimination of $\hat{a}$ and $\hat{P}$.

We want an approximate solution... Let us move into the Fourier domain and assume that $\kappa, \gamma, \Delta \gg \omega$. This allows us to neglect the $-i\omega\hat{a}$ and $-i\omega\hat{P}$ terms that appear

on the left hand side.

$$0 = \hat{a}_{\text{in}}\sqrt{\kappa_{\text{out}}} - \frac{\hat{a}\kappa}{2} + \hat{a_{\text{loss}}}\sqrt{\kappa_{\text{loss}}} + ig\sqrt{N}\hat{P} \tag{7.11}$$

$$0 = i\hat{a}g\sqrt{N} + \sqrt{\gamma}\hat{F}_p + \hat{P}\left(-\frac{\gamma}{2} - i\Delta\right) + \frac{1}{2}i\hat{S}\Omega \tag{7.12}$$

$$-i\omega\hat{S} = \frac{1}{2}i\hat{P}\Omega^* + \hat{F}_s\sqrt{\gamma_s} - \frac{\hat{S}\gamma_s}{2} \tag{7.13}$$

Since we are working in vacuum, normal ordered products of our noise operators will give zero in expectation values. Thus, we can neglect the operators $\hat{F}_s, \hat{F}_p, \hat{a}_{loss}$.

$$\hat{S} = \frac{iP\Omega^*}{\gamma_S - 2i\omega} \tag{7.14}$$

from which we obtain

$$0 = iag\sqrt{N} + P\left(\frac{1}{2}(-\gamma - 2i\Delta) - \frac{\Omega\Omega^*}{2(\gamma_S - 2i\omega)}\right) \tag{7.15}$$

$$\Rightarrow P = \frac{iag\sqrt{N}}{\frac{1}{2}\left(\gamma + \frac{\Omega\Omega^*}{\gamma_S - 2i\omega} + 2i\Delta\right)} \tag{7.16}$$

From our first equation, we now get

$$0 = -\frac{2\hat{a}g^2N}{\gamma + 2i\Delta + \frac{\Omega\Omega^*}{\gamma_s - 2i\omega}} + \hat{a}_{\text{in}}\sqrt{\kappa_{\text{out}}} - \frac{\hat{a}\kappa}{2} \tag{7.17}$$

$$= \hat{a}_{\text{in}}\kappa_{\text{out}} - \hat{a}\sqrt{\kappa_{\text{out}}}\left(\frac{\kappa}{2} + \frac{2g^2N}{\gamma + 2i\Delta + \frac{\Omega\Omega^*}{\gamma_s - 2i\omega}}\right) \tag{7.18}$$

Using the input-output relation $\hat{a}_{\text{in}} + \hat{a}_{\text{out}} = \hat{a}\sqrt{\kappa_{\text{out}}}$ and inserting the cooperativity $C = \frac{4g^2N}{\gamma\kappa}$, we obtain the reflection coefficient

$$r = \frac{\hat{a}_{\text{out}}}{\hat{a}_{\text{in}}} = -1 + \frac{2\kappa_{\text{out}}}{\kappa\left(1 + \frac{\gamma C}{\gamma + 2i\Delta + \frac{\Omega\Omega^*}{\gamma_s - 2i\omega}}\right)} \tag{7.19}$$

We now want to control the properties of this reflection coefficient such that we can mimic the optimal response of the filter cavity we found in Section 6.3 of the previous chapter.

7.3.1.1 Lossless solution

If we remove losses, we are left with

$$r = -1 + \frac{2}{\left(1 + \frac{\gamma C}{\gamma + 2i\Delta - \frac{\Omega\Omega^*}{2i\omega}}\right)} \tag{7.20}$$

If we further make the approximation $(C + 1) \approx C$, (which is valid for $C \gg 1$), we obtain a reflection coefficient

$$r = \frac{\Omega\Omega^* + 2i\omega(\gamma C - 2i\Delta)}{\Omega\Omega^* - 2i\omega(\gamma C + 2i\Delta)} \tag{7.21}$$

We have a resonance when r reaches its maximal value (i.e., where $r \to -1$) at

$$\omega_{res} = -\frac{i|\Omega|^2}{2\gamma C + 4i\Delta} \tag{7.22}$$

The real and imaginary parts of r are

$$\mathcal{R} = \frac{\left(4\Delta\omega + \Omega^2\right)^2 - 4\gamma^2 C^2\omega^2}{4\gamma^2 C^2\omega^2 + \left(4\Delta\omega + \Omega^2\right)^2} \tag{7.23}$$

$$\mathcal{I} = \frac{4\gamma C\omega\left(4\Delta\omega + \Omega^2\right)}{4\gamma^2 C^2\omega^2 + \left(4\Delta\omega + \Omega^2\right)^2} \tag{7.24}$$

which gives a scattering angle $\theta = \mathrm{Arg}(r) = 2\tan^{-1}\left(\frac{\mathcal{I}}{\sqrt{\mathcal{R}^2 + \mathcal{I}^2} + \mathcal{R}}\right)$

$$\theta = 2\tan^{-1}\left(\frac{2\gamma C\omega}{4\Delta\omega + \Omega^2}\right), \tag{7.25}$$

that we want to use to mimic the filter cavity from Section 6.3. The squeezing rotation angle φ is then given by

$$\varphi(\omega) = \frac{\theta(\omega + \omega_i) + \theta(-\omega + \omega_i)}{2} \tag{7.26}$$

$$= \tan^{-1}\left(\frac{2\gamma C\left(\omega_i - \omega\right)}{4\Delta\left(\omega_i - \omega\right) + \Omega^2}\right) + \tan^{-1}\left(\frac{2\gamma C\left(\omega_i + \omega\right)}{4\Delta\left(\omega_i + \omega\right) + \Omega^2}\right) \tag{7.27}$$

where ω_i is the frequency of the interferometer light.

7.3.1.2 Setting ω_i

Since we want our squeezing rotation angle φ to give values between 0 and $\pi/2$, or equivalently, between $\pi/2$ and π, we can make use of this requirement to set our ω_i. We set $\varphi(\omega = 0) = \frac{\pi}{2}$, and solve for ω_i.

$$2\tan^{-1}\left(\frac{2\gamma C\omega_i}{4\Delta\omega_i + \Omega^2}\right) = \frac{\pi}{2} \tag{7.28}$$

$$\Rightarrow \frac{2\gamma C\omega_i}{4\Delta\omega_i + \Omega^2} = 1 \tag{7.29}$$

$$\Rightarrow \omega_i = \frac{\Omega^2}{2\gamma C - 4\Delta} \tag{7.30}$$

Here we note that by setting ω_i we can counteract the negative effects of finite cooperativity C. This parameter is extremely sensitive, and crucially, depends strongly on the position of the atomic resonance. By making different approximations for the solutions to our equations, the calculated value of the atomic resonance will change, and hence the correct value of ω_i will be altered.

7.3.2 Setting Ω

The filter cavity that we are trying to mimic has a bandwidth κ that controls the rate at which the memory is accessed. We can modify the bandwidth by setting the coupling laser frequency, Ω. We found that the filter cavity should have $\kappa = \sqrt{2}g_{\text{LIGO}}$. We need to compute an expression for the effective bandwidth of the cavity-atoms system. This rate is related to the decay rate of the storage state S into the cavity mode a_{out}. We want to find some expression for $\langle \hat{a}^\dagger_{\text{out}}\hat{a}_{\text{out}}\rangle$ as a function of the population $\hat{S}^\dagger\hat{S}$. Using our adiabatically eliminated equations, we can write (assuming $\gamma_s = \kappa_{\text{loss}} = 0$)

$$\hat{a}_{\text{out}} = -\frac{S\Omega\sqrt{\gamma C}}{\gamma + \gamma C + 2i\Delta}, \tag{7.31}$$

and thus

$$\langle \hat{a}^\dagger_{\text{out}}\hat{a}_{\text{out}}\rangle = \underbrace{\frac{\gamma C\Omega^2}{\gamma^2(C+1)^2 + 4\Delta^2}}_{\text{effective bandwidth}} \langle \hat{S}^\dagger\hat{S}\rangle \tag{7.32}$$

We can therefore set

$$\Omega = \frac{\sqrt[4]{2}\sqrt{g_{\text{LIGO}}}\sqrt{\gamma^2(C+1)^2 + 4\Delta^2}}{\sqrt{\gamma C}} \tag{7.33}$$

7.3.3 Limiting cases

We now consider two limiting cases, firstly the so-called EIT limit, where we are on resonance $\Delta = 0$, and Raman limit, where we are far detuned $\Delta \gg C\gamma$.

7.3.3.1 EIT limit ($\Delta = 0$)

In this case, our equations reduce to

$$r = \frac{\Omega\Omega^* + 2i\gamma C\omega}{\Omega\Omega^* - 2i\gamma C\omega} \tag{7.34}$$

$$= \frac{\Omega^2/\gamma C + 2i\omega}{\Omega^2/\gamma C - 2i\omega} \tag{7.35}$$

and

$$\theta = 2\tan^{-1}\left(\frac{2\gamma C\omega}{\Omega^2}\right) \tag{7.36}$$

This maps on exactly to the case where we have a filter cavity (6.64) with $\Omega^2/\gamma C = \kappa_{\text{eff}}$. In accordance with our analysis for the filter cavity, in order to have the optimal parameters, we should set $\Omega = (\sqrt{2}g_{\text{LIGO}}\gamma C)^{1/2}$ and $\omega_i = -\frac{1}{\sqrt{2}}g_{\text{LIGO}}$.

7.3.3.2 Raman limit

In the opposite extreme, we have $\Delta \gg C\gamma$, and we obtain

$$r = -1 + \frac{2}{\left(1 + \frac{\gamma C}{\gamma + 2i\Delta - \frac{\Omega\Omega^*}{2i\omega}}\right)} \tag{7.37}$$

$$\approx -1 + \frac{2}{1 + \frac{\gamma C}{\frac{i|\Omega|^2}{2\omega} + 2i\Delta}} \tag{7.38}$$

The condition $2i\Delta - \frac{\Omega^2}{2i\omega} = 0$ leads to the changing from $r = -1$, to $r = 1$ and then back again i.e., the phase changes rapidly around the region of this resonance, which occurs at $\omega = -\frac{\Omega^2}{4\Delta}$. This rapid change around the resonance is what we exploit to mimic the filter cavity response.

7.4 Full solution

In the previous section, we used adiabatic elimination to obtain simple analytic results. However, we do no have to assume the conditions for adiabatic elimination, and instead produce a more precise solution where we keep all the terms. In Fourier space, our equations of motion are now

$$-i\omega\hat{a} = \hat{a}_{\text{in}}\sqrt{\kappa_{\text{out}}} - \frac{\hat{a}\kappa}{2} + ig\sqrt{N}\hat{P} \tag{7.39}$$

$$-i\omega\hat{P} = i\hat{a}g\sqrt{N} + \hat{P}\left(-\frac{\gamma}{2} - i\Delta\right) + \frac{1}{2}i\hat{S}\Omega \tag{7.40}$$

$$-i\omega\hat{S} = -\frac{\hat{S}\gamma_s}{2} + \frac{1}{2}i\hat{P}\Omega^* \tag{7.41}$$

Again, setting our noise operators $\hat{F}_s = \hat{F}_p = \hat{a}_{loss} = 0$, we have

$$\hat{S} = \frac{i\hat{P}\Omega^*}{\gamma_s - 2i\omega} \tag{7.42}$$

from which we obtain

$$0 = iag\sqrt{N} + P\left(-\frac{\gamma}{2} - i\Delta - \frac{\Omega\Omega^*}{2(\gamma s - 2i\omega)} + i\omega\right) \tag{7.43}$$

$$\Rightarrow \hat{P} = \frac{i\hat{a}g\sqrt{N}}{\frac{\gamma}{2} + i\Delta + \frac{\Omega\Omega^*}{2(\gamma_s - 2i\omega)} - i\omega} \tag{7.44}$$

From our first equation, we now get

$$0 = \hat{a}_{\text{in}}\sqrt{\kappa_{\text{out}}} - \hat{a}\left(\frac{\kappa}{2} + \frac{g^2 N}{\frac{\gamma}{2} + i\Delta + \frac{\Omega\Omega^*}{2(\gamma_s - 2i\omega)} - i\omega} - i\omega\right) \tag{7.45}$$

$$= \hat{a}_{\text{in}}\kappa_{\text{out}} - \hat{a}f \tag{7.46}$$

Using the input-output relation $\hat{a}_{\text{in}} + \hat{a}_{\text{out}} = \hat{a}\sqrt{\kappa_{\text{out}}}$, we obtain

$$r = \frac{a_{out}}{a_{in}} = -1 + \frac{\kappa_{out}}{f} \tag{7.47}$$

$$= -1 + \frac{2\kappa_{\text{out}}}{\frac{\gamma C\kappa}{\gamma + 2i(\Delta - \omega) + \frac{\Omega\Omega^*}{\gamma_s - 2i\omega}} + \kappa - 2i\omega} \tag{7.48}$$

$$= -1 + \frac{2\kappa\left(1 - \kappa_{\text{loss}}\right)}{\frac{\gamma C\kappa}{\gamma + 2i(\Delta - \omega) + \frac{\Omega\Omega^*}{\gamma_s - 2i\omega}} + \kappa - 2i\omega} \tag{7.49}$$

where here κ_{loss} is expressed as a fraction of κ.

Although in principle this expression is more precise than the adiabatically eliminated solutions, in the parameter regime we consider, the adiabatic approximation holds, so the differences between the two solutions are minor. As such, to investigate the losses in the system, we proceed with the adiabatically eliminated solutions.

7.4.1 EIT in the presence of losses

Now we are in a position to analyse exactly how losses such as finite cooperativity C and finite lifetimes of the storage state γ_s, and cavity loss κ_{loss}. Unless otherwise stated, for all the plots given below, we use the parameters $\Delta/2\pi = 10^9$ Hz, $\kappa/2\pi = 10^9$ Hz, $\gamma/2\pi = 10^6$ Hz, $C = 5$, $g_{\text{LIGO}}/2\pi = 60$ Hz, $\kappa_{\text{LIGO}}/2\pi = 450$ Hz and a squeezing parameter $S = 10$ dB. The first thing to ensure is that perfect EIT can reproduce the broadband suppression. Even with a modest cooperativity $C = 5$, we can reproduce the optimal suppression shown as ϕ_{optimal} in Fig. 7.2. As we can
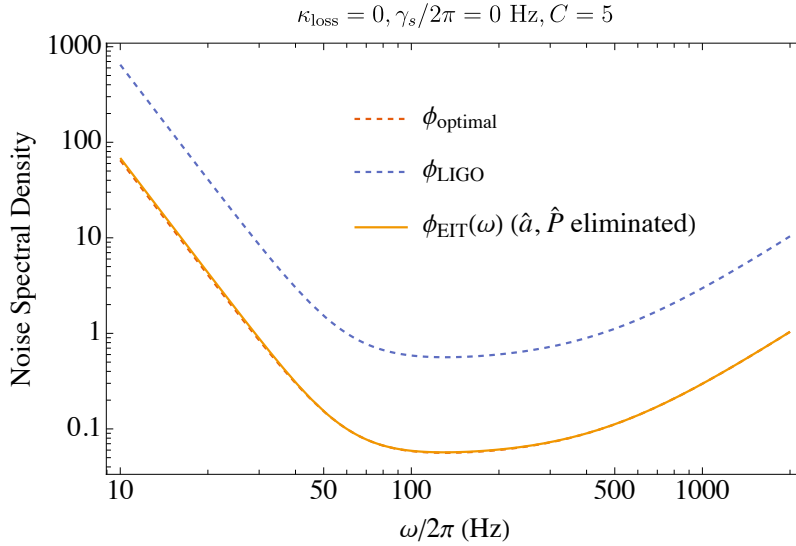
Figure 7.2: **Noise spectral density** with finite cooperativity $C = 5$ with an EIT scheme in the Raman configuration. The other losses κ_{loss} and γ_s are set to zero.

see from Fig. 7.3, worsening the cooperativity to a relatively low $C = 3$ can still produce a broadband suppression very close to what is achievable with the optimal frequency rotation ϕ_{optimal}. The protocol is relatively robust to cavity loss κ_{loss} as well. In Fig. 7.4, and in Fig. 7.5, we have can see the effect of $\kappa_{\text{loss}} = 0.01, 0.05$, respectively. There is, in essence, a broadband worsening of the noise suppression, as
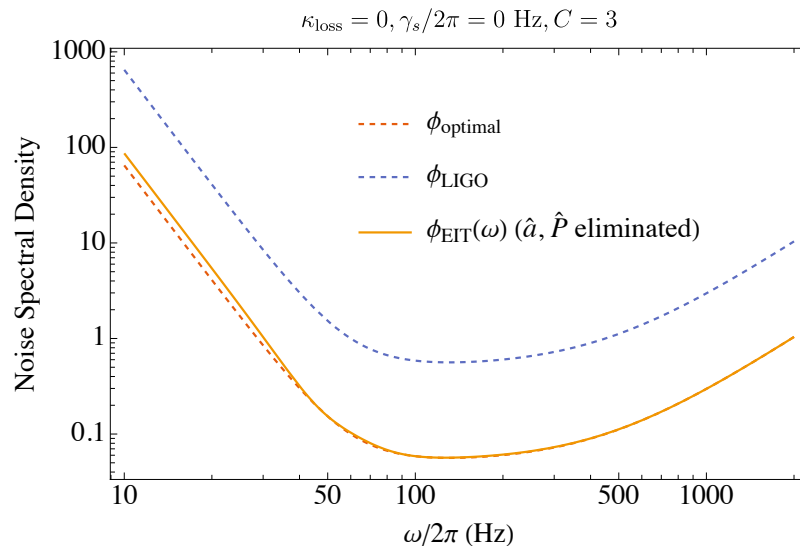
Figure 7.3: **Noise spectral density** with finite cooperativity $C = 3$ with an EIT scheme in the Raman configuration. The other losses κ_{loss} and γ_s are set to zero.

expected if the squeezed vacuum is being lost and replaced by un-squeezed vacuum, from the leaking of the cavity. Adding some loss from the storage state $\gamma_s/2\pi = 20, 30$ Hz produces a worsening around the frequency of γ_s, as can be seen in Fig. 7.6 and Fig. 7.7. Finally, we can examine the combination of all these errors. We find that for the parameters used, the cavity loss κ_{loss} dominates Fig. 7.8 the effects of loss from the storage state. However, we are still seeing, even in the worst case Fig. 7.9, a broadband noise suppression of more than 5dB, given input squeezing of 10dB.
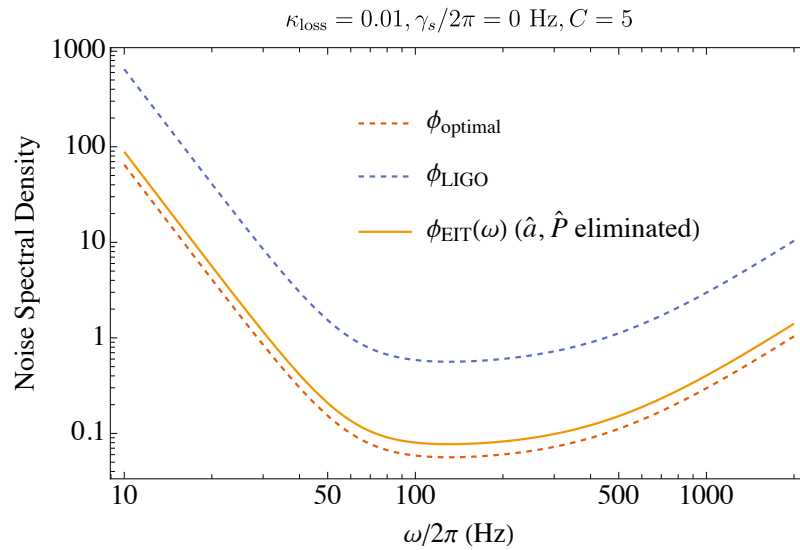
Figure 7.4: **Noise spectral density** with $\kappa_{\mathrm{loss}} = 0.01$, i.e., a 1% loss of light from the 'perfect' mirror. We otherwise have $C = 5$, $\gamma_s = 0$.
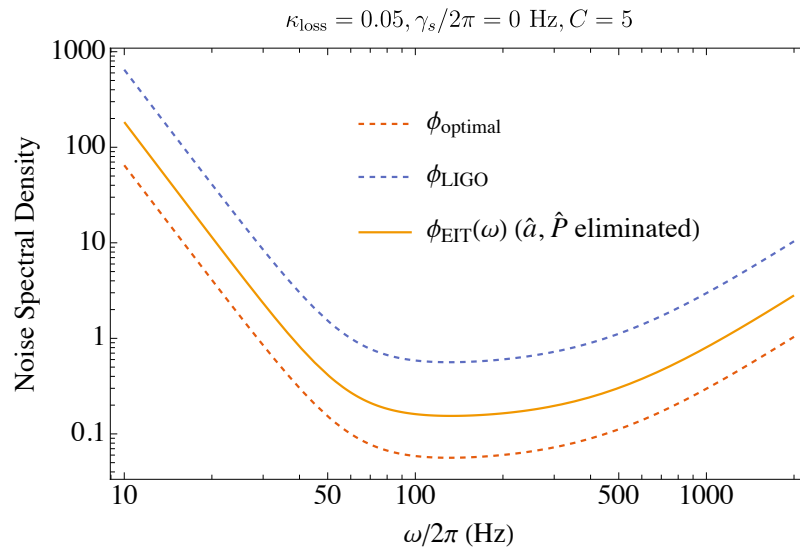
Figure 7.5: **Noise spectral density** with $\kappa_{\mathrm{loss}} = 0.05$, i.e., a 5% loss of light from the 'perfect' mirror. We otherwise have $C = 5$, $\gamma_s = 0$.
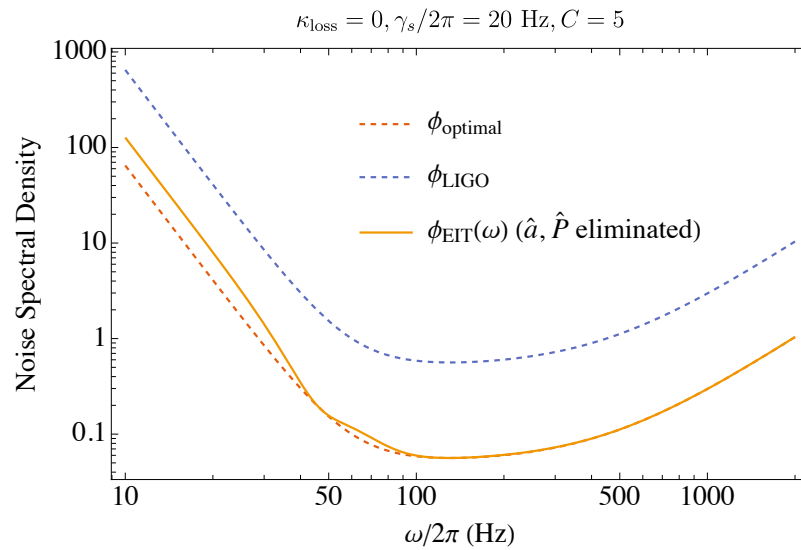
Figure 7.6: **Noise spectral density** with $\gamma_s/2\pi = 20$ Hz. We otherwise have $C = 5$, $\kappa_{\text{loss}} = 0$.
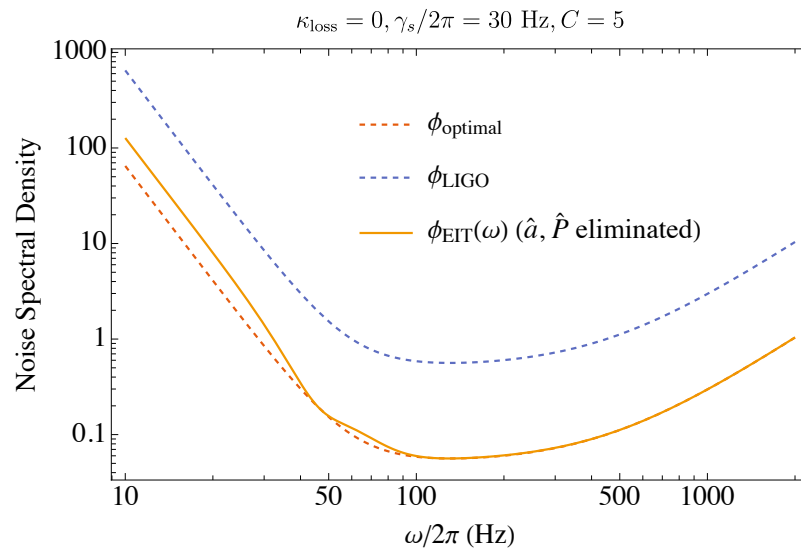
Figure 7.7: **Noise spectral density** with $\gamma_s/2\pi = 30$ Hz. We otherwise have $C = 5$, $\kappa_{\text{loss}} = 0$.
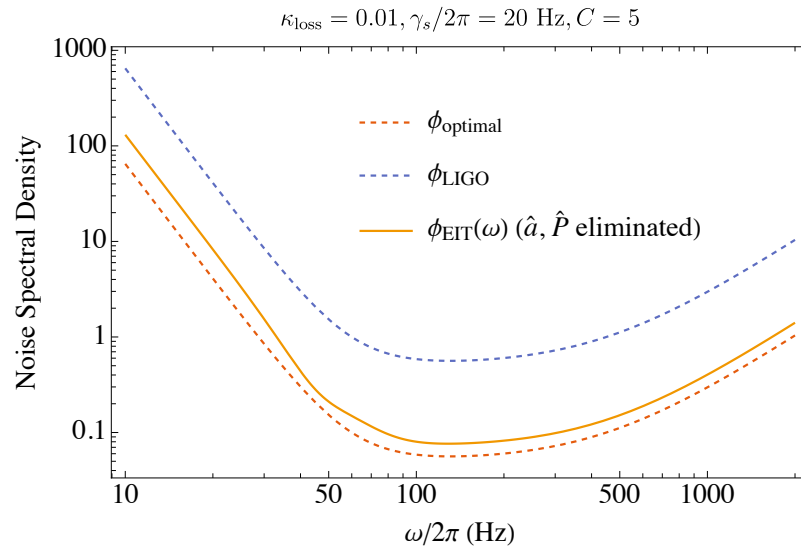
Figure 7.8: **Noise spectral density** with combined losses $\gamma_s/2\pi = 20$ Hz, $\kappa_{\text{loss}} = 0.01$ and $C = 5$.
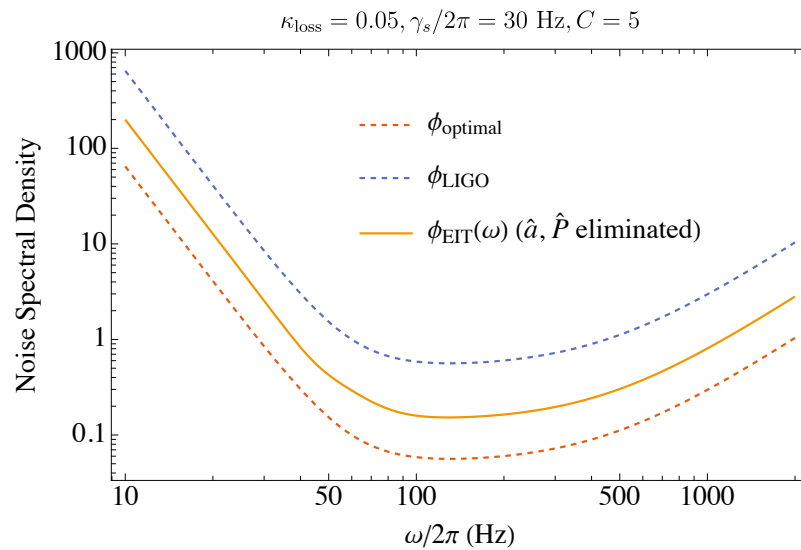
Figure 7.9: **Noise spectral density** with combined losses $\gamma_s/2\pi = 30$ Hz, $\kappa_{\text{loss}} = 0.05$ and $C = 5$.

7.5 Motional averaging
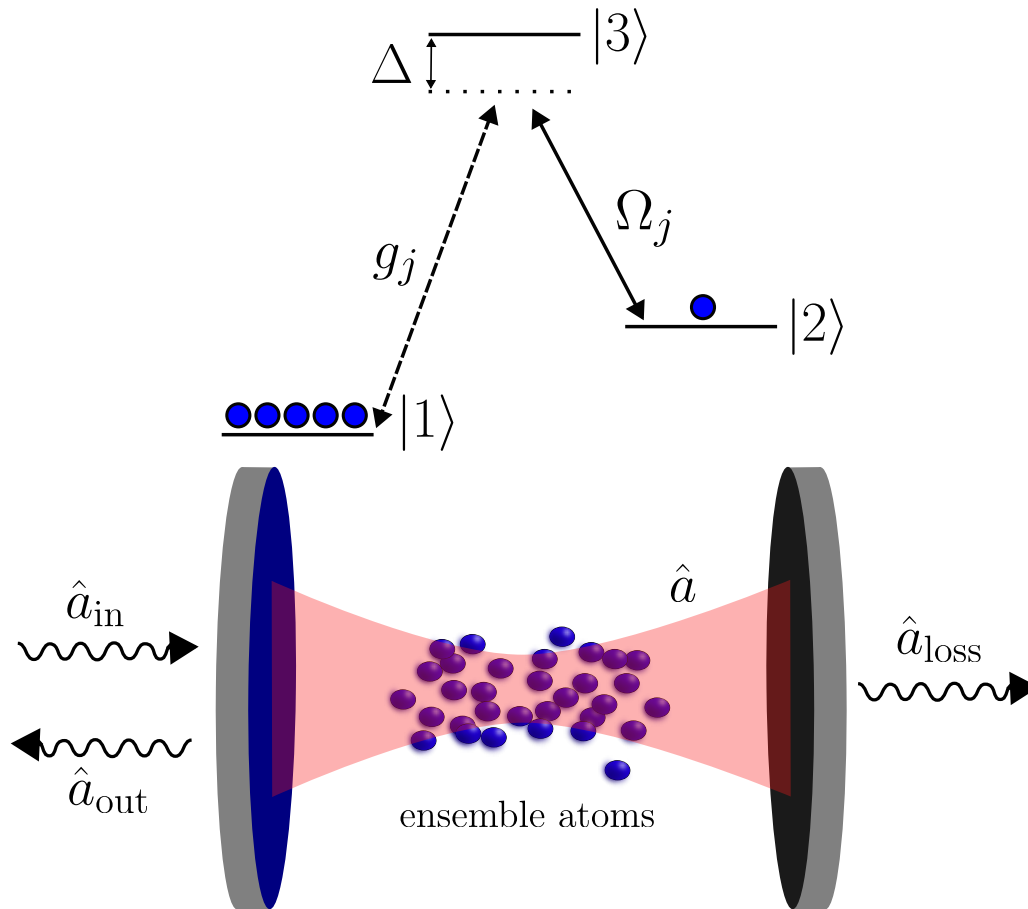
Figure 7.10: **Motional averaging using an atomic ensemble.** The pump laser prepares atoms in the state $|1\rangle$ shown. This state is then coupled to the cavity field $\hat{a}$ with coupling strength g_j, which is different for every atom. A classical drive Ω_j couples the excited state $|3\rangle$ to the storage state $|2\rangle$. The detuning Δ is chosen large to reduce the effects of Doppler broadening.

Our analysis shows that the EIT scheme can produce broadband suppression of noise. However, there are additional noise sources present in real life experiments that we have not yet taken into account. Instead of assuming that the atoms all experience the same coupling to these beams, we instead treat the couplings generally, allowing for the ensemble atoms to dynamically move in and out of the light fields within the

cavity.

We will return to the full equations of motion (7.5) and treat them more completely. We now consider the full setup, as shown in Fig. 7.10, where the ensemble atoms can move in and out of the cavity light beam $\hat{a}$.

7.5.1 Adiabatic elimination of σ_{13}

We will take $\Omega^{(j)}(t)$ and $g^{(j)}(t)$ to have real modes. We can re-write equation (7.5)

$$\frac{d\sigma_{13}^{(j)}}{dt} = -K\sigma_{13}^{(j)} + ig_j(t)a + i\frac{\Omega_j}{2}\sigma_{12}^{(j)} \tag{7.50}$$

where $K = \frac{\gamma}{2} + i\Delta$. Multiplying by $M = Ce^{Kt}$ gives a total derivative on the LHS

$$\frac{d\sigma_{13}^{(j)}}{dt}M + KM\sigma_{13}^{(j)} = \frac{d\sigma_{13}^{(j)}}{dt}M + M'\sigma_{13}^{(j)} = \frac{d}{dt}(M\sigma_{13}) \tag{7.51}$$

$$= iMg_j(t)a + iM\frac{\Omega(t)}{2}\sigma_{12}^{(j)} \tag{7.52}$$

where $M' = KM$. Substituting $\Omega(t) = \Omega_{xy}\sin(k(z_j(0) + v_z^{(j)}(0)t))$ and $g(t) = g_{xy}\sin(k(z_j(0) + v_z^{(j)}(0)t))$, and integrating, we get

$$\sigma_{13}^{(j)} = e^{-Kt}\left(ig_{xy}a\int e^{Kt}\sin(k(z_j(0) + v_z^{(j)}(0)t))dt + \frac{i\Omega_{xy}}{2}\sigma_{12}^{(j)}\int e^{Kt}\sin(k(z_j(0) + v_z^{(j)}(0)t))dt\right) \tag{7.53}$$

$$= \frac{g_{xy}}{2}af_{int} + \frac{\Omega_{xy}}{4}\sigma_{12}^{(j)}f_{int} \tag{7.54}$$

where

$$f_{int} = 2ie^{-Kt}\int e^{Kt}\sin(k(z_j(0) + v_z^{(j)}(0)t))dt \tag{7.55}$$

$$= \frac{e^{ikz_j(t)}}{\frac{\gamma}{2} - i\Delta + ikv_z^{(j)}(0)} + \frac{e^{-ikz_j(t)}}{-\frac{\gamma}{2} + i\Delta + ikv_z^{(j)}(0)} \tag{7.56}$$

and $z_j(t) = z_j(0) + v_z(0)t$. Now, we can eliminate σ_{13} from our equations to obtain

$$\dot{\hat{a}} = -\frac{\kappa}{2}\hat{a} + \sum_{j=0}^{N-1} g^{(j)}(t)\left(\frac{g_{xy}^{(j)}}{4}a + \frac{\Omega_{xy}^{(j)}}{8}\hat{\sigma}_{12}^{(j)}\right)f_j(\gamma, \Delta, k) + \sqrt{\kappa_{\text{in}}}\hat{a}_{\text{in}} \tag{7.57}$$

$$= \left(-\frac{\kappa}{2} + \sum_{j=0}^{N-1}|g_{xy}^{(j)}|^2 f_j(\gamma, \Delta, k)\right)a + \sum_{j=0}^{N-1}\frac{1}{8}g_{xy}^{(j)}(t)\Omega_{xy}^{(j)}f_j(\gamma, \Delta, k)\sigma_{12}^{(j)} + \sqrt{\kappa_{\text{in}}}\hat{a}_{\text{in}} \tag{7.58}$$

$$= \mathcal{A}(t)\hat{a} + \sum_{j=1}^{N}\mathcal{B}_j(t)\sigma_{12}^{(j)} + \sqrt{\kappa_{\text{in}}}\hat{a}_{\text{in}} \tag{7.59}$$

and

$$\dot{\hat{\sigma}}_{12}^{(j)} = -\frac{1}{2}\hat{\sigma}_{12}^{(j)}\gamma_s + \frac{\Omega_{xy}^{(j)}}{8}\left(g_{xy}^{(j)}\hat{a} + \frac{\Omega_{xy}^{(j)}}{2}\hat{\sigma}_{12}^{(j)}\right)f_j(\gamma, \delta, k) \tag{7.60}$$

$$= \frac{1}{8}g_{xy}^{(j)}\Omega_{xy}^{(j)}\hat{a}f_j(\gamma, \Delta, k) + \left(\frac{1}{16}|\Omega_{xy}|^2 f_j(\gamma, \Delta, k) - \frac{1}{2}\gamma_s\right)\hat{\sigma}_{12}^{(j)} \tag{7.61}$$

$$= \mathcal{B}_j\hat{a} + \mathcal{C}_j(t)\hat{\sigma}_{12}^{(j)} \tag{7.62}$$

where

$$\mathcal{A}(t) = -\frac{\kappa}{2} + \sum_{j=1}^{N}|g_{xy}^{(j)}|^2 f_j(\gamma, \Delta, k) \tag{7.63}$$

$$\mathcal{B}_j(t) = \frac{1}{8}g_{xy}^{(j)}(t)\Omega_{xy}^{(j)}(t)f_j(\gamma, \Delta, k) \tag{7.64}$$

$$\mathcal{C}_j(t) = \frac{1}{16}|\Omega_{xy}|^2 f_j(\gamma, \Delta, k) - \frac{1}{2}\gamma_s \tag{7.65}$$

$$f_j(\gamma, \Delta, k) = 2i\sin(k(z_j(0) + v_z^{(j)}(0)t))f_{int} \tag{7.66}$$

$$= \frac{1 - e^{-2ikz_j(t)}}{-\frac{\gamma}{2} - i\Delta + ikv_z(0)} + \frac{-1 + e^{2ikz_j(t)}}{\frac{\gamma}{2} + i\Delta + ikv_z(0)} \tag{7.67}$$

We can now split our operators into a time-independent mean value and (time-dependent) fluctuations. When taking the average of f_j, we neglect the contribution from Doppler broadening and assume the exponential terms average to zero. This

gives

$$\bar{f}_j = = \frac{-1}{\frac{\gamma}{2} - i\left(\Delta - k v_z(0)\right)} - \frac{1}{\frac{\gamma}{2} - i\left(\Delta + k v_z(0)\right)} \tag{7.68}$$

$$= \frac{-4\gamma + 8i\Delta}{4k^2v^2 + (\gamma - 2i\Delta)^2} \tag{7.69}$$

and

$$\delta f(t) = \frac{e^{2ikz_j(t)}}{\frac{\gamma}{2} - i\left(\Delta - k v_z(0)\right)} + \frac{e^{-2ikz_j(t)}}{\frac{\gamma}{2} - i\left(\Delta + k v_z(0)\right)} \tag{7.70}$$

$$\mathcal{A}(t) = \underbrace{-\frac{\kappa}{2} + \sum_{j=1}^{N} |g_{xy}^{(j)}|^2 \bar{f}_j}_{\bar{\mathcal{A}}} + \underbrace{\sum_{j=1}^{N} |g_{xy}^{(j)}|^2 \delta f(t)}_{\delta \mathcal{A}(t)} \tag{7.71}$$

$$\mathcal{B}_j(t) = \underbrace{\frac{1}{8} g_{xy}^{(j)}(t) \Omega_{xy}^{(j)}(t) \bar{f}_j}_{\bar{\mathcal{B}}} + \underbrace{\frac{1}{8} g_{xy}^{(j)}(t) \Omega_{xy}^{(j)}(t) \delta f(t)}_{\delta \mathcal{B}(t)} \tag{7.72}$$

$$\mathcal{C}_j(t) = \underbrace{\frac{1}{16} |\Omega_{xy}|^2 \bar{f}_j + \frac{1}{2} \gamma_s}_{\bar{\mathcal{C}}} + \underbrace{\frac{1}{16} |\Omega_{xy}|^2 \delta f(t)}_{\delta \mathcal{C}(t)} \tag{7.73}$$

Here we note that

$$\Omega_{xy}^{(j)}(t) = \Omega e^{\frac{-x_j^2(t) - y_j^2(t)}{w^2}} \tag{7.74}$$

$$g_{xy}^{(j)}(t) = g e^{\frac{-x_j^2(t) - y_j^2(t)}{w^2}} \tag{7.75}$$

i.e., both have a Gaussian shape. This reflects the Gaussian shape of the light beam in the transverse direction, and the sinusoidal term that we included earlier describes the oscillations in the light beam electric field. To summarise, we have

$$\dot{\hat{a}} = \mathcal{A}(t)\hat{a} + \sum_{j=1}^{N} \mathcal{B}_j(t)\hat{\sigma}_{12}^{(j)} + \sqrt{\kappa_{\text{in}}}\hat{a}_{\text{in}} \tag{7.76}$$

$$\dot{\hat{\sigma}}_{12}^{(j)} = \mathcal{B}_j \hat{a} + \mathcal{C}_j(t)\hat{\sigma}_{12}^{(j)} \tag{7.77}$$

The $(N+1) \times (N+1)$ equations can be written in a coupling matrix form

$$\dot{\mathbf{x}} = \mathbf{M}'(t)\mathbf{x}(t) + \sqrt{\kappa}\hat{\mathbf{a}}_{in} \tag{7.78}$$

117

where $\mathbf{x}(t) = \left(\hat{a}, \hat{\sigma}_{21}^{(0)}, \hat{\sigma}_{21}^{(1)}, \ldots, \hat{\sigma}_{21}^{(N-1)}\right)^T$, the elements of our basis are $\mathcal{B}_i = \mathbf{x}_i \mathbf{v}_i$ and $\mathbf{v}_i = (0, 0, \ldots, 1_i, 0, 0, \ldots)^T$. The coupling matrix $\mathbf{M}' = \mathbf{M}'_0 + \mathbf{M}'_1$ where

$$\mathbf{M}'_0 = \begin{pmatrix} \bar{\mathcal{A}} & \bar{\mathcal{B}} & \bar{\mathcal{B}} & \bar{\mathcal{B}} & \ldots & \bar{\mathcal{B}} \\ \bar{\mathcal{B}} & \bar{\mathcal{C}} & 0 & 0 & \ldots & 0 \\ \bar{\mathcal{B}} & 0 & \bar{\mathcal{C}} & 0 & \ldots & 0 \\ \vdots & \vdots & \vdots & \ddots & & \vdots \\ \vdots & \vdots & \vdots & & \ddots & \vdots \\ \bar{\mathcal{B}} & 0 & 0 & \ldots & \ldots & \bar{\mathcal{C}} \end{pmatrix} \tag{7.79}$$

$$\mathbf{M}'_1 = \begin{pmatrix} \delta\mathcal{A} & \delta\mathcal{B}_0 & \delta\mathcal{B}_1 & \delta\mathcal{B}_2 & \ldots & \delta\mathcal{B}_{N-1} \\ \delta\mathcal{B}_0 & \delta\mathcal{C}_0 & 0 & 0 & \ldots & 0 \\ \delta\mathcal{B}_1 & 0 & \delta\mathcal{C}_1 & 0 & \ldots & 0 \\ \vdots & \vdots & \vdots & \ddots & & \vdots \\ \vdots & \vdots & \vdots & & \ddots & \vdots \\ \delta\mathcal{B}_{N-1} & 0 & 0 & \ldots & \ldots & \delta\mathcal{C}_{N-1} \end{pmatrix} \tag{7.80}$$

This matrix equation describes the coupling to individual modes. In the analysis above, it was advantageous to introduce collective mode operators, which we generalise here to produce a collective mode description of the system.

7.5.2 Change of basis

We now define

$$\hat{S}_k = \frac{1}{\sqrt{N}} \sum_{\ell=0}^{N-1} e^{ik\ell\frac{2\pi}{N}} \hat{\sigma}_{12}^{(\ell)} \tag{7.81}$$

with inverse

$$\hat{\sigma}_{12}^{(j)} = \frac{1}{\sqrt{N}} \sum_{\ell=0}^{N-1} e^{-ij\ell\frac{2\pi}{N}} \hat{S}_\ell \tag{7.82}$$

This $\hat{S}_k$ operator is the generalisation of the operator $\hat{S} = \hat{S}_{k=0}$ that we wrote down before. The operator $\hat{S}_0^\dagger$ generates the Dicke state when acting on the vacuum, i.e.,

it excites the atom from the ground to the storage state. Note the orthogonality condition

$$\sum_{n=0}^{N-1} e^{\frac{i2\pi}{N}(k-k')n} = N \ \delta_{kk'} \tag{7.83}$$

In this basis, we have

$$\dot{\hat{a}} = \mathcal{A}(t)\hat{a} + \frac{1}{\sqrt{N}}\sum_{j=0}^{N-1}\sum_{\ell=0}^{N-1}\bar{\mathcal{B}}e^{-ij\ell\frac{2\pi}{N}}\hat{S}_\ell + \frac{1}{\sqrt{N}}\sum_{j=0}^{N-1}\sum_{\ell=0}^{N-1}\delta\mathcal{B}_j(t)e^{-ij\ell\frac{2\pi}{N}}\hat{S}_\ell + \sqrt{\kappa_{\mathrm{in}}}\hat{a}_{\mathrm{in}}$$

$$\tag{7.84}$$

$$= \mathcal{A}(t)\hat{a} + \frac{\bar{\mathcal{B}}}{\sqrt{N}}\sum_{\ell=0}^{N-1}\underbrace{\sum_{j=0}^{N-1}e^{-ij\ell\frac{2\pi}{N}}}_{N\delta_{\ell 0}}\hat{S}_\ell + \sum_{\ell=0}^{N-1}\underbrace{\frac{1}{\sqrt{N}}\sum_{j=0}^{N-1}\delta\mathcal{B}_j(t)e^{-ij\ell\frac{2\pi}{N}}}_{\equiv\delta\mathcal{B}_\ell^{\hat{a}}}\hat{S}_\ell + \sqrt{\kappa_{\mathrm{in}}}\hat{a}_{\mathrm{in}}$$

$$\tag{7.85}$$

$$= \bar{\mathcal{A}}\hat{a} + \delta\mathcal{A}(t)\hat{a} + \bar{\mathcal{B}}\sqrt{N}\hat{S}_0 + \sum_{\ell=0}^{N-1}\delta B_\ell^{\hat{a}}(t)\hat{S}_\ell + \sqrt{\kappa_{\mathrm{in}}}\hat{a}_{\mathrm{in}} \tag{7.86}$$

where we have defined

$$\delta\mathcal{B}_\ell^{\hat{a}}(t) \equiv \frac{1}{\sqrt{N}}\sum_{j=0}^{N-1}\delta\mathcal{B}_j(t)e^{-ij\ell\frac{2\pi}{N}} \tag{7.87}$$

Summing (7.77) over j, and writing $\mathcal{C}_j(t) = \bar{\mathcal{C}} + \delta\mathcal{C}_j(t)$, we can write an expression for $\dot{\hat{S}}_\ell$.

$$\frac{1}{\sqrt{N}} \sum_{j=0}^{N-1} e^{ij\ell\frac{2\pi}{N}} \dot{\hat{\sigma}}_{12}^{(j)} = \frac{1}{\sqrt{N}} \sum_{j=0}^{N-1} \mathcal{B}_j(t) e^{ij\ell\frac{2\pi}{N}} \hat{a} + \sum_{j=0}^{N-1} \sum_{\ell'=0}^{N-1} e^{ij\ell\frac{2\pi}{N}} \mathcal{C}_j(t) e^{-ij\ell'\frac{2\pi}{N}} \hat{S}_{\ell'}$$

(7.88)

$$\Rightarrow \dot{\hat{S}}_\ell = \sqrt{N}\bar{\mathcal{B}}\delta_{\ell 0}\hat{a} + \underbrace{\sum_{j=0}^{N-1} \delta\mathcal{B}_j(t) e^{ij\ell\frac{2\pi}{N}}}_{=\delta\mathcal{B}_{-\ell}^{\hat{a}}(t)} \hat{a} + \bar{\mathcal{C}}\hat{S}_\ell + \sum_{\ell'=0}^{N-1} \underbrace{\sum_{j=0}^{N-1} e^{ij(\ell-\ell')\frac{2\pi}{N}} \delta\mathcal{C}_j(t)}_{\equiv\delta\mathcal{C}_{\ell,\ell'}(t)} \hat{S}_{\ell'} \quad (7.89)$$

$$= \sqrt{N}\bar{\mathcal{B}}\delta_{\ell 0}\hat{a} + \delta\mathcal{B}_{-\ell}^{\hat{a}}(t)\hat{a} + \bar{\mathcal{C}}\hat{S}_\ell + \sum_{\ell'=0}^{N-1} \delta\mathcal{C}_{\ell,\ell'}(t)\hat{S}_{\ell'} \tag{7.90}$$

In this new basis, we have

$$\dot{\hat{a}} = \bar{\mathcal{A}}\hat{a} + \bar{\mathcal{B}}\sqrt{N}\hat{S}_0 + \mathcal{A}(t)\hat{a} + \sum_{\ell=0}^{N-1} B_\ell^{\hat{a}}(t)\hat{S}_\ell + \sqrt{\kappa_{\text{in}}}\hat{a}_{\text{in}} \tag{7.91}$$

$$\dot{\hat{S}}_\ell = \sqrt{N}\bar{\mathcal{B}}\delta_{\ell 0}\hat{a} + \delta\mathcal{B}_{-\ell}^{\hat{a}}(t)\hat{a} + \bar{\mathcal{C}}\hat{S}_\ell + \sum_{\ell'=0}^{N-1} \delta\mathcal{C}_{\ell,\ell'}(t)\hat{S}_{\ell'} \tag{7.92}$$

We have now the matrix equation $\mathbf{y}'(t) = \mathbf{M}\mathbf{y}(t) + \sqrt{\kappa}\hat{\mathbf{a}}_{in}(t)$, where $\mathbf{M} = \bar{\mathbf{M}} + \delta\mathbf{M}(t)$ and

$$\bar{\mathbf{M}} = \begin{pmatrix} \bar{\mathcal{A}} & \sqrt{N}\bar{\mathcal{B}} & 0 & \cdots & 0 \\ \sqrt{N}\bar{\mathcal{B}} & \bar{\mathcal{C}} & & & \\ 0 & & \bar{\mathcal{C}} & & \\ \vdots & & & \ddots & \\ 0 & & & & \bar{\mathcal{C}} \end{pmatrix} \tag{7.93}$$

and,

$$\delta\mathbf{M}(t) = \begin{pmatrix} \delta\mathcal{A}(t) & \delta\mathcal{B}_\ell^{\hat{a}}(t) \\ \delta\mathcal{B}_{-\ell}^{\hat{a}}(t) & \delta\mathcal{C}_{\ell,\ell'}(t) \end{pmatrix} \tag{7.94}$$

$$= \begin{pmatrix} \delta\mathcal{A}(t) & \delta\mathcal{B}_0^{\hat{a}}(t) & \delta\mathcal{B}_1^{\hat{a}}(t) & \dots & \delta\mathcal{B}_{N-1}^{\hat{a}}(t) \\ \delta\mathcal{B}_0^{\hat{a}}(t) & \delta\mathcal{C}_{0,0}(t) & \delta\mathcal{C}_{0,1}(t) & \dots & \delta\mathcal{C}_{0,N-1}(t) \\ \delta\mathcal{B}_{-1}^{\hat{a}}(t) & \delta\mathcal{C}_{1,0}(t) & \delta\mathcal{C}_{1,1}(t) & & \vdots \\ \vdots & \vdots & & \ddots & \\ \delta\mathcal{B}_{1-N}^{\hat{a}}(t) & \delta\mathcal{C}_{N-1,0}(t) & \dots & & \delta\mathcal{C}_{N-1,N-1}(t) \end{pmatrix} \tag{7.95}$$

Here we can see that the coefficient $\mathcal{A}$ couples the light field to itself, that $\mathcal{C}$ couples the $\hat{S}_\ell$ modes to each other, and it is $\mathcal{B}_\ell^{\hat{a}}$ that couples the atoms to the light field. The description in terms of only the coupling matrix $\bar{\mathbf{M}}$ reduces exactly to the EIT description that we derived above, with the fluctuations $\delta\mathbf{M}(t)$ corresponding to additional noise terms that we will quantify below.

7.6 Perturbation expansion

To quantify the degree to which the motional averaging will introduce extra noise, we wish to perform a perturbation expansion up to second order. Recall our coupling matrix equation

$$\mathbf{y}'(t) = \mathbf{M}(t)\mathbf{y}(t) + \sqrt{\kappa}\hat{\mathbf{a}}_{in}(t), \tag{7.96}$$

where $\mathbf{y}, \hat{\mathbf{a}}_{in}$ are both vectors, and $\mathbf{M}$ is the coupling matrix for the system of differential equations. We will now expand

$$\mathbf{y}(t) = \mathbf{y}_0(t) + \lambda\mathbf{y}_1(t) + \lambda^2\mathbf{y}_2(t) \tag{7.97}$$

$$\mathbf{M}(t) = \bar{\mathbf{M}} + \lambda\delta\mathbf{M}(t), \tag{7.98}$$

where λ is a parameter we will use to keep track of the order of the perturbation. Inserting these into (7.96), and equating orders of λ

$$\mathbf{y}_0'(t) = \bar{\mathbf{M}}y_0(t) + \sqrt{\kappa}\hat{\mathbf{a}}_{in} \tag{7.99}$$

$$\mathbf{y}_1'(t) = \delta\mathbf{M}(t)\mathbf{y}_0(t) + \bar{\mathbf{M}}\mathbf{y}_1(t) \tag{7.100}$$

$$\mathbf{y}_2'(t) = \delta\mathbf{M}(t)\mathbf{y}_1(t) + \bar{\mathbf{M}}\mathbf{y}_2(t) \tag{7.101}$$

Moving to the Fourier domain, we obtain

$$-i\omega\mathbf{y}_0(\omega) = \bar{\mathbf{M}}\mathbf{y}_0(\omega) + \sqrt{\kappa}\hat{\mathbf{a}}_{in}(\omega) \tag{7.102}$$

$$-i\omega\mathbf{y}_1(\omega) = \bar{\mathbf{M}}\mathbf{y}_1(\omega) + \int \delta\mathbf{M}(\omega - \omega')\mathbf{y}_0(\omega')d\omega' \tag{7.103}$$

$$-i\omega\mathbf{y}_2(\omega) = \bar{\mathbf{M}}\mathbf{y}_2(\omega) + \int \delta\mathbf{M}(\omega - \omega')\mathbf{y}_1(\omega')d\omega' \tag{7.104}$$

where the integrals result from the convolution theorem for products in Fourier space. The solution to the 0th order equation is

$$\mathbf{y}_0(\omega) = -\left[i\omega + \bar{\mathbf{M}}\right]^{-1}\sqrt{\kappa}\hat{\mathbf{a}}_{in}(\omega) \tag{7.105}$$

Plugging this into the first order equation gives

$$\mathbf{y}_1(\omega) = \left[i\omega + \bar{\mathbf{M}}\right]^{-1}\left(\int_{-\infty}^{\infty} \delta\mathbf{M}(\omega - \omega')\left[i\omega' + \bar{\mathbf{M}}\right]^{-1}\sqrt{\kappa}\hat{\mathbf{a}}_{in}(\omega')d\omega'\right) \tag{7.106}$$

and finally plugging this into the second order equation gives

$$\mathbf{y}_2(\omega) = -\left[i\omega + \bar{\mathbf{M}}\right]^{-1}\left(\int_{-\infty}^{\infty} \delta\mathbf{M}(\omega - \omega')\left[i\omega' + \bar{\mathbf{M}}\right]^{-1}\right.$$
$$\left.\left(\int_{-\infty}^{\infty} \delta\mathbf{M}(\omega' - \omega'')\left[i\omega'' + \bar{\mathbf{M}}\right]^{-1}\sqrt{\kappa}\hat{\mathbf{a}}_{in}(\omega'')d\omega''\right)d\omega'\right) \tag{7.107}$$

7.6.1 Expression for inverse matrix

Since $\bar{\mathbf{M}}$ is in block diagonal form, we can invert it fairly easily. We call the 2×2 matrix in the top left corner $\mathbf{T}$ and find the inverse

$$\mathbf{T} + i\omega = \begin{pmatrix} \bar{\mathcal{A}} + i\omega & \sqrt{N}\bar{\mathcal{B}} \\ \sqrt{N}\bar{\mathcal{B}} & \bar{\mathcal{C}} + i\omega \end{pmatrix} \tag{7.108}$$

$$\Rightarrow (\mathbf{T} + i\omega)^{-1} = \hat{\mathcal{T}} = \frac{1}{(\bar{\mathcal{A}} + i\omega)(\bar{\mathcal{C}} + i\omega) - N\bar{\mathcal{B}}^2}\begin{pmatrix} \bar{\mathcal{C}} + i\omega & \sqrt{N}\bar{\mathcal{B}} \\ \sqrt{N}\bar{\mathcal{B}} & \bar{\mathcal{A}} + i\omega \end{pmatrix} \tag{7.109}$$

The rest of the entries are simply $\bar{\mathcal{C}} + i\omega$ so the reciprocal will be taken in the inverse matrix $(\mathbf{M_0} + i\omega)^{-1}$. i.e., we have

$$(\bar{\mathbf{M}} + i\omega)^{-1} = \mathbf{W}(\omega) = \begin{pmatrix} \hat{\mathcal{T}} & 0 & \dots & 0 \\ 0 & \frac{1}{\bar{\mathcal{C}}+i\omega} & 0 & \vdots \\ \vdots & & \ddots & 0 \\ 0 & \dots & 0 & \frac{1}{\bar{\mathcal{C}}+i\omega} \end{pmatrix} \tag{7.110}$$

Note that the S_0 mode (the symmetric Dicke state) is the mode that is ultimately being coupled by the propagator $\mathbf{W}$.

7.6.2 Solution to the average equations of motion

We will now show that our zeroth order solution is equal to the EIT solution derived in the previous section. The zeroth order term $\hat{a}$ is the zeroth component of $\mathbf{y}_0$

$$\mathbf{y}_0 = - \left[i\omega + \mathbf{M}_0 \right]^{-1} \sqrt{\kappa} \hat{\mathbf{a}}_{in} \tag{7.111}$$

$$= -\sqrt{\kappa} \mathbf{W} \hat{a}_{in}(\omega) \mathbf{e}_0 \tag{7.112}$$

where $\mathbf{e}_0$ is a basis vector. In order to extract the zeroth component (the one corresponding to $\hat{a}$), we left multiply by the basis vector $\mathbf{e}_0^\dagger$, giving

$$\hat{a}^{(0)}(\omega) = -\mathbf{e}_0^\dagger \mathbf{W}(\omega) \sqrt{\kappa_{in}} \hat{a}_{in}(\omega) \tag{7.113}$$

$$= -\mathbf{W}_{00}(\omega) \sqrt{\kappa_{in}} \hat{a}_{in}(\omega), \tag{7.114}$$

where

$$\mathbf{W}_{00} = \frac{\bar{\mathcal{C}} + i\omega}{(\bar{\mathcal{A}} + i\omega)(\bar{\mathcal{C}} + i\omega) - N\bar{\mathcal{B}}^2}. \tag{7.115}$$

We can now find a reflection coefficient using the now familiar input-output relation

$$\hat{a}_{\text{in}} + \hat{a}_{\text{out}} = \sqrt{\kappa_{\text{out}}} \hat{a}. \tag{7.116}$$

We have

$$\hat{a}_{\text{in}} + \hat{a}_{\text{out}} = -\kappa \hat{a}_{\text{in}} \mathbf{W}_{00} \tag{7.117}$$

$$\Rightarrow \frac{\hat{a}_{\text{out}}}{\hat{a}_{\text{in}}} = -1 - \kappa \mathbf{W}_{00} \tag{7.118}$$

We assume that we are far-detuned $\Delta \ll k v_z(0)$ such that we can neglect the effects of Doppler broadening, and write

$$r = -1 - \frac{\kappa\left(-\frac{\Omega^2}{4\left(\frac{\gamma}{2}+i\Delta\right)} - \frac{\gamma_s}{2} + i\omega\right)}{\left(-\frac{\gamma C\kappa}{\frac{\gamma}{2}+i\Delta} - \frac{\kappa}{2} + i\omega\right)\left(-\frac{\Omega^2}{4\left(\frac{\gamma}{2}+i\Delta\right)} - \frac{\gamma_s}{2} + i\omega\right) - \frac{\gamma C\kappa\Omega^2}{16\left(\frac{\gamma}{2}+i\Delta\right)^2}}. \tag{7.119}$$

When $\gamma_s = 0$, we have

$$r = -1 - \frac{\kappa}{-\frac{\gamma C\kappa\Omega^2}{16\left(\frac{\gamma}{2}+i\Delta\right)^2\left(i\omega - \frac{\Omega^2}{4\left(\frac{\gamma}{2}+i\Delta\right)}\right)} - \frac{\gamma C\kappa}{\frac{\gamma}{2}+i\Delta} - \frac{\kappa}{2} + i\omega} \tag{7.120}$$

This is of the same functional form as if we adiabatically eliminate $\hat{P}$ in the standard EIT equations from above, where we have made the rescalings $\Omega \to \sqrt{2}\Omega$ and $g \to \sqrt{2}g$. In Fig. 7.11, we plot this noise spectral density for this zeroth order correction alongside the standard EIT solution. As before, without losses we can reach the noise floor provided by the optimal angle ϕ_{optimal}.
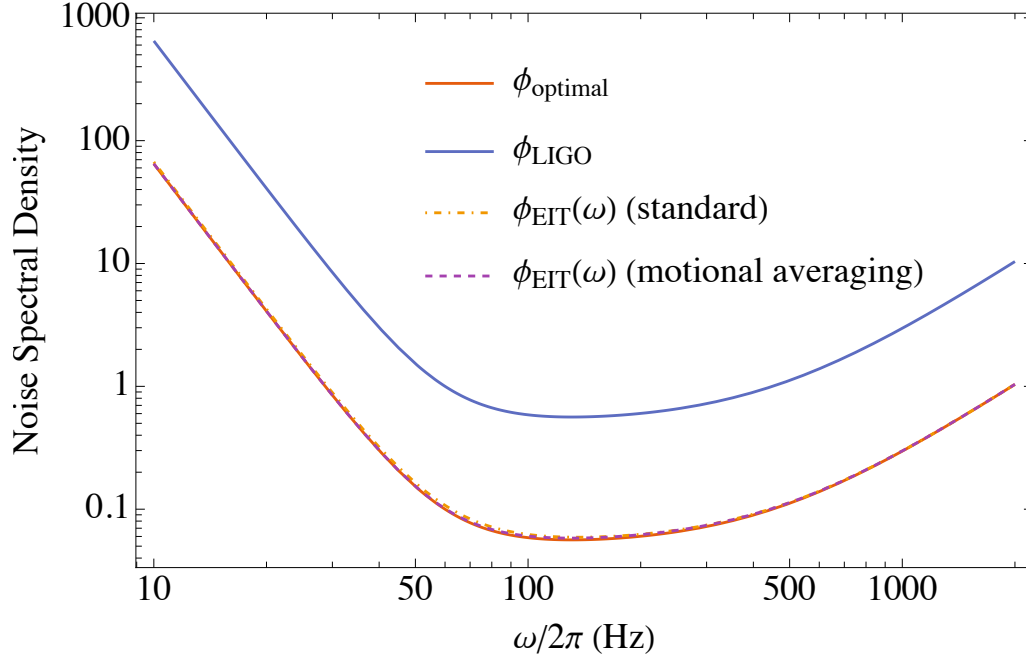
Figure 7.11: **Comparison of the noise spectral density** of standard EIT (dot-dashed), with the zeroth order motional averaging solution (dashed). We have broadband suppression of the noise compared to the unsqueezed ϕ_{LIGO}, and reach the level of the optimal solution ϕ_{optimal} when we have turned off losses due to the cavity and finite lifetime of the storage state.

7.7 Higher order corrections and noise spectral density

The first order correction to $\hat{a}$ is

$$\hat{a}^{(1)}(\omega) = \mathbf{e}_0^\dagger \mathbf{W}(\omega) \int_{-\infty}^{\infty} \delta\mathbf{M}(\omega - \omega') \mathbf{W}(\omega') \mathbf{e}_0 \sqrt{\kappa_{in}} \hat{a}_{in}(\omega') d\omega' \tag{7.121}$$

$$= \sum_{ij} \mathbf{W}_{0i}(\omega) \int_{-\infty}^{\infty} \delta\mathbf{M}_{ij}(\omega - \omega') \mathbf{W}_{j0}(\omega') \sqrt{\kappa_{in}} \hat{a}_{in}(\omega') d\omega' \tag{7.122}$$

125

and the second order correction is

$$\hat{a}^{(2)}(\omega) = -\mathbf{e}_0^\dagger \mathbf{W}(\omega) \left(\int_{-\infty}^{\infty} \delta\mathbf{M}(\omega - \omega')\mathbf{W}(\omega') \right.$$

$$\left. \times \left(\int_{-\infty}^{\infty} \delta\mathbf{M}(\omega' - \omega'')\mathbf{W}(\omega'')\mathbf{e}_0\sqrt{\kappa_{in}}\hat{a}_{in}(\omega'')d\omega'' \right) d\omega' \right) \tag{7.123}$$

$$= -\sum_{ijk\ell} \mathbf{W}_{0i}(\omega) \left(\int_{-\infty}^{\infty} \delta\mathbf{M}_{ij}(\omega - \omega')\mathbf{W}_{jk}(\omega') \right)$$

$$\times \left(\int_{-\infty}^{\infty} \delta\mathbf{M}_{k\ell}(\omega' - \omega'')\mathbf{W}_{\ell 0}(\omega'')\sqrt{\kappa_{in}}\hat{a}_{in}(\omega'')d\omega'' \right) d\omega' \tag{7.124}$$

$$= -\sqrt{\kappa_{in}} \int_{-\infty}^{\infty} \sum_{ijk\ell} \mathbf{W}_{0i}(\omega)\delta\mathbf{M}_{ij}(\omega - \omega')\mathbf{W}_{jk}(\omega')\delta\mathbf{M}_{k\ell}(\omega' - \omega'')$$

$$\times \mathbf{W}_{\ell 0}(\omega'')\sqrt{\kappa_{in}}\hat{a}_{in}(\omega'')d\omega''d\omega' \tag{7.125}$$

7.7.1 Noise spectral density to second order

We want to compute the noise spectral density which can be achieved by a single computation (see Appendix 7.12) of expectation values of the generalised quadrature operator $\hat{Y}(\omega, \theta) = \frac{e^{i\theta}a(-\omega)^\dagger + e^{-i\theta}a(\omega)}{2}$ expanded to second order

$$Y^\dagger(\omega_1, \theta)Y(\omega_2, \theta) = \frac{1}{4}\left(e^{2i\theta}a_0\left(\omega_1\right)^\dagger \cdot a_2\left(-\omega_2\right)^\dagger + e^{2i\theta}a_2\left(\omega_1\right)^\dagger \cdot a_0\left(-\omega_2\right)^\dagger \right.$$

$$+ e^{-2i\theta}a_0\left(-\omega_1\right) \cdot a_2\left(\omega_2\right) + e^{-2i\theta}a_2\left(-\omega_1\right) \cdot a_0\left(\omega_2\right)$$

$$+ a_0\left(\omega_1\right)^\dagger \cdot a_2\left(\omega_2\right) + a_2\left(\omega_1\right)^\dagger \cdot a_0\left(\omega_2\right)$$

$$\left. + a_0\left(-\omega_1\right) \cdot a_2\left(-\omega_2\right)^\dagger + a_2\left(-\omega_1\right) \cdot a_0\left(-\omega_2\right)^\dagger \right) \tag{7.126}$$

where we have thrown away $a_1 a_1$ terms, which were argued in [94] were negligible. After some algebra (see Appendix 7.11), we obtain

$$\langle Y^\dagger(\omega_1, \theta)Y(\omega_2, \theta) \rangle$$

$$= \frac{\kappa_{in}}{8}\delta(\omega_1 - \omega_2)\int d\tau d\omega' \sum_{\ell} \cosh^2(r)\mathcal{T}(-\omega_1) + \sinh^2(r)\mathcal{T}(\omega_1)$$

$$+ \sinh(2r)\Big(\mathcal{U}(\omega_1) + \mathcal{U}(-\omega_1) + \mathcal{V}(\omega_1) + \mathcal{V}(-\omega_1)\Big) \tag{7.127}$$

where

$$
\begin{aligned}
\mathcal{T}(\omega_1) = {}& 2\mathbf{W}_{00}\left(\omega_1\right)W_D(\omega')^* e^{i\tau(\omega'-\omega_1)}\Big(\mathbf{W}_{01}\left(\omega_1\right)^*\mathbf{W}_{00}\left(\omega_1\right)^*\left(\delta\mathcal{B}_\ell(t')\delta\mathcal{C}_\ell(t)\right)^* \\
& + \mathbf{W}_{10}\left(\omega_1\right)^*\left(\mathbf{W}_{00}\left(\omega_1\right)^*\left(\delta\mathcal{B}_\ell(t)\delta\mathcal{C}_\ell(t')\right)^* + \mathbf{W}_{01}\left(\omega_1\right)^*\left(\delta\mathcal{C}_\ell(t)\delta\mathcal{C}_\ell(t')\right)^*\right) \\
& + \left(\mathbf{W}_{00}\left(\omega_1\right)^*\right)^2\left(\delta\mathcal{B}_\ell(t)\delta\mathcal{B}_\ell(t')\right)^*\Big) \\
& + 2\mathbf{W}_{00}\left(\omega_1\right)^* W_D(\omega')e^{i\tau(\omega_1-\omega')}\Big(\mathbf{W}_{00}\left(\omega_1\right)\delta\mathcal{B}_\ell(t) + \mathbf{W}_{01}\left(\omega_1\right)\delta\mathcal{C}_\ell(t)\Big) \\
& \left(\mathbf{W}_{00}\left(\omega_1\right)\delta\mathcal{B}_\ell(t') + \mathbf{W}_{10}\left(\omega_1\right)\delta\mathcal{C}_\ell(t')\right) \tag{7.128}
\end{aligned}
$$

$$
\begin{aligned}
\mathcal{U}(\omega_1) = {}& \mathbf{W}_{00}\left(-\omega_1\right)^* W_D(\omega')^*\left(-e^{i(2\theta+\tau(\omega'-\omega_1))}\right) \\
& \Big(\mathbf{W}_{01}\left(\omega_1\right)^*\mathbf{W}_{00}\left(\omega_1\right)^*\left(\delta\mathcal{B}_\ell(t')\delta\mathcal{C}_\ell(t)\right)^* + \mathbf{W}_{10}\left(\omega_1\right)^*\Big(\mathbf{W}_{00}\left(\omega_1\right)^*\left(\delta\mathcal{B}_\ell(t)\delta\mathcal{C}_\ell(t')\right)^* \\
& + \mathbf{W}_{01}\left(\omega_1\right)^*\left(\delta\mathcal{C}_\ell(t)\delta\mathcal{C}_\ell(t')\right)^*\Big) + \left(\mathbf{W}_{00}\left(\omega_1\right)^*\right)^2\left(\delta\mathcal{B}_\ell(t)\delta\mathcal{B}_\ell(t')\right)^*\Big) \tag{7.129}
\end{aligned}
$$

and

$$
\begin{aligned}
\mathcal{V}(\omega_1) = {}& \mathbf{W}_{00}\left(-\omega_1\right)W_D(\omega')e^{-i(2\theta+\tau(\omega'-\omega_1))}\Big(\mathbf{W}_{00}\left(\omega_1\right)\delta\mathcal{B}_\ell(t) \\
& + \mathbf{W}_{01}\left(\omega_1\right)\delta\mathcal{C}_\ell(t)\Big)\left(\mathbf{W}_{00}\left(\omega_1\right)\delta\mathcal{B}_\ell(t') + \mathbf{W}_{10}\left(\omega_1\right)\delta\mathcal{C}_\ell(t')\right) \tag{7.130}
\end{aligned}
$$

7.8 Atomic billiards simulation

To evaluate the average and second order correction, we need atomic trajectories $\mathcal{A}(t)$, $\mathcal{B}(t)$ and $\mathcal{C}(t)$, which are provided by an atomic billiard simulation. We simulate N atoms with a thermal velocity distribution inside a box with variable geometry, to allow for both rectangular and circular cross-sections.

With large enough N, the values of $\bar{\mathcal{A}}$, $\bar{\mathcal{B}}$ and $\bar{\mathcal{C}}$ from the simulation can reproduce the broadband noise suppression in the average case, as shown in Fig. 7.12. The simulation will be used to produce the second order correction to the noise spectral density in future work. To do this, the formula (7.127) will be included in the simulation, making use of the atomic trajectories in the calculation for the NSD.
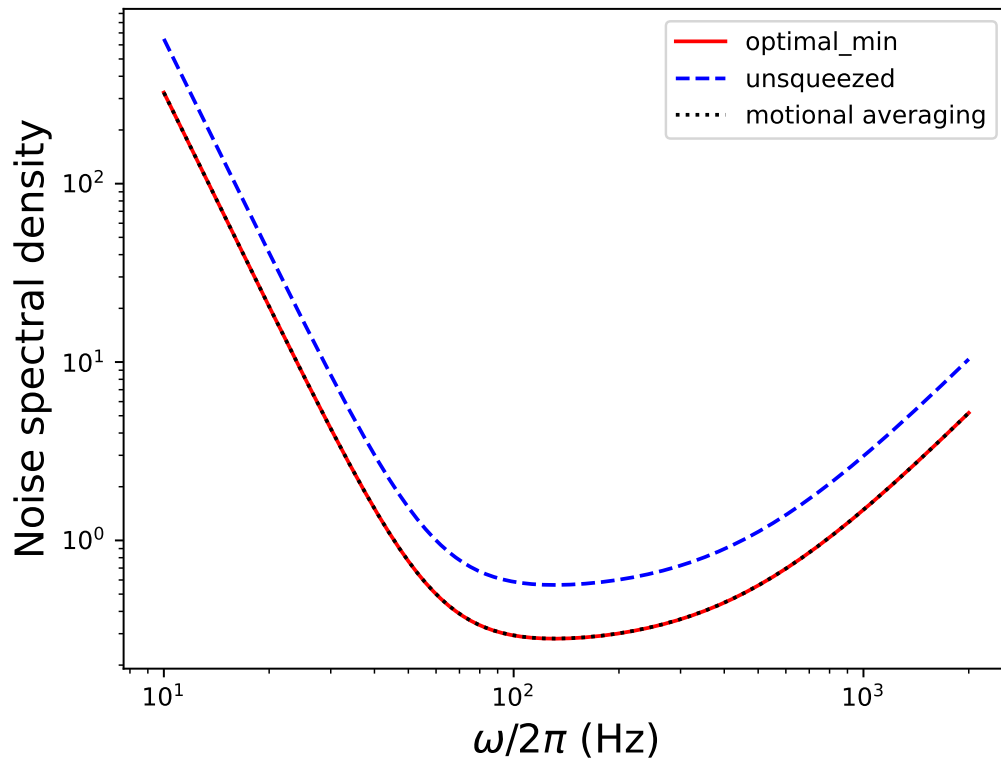
Figure 7.12: **Calculation of the noise spectral density from an atomic billiard simulation.** The motional averaging here is computed to lowest order only, i.e., without the second order correction. Without losses, we can reproduce the optimal broadband suppression from the optimal squeezing angle.

7.9   Summary and Conclusions

In these chapters, we have shown that frequency-dependent squeezing can improve the performance of gravitational wave interferometers such as the one used by VIRGO and LIGO. We derived the optimal squeezing angle needed to produce broadband suppression of noise, and showed that a filter cavity could produce this squeezing angle. However, such a filter cavity would be experimentally cumbersome, so we investigated another model, EIT using an atomic ensemble, to see whether it could produce the same effect. Initially, we assumed the coupling constants for each atom were equal, and solved the equations of motion to investigate the performance of this scheme with losses. We found that even with large losses, we were able to produce a noise suppression that would improve the sensitivity of detection. We then analysed the motional averaging aspect of the scheme, and treated the couplings in more detail, finding that, to first order, the motional averaging equations are equal to the ones for standard EIT. We used an atomic billiard simulation to verify our equations to first order. To quantify the effects of ensemble atoms moving in and out of the cavity beam by expanding the cavity mode operator to second order, and computing the noise spectral density. Future work will involve using our atomic billiard simulation to compute the additional error terms using our expression for the second order correction, such that we can fully characterise the effects of various noise sources, as well as the error introduced by the ensemble dynamics. Due to the length of the equation (7.127), checking for errors will be a relatively involved process.

7.10 Appendix: Derivation of atomic Hamiltonian

In this appendix, we derive the Hamiltonian and some additional theory that forms the basis for this chapter. Here we will derive the Hamiltonian for a 3-level atom coupled by two fields in the Λ configuration. We will write our atomic Hamiltonian assuming the energy of each level is $E_i = \hbar\omega_i$. We obtain

$$\hat{H}_0 = \sum_i \hbar\omega_i \hat{\sigma}_{ii}$$

Defining $\omega_{ij} = \omega_i - \omega_j$, we will make a constant offset to the Hamiltonian (i.e., defining the state $|1\rangle$ as the reference energy level. We obtain

$$\hat{H}_0 = \hbar\omega_{31}\hat{\sigma}_{33} + \hbar\omega_{21}\hat{\sigma}_{22} = \sum_i \hbar\omega_{i1}\hat{\sigma}_{ii}$$

7.10.1 Inclusion of dipole interaction

Suppose our 3-level atom is illuminated with two light frequencies ν_1 and ν_2, as in Fig. 7.13. One of these we will take to be a quantum field, with an electric field component given by

$$\hat{\mathbf{E}}_1(z) = \boldsymbol{\epsilon}_1 \left(\frac{\hbar\omega_1}{2\epsilon_0 V}\right)^{1/2} \left(\hat{a}e^{i\nu_1 z/c} + \hat{a}^\dagger e^{-i\nu_1 z/c}\right) \tag{7.131}$$

where $\hat{a}$ is the mode annihilation operator with frequency ν_1, $\boldsymbol{\epsilon}_1$ is the polarisation unit vector, V is the quantization volume for the field, ϵ_0 is the permittivity of free space and c is the speed of light in a vacuum. The inclusion of this quantum field alters our Hamiltonian

$$\hat{H}_0 = \hbar\nu_1 \hat{a}^\dagger \hat{a} + \hbar\omega_{31}\hat{\sigma}_{33} + \hbar\omega_{21}\hat{\sigma}_{22}$$

ν_1 is the central frequency of the cavity. We drive the other atomic transition with a classical control field at frequency ν_2

$$\boldsymbol{E}_2(z,t) = \boldsymbol{\epsilon}_2 \mathcal{E}_2(t) \cos(\nu_2(t - z/c)). \tag{7.132}$$

Both fields interact with the atoms via the dipole force. We define $\hat{H}_{\text{int}} = -\hat{\boldsymbol{d}} \cdot \hat{\boldsymbol{E}}$, where $\hat{\boldsymbol{d}}$ is the dipole moment.

$$\hat{H}_{\text{int}} = -\hat{\boldsymbol{d}} \cdot \left[\boldsymbol{E}_2(z,t) + \hat{\boldsymbol{E}}_1(z)\right] \tag{7.133}$$
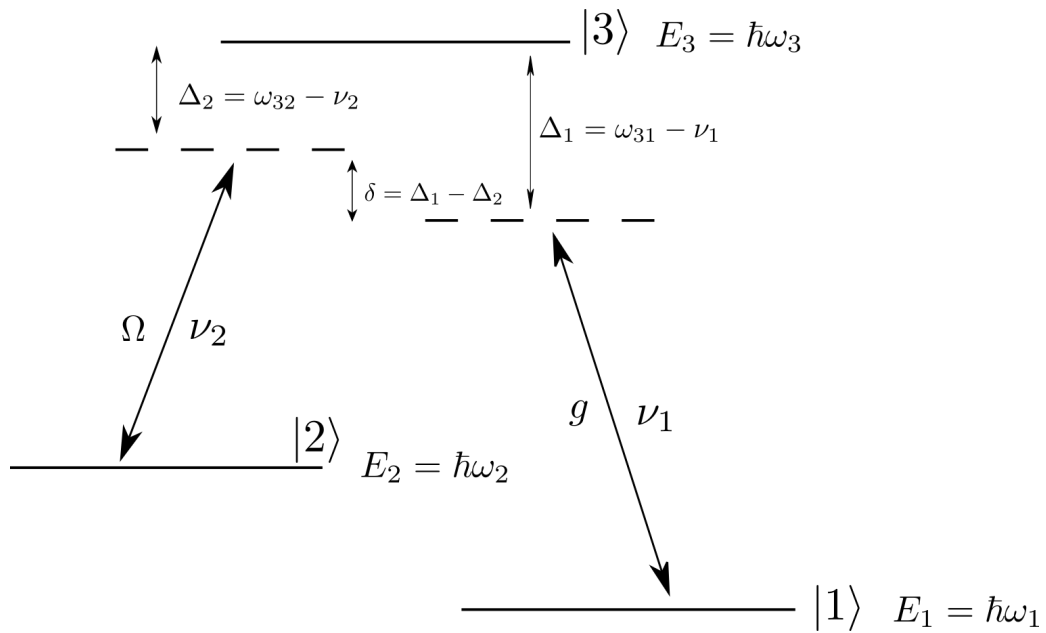
Figure 7.13: **A 3-level atom in Λ configuration** illuminated by a cavity field with coupling strength g and frequency ν_1, as well as a classical field Ω with frequency ν_2. The states $|1\rangle$ and $|2\rangle$ are detuned from the state $|3\rangle$ by the detunings Δ_1 and Δ_2, respectively.

This Hamiltonian tells us how the energy of an atomic transition is affected by our quantum ($\hat{E}_1$) and classical (E_2) fields. The dipole operator is

$$\hat{d} = \sum_{ij} \hat{\sigma}_{ij} \langle i|\hat{d}|j \rangle$$

However, we assume that the transition $|2\rangle \leftrightarrow |1\rangle$ is dipole forbidden, so the matrix elements $\langle 2|\hat{d}|1\rangle = \langle 1|\hat{d}|2\rangle = 0$. We additionally assume that the atomic states don't have their own permanent dipole, so terms of the form $\langle i|\hat{d}|i\rangle = 0$. We are thus left with a dipole operator

$$\hat{d} = \hat{\sigma}_{23} \langle 2|\hat{d}|3\rangle + \hat{\sigma}_{32} \langle 3|\hat{d}|2\rangle + \hat{\sigma}_{13} \langle 1|\hat{d}|3\rangle + \hat{\sigma}_{31} \langle 3|\hat{d}|1\rangle$$

We will further assume that the signal (quantum) field couples only the $|1\rangle \rightarrow |3\rangle$ transitions via the polarisation $\boldsymbol{\epsilon}_1$, whilst the control field couples the $|s\rangle \rightarrow |e\rangle$ transitions via $\boldsymbol{\epsilon}_2$, so $\langle 3|\hat{d} \cdot \boldsymbol{\epsilon}_2|1\rangle = 0$ and $\langle 3|\hat{d} \cdot \boldsymbol{\epsilon}_1|2\rangle = 0$. In practice, this can be achieved by having different polarisations for the two beams. With this in mind, the dot products are

$$-\hat{\boldsymbol{d}} \cdot \boldsymbol{E}_1 = - \left(\frac{\hbar \nu_1}{2\epsilon_0 V} \right)^{1/2} \left(\hat{\sigma}_{31} \langle 3|\hat{\boldsymbol{d}} \cdot \boldsymbol{\epsilon}_1|1\rangle + \sigma_{13} \langle 1|\hat{\boldsymbol{d}} \cdot \boldsymbol{\epsilon}_1|3\rangle \right) \left(\hat{a} e^{i\nu_1 z/c} + \hat{a}^\dagger e^{-i\nu_1 z/c} \right)$$
(7.134)

$$= -\hbar \left(g\hat{\sigma}_{31} + g^* \sigma_{13} \right) \left(\hat{a} e^{i\nu_1 z/c} + \hat{a}^\dagger e^{-i\nu_1 z/c} \right)$$
(7.135)

$$-\hat{\boldsymbol{d}} \cdot \boldsymbol{E}_2 = -\frac{\mathcal{E}_2}{2} \left(\hat{\sigma}_{32} \langle 3|\hat{\boldsymbol{d}} \cdot \boldsymbol{\epsilon}_2|2\rangle + \sigma_{23} \langle 2|\hat{\boldsymbol{d}} \cdot \boldsymbol{\epsilon}_2|3\rangle \right) \left(e^{i\nu_2(t-z/c)} + e^{-i\nu_2(t-z/c)} \right)$$ (7.136)

$$= -\hbar \left(\Omega \hat{\sigma}_{32} + \Omega^* \sigma_{23} \right) \left(e^{i\nu_2(t-z/c)} + e^{-i\nu_2(t-z/c)} \right)$$
(7.137)

Where we have defined

$$\Omega(t) = \frac{\mathcal{E}_2(t)}{\hbar} \langle 3|\hat{\boldsymbol{d}} \cdot \boldsymbol{\epsilon}_2|2\rangle, \qquad g = \left(\frac{\nu_1}{2\hbar\epsilon_0 V} \right)^{1/2} \langle 3|\hat{\boldsymbol{d}} \cdot \boldsymbol{\epsilon}_1|1\rangle$$
(7.138)

Where Ω is the Rabi frequency for the transition between states 3 and 2. That is, given a perfectly resonant $\Delta_1 = 0$ transition, the atom would be excited from $|2\rangle$ to $|3\rangle$ at a rate of Ω.

g and Ω encode how the quantum and classical light couple to their transitions. i.e., they translate from the fields $\hat{E}_1$ and E_2 into an energy that appears in the Hamiltonian.

7.10.1.1 Rotating wave approximation

We will transform into the interaction picture via a unitary transformation. The general action of a unitary operator is defined by

$$H \to UHU^\dagger + i\hbar \dot{U}U^\dagger \tag{7.139}$$

We will choose the unitary $\hat{U}(t) = e^{it(\hat{a}^\dagger a + \omega_{21}\sigma_{\hat{2},2} + \omega_{31}\sigma_{\hat{3},3})}$ (this defines the interaction picture)

7.10.1.2 Action of the operators

Since all the parts of the unitary commute, we can evaluate the action separately $U = U_1 U_2 = U_2 U_1$, where

$$U_1 = \exp\left(it\left(\omega_{21}\hat{\sigma}_{2,2} + \omega_{31}\hat{\sigma}_{3,3} + \nu_1\right)\right) \tag{7.140}$$

$$= -\hat{\sigma}_{2,2} - \hat{\sigma}_{3,3} + \hat{\sigma}_{2,2}e^{it\omega_{21}} + \hat{\sigma}_{3,3}e^{it\omega_{31}} + 1 \tag{7.141}$$

where we took a series expansion and made use of the orthogonality of the $\hat{\sigma}$ operators. and $U_2 = e^{it\nu_1\hat{a}^\dagger\hat{a}}$

This unitary acts on $\sigma_{\alpha\beta}$ as

$$U\sigma_{32}U^\dagger = \hat{\sigma}_{32}e^{it\omega_{32}} \tag{7.142}$$

$$U\sigma_{23}U^\dagger = \hat{\sigma}_{23}e^{-it\omega_{32}} \tag{7.143}$$

$$U\sigma_{31}U^\dagger = \hat{\sigma_{3,1}}e^{it\omega_{31}} \tag{7.144}$$

$$U\sigma_{13}U^\dagger = \hat{\sigma_{1,3}}e^{-it\omega_{31}} \tag{7.145}$$

and

$$e^{i\nu_1 t\hat{a}^\dagger\hat{a}}\hat{a}e^{-i\nu_1 t\hat{a}^\dagger\hat{a}} = e^{-i\nu_1 t}\hat{a} \tag{7.146}$$

$$e^{i\nu_1 t\hat{a}^\dagger\hat{a}}\hat{a}^\dagger e^{-i\nu_1 t\hat{a}^\dagger\hat{a}} = e^{i\nu_1 t}\hat{a}^\dagger \tag{7.147}$$

Our dot products in the interaction picture are

$$U\left(-\hat{\boldsymbol{d}} \cdot \boldsymbol{E}_1\right) U^\dagger = -\hbar\left(g\hat{\sigma}_{31}e^{it\omega_{31}} + g^*\sigma_{13}e^{-it\omega_{31}}\right)\left(\hat{a}e^{-i\nu_1 t}e^{i\nu_1 z/c} + \hat{a}^\dagger e^{i\nu_1 t}e^{-i\nu_1 z/c}\right)$$

$$(7.148)$$

$$= -\hbar\left(g^*\hat{\sigma}_{1,3}\hat{a}^\dagger e^{-\frac{i(ct(\omega_{31}-\nu_1)+\nu_1 z)}{c}} + \hat{a}g^*\hat{\sigma}_{1,3}e^{i\left(\frac{\nu_1 z}{c}-t(\nu_1+\omega_{31})\right)}\right.$$

$$\left. + g\hat{\sigma}_{3,1}\hat{a}^\dagger e^{it(\nu_1+\omega_{31})-\frac{i\nu_1 z}{c}} + \hat{a}g\hat{\sigma}_{3,1}e^{\frac{i(ct(\omega_{31}-\nu_1)+\nu_1 z)}{c}}\right) \qquad (7.149)$$

$$- \hbar\left(g^*\hat{\sigma}_{1,3}\hat{a}^\dagger e^{-i\left(\nu_1\left(\frac{z}{c}-t\right)+t\omega_{31}\right)} + \hat{a}g\hat{\sigma}_{3,1}e^{\frac{i(ct\omega_{31}+\nu_1(z-ct))}{c}}\right) \qquad (7.150)$$

$$= -\hbar\left(g^*\hat{\sigma}_{1,3}\hat{a}^\dagger e^{-\frac{i\nu_1 z}{c}-it(\omega_{31}-\nu_1)} + \hat{a}g\hat{\sigma}_{3,1}e^{\frac{i\nu_1 z}{c}+it(\omega_{31}-\nu_1)}\right) \qquad (7.151)$$

$$U\left(-\hat{\boldsymbol{d}} \cdot \boldsymbol{E}_2\right) U^\dagger = -\hbar\left(\Omega\hat{\sigma}_{32}e^{it\omega_{32}} + \Omega^*\sigma_{23}e^{-it\omega_{32}}\right)\left(e^{i\nu_2(t-z/c)} + e^{-i\nu_2(t-z/c)}\right) \qquad (7.152)$$

$$= -\Omega^*\hbar\hat{\sigma}_{2,3}e^{-it(\nu_2+\omega_{32})} - \Omega^*\hbar\hat{\sigma}_{2,3}e^{it(\nu_2-\omega_{32})}$$

$$+ \Omega\hbar\hat{\sigma}_{3,2}\left(-e^{-it(\nu_2-\omega_{32})}\right) - \Omega\hbar\hat{\sigma}_{3,2}e^{it(\nu_2+\omega_{32})} \qquad (7.153)$$

$$\approx -\hbar\left(\Omega^*\hat{\sigma}_{2,3}e^{-\frac{i(ct(\omega_{32}-\nu_2)+\nu_2 z)}{c}} + \Omega\hat{\sigma}_{3,2}e^{\frac{i(ct(\omega_{32}-\nu_2)+\nu_2 z)}{c}}\right) \qquad (7.154)$$

We have taken the rotating wave approximation (which discards terms $\propto e^{\pm i(\nu+\omega_{ij})t}$. Then transforming back to the Schrödinger picture, we obtain

$$\hat{H} = H_0 - \hbar\left(g^*\hat{\sigma}_{1,3}\hat{a}^\dagger e^{-\frac{i\nu_1 z}{c}} + \hat{a}g\hat{\sigma}_{3,1}e^{\frac{i\nu_1 z}{c}} + \Omega^*\hat{\sigma}_{2,3}e^{\frac{i\nu_2(ct-z)}{c}} + \Omega\hat{\sigma}_{3,2}e^{-i\nu_2\left(t-\frac{z}{c}\right)}\right)$$

$$(7.155)$$

7.10.2 Rotating frame

We now move to a rotating frame given by the unitary

$$R = \exp\left(-it\left(\nu_1\hat{\sigma}_{1,1} + \nu_2\hat{\sigma}_{2,2} + \nu_1\hat{a}^\dagger\hat{a}\right)\right)$$

We again split the action of this unitary in two: $R = R_1 U_2$, where U_2 is the same as above.

$$R_1 = \exp\left(-it\left(\nu_1\hat{\sigma}_{1,1} + \nu_2\hat{\sigma}_{2,2}\right)\right) \qquad (7.156)$$

$$= -\hat{\sigma}_{1,1} - \hat{\sigma}_{2,2} + \hat{\sigma}_{1,1}e^{-i\nu_1 t} + \hat{\sigma}_{2,2}e^{-i\nu_2 t} + 1 \qquad (7.157)$$

where we again took a series expansion and used the orthogonality of the σ operators.

The operator R has the actions

$$\hat{\sigma_{3,2}} \rightarrow \hat{\sigma_{3,2}}e^{i\nu_2 t} \tag{7.158}$$

$$\hat{\sigma_{2,3}} \rightarrow \hat{\sigma_{2,3}}e^{-i\nu_2 t} \tag{7.159}$$

$$\hat{\sigma_{3,1}} \rightarrow \hat{\sigma_{3,1}}e^{i\nu_1 t} \tag{7.160}$$

$$\hat{\sigma_{1,3}} \rightarrow \hat{\sigma_{1,3}}e^{-i\nu_1 t} \tag{7.161}$$

$$\hat{a} \rightarrow \hat{a}e^{-i\nu_1 t} \tag{7.162}$$

$$\hat{a}^\dagger \rightarrow \hat{a}^\dagger e^{i\nu_1 t} \tag{7.163}$$

Now, under these transformations, we have

$$\hat{H}_{\text{int}} = -\hbar \left(g^* \hat{\sigma_{1,3}}\hat{a}^\dagger e^{-\frac{i\nu_1 z}{c}} + \hat{a}g\hat{\sigma_{3,1}}e^{\frac{i\nu_1 z}{c}} + \Omega^* \hat{\sigma_{2,3}}e^{\frac{i\nu_2(ct-z)}{c}-i\nu_2 t} + \Omega\hat{\sigma_{3,2}}e^{i\nu_2 t - i\nu_2\left(t-\frac{z}{c}\right)} \right) \tag{7.164}$$

$$= -\hbar \left(\Omega\hat{\sigma}_{32} + \Omega^*\hat{\sigma}_{23} + g\hat{\sigma}_{31}\hat{a} + g^*\hat{\sigma}_{13}\hat{a}^\dagger \right) \tag{7.165}$$

where in the last line, we have defined

$$\hat{\sigma_{2,3}} \rightarrow \hat{\sigma_{2,3}}e^{\frac{i\nu_2 z}{c}} \tag{7.166}$$

$$\hat{a}^\dagger \rightarrow \hat{a}^\dagger e^{i\nu_1 t} \tag{7.167}$$

$$\hat{\sigma_{1,3}} \rightarrow \hat{\sigma_{1,3}}e^{-i\nu_1\left(t-\frac{z}{c}\right)} \tag{7.168}$$

The full Hamiltonian in the rotating frame is then written

$$\hat{H} = \hbar\nu_1\hat{a}^\dagger\hat{a} + \hbar\omega_{31}\hat{\sigma}_{33} + \hbar\omega_{21}\hat{\sigma}_{22} + i\hbar\dot{R}R^\dagger + \hat{H}_{\text{int}} \tag{7.169}$$

$$= \hbar(\omega_{31} - \nu_1)\hat{\sigma}_{33} + \hbar(\omega_{21} + \nu_2 - \nu_1)\hat{\sigma}_{22} + H_{int} \tag{7.170}$$

$$= \hbar(\omega_{31} - \nu_1)\hat{\sigma}_{33} + \hbar(\omega_{31} - \omega_{32} + \nu_2 - \nu_1)\hat{\sigma}_{22} + H_{int} \tag{7.171}$$

$$= \hbar\Delta_1\hat{\sigma}_{33} + \hbar\delta\hat{\sigma}_{22} - \hbar\left(\Omega\hat{\sigma}_{32} + \Omega^*\hat{\sigma}_{23} + g\hat{\sigma}_{31}\hat{a} + g^*\hat{\sigma}_{13}\hat{a}^\dagger\right) \tag{7.172}$$

where we have used $\sigma_{11} + \sigma_{22} + \sigma_{33} = 1$, $\Delta_1 = \omega_{31} - \nu_1$, $\Delta_2 = \omega_{32} - \nu_2$, $\delta = \Delta_1 - \Delta_2$ and that $\omega_{31} = \omega_{32} + \omega_{21} \Rightarrow \omega_{21} = \omega_{31} - \omega_{32}$.

7.11 Appendix: Derivation of quadrature operator expectation values

Here we will show in detail how the expression (7.127) was obtained. Recall the second order expansion of the quadrature operator

$$
\begin{aligned}
Y^\dagger(\omega_1,\theta)Y(\omega_2,\theta) = \frac{1}{4}\Big(&e^{2i\theta}a_0\left(\omega_1\right)^\dagger \cdot a_2\left(-\omega_2\right)^\dagger + e^{2i\theta}a_2\left(\omega_1\right)^\dagger \cdot a_0\left(-\omega_2\right)^\dagger \\
&+ e^{-2i\theta}a_0\left(-\omega_1\right)\cdot a_2\left(\omega_2\right) + e^{-2i\theta}a_2\left(-\omega_1\right)\cdot a_0\left(\omega_2\right) \\
&+ a_0\left(\omega_1\right)^\dagger \cdot a_2\left(\omega_2\right) + a_2\left(\omega_1\right)^\dagger \cdot a_0\left(\omega_2\right) \\
&+ a_0\left(-\omega_1\right)\cdot a_2\left(-\omega_2\right)^\dagger + a_2\left(-\omega_1\right)\cdot a_0\left(-\omega_2\right)^\dagger\Big) \qquad (7.173)
\end{aligned}
$$

and the expressions for $\hat{a}_0$ and $\hat{a}_2$.

$$
\hat{a}^{(0)}(\omega) = -\mathbf{W}_{00}(\omega)\sqrt{\kappa_{in}}\hat{a}_{in}(\omega) \tag{7.174}
$$

$$
\hat{a}^{(2)}(\omega) = -\sqrt{\kappa_{in}}\int_{-\infty}^{\infty}\sum_{ijk\ell}\mathbf{W}_{0i}(\omega)\delta\mathbf{M}_{ij}(\omega-\omega')\mathbf{W}_{jk}(\omega')\delta\mathbf{M}_{k\ell}(\omega'-\omega'')
$$
$$
\times \mathbf{W}_{\ell 0}(\omega'')\sqrt{\kappa_{in}}\hat{a}_{in}(\omega'')d\omega''d\omega' \tag{7.175}
$$

We will perform the calculation for the term (which should be understood to be thermally and quantum averaged)

$$
\langle\hat{a}_2^\dagger(\omega_1)\hat{a}_0(\omega_2)\rangle = \kappa_{in}\sum_{ijk\ell}\int_{-\infty}^{\infty}\Big[\mathbf{W}_{0i}(\omega_1)\delta\mathbf{M}_{ij}(\omega_1-\omega')\mathbf{W}_{jk}(\omega')\delta\mathbf{M}_{k\ell}(\omega'-\omega'')\mathbf{W}_{\ell 0}(\omega'')\Big]^*
$$
$$
\langle\hat{a}_{in}^\dagger(\omega'')\hat{a}_{in}(\omega_2)\rangle\,\mathbf{W}_{00}(\omega_2)d\omega''d\omega' \tag{7.176}
$$

To proceed, we use the standard commutator relation $[\hat{a}_{in}(\omega),\hat{a}_{in}^\dagger(\omega')] = \delta(\omega-\omega')$ and the transformation rules for squeezed states

$$
\hat{a}_{in}(\omega) \to \cosh(r)\hat{a}_{in}(\omega) - e^{i\phi_{sq}}\sinh(r)\hat{a}_{in}^\dagger(-\omega) \tag{7.177}
$$
$$
\hat{a}_{in}^\dagger(\omega) \to \cosh(r)\hat{a}_{in}^\dagger(\omega) - e^{-i\phi_{sq}}\sinh(r)\hat{a}_{in}(-\omega) \tag{7.178}
$$

where r is the squeezing parameter and ϕ_{sq} is the (fixed) squeezing angle of the incident light. Below, we set $\phi_{sq} = 0$, corresponding to squeezing in $\hat{P}$, and use $\langle\hat{a}_{in}^\dagger(\omega'')\hat{a}_{in}(\omega_2)\rangle = \delta(\omega''-\omega_2)\sinh^2(r)$. We thus have

$$\langle \hat{a}_2^\dagger(\omega_1)\hat{a}_0(\omega_2)\rangle =$$
$$\kappa_{in}\sinh^2(r)\sum_{ijk\ell}\int_{-\infty}^{\infty}\left[\mathbf{W}_{0i}(\omega_1)\mathbf{W}_{jk}(\omega')\delta\mathbf{M}_{ij}(\omega_1-\omega')\delta\mathbf{M}_{k\ell}(\omega'-\omega_2)\mathbf{W}_{\ell 0}(\omega_2)\right]^*\mathbf{W}_{00}(\omega_2)d\omega'$$

$$(7.179)$$

Now we will write the Fourier transform

$$\delta\mathbf{M}_{ij}(\omega_1-\omega')=\frac{1}{\sqrt{2\pi}}\int\delta\mathbf{M}_{ij}(t)e^{i(\omega_1-\omega')t} \tag{7.180}$$

$$\langle \hat{a}_2^\dagger(\omega_1)\hat{a}_0(\omega_2)\rangle =$$
$$\kappa_{in}\sum_{ijk\ell}\int_{-\infty}^{\infty}\left[\mathbf{W}_{0i}(\omega_1)\delta\mathbf{M}_{ij}(t)e^{i(\omega_1-\omega')t}\mathbf{W}_{jk}(\omega')\delta\mathbf{M}_{k\ell}(t')e^{i(\omega'-\omega_2)t'}\mathbf{W}_{\ell 0}(\omega_2)\right]^*\mathbf{W}_{00}(\omega_2)d\omega'dtdt'$$

$$(7.181)$$

Now we assume that the noise process is stationary and thus that $\delta M(t)\delta M(t') = F(t-t') = F(\tau)$. We then make a coordinate transformation $\tau = t-t'$ and $s = t+t'$. with $dtdt' = |J|d\tau ds$, where the Jacobian determinant is $|J| = \frac{\partial t}{\partial \tau}\frac{\partial t'}{\partial s} - \frac{\partial t}{\partial s}\frac{\partial t'}{\partial \tau} = \frac{1}{2}$. Now we get

$$\langle \hat{a}_2^\dagger(\omega_1)\hat{a}_0(\omega_2)\rangle =$$
$$\frac{\kappa_{in}}{2\pi}|J|\sum_{ijk\ell}\int_{-\infty}^{\infty}\left[\mathbf{W}_{0i}(\omega_1)\mathbf{W}_{jk}(\omega')F(\tau)\mathbf{W}_{\ell 0}(\omega_2)\right]^*e^{-\frac{i}{2}\tau(\omega_1+\omega_2-2\omega')}e^{-\frac{i}{2}s(\omega_1-\omega_2)}\mathbf{W}_{00}(\omega_2)d\omega'd\tau ds$$

$$(7.182)$$

The integral

$$\frac{1}{2\pi}\int_{-\infty}^{\infty}e^{-\frac{i}{2}s(\omega_1-\omega_2)}ds = \delta\left(\frac{\omega_1-\omega_2}{2}\right) = 2\delta(\omega_1-\omega_2), \tag{7.183}$$

cancels the contribution from $|J|$, and yields

$$\langle \hat{a}_2^\dagger(\omega_1)\hat{a}_0(\omega_2)\rangle =$$
$$\kappa_{in}\delta(\omega_1-\omega_2)\sum_{ijk\ell}\int_{-\infty}^{\infty}\left[\mathbf{W}_{0i}(\omega_1)\mathbf{W}_{jk}(\omega')F(\tau)\mathbf{W}_{\ell 0}(\omega_2)\right]^*\mathbf{W}_{00}(\omega_2)e^{-i\tau(\omega_1-\omega')}d\omega'd\tau$$

$$(7.184)$$

after performing the integral ds. Now we assume that the dominant coupling is from the terms with index 0 or 1 to the $N - 1$ continuum states. Thus, we can ignore the 0,1 terms in $\mathbf{W}_{jk}$ and write $\mathbf{W}_{jk}(\omega) = \delta_{jk}W_D(\omega) = \delta_{jk}\frac{1}{\mathcal{C}+i\omega}$. This allows us to sum over the index k, to obtain.

$$\langle\hat{a}_2^\dagger(\omega_1)\hat{a}_0(\omega_2)\rangle = \kappa_{in}\delta(\omega_1 - \omega_2)\sum_{ij\ell}\int_{-\infty}^{\infty}\left[\mathbf{W}_{0i}(\omega_1)\mathbf{W}_D(\omega')\delta\mathbf{M}_{ij}(t)\delta\mathbf{M}_{j\ell}(t')\mathbf{W}_{\ell 0}(\omega_2)\right]^*$$
$$\mathbf{W}_{00}(\omega_2)e^{-i\tau(\omega_1-\omega')}d\omega'd\tau \tag{7.185}$$

and now the index $j > 1$. We also have that the index $i \leq 1$ and $\ell \leq 1$ due to the restriction imposed by $\mathbf{W}_{0i}$ and $\mathbf{W}_{\ell 0}$. To obtain the final expression, we approximate our atomic ensemble as an ideal gas, i.e., that trajectories of different atoms are uncorrelated. Thus, products $\delta\mathbf{M}_{ij}\delta\mathbf{M}_{j\ell}$ average to zero unless the atom number is the same, and we can evaluate the sums over i and j.

The calculation of the other terms proceeds in an analogous way, with the expectation values of $\hat{a}_{\text{in}}$ given by

$$\langle\hat{a}_{in}^\dagger(\omega_1)\hat{a}_{in}(\omega_2)\rangle = \sinh^2(r)\delta(\omega_2 - \omega_1) \tag{7.186}$$
$$\langle\hat{a}_{in}(\omega_1)\hat{a}_{in}(\omega_2)\rangle = -\cosh(r)\sinh(r)\delta(\omega_2 + \omega_1) \tag{7.187}$$
$$\langle\hat{a}_{in}^\dagger(\omega_1)\hat{a}_{in}^\dagger(\omega_2)\rangle = -\cosh(r)\sinh(r)\delta(\omega_2 + \omega_1) \tag{7.188}$$
$$\langle\hat{a}_{in}(\omega_1)\hat{a}_{in}^\dagger(\omega_2)\rangle = \cosh^2(r)\delta(\omega_1 - \omega_2) \tag{7.189}$$

7.12 Appendix: Single angle noise spectral density

To compute the noise spectral density, we need to compute $S_{\delta I}\delta(\omega-\omega') = \frac{1}{2}\langle\delta I^\dagger\delta I + \delta I\delta I^\dagger\rangle$. In general, the evaluation of these expectation values of $I = -P - \mathcal{A}X$ involves writing the expectation value in terms of the generalised quadrature operator

$$\langle\hat{Y}^\dagger(\omega,\theta)\hat{Y}(\omega',\theta')\rangle = \langle\hat{Y}(\omega',\theta')\hat{Y}^\dagger(\omega,\theta)\rangle \tag{7.190}$$
$$= \frac{1}{4}\delta(\omega-\omega')\Big(\cos(\theta-\theta') - i\sin(\theta-\theta')$$
$$- S|t|^2\sin(\theta-\phi)\sin(\phi-\theta')$$
$$+ \frac{|t|^2\cos(\theta-\phi)\cos(\phi-\theta')}{S} - |t|^2\cos(\theta-\theta')\Big), \tag{7.191}$$

depending on the precise value of $\mathcal{A}$. The above formula is computed by noting that all the normal-ordered products of our operators give zero, so we simply need to perform a commutation to get our terms into normal order (which gives the term proportional to $\delta(\omega - \omega')$), and then the remaining operators can be discarded inside the expectation value.

It is advantageous if we can write this result using a single angle, such that we only need to compute it once. We write the homodyne intensity as

$$\mathcal{N}(\omega)(\cos(\theta(\omega))X + \sin(\theta(\omega))P) = I \tag{7.192}$$
$$= \mathcal{N}(\omega)Y(\theta(\omega)) \tag{7.193}$$

From here we get that $\mathcal{A} = \cot(\theta(\omega))$ and

$$\theta = \cot^{-1}(\mathcal{A}) \tag{7.194}$$
$$\mathcal{N}(\omega) = -\csc(\theta) \tag{7.195}$$
$$= -\mathcal{A}\sqrt{1 + \frac{1}{\mathcal{A}^2}} \tag{7.196}$$
$$= -\sqrt{1 + \mathcal{A}^2}. \tag{7.197}$$

Chapter 8

Conclusions

This thesis has investigated various ways that light and matter can interface to give us better control and sensitivity of quantum systems. We have analysed systems from an emitter number $N = 1$, all the way to a system with $N \sim 10^6$ emitters. We first developed a model of quantum dots embedded in a photonic crystal waveguide, and used it to analyse our recent experimental work that showed time-energy entanglement via the scattering off a single quantum dot. Our results improved our understanding of these single emitter systems and their associated single-photon nonlinearity. This nonlinearity and resulting quantum entanglement holds significance in several quantum technologies, including quantum computing, quantum cryptography and quantum teleportation. We then extended this model to a system with $N = 2$, also with an accompanying experiment. We investigated the rich physics associated with the coupling between these dots, showing that the emitter decay rate Γ can be modified to produce super- and subradiance. We showed that, in many cases, the complicated system dynamics can be understood by a much simpler model, using an effective Hamiltonian formalism. We derived several results that give us insight into the dynamics observed in the experiment. We also showed some features of the model that have not yet been observed in our experiment, both analytically via perturbation theory and with our simulation of the full system dynamics. In the cases of both $N = 1$ and $N = 2$, our model produced excellent agreement with the experimental data, as shown by several comparisons between experiment and theory.

We then moved on to a system with $N \sim 10 - 100$ – atomic arrays. We proposed and benchmarked a novel sensing protocol using cooperative enhancement to improve the coupling between two impurities embedded in this lattice. The protocol is rather general and, in principle, can be applied to other coupled systems of emitters. We analysed the effects of lattice disorder for our specific model, finding that the system is robust to most lattice disorder. Our approach is expected to be implementable in current state-of-the-art platforms, pushing forward the state of the art in sensing capability.

Finally, we investigated a system with $N \sim 10^6$ – atomic ensembles. We showed that an atomic ensemble quantum memory in a cavity can produce the appropriate squeezing rotation to produce broadband noise suppression for a gravitational wave interferometer. We analysed the various imperfections that could be detrimental to the performance of such a protocol, finding that even with large losses, we could still produce a significant improvement to the sensitivity. These results hold promise for improving the state of the art in gravitational wave astronomy, allowing us to see further and fainter objects in our universe.

We have contributed models describing $N = 1$ and $N = 2$ quantum emitters

embedded in photonic crystal waveguides, as well as an analysis of the physics underlying these models. Potential future research directions include the analysis of pulsed excitation, as well as the effects of different driving regimes, including the strength and driving method (i.e., through the waveguide vs from the top). We contributed a novel sensing scheme that can be realised in current state-of-the-art platforms. This scheme could be extended to beyond the single-excitation regime, where it may be possible to exploit the strong photon nonlinearities that will occur to further improve the sensitivity. It would also be of interest to perform an explicit analysis to see how the protocol performs when implemented in other platforms, including, e.g., photonic crystal waveguides. We contributed a novel noise analysis of motionally-averaged EIT that can be used to enhance the sensitivity of gravitational wave detectors. Future directions for this work include an analysis of the vapour cell in which the atomic ensemble is housed. Decreasing the size of the cell will improve the degree of motional averaging, but will increase the number of collisions with the cell wall, which introduces another source of error. It is thus of interest to find the optimal cell size and geometry.

The work in this thesis is a stepping stone to a wide range of quantum enhanced technologies, including quantum computers, quantum networks, and quantum metrology devices. Research into the interaction between light and matter will be of continuing importance in the future, due to its role in transforming and shaping the modern world.

Bibliography

[1] S. Liu, O. A. D. Sandberg, M. L. Chan, B. Schrinski, Y. Anyfantaki, R. B. Nielsen, R. G. Larsen, A. Skalkin, Y. Wang, L. Midolo, S. Scholz, A. D. Wieck, A. Ludwig, A. S. Sørensen, A. Tiranov, and P. Lodahl, "Violation of Bell inequality by photon scattering on a two-level emitter," Jun. 2023. [Online]. Available: http://arxiv.org/abs/2306.12801

[2] A. Tiranov, V. Angelopoulou, C. J. van Diepen, B. Schrinski, O. A. D. Sandberg, Y. Wang, L. Midolo, S. Scholz, A. D. Wieck, A. Ludwig, A. S. Sørensen, and P. Lodahl, "Collective super- and subradiant dynamics between distant optical quantum emitters," *Science*, vol. 379, no. 6630, pp. 389–393, Jan. 2023. [Online]. Available: https://www.science.org/doi/full/10.1126/science.ade9324

[3] D. V. Martynov, E. D. Hall, B. P. Abbott, R. Abbott, T. D. Abbott, C. Adams, R. X. Adhikari, R. A. Anderson, S. B. Anderson, K. Arai, M. A. Arain, S. M. Aston, L. Austin, S. W. Ballmer, M. Barbet, D. Barker, B. Barr, L. Barsotti, J. Bartlett, M. A. Barton, I. Bartos, J. C. Batch, A. S. Bell, I. Belopolski, J. Bergman, J. Betzwieser, G. Billingsley, J. Birch, S. Biscans, C. Biwer, E. Black, C. D. Blair, C. Bogan, C. Bond, R. Bork, D. O. Bridges, A. F. Brooks, D. D. Brown, L. Carbone, C. Celerier, G. Ciani, F. Clara, D. Cook, S. T. Countryman, M. J. Cowart, D. C. Coyne, A. Cumming, L. Cunningham, M. Damjanic, R. Dannenberg, K. Danzmann, C. F. D. S. Costa, E. J. Daw, D. DeBra, R. T. DeRosa, R. DeSalvo, K. L. Dooley, S. Doravari, J. C. Driggers, S. E. Dwyer, A. Effler, T. Etzel, M. Evans, T. M. Evans, M. Factourovich, H. Fair, D. Feldbaum, R. P. Fisher, S. Foley, M. Frede, A. Freise, P. Fritschel, V. V. Frolov, P. Fulda, M. Fyffe, V. Galdi, J. A. Giaime, K. D. Giardina, J. R. Gleason, R. Goetz, S. Gras, C. Gray, R. J. S. Greenhalgh, H. Grote, C. J. Guido, K. E. Gushwa, E. K. Gustafson, R. Gustafson, G. Hammond, J. Hanks, J. Hanson, T. Hardwick, G. M. Harry, K. Haughian, J. Heefner, M. C. Heintze, A. W. Heptonstall, D. Hoak, J. Hough, A. Ivanov, K. Izumi, M. Jacobson, E. James, R. Jones, S. Kandhasamy,

S. Karki, M. Kasprzack, S. Kaufer, K. Kawabe, W. Kells, N. Kijbunchoo, E. J. King, P. J. King, D. L. Kinzel, J. S. Kissel, K. Kokeyama, W. Z. Korth, G. Kuehn, P. Kwee, M. Landry, B. Lantz, A. L. Roux, B. M. Levine, J. B. Lewis, V. Lhuillier, N. A. Lockerbie, M. Lormand, M. J. Lubinski, A. P. Lundgren, T. MacDonald, M. MacInnis, D. M. Macleod, M. Mageswaran, K. Mailand, S. M'arka, Z. M'arka, A. S. Markosyan, E. Maros, I. W. Martin, R. M. Martin, J. N. Marx, K. Mason, T. J. Massinger, F. Matichard, N. Mavalvala, R. McCarthy, D. E. McClelland, S. McCormick, G. McIntyre, J. McIver, E. L. Merilh, M. S. Meyer, P. M. Meyers, J. Miller, R. Mittleman, G. Moreno, C. L. Mueller, G. Mueller, A. Mullavey, J. Munch, P. G. Murray, L. K. Nuttall, J. Oberling, J. O'Dell, P. Oppermann, R. J. Oram, B. O'Reilly, C. Osthelder, D. J. Ottaway, H. Overmier, J. R. Palamos, H. R. Paris, W. Parker, Z. Patrick, A. Pele, S. Penn, M. Phelps, M. Pickenpack, V. Piero, I. Pinto, J. Poeld, M. Principe, L. Prokhorov, O. Puncken, V. Quetschke, E. A. Quintero, F. J. Raab, H. Radkins, P. Raffai, C. R. Ramet, C. M. Reed, S. Reid, D. H. Reitze, N. A. Robertson, J. G. Rollins, V. J. Roma, J. H. Romie, S. Rowan, K. Ryan, T. Sadecki, E. J. Sanchez, V. Sandberg, V. Sannibale, R. L. Savage, R. M. S. Schofield, B. Schultz, P. Schwinberg, D. Sellers, A. Sevigny, D. A. Shaddock, Z. Shao, B. Shapiro, P. Shawhan, D. H. Shoemaker, D. Sigg, B. J. J. Slagmolen, J. R. Smith, M. R. Smith, N. D. Smith-Lefebvre, B. Sorazu, A. Staley, A. J. Stein, A. Stochino, K. A. Strain, R. Taylor, M. Thomas, P. Thomas, K. A. Thorne, E. Thrane, K. V. Tokmakov, C. I. Torrie, G. Traylor, G. Vajente, G. Valdes, A. A. van Veggel, M. Vargas, A. Vecchio, P. J. Veitch, K. Venkateswara, T. Vo, C. Vorvick, S. J. Waldman, M. Walker, R. L. Ward, J. Warner, B. Weaver, R. Weiss, T. Welborn, P. Wessels, C. Wilkinson, P. A. Willems, L. Williams, B. Willke, I. Wilmut, L. Winkelmann, C. C. Wipf, J. Worden, G. Wu, H. Yamamoto, C. C. Yancey, H. Yu, L. Zhang, M. E. Zucker, and J. Zweizig, "The Sensitivity of the Advanced LIGO Detectors at the Beginning of Gravitational Wave Astronomy," *Physical Review D*, vol. 93, no. 11, p. 112004, Jun. 2016. [Online]. Available: http://arxiv.org/abs/1604.00439

[4] "Image Use Policy." [Online]. Available: https://www.ligo.caltech.edu/page/image-use-policy

[5] M. D. Lukin, "Colloquium: Trapping and manipulating photon states in atomic ensembles," *Reviews of Modern Physics*, vol. 75, no. 2, pp. 457–472, Apr. 2003. [Online]. Available: https://link.aps.org/doi/10.1103/RevModPhys.75.457

[6] J. P. Dowling and G. J. Milburn, "Quantum technology: The second quantum revolution," *Philosophical Transactions of the Royal Society of London. Series A: Mathematical, Physical and Engineering Sciences*, vol. 361, no. 1809, pp. 1655–1674, Jun. 2003. [Online]. Available: https://royalsocietypublishing.org/doi/10.1098/rsta.2003.1227

[7] D. E. Chang, V. Vuletić, and M. D. Lukin, "Quantum nonlinear optics — photon by photon," *Nature Photonics*, vol. 8, no. 9, pp. 685–694, Sep. 2014. [Online]. Available: https://www.nature.com/articles/nphoton.2014.192

[8] P. A. Franken and J. F. Ward, "Optical Harmonics and Nonlinear Phenomena," *Reviews of Modern Physics*, vol. 35, no. 1, pp. 23–39, Jan. 1963. [Online]. Available: https://link.aps.org/doi/10.1103/RevModPhys.35.23

[9] G. J. Milburn, "Quantum optical Fredkin gate," *Physical Review Letters*, vol. 62, no. 18, pp. 2124–2127, May 1989. [Online]. Available: https://link.aps.org/doi/10.1103/PhysRevLett.62.2124

[10] N. Imoto, H. A. Haus, and Y. Yamamoto, "Quantum nondemolition measurement of the photon number via the optical Kerr effect," *Physical Review A*, vol. 32, no. 4, pp. 2287–2292, Oct. 1985. [Online]. Available: https://link.aps.org/doi/10.1103/PhysRevA.32.2287

[11] S. E. Harris, J. E. Field, and A. Imamoğlu, "Nonlinear optical processes using electromagnetically induced transparency," *Physical Review Letters*, vol. 64, no. 10, pp. 1107–1110, Mar. 1990. [Online]. Available: https://link.aps.org/doi/10.1103/PhysRevLett.64.1107

[12] M. D. Lukin and A. Imamoğlu, "Controlling photons using electromagnetically induced transparency," *Nature*, vol. 413, no. 6853, pp. 273–276, Sep. 2001. [Online]. Available: https://www.nature.com/articles/35095000

[13] G. Kirchmair, B. Vlastakis, Z. Leghtas, S. E. Nigg, H. Paik, E. Ginossar, M. Mirrahimi, L. Frunzio, S. M. Girvin, and R. J. Schoelkopf, "Observation of quantum state collapse and revival due to the single-photon Kerr effect," *Nature*, vol. 495, no. 7440, pp. 205–209, Mar. 2013. [Online]. Available: https://www.nature.com/articles/nature11902

[14] J. Benhelm, G. Kirchmair, C. F. Roos, and R. Blatt, "Towards fault-tolerant quantum computing with trapped ions," *Nature Physics*,

vol. 4, no. 6, pp. 463–466, Jun. 2008. [Online]. Available: https://www.nature.com/articles/nphys961

[15] H. Häffner, C. F. Roos, and R. Blatt, "Quantum computing with trapped ions," *Physics Reports*, vol. 469, no. 4, pp. 155–203, Dec. 2008. [Online]. Available: https://www.sciencedirect.com/science/article/pii/S0370157308003463

[16] K. Mølmer and A. Sørensen, "Multiparticle Entanglement of Hot Trapped Ions," *Physical Review Letters*, vol. 82, no. 9, pp. 1835–1838, Mar. 1999. [Online]. Available: https://link.aps.org/doi/10.1103/PhysRevLett.82.1835

[17] J. Majer, J. M. Chow, J. M. Gambetta, J. Koch, B. R. Johnson, J. A. Schreier, L. Frunzio, D. I. Schuster, A. A. Houck, A. Wallraff, A. Blais, M. H. Devoret, S. M. Girvin, and R. J. Schoelkopf, "Coupling superconducting qubits via a cavity bus," *Nature*, vol. 449, no. 7161, pp. 443–447, Sep. 2007. [Online]. Available: https://www.nature.com/articles/nature06184

[18] E. Jeffrey, D. Sank, J. Y. Mutus, T. C. White, J. Kelly, R. Barends, Y. Chen, Z. Chen, B. Chiaro, A. Dunsworth, A. Megrant, P. J. J. O'Malley, C. Neill, P. Roushan, A. Vainsencher, J. Wenner, A. N. Cleland, and J. M. Martinis, "Fast Accurate State Measurement with Superconducting Qubits," *Physical Review Letters*, vol. 112, no. 19, p. 190504, May 2014. [Online]. Available: https://link.aps.org/doi/10.1103/PhysRevLett.112.190504

[19] P. Krantz, M. Kjaergaard, F. Yan, T. P. Orlando, S. Gustavsson, and W. D. Oliver, "A quantum engineer's guide to superconducting qubits," *Applied Physics Reviews*, vol. 6, no. 2, p. 021318, Jun. 2019. [Online]. Available: https://doi.org/10.1063/1.5089550

[20] D. Loss and D. P. DiVincenzo, "Quantum computation with quantum dots," *Physical Review A*, vol. 57, no. 1, pp. 120–126, Jan. 1998. [Online]. Available: https://link.aps.org/doi/10.1103/PhysRevA.57.120

[21] A. Javadi, I. Söllner, M. Arcari, S. L. Hansen, L. Midolo, S. Mahmoodian, G. Kiršanskė, T. Pregnolato, E. H. Lee, J. D. Song, S. Stobbe, and P. Lodahl, "Single-photon non-linear optics with a quantum dot in a waveguide," *Nature Communications*, vol. 6, no. 1, p. 8655, Oct. 2015. [Online]. Available: https://www.nature.com/articles/ncomms9655

[22] P. Lodahl, S. Mahmoodian, and S. Stobbe, "Interfacing single photons and single quantum dots with photonic nanostructures," *Reviews of Modern*

146

Physics, vol. 87, no. 2, pp. 347–400, May 2015. [Online]. Available: https://link.aps.org/doi/10.1103/RevModPhys.87.347

[23] M. Endres, H. Bernien, A. Keesling, H. Levine, E. R. Anschuetz, A. Krajenbrink, C. Senko, V. Vuletic, M. Greiner, and M. D. Lukin, "Atom-by-atom assembly of defect-free one-dimensional cold atom arrays," *Science*, vol. 354, no. 6315, pp. 1024–1027, Nov. 2016. [Online]. Available: https://www.science.org/doi/10.1126/science.aah3752

[24] K. Hammerer, A. S. Sørensen, and E. S. Polzik, "Quantum interface between light and atomic ensembles," *Reviews of Modern Physics*, vol. 82, no. 2, pp. 1041–1093, Apr. 2010. [Online]. Available: https://link.aps.org/doi/10.1103/RevModPhys.82.1041

[25] K. M. Watson, "Multiple Scattering by Quantum-Mechanical Systems," *Physical Review*, vol. 105, no. 4, pp. 1388–1398, Feb. 1957. [Online]. Available: https://link.aps.org/doi/10.1103/PhysRev.105.1388

[26] R. Kaiser, "Quantum multiple scattering," *Journal of Modern Optics*, vol. 56, no. 18-19, pp. 2082–2088, Oct. 2009. [Online]. Available: https://doi.org/10.1080/09500340903082663

[27] N. Sangouard, C. Simon, H. de Riedmatten, and N. Gisin, "Quantum repeaters based on atomic ensembles and linear optics," *Reviews of Modern Physics*, vol. 83, no. 1, pp. 33–80, Mar. 2011. [Online]. Available: https://link.aps.org/doi/10.1103/RevModPhys.83.33

[28] R. H. Dicke, "Coherence in Spontaneous Radiation Processes," *Physical Review*, vol. 93, no. 1, pp. 99–110, Jan. 1954. [Online]. Available: https://link.aps.org/doi/10.1103/PhysRev.93.99

[29] M. Gross and S. Haroche, "Superradiance: An essay on the theory of collective spontaneous emission," *Physics Reports*, vol. 93, no. 5, pp. 301–396, Dec. 1982. [Online]. Available: https://www.sciencedirect.com/science/article/pii/0370157382901028

[30] A. S. Sheremet, M. I. Petrov, I. V. Iorsh, A. V. Poshakinskiy, and A. N. Poddubny, "Waveguide quantum electrodynamics: Collective radiance and photon-photon correlations," *Reviews of Modern Physics*, vol. 95, no. 1, p. 015002, Mar. 2023. [Online]. Available: https://link.aps.org/doi/10.1103/RevModPhys.95.015002

[31] B. R. Mollow, "Pure-state analysis of resonant light scattering: Radiative damping, saturation, and multiphoton effects," *Physical Review A*, vol. 12, no. 5, pp. 1919–1943, Nov. 1975. [Online]. Available: https://link.aps.org/doi/10.1103/PhysRevA.12.1919

[32] T. Caneva, M. T. Manzoni, T. Shi, J. S. Douglas, J. I. Cirac, and D. E. Chang, "Quantum dynamics of propagating photons with strong interactions: A generalized input–output formalism," *New Journal of Physics*, vol. 17, no. 11, p. 113001, Oct. 2015. [Online]. Available: https://dx.doi.org/10.1088/1367-2630/17/11/113001

[33] P. Lodahl, S. Mahmoodian, S. Stobbe, A. Rauschenbeutel, P. Schneeweiss, J. Volz, H. Pichler, and P. Zoller, "Chiral quantum optics," *Nature*, vol. 541, no. 7638, pp. 473–480, Jan. 2017. [Online]. Available: https://www.nature.com/articles/nature21037

[34] H. T. Dung, L. Knöll, and D.-G. Welsch, "Resonant dipole-dipole interaction in the presence of dispersing and absorbing surroundings," *Physical Review A*, vol. 66, no. 6, p. 063810, Dec. 2002. [Online]. Available: https://link.aps.org/doi/10.1103/PhysRevA.66.063810

[35] A. Asenjo-Garcia, M. Moreno-Cardoner, A. Albrecht, H. J. Kimble, and D. E. Chang, "Exponential Improvement in Photon Storage Fidelities Using Subradiance and "Selective Radiance" in Atomic Arrays," *Physical Review X*, vol. 7, no. 3, p. 031024, Aug. 2017. [Online]. Available: http://link.aps.org/doi/10.1103/PhysRevX.7.031024

[36] A. Albrecht, L. Henriet, A. Asenjo-Garcia, P. B. Dieterle, O. Painter, and D. E. Chang, "Subradiant states of quantum bits coupled to a one-dimensional waveguide," *New Journal of Physics*, vol. 21, no. 2, p. 025003, Feb. 2019. [Online]. Available: https://iopscience.iop.org/article/10.1088/1367-2630/ab0134

[37] M. Lax, "Formal Theory of Quantum Fluctuations from a Driven State," *Physical Review*, vol. 129, no. 5, pp. 2342–2348, Mar. 1963. [Online]. Available: https://link.aps.org/doi/10.1103/PhysRev.129.2342

[38] S. Swain, "Master equation derivation of quantum regression theorem," *Journal of Physics A: Mathematical and General*, vol. 14, no. 10, p. 2577, Oct. 1981. [Online]. Available: https://dx.doi.org/10.1088/0305-4470/14/10/013

[39] M. Lax, "Quantum Noise. X. Density-Matrix Treatment of Field and Population-Difference Fluctuations," *Physical Review*, vol. 157, no. 2, pp. 213–231, May 1967. [Online]. Available: https://link.aps.org/doi/10.1103/PhysRev.157.213

[40] R. Jozsa, "Entanglement and Quantum Computation," Jul. 1997. [Online]. Available: http://arxiv.org/abs/quant-ph/9707034

[41] A. K. Ekert, "Quantum cryptography based on Bell's theorem," *Physical Review Letters*, vol. 67, no. 6, pp. 661–663, Aug. 1991. [Online]. Available: https://link.aps.org/doi/10.1103/PhysRevLett.67.661

[42] A. Ekert and R. Renner, "The ultimate physical limits of privacy," *Nature*, vol. 507, no. 7493, pp. 443–447, Mar. 2014. [Online]. Available: https://www.nature.com/articles/nature13132

[43] J. Lee and M. S. Kim, "Entanglement Teleportation via Werner States," *Physical Review Letters*, vol. 84, no. 18, pp. 4236–4239, May 2000. [Online]. Available: http://arxiv.org/abs/quant-ph/9907041

[44] M. Horodecki, P. Horodecki, and R. Horodecki, "Mixed-State Entanglement and Quantum Communication," in *Quantum Information: An Introduction to Basic Theoretical Concepts and Experiments*, ser. Springer Tracts in Modern Physics, G. Alber, T. Beth, M. Horodecki, P. Horodecki, R. Horodecki, M. Rötteler, H. Weinfurter, R. Werner, and A. Zeilinger, Eds. Berlin, Heidelberg: Springer, 2001, pp. 151–195. [Online]. Available: https://doi.org/10.1007/3-540-44678-8_5

[45] R. Horodecki, P. Horodecki, M. Horodecki, and K. Horodecki, "Quantum entanglement," *Reviews of Modern Physics*, vol. 81, no. 2, pp. 865–942, Jun. 2009. [Online]. Available: https://link.aps.org/doi/10.1103/RevModPhys.81.865

[46] D. A. B. Miller, "Are optical transistors the logical next step?" *Nature Photonics*, vol. 4, no. 1, pp. 3–5, Jan. 2010. [Online]. Available: https://www.nature.com/articles/nphoton.2009.240

[47] H. J. Kimble, "The quantum internet," *Nature*, vol. 453, no. 7198, pp. 1023–1030, Jun. 2008. [Online]. Available: https://www.nature.com/articles/nature07127

[48] A. Muthukrishnan, M. O. Scully, and M. S. Zubairy, "Quantum microscopy using photon correlations," *Journal of Optics B: Quantum and Semiclassical Optics*, vol. 6, no. 6, p. S575, May 2004. [Online]. Available: https://dx.doi.org/10.1088/1464-4266/6/6/017

[49] V. Giovannetti, S. Lloyd, and L. Maccone, "Advances in quantum metrology," *Nature Photonics*, vol. 5, no. 4, pp. 222–229, Apr. 2011. [Online]. Available: https://www.nature.com/articles/nphoton.2011.35

[50] C. K. Hong, Z. Y. Ou, and L. Mandel, "Measurement of subpicosecond time intervals between two photons by interference," *Physical Review Letters*, vol. 59, no. 18, pp. 2044–2046, Nov. 1987. [Online]. Available: https://link.aps.org/doi/10.1103/PhysRevLett.59.2044

[51] J. C. Howell, "Franson Interference: Space-like separated method for determining time-time correlations of entangled photons." [Online]. Available: https://www.pas.rochester.edu/~howell/mysite2/Tutorials/Franson%20Interference.pdf

[52] S. Manz, T. Fernholz, J. Schmiedmayer, and J.-W. Pan, "Collisional decoherence during writing and reading quantum states," *Physical Review A*, vol. 75, no. 4, p. 040101, Apr. 2007. [Online]. Available: https://link.aps.org/doi/10.1103/PhysRevA.75.040101

[53] J. H. Wesenberg and K. Mølmer, "Field Inside a Random Distribution of Parallel Dipoles," *Physical Review Letters*, vol. 93, no. 14, p. 143903, Sep. 2004. [Online]. Available: https://link.aps.org/doi/10.1103/PhysRevLett.93.143903

[54] J. A. Mlynek, A. A. Abdumalikov, C. Eichler, and A. Wallraff, "Observation of Dicke superradiance for two artificial atoms in a cavity with high decay rate," *Nature Communications*, vol. 5, no. 1, p. 5186, Nov. 2014. [Online]. Available: https://www.nature.com/articles/ncomms6186

[55] S. J. Masson and A. Asenjo-Garcia, "Universality of Dicke superradiance in arrays of quantum emitters," *Nature Communications*, vol. 13, no. 1, p. 2285, Apr. 2022. [Online]. Available: https://www.nature.com/articles/s41467-022-29805-4

[56] R. Gutzler, M. Garg, C. R. Ast, K. Kuhnke, and K. Kern, "Light–matter interaction at atomic scales," *Nature Reviews Physics*, vol. 3, no. 6, pp.

441–453, Jun. 2021. [Online]. Available: https://www.nature.com/articles/s42254-021-00306-5

[57] K. Hammerer, A. S. Sørensen, and E. S. Polzik, "Quantum interface between light and atomic ensembles," *Reviews of Modern Physics*, vol. 82, no. 2, pp. 1041–1093, Apr. 2010. [Online]. Available: https://link.aps.org/doi/10.1103/RevModPhys.82.1041

[58] C. Gonzalez-Ballestero, M. Aspelmeyer, L. Novotny, R. Quidant, and O. Romero-Isart, "Levitodynamics: Levitation and control of microscopic objects in vacuum," *Science*, vol. 374, no. 6564, p. eabg3027, Oct. 2021, publisher: American Association for the Advancement of Science. [Online]. Available: https://www.science.org/doi/full/10.1126/science.abg3027

[59] J. Rieser, M. A. Ciampini, H. Rudolph, N. Kiesel, K. Hornberger, B. A. Stickler, M. Aspelmeyer, and U. Deli, "Tunable light-induced dipole-dipole interaction between optically levitated nanoparticles," *Science*, vol. 377, no. 6609, pp. 987–990, Aug. 2022, publisher: American Association for the Advancement of Science. [Online]. Available: https://www-science-org.ezp-prod1.hul.harvard.edu/doi/full/10.1126/science.abp9941

[60] E. Vetsch, D. Reitz, G. Sagué, R. Schmidt, S. T. Dawkins, and A. Rauschenbeutel, "Optical Interface Created by Laser-Cooled Atoms Trapped in the Evanescent Field Surrounding an Optical Nanofiber," *Physical Review Letters*, vol. 104, no. 20, p. 203603, May 2010. [Online]. Available: https://link.aps.org/doi/10.1103/PhysRevLett.104.203603

[61] J. D. Hood, A. Goban, A. Asenjo-Garcia, M. Lu, S.-P. Yu, D. E. Chang, and H. J. Kimble, "Atomatom interactions around the band edge of a photonic crystal waveguide," *Proceedings of the National Academy of Sciences*, vol. 113, no. 38, pp. 10 507–10 512, Sep. 2016, publisher: Proceedings of the National Academy of Sciences. [Online]. Available: https://www.pnas.org/doi/abs/10.1073/pnas.1603788113

[62] R. J. Bettles, S. A. Gardiner, and C. S. Adams, "Enhanced Optical Cross Section via Collective Coupling of Atomic Dipoles in a 2D Array," *Physical Review Letters*, vol. 116, no. 10, p. 103602, Mar. 2016. [Online]. Available: https://link.aps.org/doi/10.1103/PhysRevLett.116.103602

[63] E. Shahmoon, D. S. Wild, M. D. Lukin, and S. F. Yelin, "Cooperative Resonances in Light Scattering from Two-Dimensional Atomic Arrays,"

Physical Review Letters, vol. 118, no. 11, p. 113601, Mar. 2017. [Online]. Available: https://link.aps.org/doi/10.1103/PhysRevLett.118.113601

[64] A. Asenjo-Garcia, M. Moreno-Cardoner, A. Albrecht, H. Kimble, and D. Chang, "Exponential Improvement in Photon Storage Fidelities Using Subradiance and Selective Radiance in Atomic Arrays," *Physical Review X*, vol. 7, no. 3, p. 031024, Aug. 2017. [Online]. Available: http://link.aps.org/doi/10.1103/PhysRevX.7.031024

[65] S. J. Masson, I. Ferrier-Barbut, L. A. Orozco, A. Browaeys, and A. Asenjo-Garcia, "Many-Body Signatures of Collective Decay in Atomic Chains," *Physical Review Letters*, vol. 125, no. 26, p. 263601, Dec. 2020. [Online]. Available: https://link.aps.org/doi/10.1103/PhysRevLett.125.263601

[66] O. Rubies-Bigorda, S. Ostermann, and S. F. Yelin, "Dynamic population of multiexcitation subradiant states in incoherently excited atomic arrays," *Physical Review A*, vol. 107, no. 5, p. L051701, May 2023. [Online]. Available: https://link.aps.org/doi/10.1103/PhysRevA.107.L051701

[67] K. Bian, W. Zheng, X. Zeng, X. Chen, R. Stöhr, A. Denisenko, S. Yang, J. Wrachtrup, and Y. Jiang, "Nanoscale electric-field imaging based on a quantum sensor and its charge-state control under ambient condition," *Nature Communications*, vol. 12, no. 1, p. 2457, Apr. 2021. [Online]. Available: https://www.nature.com/articles/s41467-021-22709-9

[68] B. J. Bloom, T. L. Nicholson, J. R. Williams, S. L. Campbell, M. Bishof, X. Zhang, W. Zhang, S. L. Bromley, and J. Ye, "An optical lattice clock with accuracy and stability at the 10-18 level," *Nature*, vol. 506, no. 7486, pp. 71–75, Feb. 2014. [Online]. Available: https://www.nature.com/articles/nature12941

[69] W. C. Campbell and P. Hamilton, "Rotation sensing with trapped ions*," *Journal of Physics B: Atomic, Molecular and Optical Physics*, vol. 50, no. 6, p. 064002, Feb. 2017. [Online]. Available: https://dx.doi.org/10.1088/1361-6455/aa5a8f

[70] C. L. Degen, F. Reinhard, and P. Cappellaro, "Quantum sensing," *Reviews of Modern Physics*, vol. 89, no. 3, p. 035002, Jul. 2017. [Online]. Available: http://link.aps.org/doi/10.1103/RevModPhys.89.035002

[71] S. Hsieh, P. Bhattacharyya, C. Zu, T. Mittiga, T. J. Smart, F. Machado, B. Kobrin, T. O. Höhn, N. Z. Rui, M. Kamrani, S. Chatterjee, S. Choi,

152

M. Zaletel, V. V. Struzhkin, J. E. Moore, V. I. Levitas, R. Jeanloz, and N. Y. Yao, "Imaging stress and magnetism at high pressures using a nanoscale quantum sensor," *Science*, vol. 366, no. 6471, pp. 1349–1354, Dec. 2019, publisher: American Association for the Advancement of Science. [Online]. Available: https://www.science.org/doi/full/10.1126/science.aaw4352

[72] M. D. Swallows, M. Bishof, Y. Lin, S. Blatt, M. J. Martin, A. M. Rey, and J. Ye, "Suppression of Collisional Shifts in a Strongly Interacting Lattice Clock," *Science*, vol. 331, no. 6020, pp. 1043–1046, Feb. 2011, publisher: American Association for the Advancement of Science. [Online]. Available: https://www.science.org/doi/abs/10.1126/science.1196442

[73] S. Krämer, L. Ostermann, and H. Ritsch, "Optimized geometries for future generation optical lattice clocks," *Europhysics Letters*, vol. 114, no. 1, p. 14003, May 2016, publisher: EDP Sciences, IOP Publishing and Società Italiana di Fisica. [Online]. Available: https://dx.doi.org/10.1209/0295-5075/114/14003

[74] S. L. Campbell, R. B. Hutson, G. E. Marti, A. Goban, N. Darkwah Oppong, R. L. McNally, L. Sonderhouse, J. M. Robinson, W. Zhang, B. J. Bloom, and J. Ye, "A Fermi-degenerate three-dimensional optical lattice clock," *Science*, vol. 358, no. 6359, pp. 90–94, Oct. 2017, publisher: American Association for the Advancement of Science. [Online]. Available: https://www.science.org/doi/full/10.1126/science.aam5538

[75] T. L. Patti, D. S. Wild, E. Shahmoon, M. D. Lukin, and S. F. Yelin, "Controlling Interactions between Quantum Emitters Using Atom Arrays," *Physical Review Letters*, vol. 126, no. 22, p. 223602, Jun. 2021. [Online]. Available: https://link.aps.org/doi/10.1103/PhysRevLett.126.223602

[76] B. Olmos, I. Lesanovsky, and J. P. Garrahan, "Out-of-equilibrium evolution of kinetically constrained many-body quantum systems under purely dissipative dynamics," *Physical Review E*, vol. 90, no. 4, p. 042147, Oct. 2014. [Online]. Available: https://link.aps.org/doi/10.1103/PhysRevE.90.042147

[77] J. Wiersig, "Enhancing the Sensitivity of Frequency and Energy Splitting Detection by Using Exceptional Points: Application to Microcavity Sensors for Single-Particle Detection," *Physical Review Letters*, vol. 112, no. 20, p. 203901, May 2014. [Online]. Available: https://link.aps.org/doi/10.1103/PhysRevLett.112.203901

[78] B. P. Abbott, R. Abbott, T. D. Abbott, M. R. Abernathy, F. Acernese, K. Ackley, C. Adams, T. Adams, P. Addesso, R. X. Adhikari, V. B. Adya, C. Affeldt, M. Agathos, K. Agatsuma, N. Aggarwal, O. D. Aguiar, L. Aiello, A. Ain, P. Ajith, B. Allen, A. Allocca, P. A. Altin, S. B. Anderson, W. G. Anderson, K. Arai, M. A. Arain, M. C. Araya, C. C. Arceneaux, J. S. Areeda, N. Arnaud, K. G. Arun, S. Ascenzi, G. Ashton, M. Ast, S. M. Aston, P. Astone, P. Aufmuth, C. Aulbert, S. Babak, P. Bacon, M. K. M. Bader, P. T. Baker, F. Baldaccini, G. Ballardin, S. W. Ballmer, J. C. Barayoga, S. E. Barclay, B. C. Barish, D. Barker, F. Barone, B. Barr, L. Barsotti, M. Barsuglia, D. Barta, J. Bartlett, M. A. Barton, I. Bartos, R. Bassiri, A. Basti, J. C. Batch, C. Baune, V. Bavigadda, M. Bazzan, B. Behnke, M. Bejger, C. Belczynski, A. S. Bell, C. J. Bell, B. K. Berger, J. Bergman, G. Bergmann, C. P. L. Berry, D. Bersanetti, A. Bertolini, J. Betzwieser, S. Bhagwat, R. Bhandare, I. A. Bilenko, G. Billingsley, J. Birch, R. Birney, O. Birnholtz, S. Biscans, A. Bisht, M. Bitossi, C. Biwer, M. A. Bizouard, J. K. Blackburn, C. D. Blair, D. G. Blair, R. M. Blair, S. Bloemen, O. Bock, T. P. Bodiya, M. Boer, G. Bogaert, C. Bogan, A. Bohe, P. Bojtos, C. Bond, F. Bondu, R. Bonnand, B. A. Boom, R. Bork, V. Boschi, S. Bose, Y. Bouffanais, A. Bozzi, C. Bradaschia, P. R. Brady, V. B. Braginsky, M. Branchesi, J. E. Brau, T. Briant, A. Brillet, M. Brinkmann, V. Brisson, P. Brockill, A. F. Brooks, D. A. Brown, D. D. Brown, N. M. Brown, C. C. Buchanan, A. Buikema, T. Bulik, H. J. Bulten, A. Buonanno, D. Buskulic, C. Buy, R. L. Byer, M. Cabero, L. Cadonati, G. Cagnoli, C. Cahillane, J. C. Bustillo, T. Callister, E. Calloni, J. B. Camp, K. C. Cannon, J. Cao, C. D. Capano, E. Capocasa, F. Carbognani, S. Caride, J. C. Diaz, C. Casentini, S. Caudill, M. Cavaglià, F. Cavalier, R. Cavalieri, G. Cella, C. B. Cepeda, L. C. Baiardi, G. Cerretani, E. Cesarini, R. Chakraborty, T. Chalermsongsak, S. J. Chamberlin, M. Chan, S. Chao, P. Charlton, E. Chassande-Mottin, H. Y. Chen, Y. Chen, C. Cheng, A. Chincarini, A. Chiummo, H. S. Cho, M. Cho, J. H. Chow, N. Christensen, Q. Chu, S. Chua, S. Chung, G. Ciani, F. Clara, J. A. Clark, F. Cleva, E. Coccia, P.-F. Cohadon, A. Colla, C. G. Collette, L. Cominsky, M. Constancio, A. Conte, L. Conti, D. Cook, T. R. Corbitt, N. Cornish, A. Corsi, S. Cortese, C. A. Costa, M. W. Coughlin, S. B. Coughlin, J.-P. Coulon, S. T. Countryman, P. Couvares, E. E. Cowan, D. M. Coward, M. J. Cowart, D. C. Coyne, R. Coyne, K. Craig, J. D. E. Creighton, T. D. Creighton, J. Cripe, S. G. Crowder, A. M. Cruise, A. Cumming, L. Cunningham, E. Cuoco, T. D. Canton, S. L. Danilishin, S. D'Antonio, K. Danzmann, N. S. Darman, C. F. Da Silva Costa, V. Dattilo, I. Dave, H. P.

154

Daveloza, M. Davier, G. S. Davies, E. J. Daw, R. Day, S. De, D. DeBra, G. Debreczeni, J. Degallaix, M. De Laurentis, S. Deléglise, W. Del Pozzo, T. Denker, T. Dent, H. Dereli, V. Dergachev, R. T. DeRosa, R. De Rosa, R. DeSalvo, S. Dhurandhar, M. C. Díaz, L. Di Fiore, M. Di Giovanni, A. Di Lieto, S. Di Pace, I. Di Palma, A. Di Virgilio, G. Dojcinoski, V. Dolique, F. Donovan, K. L. Dooley, S. Doravari, R. Douglas, T. P. Downes, M. Drago, R. W. P. Drever, J. C. Driggers, Z. Du, M. Ducrot, S. E. Dwyer, T. B. Edo, M. C. Edwards, A. Effler, H.-B. Eggenstein, P. Ehrens, J. Eichholz, S. S. Eikenberry, W. Engels, R. C. Essick, T. Etzel, M. Evans, T. M. Evans, R. Everett, M. Factourovich, V. Fafone, H. Fair, S. Fairhurst, X. Fan, Q. Fang, S. Farinon, B. Farr, W. M. Farr, M. Favata, M. Fays, H. Fehrmann, M. M. Fejer, D. Feldbaum, I. Ferrante, E. C. Ferreira, F. Ferrini, F. Fidecaro, L. S. Finn, I. Fiori, D. Fiorucci, R. P. Fisher, R. Flaminio, M. Fletcher, H. Fong, J.-D. Fournier, S. Franco, S. Frasca, F. Frasconi, M. Frede, Z. Frei, A. Freise, R. Frey, V. Frey, T. T. Fricke, P. Fritschel, V. V. Frolov, P. Fulda, M. Fyffe, H. A. G. Gabbard, J. R. Gair, L. Gammaitoni, S. G. Gaonkar, F. Garufi, A. Gatto, G. Gaur, N. Gehrels, G. Gemme, B. Gendre, E. Genin, A. Gennai, J. George, L. Gergely, V. Germain, A. Ghosh, A. Ghosh, S. Ghosh, J. A. Giaime, K. D. Giardina, A. Giazotto, K. Gill, A. Glaefke, J. R. Gleason, E. Goetz, R. Goetz, L. Gondan, G. González, J. M. G. Castro, A. Gopakumar, N. A. Gordon, M. L. Gorodetsky, S. E. Gossan, M. Gosselin, R. Gouaty, C. Graef, P. B. Graff, M. Granata, A. Grant, S. Gras, C. Gray, G. Greco, A. C. Green, R. J. S. Greenhalgh, P. Groot, H. Grote, S. Grunewald, G. M. Guidi, X. Guo, A. Gupta, M. K. Gupta, K. E. Gushwa, E. K. Gustafson, R. Gustafson, J. J. Hacker, B. R. Hall, E. D. Hall, G. Hammond, M. Haney, M. M. Hanke, J. Hanks, C. Hanna, M. D. Hannam, J. Hanson, T. Hardwick, J. Harms, G. M. Harry, I. W. Harry, M. J. Hart, M. T. Hartman, C.-J. Haster, K. Haughian, J. Healy, J. Heefner, A. Heidmann, M. C. Heintze, G. Heinzel, H. Heitmann, P. Hello, G. Hemming, M. Hendry, I. S. Heng, J. Hennig, A. W. Heptonstall, M. Heurs, S. Hild, D. Hoak, K. A. Hodge, D. Hofman, S. E. Hollitt, K. Holt, D. E. Holz, P. Hopkins, D. J. Hosken, J. Hough, E. A. Houston, E. J. Howell, Y. M. Hu, S. Huang, E. A. Huerta, D. Huet, B. Hughey, S. Husa, S. H. Huttner, T. Huynh-Dinh, A. Idrisy, N. Indik, D. R. Ingram, R. Inta, H. N. Isa, J.-M. Isac, M. Isi, G. Islas, T. Isogai, B. R. Iyer, K. Izumi, M. B. Jacobson, T. Jacqmin, H. Jang, K. Jani, P. Jaranowski, S. Jawahar, F. Jiménez-Forteza, W. W. Johnson, N. K. Johnson-McDaniel, D. I. Jones, R. Jones, R. J. G. Jonker, L. Ju, K. Haris, C. V. Kalaghatgi, V. Kalogera, S. Kandhasamy, G. Kang, J. B. Kanner, S. Karki, M. Kasprzack,

155

E. Katsavounidis, W. Katzman, S. Kaufer, T. Kaur, K. Kawabe, F. Kawazoe, F. Kéfélian, M. S. Kehl, D. Keitel, D. B. Kelley, W. Kells, R. Kennedy, D. G. Keppel, J. S. Key, A. Khalaidovski, F. Y. Khalili, I. Khan, S. Khan, Z. Khan, E. A. Khazanov, N. Kijbunchoo, C. Kim, J. Kim, K. Kim, N.-G. Kim, N. Kim, Y.-M. Kim, E. J. King, P. J. King, D. L. Kinzel, J. S. Kissel, L. Kleybolte, S. Klimenko, S. M. Koehlenbeck, K. Kokeyama, S. Koley, V. Kondrashov, A. Kontos, S. Koranda, M. Korobko, W. Z. Korth, I. Kowalska, D. B. Kozak, V. Kringel, B. Krishnan, A. Królak, C. Krueger, G. Kuehn, P. Kumar, R. Kumar, L. Kuo, A. Kutynia, P. Kwee, B. D. Lackey, M. Landry, J. Lange, B. Lantz, P. D. Lasky, A. Lazzarini, C. Lazzaro, P. Leaci, S. Leavey, E. O. Lebigot, C. H. Lee, H. K. Lee, H. M. Lee, K. Lee, A. Lenon, M. Leonardi, J. R. Leong, N. Leroy, N. Letendre, Y. Levin, B. M. Levine, T. G. F. Li, A. Libson, T. B. Littenberg, N. A. Lockerbie, J. Logue, A. L. Lombardi, L. T. London, J. E. Lord, M. Lorenzini, V. Loriette, M. Lormand, G. Losurdo, J. D. Lough, C. O. Lousto, G. Lovelace, H. Lück, A. P. Lundgren, J. Luo, R. Lynch, Y. Ma, T. MacDonald, B. Machenschalk, M. MacInnis, D. M. Macleod, F. Magaña-Sandoval, R. M. Magee, M. Mageswaran, E. Majorana, I. Maksimovic, V. Malvezzi, N. Man, I. Mandel, V. Mandic, V. Mangano, G. L. Mansell, M. Manske, M. Mantovani, F. Marchesoni, F. Marion, S. Márka, Z. Márka, A. S. Markosyan, E. Maros, F. Martelli, L. Martellini, I. W. Martin, R. M. Martin, D. V. Martynov, J. N. Marx, K. Mason, A. Masserot, T. J. Massinger, M. Masso-Reid, F. Matichard, L. Matone, N. Mavalvala, N. Mazumder, G. Mazzolo, R. McCarthy, D. E. McClelland, S. McCormick, S. C. McGuire, G. McIntyre, J. McIver, D. J. McManus, S. T. McWilliams, D. Meacher, G. D. Meadors, J. Meidam, A. Melatos, G. Mendell, D. Mendoza-Gandara, R. A. Mercer, E. Merilh, M. Merzougui, S. Meshkov, C. Messenger, C. Messick, P. M. Meyers, F. Mezzani, H. Miao, C. Michel, H. Middleton, E. E. Mikhailov, L. Milano, J. Miller, M. Millhouse, Y. Minenkov, J. Ming, S. Mirshekari, C. Mishra, S. Mitra, V. P. Mitrofanov, G. Mitselmakher, R. Mittleman, A. Moggi, M. Mohan, S. R. P. Mohapatra, M. Montani, B. C. Moore, C. J. Moore, D. Moraru, G. Moreno, S. R. Morriss, K. Mossavi, B. Mours, C. M. Mow-Lowry, C. L. Mueller, G. Mueller, A. W. Muir, A. Mukherjee, D. Mukherjee, S. Mukherjee, N. Mukund, A. Mullavey, J. Munch, D. J. Murphy, P. G. Murray, A. Mytidis, I. Nardecchia, L. Naticchioni, R. K. Nayak, V. Necula, K. Nedkova, G. Nelemans, M. Neri, A. Neunzert, G. Newton, T. T. Nguyen, A. B. Nielsen, S. Nissanke, A. Nitz, F. Nocera, D. Nolting, M. E. N. Normandin, L. K. Nuttall, J. Oberling, E. Ochsner, J. O'Dell, E. Oelker, G. H. Ogin, J. J. Oh, S. H. Oh, F. Ohme,

M. Oliver, P. Oppermann, R. J. Oram, B. O'Reilly, R. O'Shaughnessy, C. D. Ott, D. J. Ottaway, R. S. Ottens, H. Overmier, B. J. Owen, A. Pai, S. A. Pai, J. R. Palamos, O. Palashov, C. Palomba, A. Pal-Singh, H. Pan, Y. Pan, C. Pankow, F. Pannarale, B. C. Pant, F. Paoletti, A. Paoli, M. A. Papa, H. R. Paris, W. Parker, D. Pascucci, A. Pasqualetti, R. Passaquieti, D. Passuello, B. Patricelli, Z. Patrick, B. L. Pearlstone, M. Pedraza, R. Pedurand, L. Pekowsky, A. Pele, S. Penn, A. Perreca, H. P. Pfeiffer, M. Phelps, O. Piccinni, M. Pichot, M. Pickenpack, F. Piergiovanni, V. Pierro, G. Pillant, L. Pinard, I. M. Pinto, M. Pitkin, J. H. Poeld, R. Poggiani, P. Popolizio, A. Post, J. Powell, J. Prasad, V. Predoi, S. S. Premachandra, T. Prestegard, L. R. Price, M. Prijatelj, M. Principe, S. Privitera, R. Prix, G. A. Prodi, L. Prokhorov, O. Puncken, M. Punturo, P. Puppo, M. Pürrer, H. Qi, J. Qin, V. Quetschke, E. A. Quintero, R. Quitzow-James, F. J. Raab, D. S. Rabeling, H. Radkins, P. Raffai, S. Raja, M. Rakhmanov, C. R. Ramet, P. Rapagnani, V. Raymond, M. Razzano, V. Re, J. Read, C. M. Reed, T. Regimbau, L. Rei, S. Reid, D. H. Reitze, H. Rew, S. D. Reyes, F. Ricci, K. Riles, N. A. Robertson, R. Robie, F. Robinet, A. Rocchi, L. Rolland, J. G. Rollins, V. J. Roma, J. D. Romano, R. Romano, G. Romanov, J. H. Romie, D. Rosińska, S. Rowan, A. Rüdiger, P. Ruggi, K. Ryan, S. Sachdev, T. Sadecki, L. Sadeghian, L. Salconi, M. Saleem, F. Salemi, A. Samajdar, L. Sammut, L. M. Sampson, E. J. Sanchez, V. Sandberg, B. Sandeen, G. H. Sanders, J. R. Sanders, B. Sassolas, B. S. Sathyaprakash, P. R. Saulson, O. Sauter, R. L. Savage, A. Sawadsky, P. Schale, R. Schilling, J. Schmidt, P. Schmidt, R. Schnabel, R. M. S. Schofield, A. Schönbeck, E. Schreiber, D. Schuette, B. F. Schutz, J. Scott, S. M. Scott, D. Sellers, A. S. Sengupta, D. Sentenac, V. Sequino, A. Sergeev, G. Serna, Y. Setyawati, A. Sevigny, D. A. Shaddock, T. Shaffer, S. Shah, M. S. Shahriar, M. Shaltev, Z. Shao, B. Shapiro, P. Shawhan, A. Sheperd, D. H. Shoemaker, D. M. Shoemaker, K. Siellez, X. Siemens, D. Sigg, A. D. Silva, D. Simakov, A. Singer, L. P. Singer, A. Singh, R. Singh, A. Singhal, A. M. Sintes, B. J. J. Slagmolen, J. R. Smith, M. R. Smith, N. D. Smith, R. J. E. Smith, E. J. Son, B. Sorazu, F. Sorrentino, T. Souradeep, A. K. Srivastava, A. Staley, M. Steinke, J. Steinlechner, S. Steinlechner, D. Steinmeyer, B. C. Stephens, S. P. Stevenson, R. Stone, K. A. Strain, N. Straniero, G. Stratta, N. A. Strauss, S. Strigin, R. Sturani, A. L. Stuver, T. Z. Summerscales, L. Sun, P. J. Sutton, B. L. Swinkels, M. J. Szczepańczyk, M. Tacca, D. Talukder, D. B. Tanner, M. Tápai, S. P. Tarabrin, A. Taracchini, R. Taylor, T. Theeg, M. P. Thirugnanasambandam, E. G. Thomas, M. Thomas, P. Thomas, K. A. Thorne, K. S. Thorne, E. Thrane,

S. Tiwari, V. Tiwari, K. V. Tokmakov, C. Tomlinson, M. Tonelli, C. V. Torres, C. I. Torrie, D. Töyrä, F. Travasso, G. Traylor, D. Trifirò, M. C. Tringali, L. Trozzo, M. Tse, M. Turconi, D. Tuyenbayev, D. Ugolini, C. S. Unnikrishnan, A. L. Urban, S. A. Usman, H. Vahlbruch, G. Vajente, G. Valdes, M. Vallisneri, N. Van Bakel, M. Van Beuzekom, J. F. J. Van Den Brand, C. Van Den Broeck, D. C. Vander-Hyde, L. Van Der Schaaf, J. V. Van Heijningen, A. A. Van Veggel, M. Vardaro, S. Vass, M. Vasúth, R. Vaulin, A. Vecchio, G. Vedovato, J. Veitch, P. J. Veitch, K. Venkateswara, D. Verkindt, F. Vetrano, A. Viceré, S. Vinciguerra, D. J. Vine, J.-Y. Vinet, S. Vitale, T. Vo, H. Vocca, C. Vorvick, D. Voss, W. D. Vousden, S. P. Vyatchanin, A. R. Wade, L. E. Wade, M. Wade, S. J. Waldman, M. Walker, L. Wallace, S. Walsh, G. Wang, H. Wang, M. Wang, X. Wang, Y. Wang, H. Ward, R. L. Ward, J. Warner, M. Was, B. Weaver, L.-W. Wei, M. Weinert, A. J. Weinstein, R. Weiss, T. Welborn, L. Wen, P. Weßels, T. Westphal, K. Wette, J. T. Whelan, S. E. Whitcomb, D. J. White, B. F. Whiting, K. Wiesner, C. Wilkinson, P. A. Willems, L. Williams, R. D. Williams, A. R. Williamson, J. L. Willis, B. Willke, M. H. Wimmer, L. Winkelmann, W. Winkler, C. C. Wipf, A. G. Wiseman, H. Wittel, G. Woan, J. Worden, J. L. Wright, G. Wu, J. Yablon, I. Yakushin, W. Yam, H. Yamamoto, C. C. Yancey, M. J. Yap, H. Yu, M. Yvert, A. Zadrożny, L. Zangrando, M. Zanolin, J.-P. Zendri, M. Zevin, F. Zhang, L. Zhang, M. Zhang, Y. Zhang, C. Zhao, M. Zhou, Z. Zhou, X. J. Zhu, M. E. Zucker, S. E. Zuraw, J. Zweizig, and LIGO Scientific Collaboration and Virgo Collaboration, "Observation of Gravitational Waves from a Binary Black Hole Merger," *Physical Review Letters*, vol. 116, no. 6, p. 061102, Feb. 2016. [Online]. Available: https://link.aps.org/doi/10.1103/PhysRevLett.116.061102

[79] LIGO Scientific Collaboration and Virgo Collaboration, B. P. Abbott, R. Abbott, T. D. Abbott, F. Acernese, K. Ackley, C. Adams, T. Adams, P. Addesso, R. X. Adhikari, V. B. Adya, C. Affeldt, M. Afrough, B. Agarwal, M. Agathos, K. Agatsuma, N. Aggarwal, O. D. Aguiar, L. Aiello, A. Ain, P. Ajith, B. Allen, G. Allen, A. Allocca, P. A. Altin, A. Amato, A. Ananyeva, S. B. Anderson, W. G. Anderson, S. V. Angelova, S. Antier, S. Appert, K. Arai, M. C. Araya, J. S. Areeda, N. Arnaud, K. G. Arun, S. Ascenzi, G. Ashton, M. Ast, S. M. Aston, P. Astone, D. V. Atallah, P. Aufmuth, C. Aulbert, K. AultONeal, C. Austin, A. Avila-Alvarez, S. Babak, P. Bacon, M. K. M. Bader, S. Bae, M. Bailes, P. T. Baker, F. Baldaccini, G. Ballardin, S. W. Ballmer, S. Banagiri, J. C. Barayoga, S. E. Barclay, B. C. Barish, D. Barker, K. Barkett, F. Barone, B. Barr, L. Barsotti, M. Barsuglia,

D. Barta, S. D. Barthelmy, J. Bartlett, I. Bartos, R. Bassiri, A. Basti, J. C. Batch, M. Bawaj, J. C. Bayley, M. Bazzan, B. Bécsy, C. Beer, M. Bejger, I. Belahcene, A. S. Bell, B. K. Berger, G. Bergmann, S. Bernuzzi, J. J. Bero, C. P. L. Berry, D. Bersanetti, A. Bertolini, J. Betzwieser, S. Bhagwat, R. Bhandare, I. A. Bilenko, G. Billingsley, C. R. Billman, J. Birch, R. Birney, O. Birnholtz, S. Biscans, S. Biscoveanu, A. Bisht, M. Bitossi, C. Biwer, M. A. Bizouard, J. K. Blackburn, J. Blackman, C. D. Blair, D. G. Blair, R. M. Blair, S. Bloemen, O. Bock, N. Bode, M. Boer, G. Bogaert, A. Bohe, F. Bondu, E. Bonilla, R. Bonnand, B. A. Boom, R. Bork, V. Boschi, S. Bose, K. Bossie, Y. Bouffanais, A. Bozzi, C. Bradaschia, P. R. Brady, M. Branchesi, J. E. Brau, T. Briant, A. Brillet, M. Brinkmann, V. Brisson, P. Brockill, J. E. Broida, A. F. Brooks, D. A. Brown, D. D. Brown, S. Brunett, C. C. Buchanan, A. Buikema, T. Bulik, H. J. Bulten, A. Buonanno, D. Buskulic, C. Buy, R. L. Byer, M. Cabero, L. Cadonati, G. Cagnoli, C. Cahillane, J. Calderón Bustillo, T. A. Callister, E. Calloni, J. B. Camp, M. Canepa, P. Canizares, K. C. Cannon, H. Cao, J. Cao, C. D. Capano, E. Capocasa, F. Carbognani, S. Caride, M. F. Carney, G. Carullo, J. Casanueva Diaz, C. Casentini, S. Caudill, M. Cavaglià, F. Cavalier, R. Cavalieri, G. Cella, C. B. Cepeda, P. Cerdá-Durán, G. Cerretani, E. Cesarini, S. J. Chamberlin, M. Chan, S. Chao, P. Charlton, E. Chase, E. Chassande-Mottin, D. Chatterjee, K. Chatziioannou, B. D. Cheeseboro, H. Y. Chen, X. Chen, Y. Chen, H.-P. Cheng, H. Chia, A. Chincarini, A. Chiummo, T. Chmiel, H. S. Cho, M. Cho, J. H. Chow, N. Christensen, Q. Chu, A. J. K. Chua, S. Chua, A. K. W. Chung, S. Chung, G. Ciani, R. Ciolfi, C. E. Cirelli, A. Cirone, F. Clara, J. A. Clark, P. Clearwater, F. Cleva, C. Cocchieri, E. Coccia, P.-F. Cohadon, D. Cohen, A. Colla, C. G. Collette, L. R. Cominsky, M. Constancio, L. Conti, S. J. Cooper, P. Corban, T. R. Corbitt, I. Cordero-Carrión, K. R. Corley, N. Cornish, A. Corsi, S. Cortese, C. A. Costa, M. W. Coughlin, S. B. Coughlin, J.-P. Coulon, S. T. Countryman, P. Couvares, P. B. Covas, E. E. Cowan, D. M. Coward, M. J. Cowart, D. C. Coyne, R. Coyne, J. D. E. Creighton, T. D. Creighton, J. Cripe, S. G. Crowder, T. J. Cullen, A. Cumming, L. Cunningham, E. Cuoco, T. Dal Canton, G. Dálya, S. L. Danilishin, S. D'Antonio, K. Danzmann, A. Dasgupta, C. F. Da Silva Costa, V. Dattilo, I. Dave, M. Davier, D. Davis, E. J. Daw, B. Day, S. De, D. DeBra, J. Degallaix, M. De Laurentis, S. Deléglise, W. Del Pozzo, N. Demos, T. Denker, T. Dent, R. De Pietri, V. Dergachev, R. De Rosa, R. T. DeRosa, C. De Rossi, R. DeSalvo, O. de Varona, J. Devenson, S. Dhurandhar, M. C. Díaz, T. Dietrich, L. Di Fiore, M. Di Giovanni, T. Di Girolamo, A. Di Lieto,

S. Di Pace, I. Di Palma, F. Di Renzo, Z. Doctor, V. Dolique, F. Donovan, K. L. Dooley, S. Doravari, I. Dorrington, R. Douglas, M. Dovale Álvarez, T. P. Downes, M. Drago, C. Dreissigacker, J. C. Driggers, Z. Du, M. Ducrot, R. Dudi, P. Dupej, S. E. Dwyer, T. B. Edo, M. C. Edwards, A. Effler, H.-B. Eggenstein, P. Ehrens, J. Eichholz, S. S. Eikenberry, R. A. Eisenstein, R. C. Essick, D. Estevez, Z. B. Etienne, T. Etzel, M. Evans, T. M. Evans, M. Factourovich, V. Fafone, H. Fair, S. Fairhurst, X. Fan, S. Farinon, B. Farr, W. M. Farr, E. J. Fauchon-Jones, M. Favata, M. Fays, C. Fee, H. Fehrmann, J. Feicht, M. M. Fejer, A. Fernandez-Galiana, I. Ferrante, E. C. Ferreira, F. Ferrini, F. Fidecaro, D. Finstad, I. Fiori, D. Fiorucci, M. Fishbach, R. P. Fisher, M. Fitz-Axen, R. Flaminio, M. Fletcher, H. Fong, J. A. Font, P. W. F. Forsyth, S. S. Forsyth, J.-D. Fournier, S. Frasca, F. Frasconi, Z. Frei, A. Freise, R. Frey, V. Frey, E. M. Fries, P. Fritschel, V. V. Frolov, P. Fulda, M. Fyffe, H. Gabbard, B. U. Gadre, S. M. Gaebel, J. R. Gair, L. Gammaitoni, M. R. Ganija, S. G. Gaonkar, C. Garcia-Quiros, F. Garufi, B. Gateley, S. Gaudio, G. Gaur, V. Gayathri, N. Gehrels, G. Gemme, E. Genin, A. Gennai, D. George, J. George, L. Gergely, V. Germain, S. Ghonge, A. Ghosh, A. Ghosh, S. Ghosh, J. A. Giaime, K. D. Giardina, A. Giazotto, K. Gill, L. Glover, E. Goetz, R. Goetz, S. Gomes, B. Goncharov, G. González, J. M. Gonzalez Castro, A. Gopakumar, M. L. Gorodetsky, S. E. Gossan, M. Gosselin, R. Gouaty, A. Grado, C. Graef, M. Granata, A. Grant, S. Gras, C. Gray, G. Greco, A. C. Green, E. M. Gretarsson, P. Groot, H. Grote, S. Grunewald, P. Gruning, G. M. Guidi, X. Guo, A. Gupta, M. K. Gupta, K. E. Gushwa, E. K. Gustafson, R. Gustafson, O. Halim, B. R. Hall, E. D. Hall, E. Z. Hamilton, G. Hammond, M. Haney, M. M. Hanke, J. Hanks, C. Hanna, M. D. Hannam, O. A. Hannuksela, J. Hanson, T. Hardwick, J. Harms, G. M. Harry, I. W. Harry, M. J. Hart, C.-J. Haster, K. Haughian, J. Healy, A. Heidmann, M. C. Heintze, H. Heitmann, P. Hello, G. Hemming, M. Hendry, I. S. Heng, J. Hennig, A. W. Heptonstall, M. Heurs, S. Hild, T. Hinderer, W. C. G. Ho, D. Hoak, D. Hofman, K. Holt, D. E. Holz, P. Hopkins, C. Horst, J. Hough, E. A. Houston, E. J. Howell, A. Hreibi, Y. M. Hu, E. A. Huerta, D. Huet, B. Hughey, S. Husa, S. H. Huttner, T. Huynh-Dinh, N. Indik, R. Inta, G. Intini, H. N. Isa, J.-M. Isac, M. Isi, B. R. Iyer, K. Izumi, T. Jacqmin, K. Jani, P. Jaranowski, S. Jawahar, F. Jiménez-Forteza, W. W. Johnson, N. K. Johnson-McDaniel, D. I. Jones, R. Jones, R. J. G. Jonker, L. Ju, J. Junker, C. V. Kalaghatgi, V. Kalogera, B. Kamai, S. Kandhasamy, G. Kang, J. B. Kanner, S. J. Kapadia, S. Karki, K. S. Karvinen, M. Kasprzack, W. Kastaun, M. Katolik, E. Katsavounidis, W. Katzman, S. Kaufer, K. Kawabe, F. Kéfélian, D. Keitel,

160

A. J. Kemball, R. Kennedy, C. Kent, J. S. Key, F. Y. Khalili, I. Khan, S. Khan, Z. Khan, E. A. Khazanov, N. Kijbunchoo, C. Kim, J. C. Kim, K. Kim, W. Kim, W. S. Kim, Y.-M. Kim, S. J. Kimbrell, E. J. King, P. J. King, M. Kinley-Hanlon, R. Kirchhoff, J. S. Kissel, L. Kleybolte, S. Klimenko, T. D. Knowles, P. Koch, S. M. Koehlenbeck, S. Koley, V. Kondrashov, A. Kontos, M. Korobko, W. Z. Korth, I. Kowalska, D. B. Kozak, C. Krämer, V. Kringel, B. Krishnan, A. Królak, G. Kuehn, P. Kumar, R. Kumar, S. Kumar, L. Kuo, A. Kutynia, S. Kwang, B. D. Lackey, K. H. Lai, M. Landry, R. N. Lang, J. Lange, B. Lantz, R. K. Lanza, S. L. Larson, A. Lartaux-Vollard, P. D. Lasky, M. Laxen, A. Lazzarini, C. Lazzaro, P. Leaci, S. Leavey, C. H. Lee, H. K. Lee, H. M. Lee, H. W. Lee, K. Lee, J. Lehmann, A. Lenon, E. Leon, M. Leonardi, N. Leroy, N. Letendre, Y. Levin, T. G. F. Li, S. D. Linker, T. B. Littenberg, J. Liu, X. Liu, R. K. L. Lo, N. A. Lockerbie, L. T. London, J. E. Lord, M. Lorenzini, V. Loriette, M. Lormand, G. Losurdo, J. D. Lough, C. O. Lousto, G. Lovelace, H. Lück, D. Lumaca, A. P. Lundgren, R. Lynch, Y. Ma, R. Macas, S. Macfoy, B. Machenschalk, M. MacInnis, D. M. Macleod, I. Magaña Hernandez, F. Magaña-Sandoval, L. Magaña Zertuche, R. M. Magee, E. Majorana, I. Maksimovic, N. Man, V. Mandic, V. Mangano, G. L. Mansell, M. Manske, M. Mantovani, F. Marchesoni, F. Marion, S. Márka, Z. Márka, C. Markakis, A. S. Markosyan, A. Markowitz, E. Maros, A. Marquina, P. Marsh, F. Martelli, L. Martellini, I. W. Martin, R. M. Martin, D. V. Martynov, J. N. Marx, K. Mason, E. Massera, A. Masserot, T. J. Massinger, M. Masso-Reid, S. Mastrogiovanni, A. Matas, F. Matichard, L. Matone, N. Mavalvala, N. Mazumder, R. McCarthy, D. E. McClelland, S. McCormick, L. McCuller, S. C. McGuire, G. McIntyre, J. McIver, D. J. McManus, L. McNeill, T. McRae, S. T. McWilliams, D. Meacher, G. D. Meadors, M. Mehmet, J. Meidam, E. Mejuto-Villa, A. Melatos, G. Mendell, R. A. Mercer, E. L. Merilh, M. Merzougui, S. Meshkov, C. Messenger, C. Messick, R. Metzdorff, P. M. Meyers, H. Miao, C. Michel, H. Middleton, E. E. Mikhailov, L. Milano, A. L. Miller, B. B. Miller, J. Miller, M. Millhouse, M. C. Milovich-Goff, O. Minazzoli, Y. Minenkov, J. Ming, C. Mishra, S. Mitra, V. P. Mitrofanov, G. Mitselmakher, R. Mittleman, D. Moffa, A. Moggi, K. Mogushi, M. Mohan, S. R. P. Mohapatra, I. Molina, M. Montani, C. J. Moore, D. Moraru, G. Moreno, S. Morisaki, S. R. Morriss, B. Mours, C. M. Mow-Lowry, G. Mueller, A. W. Muir, A. Mukherjee, D. Mukherjee, S. Mukherjee, N. Mukund, A. Mullavey, J. Munch, E. A. Muñiz, M. Muratore, P. G. Murray, A. Nagar, K. Napier, I. Nardecchia, L. Naticchioni, R. K. Nayak, J. Neilson, G. Nelemans, T. J. N. Nelson, M. Nery, A. Neunzert,

L. Nevin, J. M. Newport, G. Newton, K. K. Y. Ng, P. Nguyen, T. T. Nguyen, D. Nichols, A. B. Nielsen, S. Nissanke, A. Nitz, A. Noack, F. Nocera, D. Nolting, C. North, L. K. Nuttall, J. Oberling, G. D. O'Dea, G. H. Ogin, J. J. Oh, S. H. Oh, F. Ohme, M. A. Okada, M. Oliver, P. Oppermann, R. J. Oram, B. O'Reilly, R. Ormiston, L. F. Ortega, R. O'Shaughnessy, S. Ossokine, D. J. Ottaway, H. Overmier, B. J. Owen, A. E. Pace, J. Page, M. A. Page, A. Pai, S. A. Pai, J. R. Palamos, O. Palashov, C. Palomba, A. Pal-Singh, H. Pan, H.-W. Pan, B. Pang, P. T. H. Pang, C. Pankow, F. Pannarale, B. C. Pant, F. Paoletti, A. Paoli, M. A. Papa, A. Parida, W. Parker, D. Pascucci, A. Pasqualetti, R. Passaquieti, D. Passuello, M. Patil, B. Patricelli, B. L. Pearlstone, M. Pedraza, R. Pedurand, L. Pekowsky, A. Pele, S. Penn, C. J. Perez, A. Perreca, L. M. Perri, H. P. Pfeiffer, M. Phelps, O. J. Piccinni, M. Pichot, F. Piergiovanni, V. Pierro, G. Pillant, L. Pinard, I. M. Pinto, M. Pirello, M. Pitkin, M. Poe, R. Poggiani, P. Popolizio, E. K. Porter, A. Post, J. Powell, J. Prasad, J. W. W. Pratt, G. Pratten, V. Predoi, T. Prestegard, M. Prijatelj, M. Principe, S. Privitera, R. Prix, G. A. Prodi, L. G. Prokhorov, O. Puncken, M. Punturo, P. Puppo, M. Pürrer, H. Qi, V. Quetschke, E. A. Quintero, R. Quitzow-James, F. J. Raab, D. S. Rabeling, H. Radkins, P. Raffai, S. Raja, C. Rajan, B. Rajbhandari, M. Rakhmanov, K. E. Ramirez, A. Ramos-Buades, P. Rapagnani, V. Raymond, M. Razzano, J. Read, T. Regimbau, L. Rei, S. Reid, D. H. Reitze, W. Ren, S. D. Reyes, F. Ricci, P. M. Ricker, S. Rieger, K. Riles, M. Rizzo, N. A. Robertson, R. Robie, F. Robinet, A. Rocchi, L. Rolland, J. G. Rollins, V. J. Roma, J. D. Romano, R. Romano, C. L. Romel, J. H. Romie, D. Rosińska, M. P. Ross, S. Rowan, A. Rüdiger, P. Ruggi, G. Rutins, K. Ryan, S. Sachdev, T. Sadecki, L. Sadeghian, M. Sakellariadou, L. Salconi, M. Saleem, F. Salemi, A. Samajdar, L. Sammut, L. M. Sampson, E. J. Sanchez, L. E. Sanchez, N. Sanchis-Gual, V. Sandberg, J. R. Sanders, B. Sassolas, B. S. Sathyaprakash, P. R. Saulson, O. Sauter, R. L. Savage, A. Sawadsky, P. Schale, M. Scheel, J. Scheuer, J. Schmidt, P. Schmidt, R. Schnabel, R. M. S. Schofield, A. Schönbeck, E. Schreiber, D. Schuette, B. W. Schulte, B. F. Schutz, S. G. Schwalbe, J. Scott, S. M. Scott, E. Seidel, D. Sellers, A. S. Sengupta, D. Sentenac, V. Sequino, A. Sergeev, D. A. Shaddock, T. J. Shaffer, A. A. Shah, M. S. Shahriar, M. B. Shaner, L. Shao, B. Shapiro, P. Shawhan, A. Sheperd, D. H. Shoemaker, D. M. Shoemaker, K. Siellez, X. Siemens, M. Sieniawska, D. Sigg, A. D. Silva, L. P. Singer, A. Singh, A. Singhal, A. M. Sintes, B. J. J. Slagmolen, B. Smith, J. R. Smith, R. J. E. Smith, S. Somala, E. J. Son, J. A. Sonnenberg, B. Sorazu, F. Sorrentino, T. Souradeep, A. P. Spencer, A. K.

Srivastava, K. Staats, A. Staley, M. Steinke, J. Steinlechner, S. Steinlechner, D. Steinmeyer, S. P. Stevenson, R. Stone, D. J. Stops, K. A. Strain, G. Stratta, S. E. Strigin, A. Strunk, R. Sturani, A. L. Stuver, T. Z. Summerscales, L. Sun, S. Sunil, J. Suresh, P. J. Sutton, B. L. Swinkels, M. J. Szczepańczyk, M. Tacca, S. C. Tait, C. Talbot, D. Talukder, D. B. Tanner, M. Tápai, A. Taracchini, J. D. Tasson, J. A. Taylor, R. Taylor, S. V. Tewari, T. Theeg, F. Thies, E. G. Thomas, M. Thomas, P. Thomas, K. A. Thorne, K. S. Thorne, E. Thrane, S. Tiwari, V. Tiwari, K. V. Tokmakov, K. Toland, M. Tonelli, Z. Tornasi, A. Torres-Forné, C. I. Torrie, D. Töyrä, F. Travasso, G. Traylor, J. Trinastic, M. C. Tringali, L. Trozzo, K. W. Tsang, M. Tse, R. Tso, L. Tsukada, D. Tsuna, D. Tuyenbayev, K. Ueno, D. Ugolini, C. S. Unnikrishnan, A. L. Urban, S. A. Usman, H. Vahlbruch, G. Vajente, G. Valdes, M. Vallisneri, N. van Bakel, M. van Beuzekom, J. F. J. van den Brand, C. Van Den Broeck, D. C. Vander-Hyde, L. van der Schaaf, J. V. van Heijningen, A. A. van Veggel, M. Vardaro, V. Varma, S. Vass, M. Vasúth, A. Vecchio, G. Vedovato, J. Veitch, P. J. Veitch, K. Venkateswara, G. Venugopalan, D. Verkindt, F. Vetrano, A. Viceré, A. D. Viets, S. Vinciguerra, D. J. Vine, J.-Y. Vinet, S. Vitale, T. Vo, H. Vocca, C. Vorvick, S. P. Vyatchanin, A. R. Wade, L. E. Wade, M. Wade, R. Walet, M. Walker, L. Wallace, S. Walsh, G. Wang, H. Wang, J. Z. Wang, W. H. Wang, Y. F. Wang, R. L. Ward, J. Warner, M. Was, J. Watchi, B. Weaver, L.-W. Wei, M. Weinert, A. J. Weinstein, R. Weiss, L. Wen, E. K. Wessel, P. Weßels, J. Westerweck, T. Westphal, K. Wette, J. T. Whelan, S. E. Whitcomb, B. F. Whiting, C. Whittle, D. Wilken, D. Williams, R. D. Williams, A. R. Williamson, J. L. Willis, B. Willke, M. H. Wimmer, W. Winkler, C. C. Wipf, H. Wittel, G. Woan, J. Woehler, J. Wofford, K. W. K. Wong, J. Worden, J. L. Wright, D. S. Wu, D. M. Wysocki, S. Xiao, H. Yamamoto, C. C. Yancey, L. Yang, M. J. Yap, M. Yazback, H. Yu, H. Yu, M. Yvert, A. Zadrożny, M. Zanolin, T. Zelenova, J.-P. Zendri, M. Zevin, L. Zhang, M. Zhang, T. Zhang, Y.-H. Zhang, C. Zhao, M. Zhou, Z. Zhou, S. J. Zhu, X. J. Zhu, A. B. Zimmerman, M. E. Zucker, and J. Zweizig, "GW170817: Observation of Gravitational Waves from a Binary Neutron Star Inspiral," *Physical Review Letters*, vol. 119, no. 16, p. 161101, Oct. 2017. [Online]. Available: https://link.aps.org/doi/10.1103/PhysRevLett.119.161101

[80] LIGO Scientific Collaboration and Virgo Collaboration, B. P. Abbott, R. Abbott, T. D. Abbott, S. Abraham, F. Acernese, K. Ackley, C. Adams, R. X. Adhikari, V. B. Adya, C. Affeldt, M. Agathos, K. Agatsuma, N. Aggarwal, O. D. Aguiar, L. Aiello, A. Ain, P. Ajith, G. Allen, A. Allocca,

M. A. Aloy, P. A. Altin, A. Amato, A. Ananyeva, S. B. Anderson, W. G. Anderson, S. V. Angelova, S. Antier, S. Appert, K. Arai, M. C. Araya, J. S. Areeda, M. Arène, N. Arnaud, K. G. Arun, S. Ascenzi, G. Ashton, S. M. Aston, P. Astone, F. Aubin, P. Aufmuth, K. AultONeal, C. Austin, V. Avendano, A. Avila-Alvarez, S. Babak, P. Bacon, F. Badaracco, M. K. M. Bader, S. Bae, P. T. Baker, F. Baldaccini, G. Ballardin, S. W. Ballmer, S. Banagiri, J. C. Barayoga, S. E. Barclay, B. C. Barish, D. Barker, K. Barkett, S. Barnum, F. Barone, B. Barr, L. Barsotti, M. Barsuglia, D. Barta, J. Bartlett, I. Bartos, R. Bassiri, A. Basti, M. Bawaj, J. C. Bayley, M. Bazzan, B. Bécsy, M. Bejger, I. Belahcene, A. S. Bell, D. Beniwal, B. K. Berger, G. Bergmann, S. Bernuzzi, J. J. Bero, C. P. L. Berry, D. Bersanetti, A. Bertolini, J. Betzwieser, R. Bhandare, J. Bidler, I. A. Bilenko, S. A. Bilgili, G. Billingsley, J. Birch, R. Birney, O. Birnholtz, S. Biscans, S. Biscoveanu, A. Bisht, M. Bitossi, M. A. Bizouard, J. K. Blackburn, J. Blackman, C. D. Blair, D. G. Blair, R. M. Blair, S. Bloemen, N. Bode, M. Boer, Y. Boetzel, G. Bogaert, F. Bondu, E. Bonilla, R. Bonnand, P. Booker, B. A. Boom, C. D. Booth, R. Bork, V. Boschi, S. Bose, K. Bossie, V. Bossilkov, J. Bosveld, Y. Bouffanais, A. Bozzi, C. Bradaschia, P. R. Brady, A. Bramley, M. Branchesi, J. E. Brau, T. Briant, J. H. Briggs, F. Brighenti, A. Brillet, M. Brinkmann, V. Brisson, P. Brockill, A. F. Brooks, D. D. Brown, S. Brunett, A. Buikema, T. Bulik, H. J. Bulten, A. Buonanno, D. Buskulic, M. J. Bustamante Rosell, C. Buy, R. L. Byer, M. Cabero, L. Cadonati, G. Cagnoli, C. Cahillane, J. Calderón Bustillo, T. A. Callister, E. Calloni, J. B. Camp, W. A. Campbell, M. Canepa, K. C. Cannon, H. Cao, J. Cao, E. Capocasa, F. Carbognani, S. Caride, M. F. Carney, G. Carullo, J. Casanueva Diaz, C. Casentini, S. Caudill, M. Cavaglià, F. Cavalier, R. Cavalieri, G. Cella, P. Cerdá-Durán, G. Cerretani, E. Cesarini, O. Chaibi, K. Chakravarti, S. J. Chamberlin, M. Chan, S. Chao, P. Charlton, E. A. Chase, E. Chassande-Mottin, D. Chatterjee, M. Chaturvedi, K. Chatziioannou, B. D. Cheeseboro, H. Y. Chen, X. Chen, Y. Chen, H.-P. Cheng, C. K. Cheong, H. Y. Chia, A. Chincarini, A. Chiummo, G. Cho, H. S. Cho, M. Cho, N. Christensen, Q. Chu, S. Chua, K. W. Chung, S. Chung, G. Ciani, A. A. Ciobanu, R. Ciolfi, F. Cipriano, A. Cirone, F. Clara, J. A. Clark, P. Clearwater, F. Cleva, C. Cocchieri, E. Coccia, P.-F. Cohadon, D. Cohen, R. Colgan, M. Colleoni, C. G. Collette, C. Collins, L. R. Cominsky, M. Constancio, L. Conti, S. J. Cooper, P. Corban, T. R. Corbitt, I. Cordero-Carrión, K. R. Corley, N. Cornish, A. Corsi, S. Cortese, C. A. Costa, R. Cotesta, M. W. Coughlin, S. B. Coughlin, J.-P. Coulon, S. T. Countryman, P. Couvares, P. B. Covas, E. E. Cowan, D. M. Coward, M. J. Cowart, D. C. Coyne,

164

R. Coyne, J. D. E. Creighton, T. D. Creighton, J. Cripe, M. Croquette, S. G. Crowder, T. J. Cullen, A. Cumming, L. Cunningham, E. Cuoco, T. D. Canton, G. Dálya, S. L. Danilishin, S. D'Antonio, K. Danzmann, A. Dasgupta, C. F. Da Silva Costa, L. E. H. Datrier, V. Dattilo, I. Dave, M. Davier, D. Davis, E. J. Daw, D. DeBra, M. Deenadayalan, J. Degallaix, M. De Laurentis, S. Deléglise, W. Del Pozzo, L. M. DeMarchi, N. Demos, T. Dent, R. De Pietri, J. Derby, R. De Rosa, C. De Rossi, R. DeSalvo, O. de Varona, S. Dhurandhar, M. C. Díaz, T. Dietrich, L. Di Fiore, M. Di Giovanni, T. Di Girolamo, A. Di Lieto, B. Ding, S. Di Pace, I. Di Palma, F. Di Renzo, A. Dmitriev, Z. Doctor, F. Donovan, K. L. Dooley, S. Doravari, I. Dorrington, T. P. Downes, M. Drago, J. C. Driggers, Z. Du, J.-G. Ducoin, P. Dupej, S. E. Dwyer, P. J. Easter, T. B. Edo, M. C. Edwards, A. Effler, P. Ehrens, J. Eichholz, S. S. Eikenberry, M. Eisenmann, R. A. Eisenstein, R. C. Essick, H. Estelles, D. Estevez, Z. B. Etienne, T. Etzel, M. Evans, T. M. Evans, V. Fafone, H. Fair, S. Fairhurst, X. Fan, S. Farinon, B. Farr, W. M. Farr, E. J. Fauchon-Jones, M. Favata, M. Fays, M. Fazio, C. Fee, J. Feicht, M. M. Fejer, F. Feng, A. Fernandez-Galiana, I. Ferrante, E. C. Ferreira, T. A. Ferreira, F. Ferrini, F. Fidecaro, I. Fiori, D. Fiorucci, M. Fishbach, R. P. Fisher, J. M. Fishner, M. Fitz-Axen, R. Flaminio, M. Fletcher, E. Flynn, H. Fong, J. A. Font, P. W. F. Forsyth, J.-D. Fournier, S. Frasca, F. Frasconi, Z. Frei, A. Freise, R. Frey, V. Frey, P. Fritschel, V. V. Frolov, P. Fulda, M. Fyffe, H. A. Gabbard, B. U. Gadre, S. M. Gaebel, J. R. Gair, L. Gammaitoni, M. R. Ganija, S. G. Gaonkar, A. Garcia, C. García-Quirós, F. Garufi, B. Gateley, S. Gaudio, G. Gaur, V. Gayathri, G. Gemme, E. Genin, A. Gennai, D. George, J. George, L. Gergely, V. Germain, S. Ghonge, A. Ghosh, A. Ghosh, S. Ghosh, B. Giacomazzo, J. A. Giaime, K. D. Giardina, A. Giazotto, K. Gill, G. Giordano, L. Glover, P. Godwin, E. Goetz, R. Goetz, B. Goncharov, G. González, J. M. Gonzalez Castro, A. Gopakumar, M. L. Gorodetsky, S. E. Gossan, M. Gosselin, R. Gouaty, A. Grado, C. Graef, M. Granata, A. Grant, S. Gras, P. Grassia, C. Gray, R. Gray, G. Greco, A. C. Green, R. Green, E. M. Gretarsson, P. Groot, H. Grote, S. Grunewald, P. Gruning, G. M. Guidi, H. K. Gulati, Y. Guo, A. Gupta, M. K. Gupta, E. K. Gustafson, R. Gustafson, L. Haegel, O. Halim, B. R. Hall, E. D. Hall, E. Z. Hamilton, G. Hammond, M. Haney, M. M. Hanke, J. Hanks, C. Hanna, M. D. Hannam, O. A. Hannuksela, J. Hanson, T. Hardwick, K. Haris, J. Harms, G. M. Harry, I. W. Harry, C.-J. Haster, K. Haughian, F. J. Hayes, J. Healy, A. Heidmann, M. C. Heintze, H. Heitmann, P. Hello, G. Hemming, M. Hendry, I. S. Heng, J. Hennig, A. W. Heptonstall, F. Hernandez Vivanco, M. Heurs, S. Hild,

165

T. Hinderer, D. Hoak, S. Hochheim, D. Hofman, A. M. Holgado, N. A. Holland, K. Holt, D. E. Holz, P. Hopkins, C. Horst, J. Hough, E. J. Howell, C. G. Hoy, A. Hreibi, Y. Huang, E. A. Huerta, D. Huet, B. Hughey, M. Hulko, S. Husa, S. H. Huttner, T. Huynh-Dinh, B. Idzkowski, A. Iess, C. Ingram, R. Inta, G. Intini, B. Irwin, H. N. Isa, J.-M. Isac, M. Isi, B. R. Iyer, K. Izumi, T. Jacqmin, S. J. Jadhav, K. Jani, N. N. Janthalur, P. Jaranowski, A. C. Jenkins, J. Jiang, D. S. Johnson, N. K. Johnson-McDaniel, A. W. Jones, D. I. Jones, R. Jones, R. J. G. Jonker, L. Ju, J. Junker, C. V. Kalaghatgi, V. Kalogera, B. Kamai, S. Kandhasamy, G. Kang, J. B. Kanner, S. J. Kapadia, S. Karki, K. S. Karvinen, R. Kashyap, M. Kasprzack, S. Katsanevas, E. Katsavounidis, W. Katzman, S. Kaufer, K. Kawabe, N. V. Keerthana, F. Kéfélian, D. Keitel, R. Kennedy, J. S. Key, F. Y. Khalili, H. Khan, I. Khan, S. Khan, Z. Khan, E. A. Khazanov, M. Khursheed, N. Kijbunchoo, C. Kim, J. C. Kim, K. Kim, W. Kim, W. S. Kim, Y.-M. Kim, C. Kimball, E. J. King, P. J. King, M. Kinley-Hanlon, R. Kirchhoff, J. S. Kissel, L. Kleybolte, J. H. Klika, S. Klimenko, T. D. Knowles, P. Koch, S. M. Koehlenbeck, G. Koekoek, S. Koley, V. Kondrashov, A. Kontos, N. Koper, M. Korobko, W. Z. Korth, I. Kowalska, D. B. Kozak, V. Kringel, N. Krishnendu, A. Królak, G. Kuehn, A. Kumar, P. Kumar, R. Kumar, S. Kumar, L. Kuo, A. Kutynia, S. Kwang, B. D. Lackey, K. H. Lai, T. L. Lam, M. Landry, B. B. Lane, R. N. Lang, J. Lange, B. Lantz, R. K. Lanza, A. Lartaux-Vollard, P. D. Lasky, M. Laxen, A. Lazzarini, C. Lazzaro, P. Leaci, S. Leavey, Y. K. Lecoeuche, C. H. Lee, H. K. Lee, H. M. Lee, H. W. Lee, J. Lee, K. Lee, J. Lehmann, A. Lenon, N. Leroy, N. Letendre, Y. Levin, J. Li, K. J. L. Li, T. G. F. Li, X. Li, F. Lin, F. Linde, S. D. Linker, T. B. Littenberg, J. Liu, X. Liu, R. K. L. Lo, N. A. Lockerbie, L. T. London, A. Longo, M. Lorenzini, V. Loriette, M. Lormand, G. Losurdo, J. D. Lough, C. O. Lousto, G. Lovelace, M. E. Lower, H. Lück, D. Lumaca, A. P. Lundgren, R. Lynch, Y. Ma, R. Macas, S. Macfoy, M. MacInnis, D. M. Macleod, A. Macquet, F. Magaña-Sandoval, L. Magaña Zertuche, R. M. Magee, E. Majorana, I. Maksimovic, A. Malik, N. Man, V. Mandic, V. Mangano, G. L. Mansell, M. Manske, M. Mantovani, F. Marchesoni, F. Marion, S. Márka, Z. Márka, C. Markakis, A. S. Markosyan, A. Markowitz, E. Maros, A. Marquina, S. Marsat, F. Martelli, I. W. Martin, R. M. Martin, D. V. Martynov, K. Mason, E. Massera, A. Masserot, T. J. Massinger, M. Masso-Reid, S. Mastrogiovanni, A. Matas, F. Matichard, L. Matone, N. Mavalvala, N. Mazumder, J. J. McCann, R. McCarthy, D. E. McClelland, S. McCormick, L. McCuller, S. C. McGuire, J. McIver, D. J. McManus, T. McRae, S. T. McWilliams, D. Meacher, G. D. Meadors,

M. Mehmet, A. K. Mehta, J. Meidam, A. Melatos, G. Mendell, R. A. Mercer, L. Mereni, E. L. Merilh, M. Merzougui, S. Meshkov, C. Messenger, C. Messick, R. Metzdorff, P. M. Meyers, H. Miao, C. Michel, H. Middleton, E. E. Mikhailov, L. Milano, A. L. Miller, A. Miller, M. Millhouse, J. C. Mills, M. C. Milovich-Goff, O. Minazzoli, Y. Minenkov, A. Mishkin, C. Mishra, T. Mistry, S. Mitra, V. P. Mitrofanov, G. Mitselmakher, R. Mittleman, G. Mo, D. Moffa, K. Mogushi, S. R. P. Mohapatra, M. Montani, C. J. Moore, D. Moraru, G. Moreno, S. Morisaki, B. Mours, C. M. Mow-Lowry, A. Mukherjee, D. Mukherjee, S. Mukherjee, N. Mukund, A. Mullavey, J. Munch, E. A. Muñiz, M. Muratore, P. G. Murray, A. Nagar, I. Nardecchia, L. Naticchioni, R. K. Nayak, J. Neilson, G. Nelemans, T. J. N. Nelson, M. Nery, A. Neunzert, K. Y. Ng, S. Ng, P. Nguyen, D. Nichols, A. B. Nielsen, S. Nissanke, A. Nitz, F. Nocera, C. North, L. K. Nuttall, M. Obergaulinger, J. Oberling, B. D. O'Brien, G. D. O'Dea, G. H. Ogin, J. J. Oh, S. H. Oh, F. Ohme, H. Ohta, M. A. Okada, M. Oliver, P. Oppermann, R. J. Oram, B. O'Reilly, R. G. Ormiston, L. F. Ortega, R. O'Shaughnessy, S. Ossokine, D. J. Ottaway, H. Overmier, B. J. Owen, A. E. Pace, G. Pagano, M. A. Page, A. Pai, S. A. Pai, J. R. Palamos, O. Palashov, C. Palomba, A. Pal-Singh, H.-W. Pan, B. Pang, P. T. H. Pang, C. Pankow, F. Pannarale, B. C. Pant, F. Paoletti, A. Paoli, M. A. Papa, A. Parida, W. Parker, D. Pascucci, A. Pasqualetti, R. Passaquieti, D. Passuello, M. Patil, B. Patricelli, B. L. Pearlstone, C. Pedersen, M. Pedraza, R. Pedurand, A. Pele, S. Penn, A. Perego, C. J. Perez, A. Perreca, H. P. Pfeiffer, M. Phelps, K. S. Phukon, O. J. Piccinni, M. Pichot, F. Piergiovanni, G. Pillant, L. Pinard, M. Pirello, M. Pitkin, R. Poggiani, D. Y. T. Pong, S. Ponrathnam, P. Popolizio, E. K. Porter, J. Powell, A. K. Prajapati, J. Prasad, K. Prasai, R. Prasanna, G. Pratten, T. Prestegard, S. Privitera, G. A. Prodi, L. G. Prokhorov, O. Puncken, M. Punturo, P. Puppo, M. Pürrer, H. Qi, V. Quetschke, P. J. Quinonez, E. A. Quintero, R. Quitzow-James, F. J. Raab, H. Radkins, N. Radulescu, P. Raffai, S. Raja, C. Rajan, B. Rajbhandari, M. Rakhmanov, K. E. Ramirez, A. Ramos-Buades, J. Rana, K. Rao, P. Rapagnani, V. Raymond, M. Razzano, J. Read, T. Regimbau, L. Rei, S. Reid, D. H. Reitze, W. Ren, F. Ricci, C. J. Richardson, J. W. Richardson, P. M. Ricker, G. M. Riemenschneider, K. Riles, M. Rizzo, N. A. Robertson, R. Robie, F. Robinet, A. Rocchi, L. Rolland, J. G. Rollins, V. J. Roma, M. Romanelli, R. Romano, C. L. Romel, J. H. Romie, K. Rose, D. Rosińska, S. G. Rosofsky, M. P. Ross, S. Rowan, A. Rüdiger, P. Ruggi, G. Rutins, K. Ryan, S. Sachdev, T. Sadecki, M. Sakellariadou, O. Salafia, L. Salconi, M. Saleem, F. Salemi, A. Samajdar,

L. Sammut, E. J. Sanchez, L. E. Sanchez, N. Sanchis-Gual, V. Sandberg, J. R. Sanders, K. A. Santiago, N. Sarin, B. Sassolas, B. S. Sathyaprakash, P. R. Saulson, O. Sauter, R. L. Savage, P. Schale, M. Scheel, J. Scheuer, P. Schmidt, R. Schnabel, R. M. S. Schofield, A. Schönbeck, E. Schreiber, B. W. Schulte, B. F. Schutz, S. G. Schwalbe, J. Scott, S. M. Scott, E. Seidel, D. Sellers, A. S. Sengupta, N. Sennett, D. Sentenac, V. Sequino, A. Sergeev, Y. Setyawati, D. A. Shaddock, T. Shaffer, M. S. Shahriar, M. B. Shaner, L. Shao, P. Sharma, P. Shawhan, H. Shen, R. Shink, D. H. Shoemaker, D. M. Shoemaker, S. ShyamSundar, K. Siellez, M. Sieniawska, D. Sigg, A. D. Silva, L. P. Singer, N. Singh, A. Singhal, A. M. Sintes, S. Sitmukhambetov, V. Skliris, B. J. J. Slagmolen, T. J. Slaven-Blair, J. R. Smith, R. J. E. Smith, S. Somala, E. J. Son, B. Sorazu, F. Sorrentino, T. Souradeep, E. Sowell, A. P. Spencer, A. K. Srivastava, V. Srivastava, K. Staats, C. Stachie, M. Standke, D. A. Steer, M. Steinke, J. Steinlechner, S. Steinlechner, D. Steinmeyer, S. P. Stevenson, D. Stocks, R. Stone, D. J. Stops, K. A. Strain, G. Stratta, S. E. Strigin, A. Strunk, R. Sturani, A. L. Stuver, V. Sudhir, T. Z. Summerscales, L. Sun, S. Sunil, J. Suresh, P. J. Sutton, B. L. Swinkels, M. J. Szczepańczyk, M. Tacca, S. C. Tait, C. Talbot, D. Talukder, D. B. Tanner, M. Tápai, A. Taracchini, J. D. Tasson, R. Taylor, F. Thies, M. Thomas, P. Thomas, S. R. Thondapu, K. A. Thorne, E. Thrane, S. Tiwari, S. Tiwari, V. Tiwari, K. Toland, M. Tonelli, Z. Tornasi, A. Torres-Forné, C. I. Torrie, D. Töyrä, F. Travasso, G. Traylor, M. C. Tringali, A. Trovato, L. Trozzo, R. Trudeau, K. W. Tsang, M. Tse, R. Tso, L. Tsukada, D. Tsuna, D. Tuyenbayev, K. Ueno, D. Ugolini, C. S. Unnikrishnan, A. L. Urban, S. A. Usman, H. Vahlbruch, G. Vajente, G. Valdes, N. van Bakel, M. van Beuzekom, J. F. J. van den Brand, C. Van Den Broeck, D. C. Vander-Hyde, J. V. van Heijningen, L. van der Schaaf, A. A. van Veggel, M. Vardaro, V. Varma, S. Vass, M. Vasúth, A. Vecchio, G. Vedovato, J. Veitch, P. J. Veitch, K. Venkateswara, G. Venugopalan, D. Verkindt, F. Vetrano, A. Viceré, A. D. Viets, D. J. Vine, J.-Y. Vinet, S. Vitale, T. Vo, H. Vocca, C. Vorvick, S. P. Vyatchanin, A. R. Wade, L. E. Wade, M. Wade, R. Walet, M. Walker, L. Wallace, S. Walsh, G. Wang, H. Wang, J. Z. Wang, W. H. Wang, Y. F. Wang, R. L. Ward, Z. A. Warden, J. Warner, M. Was, J. Watchi, B. Weaver, L.-W. Wei, M. Weinert, A. J. Weinstein, R. Weiss, F. Wellmann, L. Wen, E. K. Wessel, P. Weßels, J. W. Westhouse, K. Wette, J. T. Whelan, L. V. White, B. F. Whiting, C. Whittle, D. M. Wilken, D. Williams, A. R. Williamson, J. L. Willis, B. Willke, M. H. Wimmer, W. Winkler, C. C. Wipf, H. Wittel, G. Woan, J. Woehler, J. K. Wofford, J. Worden, J. L. Wright, D. S. Wu, D. M. Wysocki,

168

L. Xiao, H. Yamamoto, C. C. Yancey, L. Yang, M. J. Yap, M. Yazback, D. W. Yeeles, H. Yu, H. Yu, S. H. R. Yuen, M. Yvert, A. K. Zadrożny, M. Zanolin, F. Zappa, T. Zelenova, J.-P. Zendri, M. Zevin, J. Zhang, L. Zhang, T. Zhang, C. Zhao, M. Zhou, Z. Zhou, X. J. Zhu, A. B. Zimmerman, Y. Zlochower, M. E. Zucker, and J. Zweizig, "GWTC-1: A Gravitational-Wave Transient Catalog of Compact Binary Mergers Observed by LIGO and Virgo during the First and Second Observing Runs," *Physical Review X*, vol. 9, no. 3, p. 031040, Sep. 2019. [Online]. Available: https://link.aps.org/doi/10.1103/PhysRevX.9.031040

[81] T. L. S. Collaboration, J. Aasi, B. P. Abbott, R. Abbott, T. Abbott, M. R. Abernathy, K. Ackley, C. Adams, T. Adams, P. Addesso, R. X. Adhikari, V. Adya, C. Affeldt, N. Aggarwal, O. D. Aguiar, A. Ain, P. Ajith, A. Alemic, B. Allen, D. Amariutei, S. B. Anderson, W. G. Anderson, K. Arai, M. C. Araya, C. Arceneaux, J. S. Areeda, G. Ashton, S. Ast, S. M. Aston, P. Aufmuth, C. Aulbert, B. E. Aylott, S. Babak, P. T. Baker, S. W. Ballmer, J. C. Barayoga, M. Barbet, S. Barclay, B. C. Barish, D. Barker, B. Barr, L. Barsotti, J. Bartlett, M. A. Barton, I. Bartos, R. Bassiri, J. C. Batch, C. Baune, B. Behnke, A. S. Bell, C. Bell, M. Benacquista, J. Bergman, G. Bergmann, C. P. L. Berry, J. Betzwieser, S. Bhagwat, R. Bhandare, I. A. Bilenko, G. Billingsley, J. Birch, S. Biscans, C. Biwer, J. K. Blackburn, L. Blackburn, C. D. Blair, D. Blair, O. Bock, T. P. Bodiya, P. Bojtos, C. Bond, R. Bork, M. Born, S. Bose, P. R. Brady, V. B. Braginsky, J. E. Brau, D. O. Bridges, M. Brinkmann, A. F. Brooks, D. A. Brown, D. D. Brown, N. M. Brown, S. Buchman, A. Buikema, A. Buonanno, L. Cadonati, J. C. Bustillo, J. B. Camp, K. C. Cannon, J. Cao, C. D. Capano, S. Caride, S. Caudill, M. Cavaglià, C. Cepeda, R. Chakraborty, T. Chalermsongsak, S. J. Chamberlin, S. Chao, P. Charlton, Y. Chen, H. S. Cho, M. Cho, J. H. Chow, N. Christensen, Q. Chu, S. Chung, G. Ciani, F. Clara, J. A. Clark, C. Collette, L. Cominsky, M. Constancio, D. Cook, T. R. Corbitt, N. Cornish, A. Corsi, C. A. Costa, M. W. Coughlin, S. Countryman, P. Couvares, D. M. Coward, M. J. Cowart, D. C. Coyne, R. Coyne, K. Craig, J. D. E. Creighton, T. D. Creighton, J. Cripe, S. G. Crowder, A. Cumming, L. Cunningham, C. Cutler, K. Dahl, T. D. Canton, M. Damjanic, S. L. Danilishin, K. Danzmann, L. Dartez, I. Dave, H. Daveloza, G. S. Davies, E. J. Daw, D. DeBra, W. D. Pozzo, T. Denker, T. Dent, V. Dergachev, R. T. DeRosa, R. DeSalvo, S. Dhurandhar, M. D´ıaz, I. D. Palma, G. Dojcinoski, E. Dominguez, F. Donovan, K. L. Dooley, S. Doravari, R. Douglas, T. P. Downes, J. C. Driggers, Z. Du, S. Dwyer, T. Eberle, T. Edo, M. Edwards, M. Edwards, A. Effler, H.-B. Eggenstein,

P. Ehrens, J. Eichholz, S. S. Eikenberry, R. Essick, T. Etzel, M. Evans, T. Evans, M. Factourovich, S. Fairhurst, X. Fan, Q. Fang, B. Farr, W. M. Farr, M. Favata, M. Fays, H. Fehrmann, M. M. Fejer, D. Feldbaum, E. C. Ferreira, R. P. Fisher, Z. Frei, A. Freise, R. Frey, T. T. Fricke, P. Fritschel, V. V. Frolov, S. Fuentes-Tapia, P. Fulda, M. Fyffe, J. R. Gair, S. Gaonkar, N. Gehrels, L. Á. Gergely´, J. A. Giaime, K. D. Giardina, J. Gleason, E. Goetz, R. Goetz, L. Gondan, G. González, N. Gordon, M. L. Gorodetsky, S. Gossan, S. Goßler, C. Gräf, P. B. Graff, A. Grant, S. Gras, C. Gray, R. J. S. Greenhalgh, A. M. Gretarsson, H. Grote, S. Grunewald, C. J. Guido, X. Guo, K. Gushwa, E. K. Gustafson, R. Gustafson, J. Hacker, E. D. Hall, G. Hammond, M. Hanke, J. Hanks, C. Hanna, M. D. Hannam, J. Hanson, T. Hardwick, G. M. Harry, I. W. Harry, M. Hart, M. T. Hartman, C.-J. Haster, K. Haughian, S. Hee, M. Heintze, G. Heinzel, M. Hendry, I. S. Heng, A. W. Heptonstall, M. Heurs, M. Hewitson, S. Hild, D. Hoak, K. A. Hodge, S. E. Hollitt, K. Holt, P. Hopkins, D. J. Hosken, J. Hough, E. Houston, E. J. Howell, Y. M. Hu, E. Huerta, B. Hughey, S. Husa, S. H. Huttner, M. Huynh, T. Huynh-Dinh, A. Idrisy, N. Indik, D. R. Ingram, R. Inta, G. Islas, J. C. Isler, T. Isogai, B. R. Iyer, K. Izumi, M. Jacobson, H. Jang, S. Jawahar, Y. Ji, F. Jiménez-Forteza, W. W. Johnson, D. I. Jones, R. Jones, L. Ju, K. Haris, V. Kalogera, S. Kandhasamy, G. Kang, J. B. Kanner, E. Katsavounidis, W. Katzman, H. Kaufer, S. Kaufer, T. Kaur, K. Kawabe, F. Kawazoe, G. M. Keiser, D. Keitel, D. B. Kelley, W. Kells, D. G. Keppel, J. S. Key, A. Khalaidovski, F. Y. Khalili, E. A. Khazanov, C. Kim, K. Kim, N. G. Kim, N. Kim, Y.-M. Kim, E. J. King, P. J. King, D. L. Kinzel, J. S. Kissel, S. Klimenko, J. Kline, S. Koehlenbeck, K. Kokeyama, V. Kondrashov, M. Korobko, W. Z. Korth, D. B. Kozak, V. Kringel, B. Krishnan, C. Krueger, G. Kuehn, A. Kumar, P. Kumar, L. Kuo, M. Landry, B. Lantz, S. Larson, P. D. Lasky, A. Lazzarini, C. Lazzaro, J. Le, P. Leaci, S. Leavey, E. O. Lebigot, C. H. Lee, H. K. Lee, H. M. Lee, J. R. Leong, Y. Levin, B. Levine, J. Lewis, T. G. F. Li, K. Libbrecht, A. Libson, A. C. Lin, T. B. Littenberg, N. A. Lockerbie, V. Lockett, J. Logue, A. L. Lombardi, M. Lormand, J. Lough, M. J. Lubinski, H. Lück, A. P. Lundgren, R. Lynch, Y. Ma, J. Macarthur, T. MacDonald, B. Machenschalk, M. MacInnis, D. M. Macleod, F. Magaña-Sandoval, R. Magee, M. Mageswaran, C. Maglione, K. Mailand, I. Mandel, V. Mandic, V. Mangano, G. L. Mansell, S. Márka, Z. Márka, A. Markosyan, E. Maros, I. W. Martin, R. M. Martin, D. Martynov, J. N. Marx, K. Mason, T. J. Massinger, F. Matichard, L. Matone, N. Mavalvala, N. Mazumder, G. Mazzolo, R. McCarthy, D. E. McClelland, S. McCormick, S. C. McGuire, G. McIntyre, J. McIver, K. McLin,

S. McWilliams, G. D. Meadors, M. Meinders, A. Melatos, G. Mendell, R. A. Mercer, S. Meshkov, C. Messenger, P. M. Meyers, H. Miao, H. Middleton, E. E. Mikhailov, A. Miller, J. Miller, M. Millhouse, J. Ming, S. Mirshekari, C. Mishra, S. Mitra, V. P. Mitrofanov, G. Mitselmakher, R. Mittleman, B. Moe, S. D. Mohanty, S. R. P. Mohapatra, B. Moore, D. Moraru, G. Moreno, S. R. Morriss, K. Mossavi, C. M. Mow-Lowry, C. L. Mueller, G. Mueller, S. Mukherjee, A. Mullavey, J. Munch, D. Murphy, P. G. Murray, A. Mytidis, T. Nash, R. K. Nayak, V. Necula, K. Nedkova, G. Newton, T. Nguyen, A. B. Nielsen, S. Nissanke, A. H. Nitz, D. Nolting, M. E. N. Normandin, L. K. Nuttall, E. Ochsner, J. O'Dell, E. Oelker, G. H. Ogin, J. J. Oh, S. H. Oh, F. Ohme, P. Oppermann, R. Oram, B. O'Reilly, W. Ortega, R. O'Shaughnessy, C. Osthelder, C. D. Ott, D. J. Ottaway, R. S. Ottens, H. Overmier, B. J. Owen, C. Padilla, A. Pai, S. Pai, O. Palashov, A. Pal-Singh, H. Pan, C. Pankow, F. Pannarale, B. C. Pant, M. A. Papa, H. Paris, Z. Patrick, M. Pedraza, L. Pekowsky, A. Pele, S. Penn, A. Perreca, M. Phelps, V. Pierro, I. M. Pinto, M. Pitkin, J. Poeld, A. Post, A. Poteomkin, J. Powell, J. Prasad, V. Predoi, S. Premachandra, T. Prestegard, L. R. Price, M. Principe, S. Privitera, R. Prix, L. Prokhorov, O. Puncken, M. Pürrer, J. Qin, V. Quetschke, E. Quintero, G. Quiroga, R. Quitzow-James, F. J. Raab, D. S. Rabeling, H. Radkins, P. Raffai, S. Raja, G. Rajalakshmi, M. Rakhmanov, K. Ramirez, V. Raymond, C. M. Reed, S. Reid, D. H. Reitze, O. Reula, K. Riles, N. A. Robertson, R. Robie, J. G. Rollins, V. Roma, J. D. Romano, G. Romanov, J. H. Romie, S. Rowan, A. Rüdiger, K. Ryan, S. Sachdev, T. Sadecki, L. Sadeghian, M. Saleem, F. Salemi, L. Sammut, V. Sandberg, J. R. Sanders, V. Sannibale, I. Santiago-Prieto, B. S. Sathyaprakash, P. R. Saulson, R. Savage, A. Sawadsky, J. Scheuer, R. Schilling, P. Schmidt, R. Schnabel, R. M. S. Schofield, E. Schreiber, D. Schuette, B. F. Schutz, J. Scott, S. M. Scott, D. Sellers, A. S. Sengupta, A. Sergeev, G. Serna, A. Sevigny, D. A. Shaddock, M. S. Shahriar, M. Shaltev, Z. Shao, B. Shapiro, P. Shawhan, D. H. Shoemaker, T. L. Sidery, X. Siemens, D. Sigg, A. D. Silva, D. Simakov, A. Singer, L. Singer, R. Singh, A. M. Sintes, B. J. J. Slagmolen, J. R. Smith, M. R. Smith, R. J. E. Smith, N. D. Smith-Lefebvre, E. J. Son, B. Sorazu, T. Souradeep, A. Staley, J. Stebbins, M. Steinke, J. Steinlechner, S. Steinlechner, D. Steinmeyer, B. C. Stephens, S. Steplewski, S. Stevenson, R. Stone, K. A. Strain, S. Strigin, R. Sturani, A. L. Stuver, T. Z. Summerscales, P. J. Sutton, M. Szczepanczyk, G. Szeifert, D. Talukder, D. B. Tanner, M. Tápai, S. P. Tarabrin, A. Taracchini, R. Taylor, G. Tellez, T. Theeg, M. P. Thirugnanasambandam, M. Thomas, P. Thomas, K. A. Thorne, K. S. Thorne, E. Thrane, V. Tiwari, C. Tomlinson,

C. V. Torres, C. I. Torrie, G. Traylor, M. Tse, D. Tshilumba, D. Ugolini, C. S. Unnikrishnan, A. L. Urban, S. A. Usman, H. Vahlbruch, G. Vajente, G. Valdes, M. Vallisneri, A. A. van Veggel, S. Vass, R. Vaulin, A. Vecchio, J. Veitch, P. J. Veitch, K. Venkateswara, R. Vincent-Finley, S. Vitale, T. Vo, C. Vorvick, W. D. Vousden, S. P. Vyatchanin, A. R. Wade, L. Wade, M. Wade, M. Walker, L. Wallace, S. Walsh, H. Wang, M. Wang, X. Wang, R. L. Ward, J. Warner, M. Was, B. Weaver, M. Weinert, A. J. Weinstein, R. Weiss, T. Welborn, L. Wen, P. Wessels, T. Westphal, K. Wette, J. T. Whelan, S. E. Whitcomb, D. J. White, B. F. Whiting, C. Wilkinson, L. Williams, R. Williams, A. R. Williamson, J. L. Willis, B. Willke, M. Wimmer, W. Winkler, C. C. Wipf, H. Wittel, G. Woan, J. Worden, S. Xie, J. Yablon, I. Yakushin, W. Yam, H. Yamamoto, C. C. Yancey, Q. Yang, M. Zanolin, F. Zhang, L. Zhang, M. Zhang, Y. Zhang, C. Zhao, M. Zhou, X. J. Zhu, M. E. Zucker, S. Zuraw, and J. Zweizig, "Advanced LIGO," *Classical and Quantum Gravity*, vol. 32, no. 7, p. 074001, Mar. 2015. [Online]. Available: https://dx.doi.org/10.1088/0264-9381/32/7/074001

[82] F. Acernese, M. Agathos, K. Agatsuma, D. Aisa, N. Allemandou, A. Allocca, J. Amarni, P. Astone, G. Balestri, G. Ballardin, F. Barone, J.-P. Baronick, M. Barsuglia, A. Basti, F. Basti, T. S. Bauer, V. Bavigadda, M. Bejger, M. G. Beker, C. Belczynski, D. Bersanetti, A. Bertolini, M. Bitossi, M. A. Bizouard, S. Bloemen, M. Blom, M. Boer, G. Bogaert, D. Bondi, F. Bondu, L. Bonelli, R. Bonnand, V. Boschi, L. Bosi, T. Bouedo, C. Bradaschia, M. Branchesi, T. Briant, A. Brillet, V. Brisson, T. Bulik, H. J. Bulten, D. Buskulic, C. Buy, G. Cagnoli, E. Calloni, C. Campeggi, B. Canuel, F. Carbognani, F. Cavalier, R. Cavalieri, G. Cella, E. Cesarini, E. C. Mottin, A. Chincarini, A. Chiummo, S. Chua, F. Cleva, E. Coccia, P.-F. Cohadon, A. Colla, M. Colombini, A. Conte, J.-P. Coulon, E. Cuoco, A. Dalmaz, S. D'Antonio, V. Dattilo, M. Davier, R. Day, G. Debreczeni, J. Degallaix, S. Deléglise, W. D. Pozzo, H. Dereli, R. D. Rosa, L. D. Fiore, A. D. Lieto, A. D. Virgilio, M. Doets, V. Dolique, M. Drago, M. Ducrot, G. Endrőczi, V. Fafone, S. Farinon, I. Ferrante, F. Ferrini, F. Fidecaro, I. Fiori, R. Flaminio, J.-D. Fournier, S. Franco, S. Frasca, F. Frasconi, L. Gammaitoni, F. Garufi, M. Gaspard, A. Gatto, G. Gemme, B. Gendre, E. Genin, A. Gennai, S. Ghosh, L. Giacobone, A. Giazotto, R. Gouaty, M. Granata, G. Greco, P. Groot, G. M. Guidi, J. Harms, A. Heidmann, H. Heitmann, P. Hello, G. Hemming, E. Hennes, D. Hofman, P. Jaranowski, R. J. G. Jonker, M. Kasprzack, F. Kéfélian, I. Kowalska, M. Kraan, A. Królak, A. Kutynia, C. Lazzaro, M. Leonardi,

N. Leroy, N. Letendre, T. G. F. Li, B. Lieunard, M. Lorenzini, V. Loriette, G. Losurdo, C. Magazzù, E. Majorana, I. Maksimovic, V. Malvezzi, N. Man, V. Mangano, M. Mantovani, F. Marchesoni, F. Marion, J. Marque, F. Martelli, L. Martellini, A. Masserot, D. Meacher, J. Meidam, F. Mezzani, C. Michel, L. Milano, Y. Minenkov, A. Moggi, M. Mohan, M. Montani, N. Morgado, B. Mours, F. Mul, M. F. Nagy, I. Nardecchia, L. Naticchioni, G. Nelemans, I. Neri, M. Neri, F. Nocera, E. Pacaud, C. Palomba, F. Paoletti, A. Paoli, A. Pasqualetti, R. Passaquieti, D. Passuello, M. Perciballi, S. Petit, M. Pichot, F. Piergiovanni, G. Pillant, A. Piluso, L. Pinard, R. Poggiani, M. Prijatelj, G. A. Prodi, M. Punturo, P. Puppo, D. S. Rabeling, I. Rácz, P. Rapagnani, M. Razzano, V. Re, T. Regimbau, F. Ricci, F. Robinet, A. Rocchi, L. Rolland, R. Romano, D. Rosińska, P. Ruggi, E. Saracco, B. Sassolas, F. Schimmel, D. Sentenac, V. Sequino, S. Shah, K. Siellez, N. Straniero, B. Swinkels, M. Tacca, M. Tonelli, F. Travasso, M. Turconi, G. Vajente, N. van Bakel, M. van Beuzekom, J. F. J. van den Brand, C. V. D. Broeck, M. V. van der Sluys, J. van Heijningen, M. Vasúth, G. Vedovato, J. Veitch, D. Verkindt, F. Vetrano, A. Viceré, J.-Y. Vinet, G. Visser, H. Vocca, R. Ward, M. Was, L.-W. Wei, M. Yvert, A. Z. żny, and J.-P. Zendri, "Advanced Virgo: A second-generation interferometric gravitational wave detector," *Classical and Quantum Gravity*, vol. 32, no. 2, p. 024001, Dec. 2014. [Online]. Available: https://dx.doi.org/10.1088/0264-9381/32/2/024001

[83] C. M. Caves, "Quantum-Mechanical Radiation-Pressure Fluctuations in an Interferometer," *Physical Review Letters*, vol. 45, no. 2, pp. 75–79, Jul. 1980. [Online]. Available: https://link.aps.org/doi/10.1103/PhysRevLett.45.75

[84] ——, "Quantum-mechanical noise in an interferometer," *Physical Review D*, vol. 23, no. 8, pp. 1693–1708, Apr. 1981. [Online]. Available: https://link.aps.org/doi/10.1103/PhysRevD.23.1693

[85] V. B. Braginsky and F. Ya. Khalili, "Quantum nondemolition measurements: The route from toys to tools," *Reviews of Modern Physics*, vol. 68, no. 1, pp. 1–11, Jan. 1996. [Online]. Available: https://link.aps.org/doi/10.1103/RevModPhys.68.1

[86] H. J. Kimble, Y. Levin, A. B. Matsko, K. S. Thorne, and S. P. Vyatchanin, "Conversion of conventional gravitational-wave interferometers into quantum nondemolition interferometers by modifying their input and/or output optics," *Physical Review D*, vol. 65, no. 2, p. 022002, Dec. 2001. [Online]. Available: https://link.aps.org/doi/10.1103/PhysRevD.65.022002

[87] L. McCuller, C. Whittle, D. Ganapathy, K. Komori, M. Tse, A. Fernandez-Galiana, L. Barsotti, P. Fritschel, M. MacInnis, F. Matichard, K. Mason, N. Mavalvala, R. Mittleman, H. Yu, M. E. Zucker, and M. Evans, "Frequency-Dependent Squeezing for Advanced LIGO," *Physical Review Letters*, vol. 124, no. 17, p. 171102, Apr. 2020. [Online]. Available: https://link.aps.org/doi/10.1103/PhysRevLett.124.171102

[88] Y. Zhao, N. Aritomi, E. Capocasa, M. Leonardi, M. Eisenmann, Y. Guo, E. Polini, A. Tomura, K. Arai, Y. Aso, Y.-C. Huang, R.-K. Lee, H. Lück, O. Miyakawa, P. Prat, A. Shoda, M. Tacca, R. Takahashi, H. Vahlbruch, M. Vardaro, C.-M. Wu, M. Barsuglia, and R. Flaminio, "Frequency-Dependent Squeezed Vacuum Source for Broadband Quantum Noise Reduction in Advanced Gravitational-Wave Detectors," *Physical Review Letters*, vol. 124, no. 17, p. 171101, Apr. 2020. [Online]. Available: https://link.aps.org/doi/10.1103/PhysRevLett.124.171101

[89] N. B. Phillips, A. V. Gorshkov, and I. Novikova, "Light storage in an optically thick atomic ensemble under conditions of electromagnetically induced transparency and four-wave mixing," *Physical Review A*, vol. 83, no. 6, p. 063823, Jun. 2011. [Online]. Available: https://link.aps.org/doi/10.1103/PhysRevA.83.063823

[90] A. V. Gorshkov, A. André, M. Fleischhauer, A. S. Sørensen, and M. D. Lukin, "Universal Approach to Optimal Photon Storage in Atomic Media," *Physical Review Letters*, vol. 98, no. 12, p. 123601, Mar. 2007. [Online]. Available: https://link.aps.org/doi/10.1103/PhysRevLett.98.123601

[91] A. V. Gorshkov, A. André, M. D. Lukin, and A. S. Sørensen, "Photon storage in $\ensuremath{\Lambda}$-type optically dense atomic media. II. Free-space model," *Physical Review A*, vol. 76, no. 3, p. 033805, Sep. 2007. [Online]. Available: https://link.aps.org/doi/10.1103/PhysRevA.76.033805

[92] E. E. Mikhailov, K. Goda, T. Corbitt, and N. Mavalvala, "Frequency-dependent squeeze-amplitude attenuation and squeeze-angle rotation by electromagnetically induced transparency for gravitational-wave interferometers," *Physical Review A*, vol. 73, no. 5, p. 053810, May 2006. [Online]. Available: https://link.aps.org/doi/10.1103/PhysRevA.73.053810

[93] J. Junker, D. Wilken, N. Johny, D. Steinmeyer, and M. Heurs, "Frequency-Dependent Squeezing from a Detuned Squeezer," *Physical Review*

Letters, vol. 129, no. 3, p. 033602, Jul. 2022. [Online]. Available: https://link.aps.org/doi/10.1103/PhysRevLett.129.033602

[94] J. Borregaard, M. Zugenmaier, J. M. Petersen, H. Shen, G. Vasilakis, K. Jensen, E. S. Polzik, and A. S. Sørensen, "Scalable photonic network architecture based on motional averaging in room temperature gas," *Nature Communications*, vol. 7, no. 1, p. 11356, Apr. 2016. [Online]. Available: https://www.nature.com/articles/ncomms11356